
HMS
آزمایشگاه تحقیقاتی
حسگر مواد صبا

اینکه ما روی علم و فنّاوری تکیه میکنیم، فقط به خاطر این نیست که میخواهیم نِصاب علمی خودمان را بالا ببریم؛ پیشرفت علم و فنّاوری به پیشرفت اقتصاد کمک میکند؛ بنگاه‌هایی که دانش‌بنیان هستند میتوانند به اقتصاد ملّی کمک کنند.

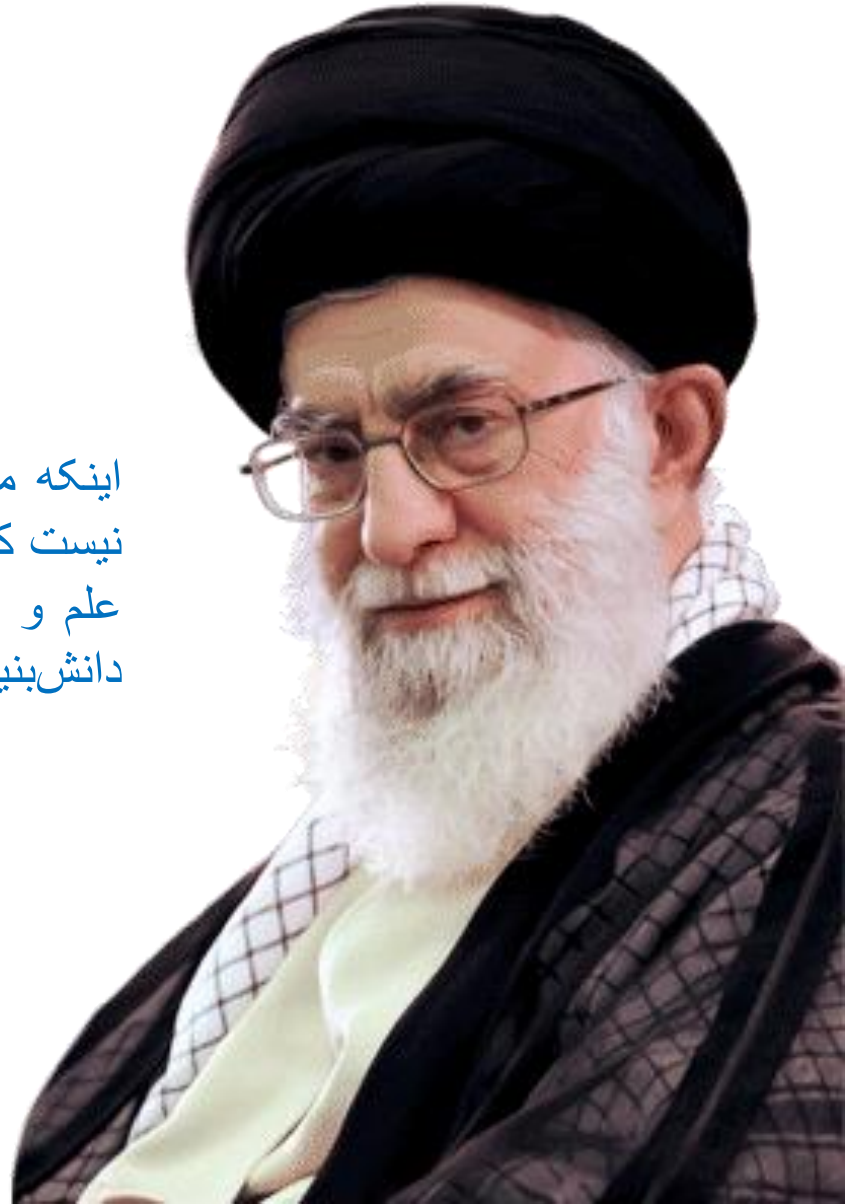

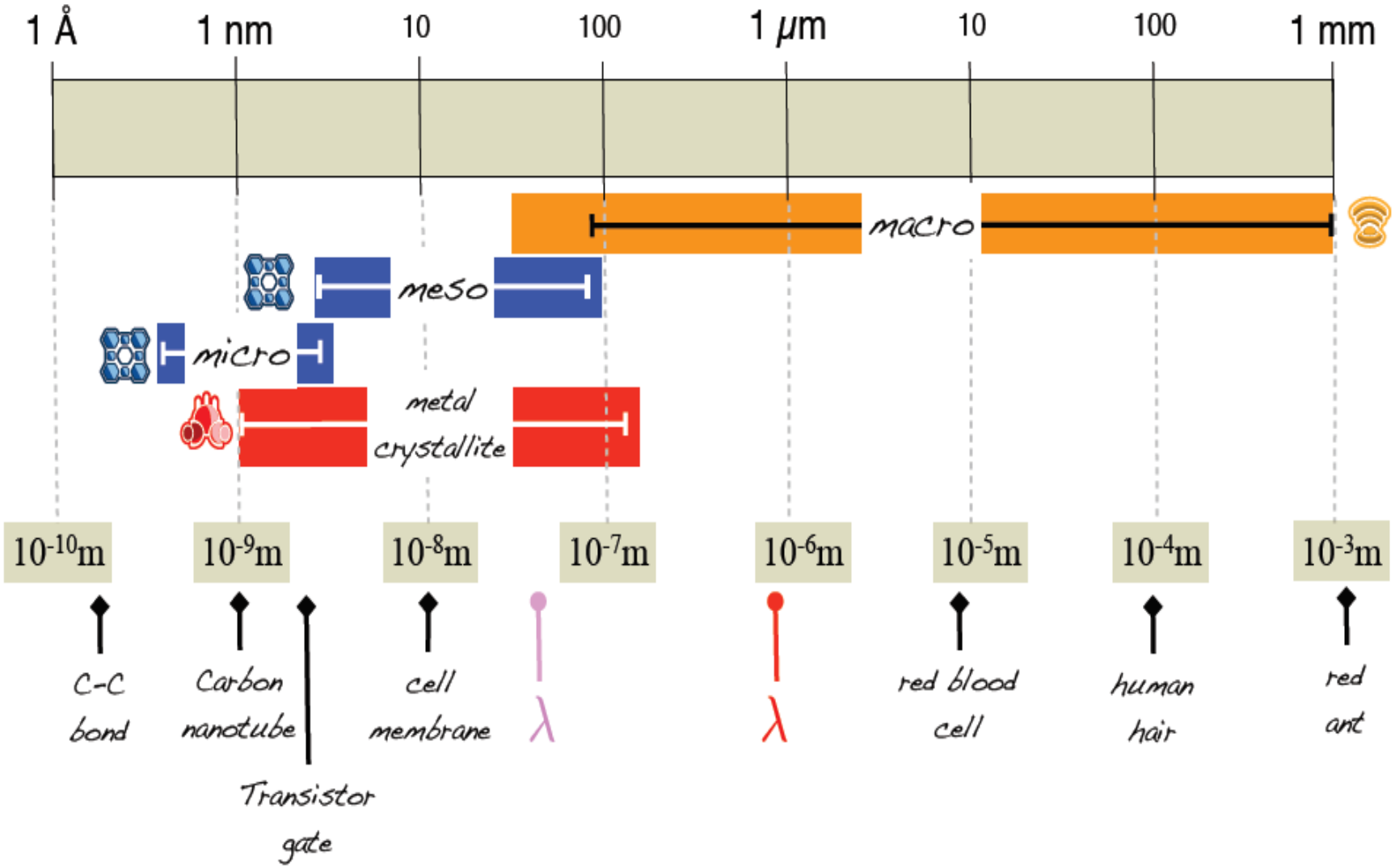
1 Å
1 nm
10
100
1 μm
10
100
1 mm
macro
meso
micro
metal
crystallite
10-10m
10-9m
10-8m
10-7m
10-6m
10-5m
10-4m
10-3m
C-C
bond
Carbon
nanotube
Transistor
gate
cell
membrane
λ
λ
red blood
cell
human
hair
red
ant

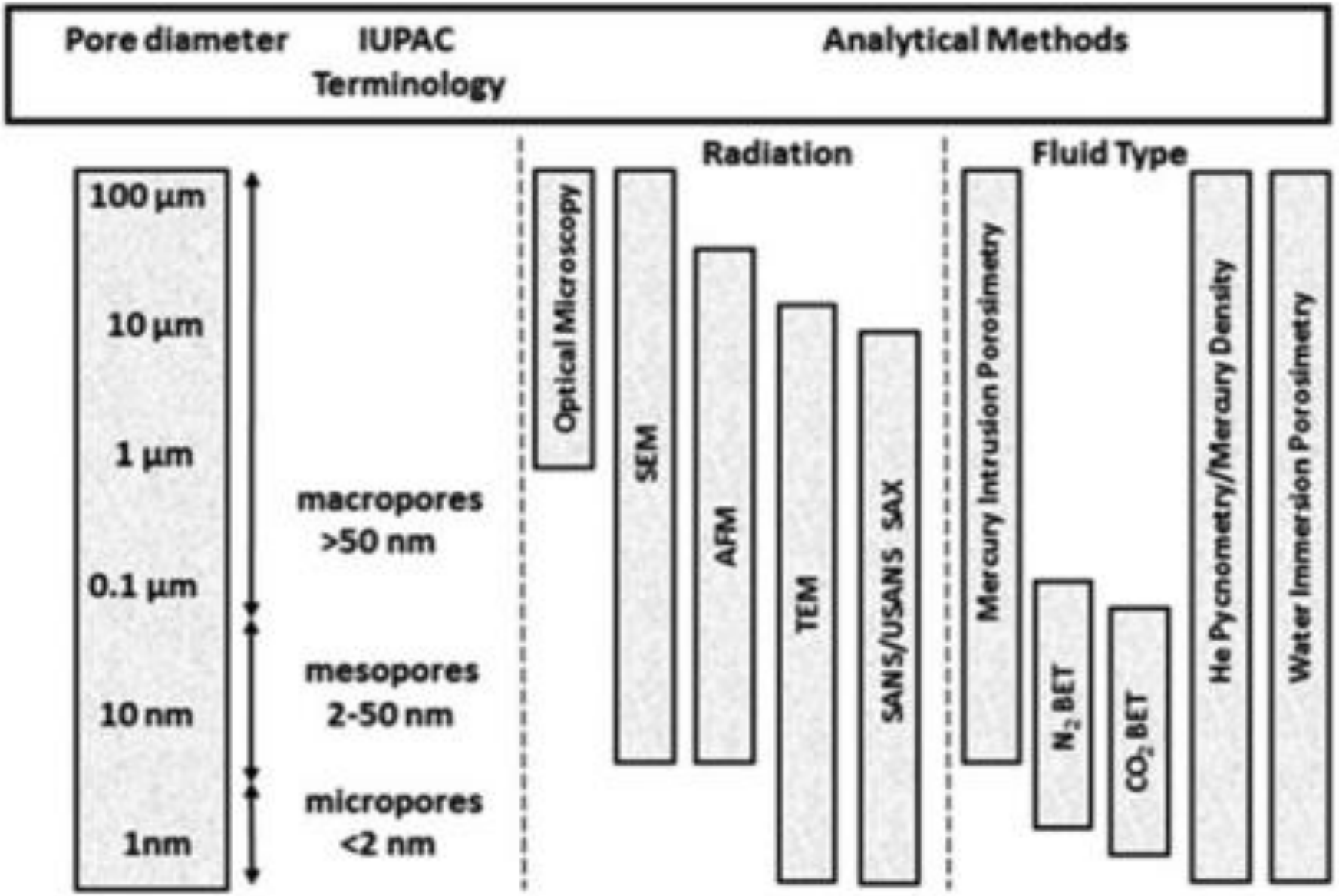

Fig. 2.1 Methods used to determine porosity and pore size distribution (PSD) (Anovitz and Cole 2015)

Size- and Shape-Dependent Catalytic Performances

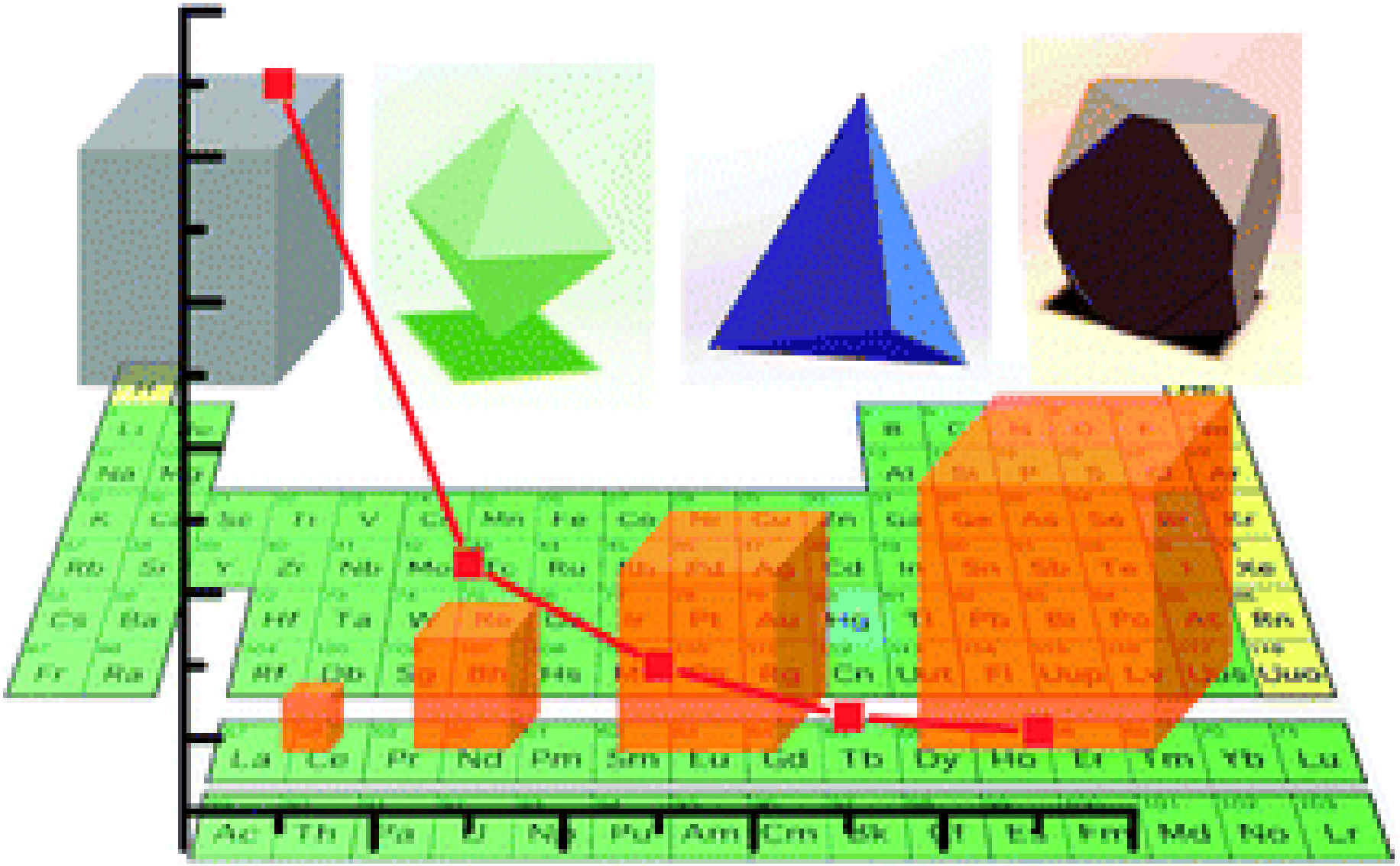

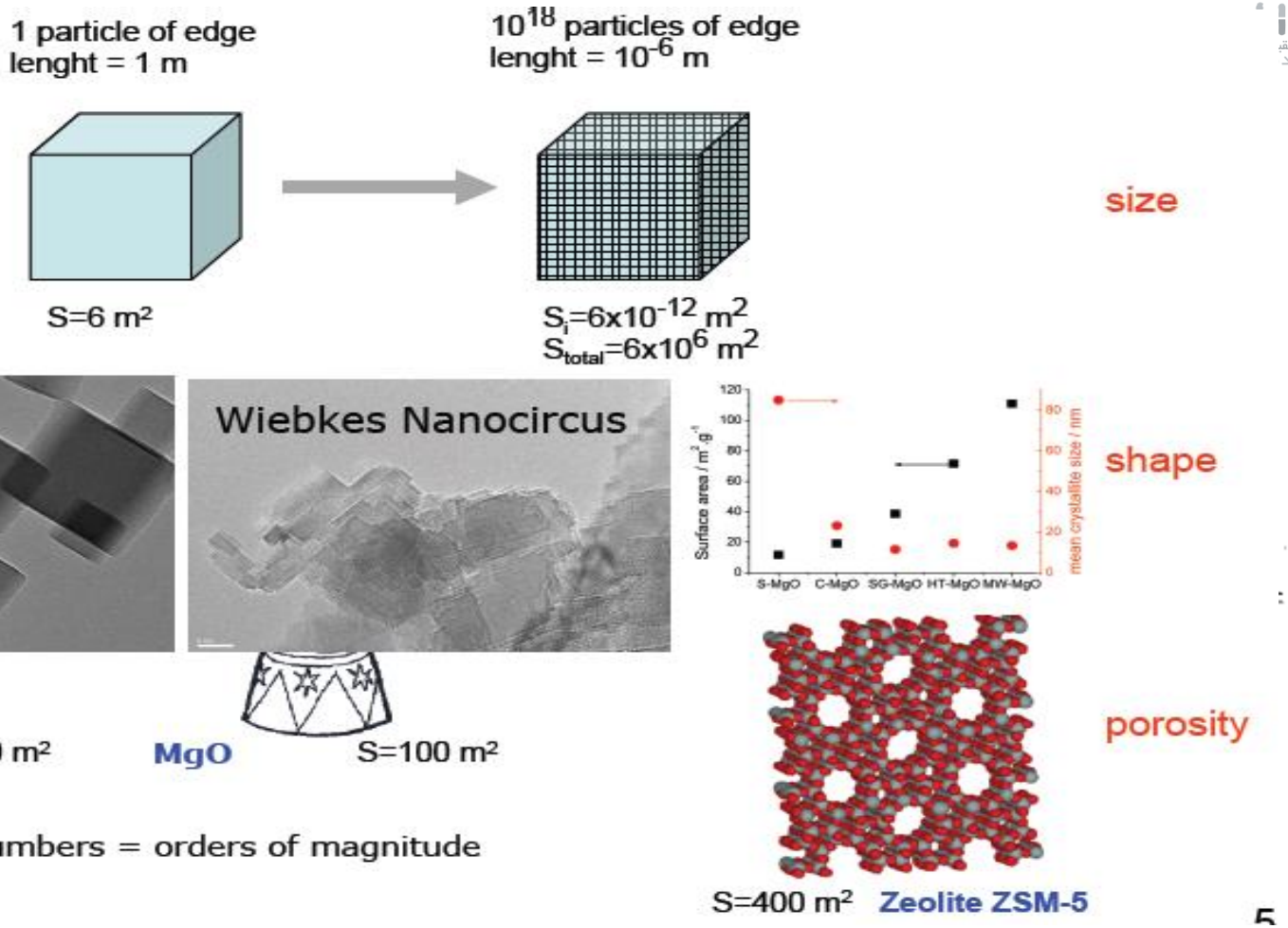

sS==
s/V=4pr2/4/3pr3=3/pr

fractal demation ارزیابی بعد خود متشابه

saxs-sans - (سختی سطح – تخلخل)

- Surface area from particle size distribution

  Dynamic light scattering

  Measures Brownian motion and relates this to the size of the particles by using a correlation function and the Stokes-Einstein equation

  Non-spherical particles will be measured as equivalent spheres

$$D_0 = \frac{kT}{6\pi\eta R}$$

D= Diffusion coefficient
k= Boltzmann constant
T= absolute temperature
η= dynamic viscosity of the solvent
R= radius of the particle

- Microscopy

  Shape analysis

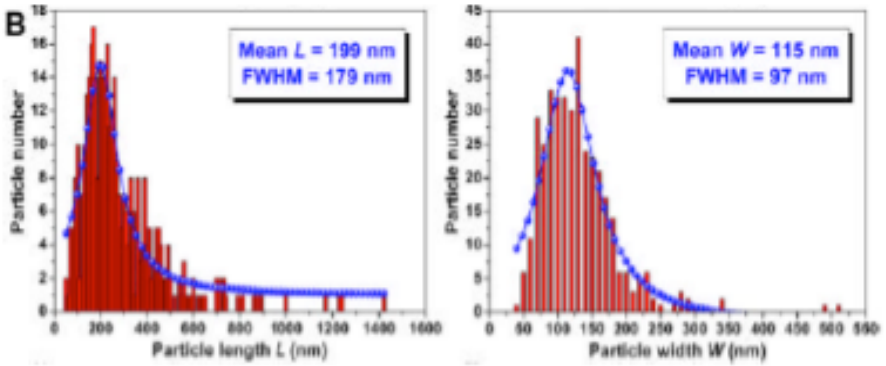

- Small angle X-ray scattering

  Scattering of X-rays by small domains of uniform matter (crystalline or amorphous), for which the electron density ρ^e is different from the continuous medium

  The central peak of scattered intensity gets broader as the domain size (particles, voids) decreases

  SAXS parameters (mean size / size distribution / specific surface area) are derived from analysis of the profile of the SAXS curve

- Mercury porosimetry

- Gas Adsorption

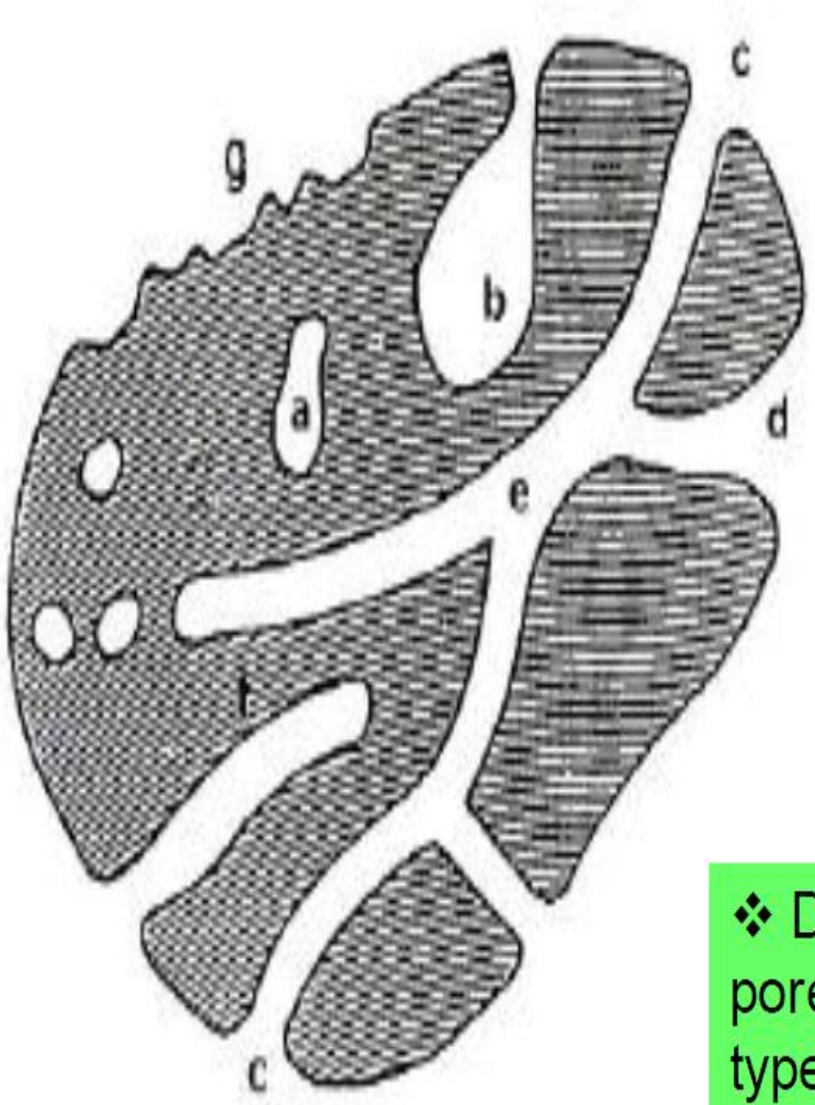

IUPAC

a - closed pores

b,f - pen only at one end

c,d,g - open

e - open at two ends (through)

❖ Different types and/or shapes of pores will generate different hysteresis types in the adsorption-desorption isotherms

Applications

- Paints and coatings
- Aerospace
- Pharmaceutics
- Nanotubes
- Carbon Black
- Electronics
- Ceramics
- Catalysts
- Activated Carbons
- Fuel Cell Electrodes
- Adsorbents

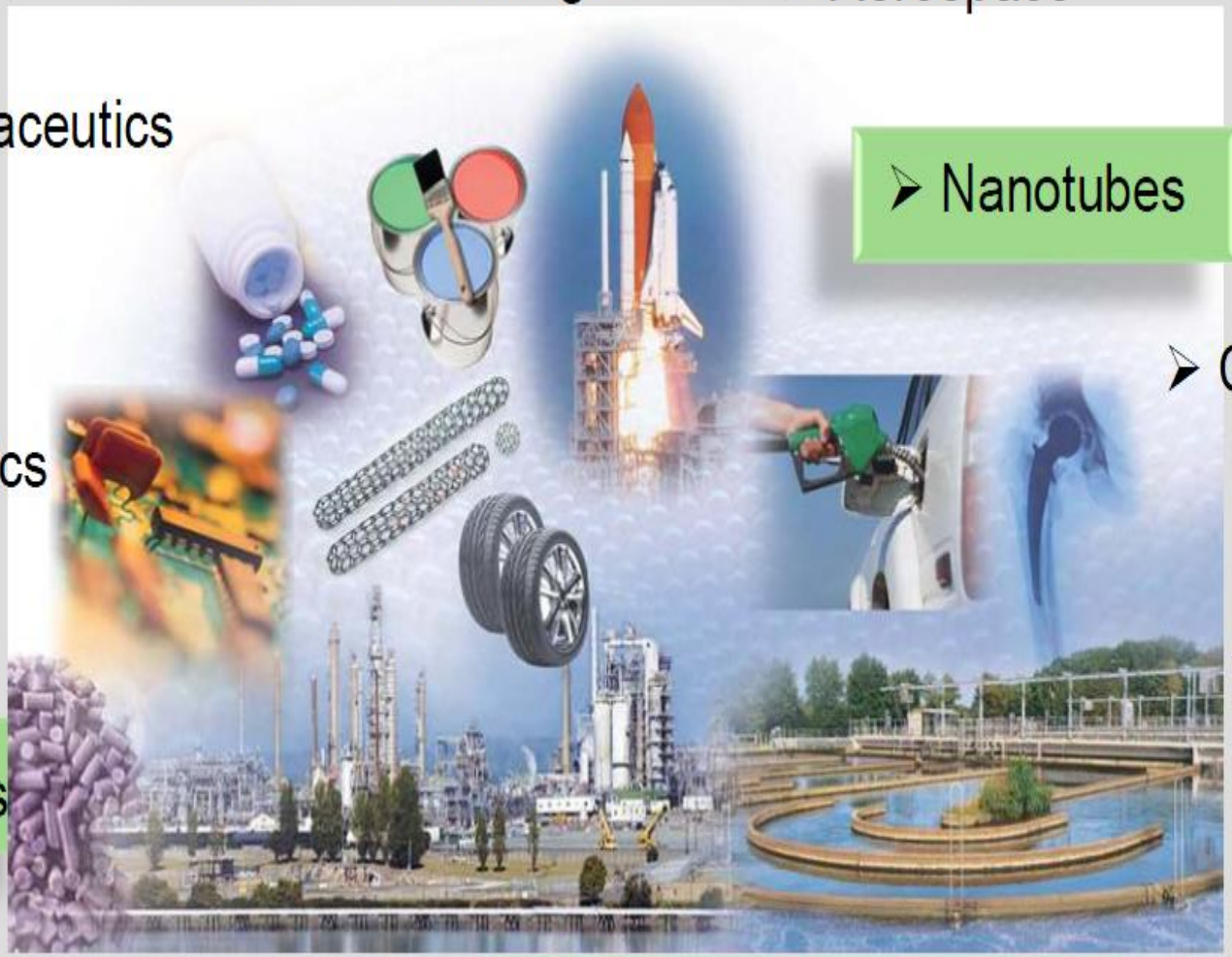

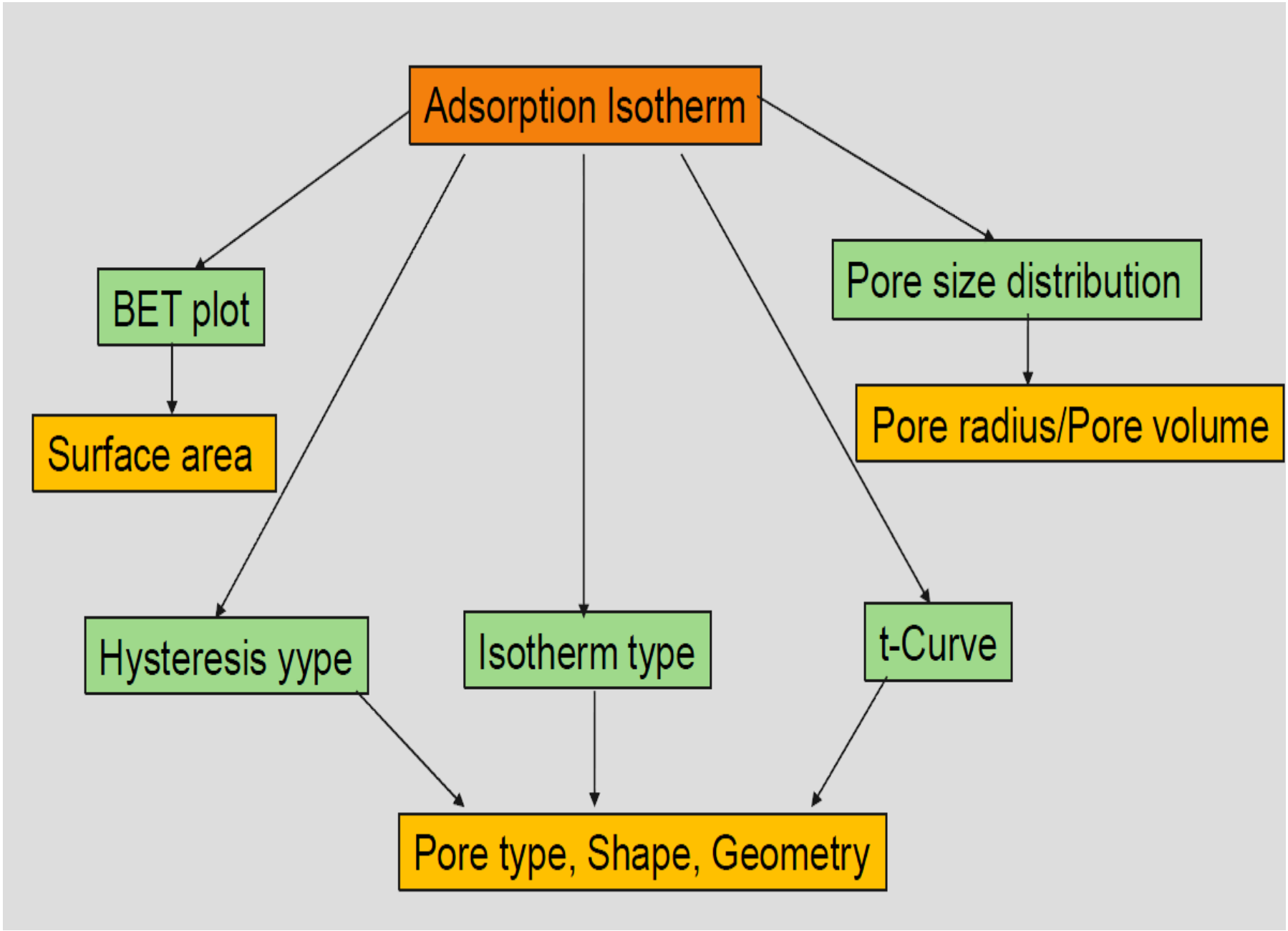
Adsorption Isotherm
BET plot
Surface area
Pore size distribution
Pore radius/Pore volume
Hysteresis yype
Isotherm type
t-Curve
Pore type, Shape, Geometry

کاربرد

Oil industry

- Oil refinerly (Cracking, Reforming, Hydrodesulfurization, etc.)
- Polimer and petrochemical product synthesis
- Liquid fuel synthesis from CO and H_2 (FT reaction, Fe/CO)

Car industry

- Exhaust gas catalyst

Chemical industry

- Ammonia synthesis from N_2 and H_2 (Fe/CO)
- HNO_3 synthesis from ammonia

Fuell cell industry

- Electrode catalyst of fuel cell

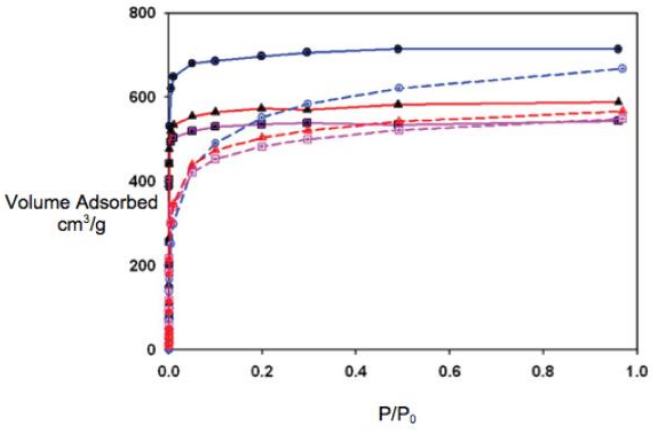

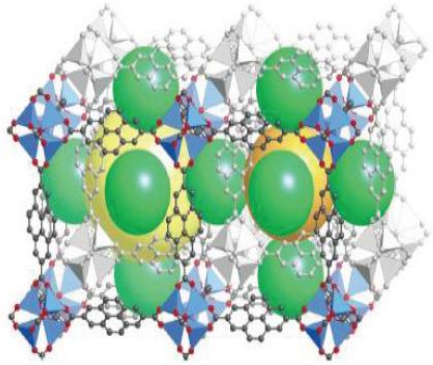

Figure 12: The structure of catenated IRMOF-13. Orange and yellow represent non-catenated pore volumes. Green represents catenated pore volume.

Catalysts	BET Surface Areas m^2/g	Micro Pore Volume V[=] liquid N_2 volume cm^3/g	Meso Pore Volume V[=] liquid N_2 volume cm^3/g	Average Pore Diameter nm
100 % Co_3O_4	185.2	0.009	0.66	2.2, 18*
50/50 Co_3O_4/CeO_2	180.3	0.008	0.66	2.2, 14*
25/25/50 $Ag_2O/Co_3O_4/CeO_2$	148.0	0.005	0.50	2.2

*Catalysts gave 2 average pore diameters

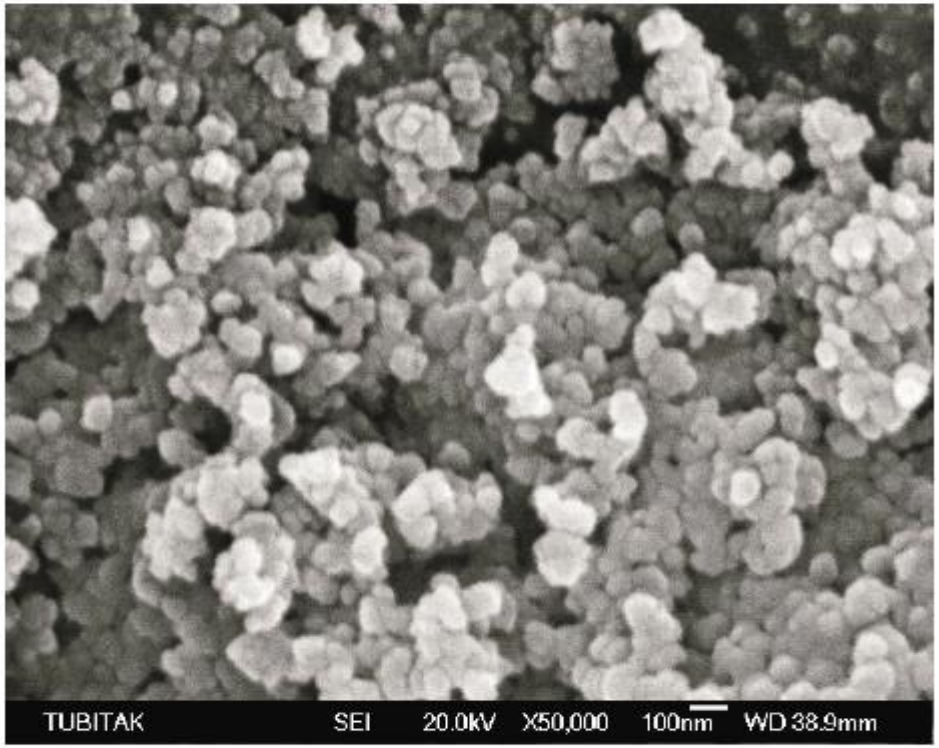

(A)

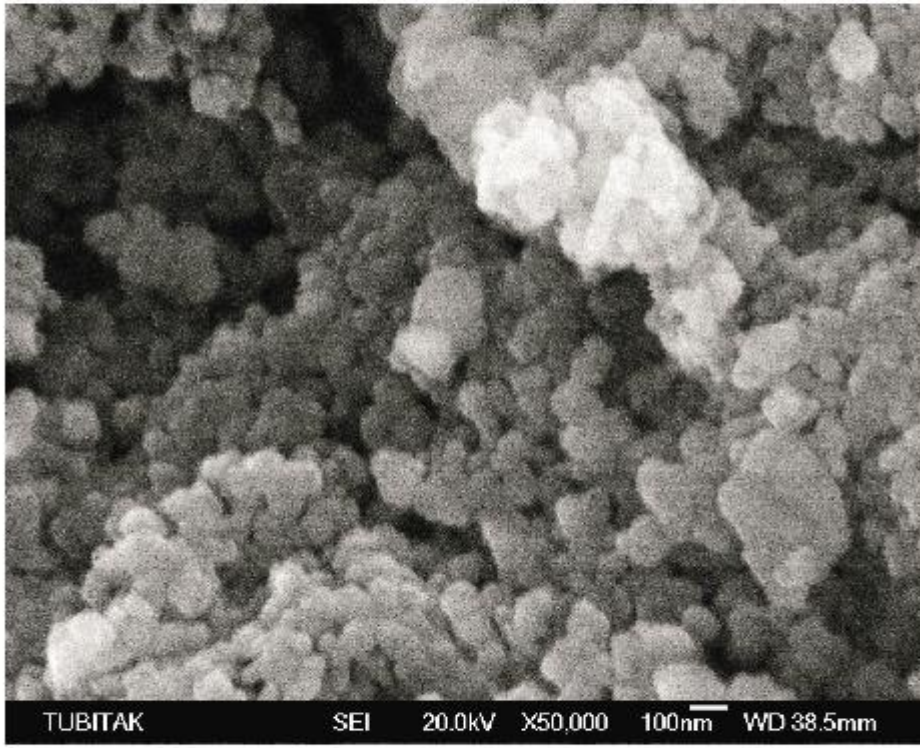

(B)

Figure 2. Scanning electron microscopy photograph of 50/50 Co_3O_4/CeO_2 (A) and 25/25/50 $Ag_2O/Co_3O_4/CeO_2$ (B).

تعیین ذرات در مقیاس نانو

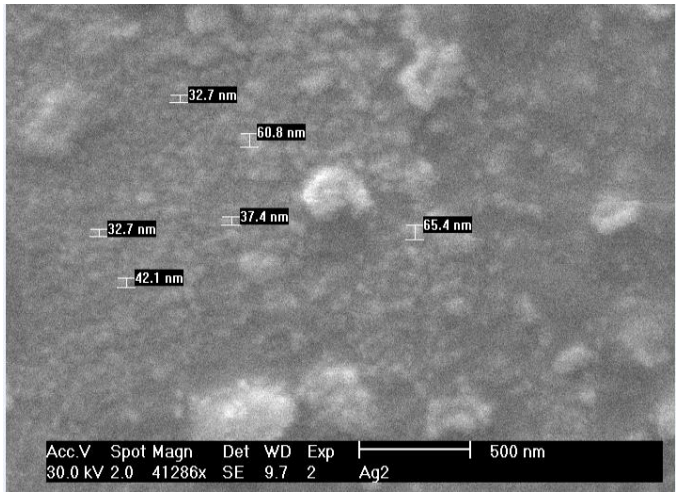

- Pore Volume Data

Total pore volume for pores with Radius less than 15.93 Å at P/Po = 0.395090	5.787e-01 cc/g
BJH method cumulative adsorption pore volume	2.103e+00 cc/g
BJH method cumulative desorption pore volume	2.192e+00 cc/g
DH method cumulative adsorption pore volume	2.054e+00 cc/g
DH method cumulative desorption pore volume	2.146e+00 cc/g
HK method cumulative pore volume	4.257e-01 cc/g
SF method cumulative pore volume	4.358e-01 cc/g
NLDFT method cumulative pore volume	1.904e+00 cc/g

- Pore Size Data

Average pore Radius	3.505e+01 Å
BJH method adsorption pore Radius (Mode Dv(r))	1.698e+01 Å
BJH method desorption pore Radius (Mode Dv(r))	1.710e+01 Å
DH method adsorption pore Radius (Mode Dv(r))	1.698e+01 Å
DH method desorption pore Radius (Mode Dv(r))	1.710e+01 Å
HK method pore Radius (Mode)	1.838e+00 Å
SF method pore Radius (Mode)	2.261e+00 Å
NLDFT pore Radius (Mode)	2.376e+01 Å

$$\tau = \frac{K\lambda}{\beta cos\theta}$$

رابطه‌ی شرر: $D=(0.9\times\lambda)/(\beta\cos\theta)$

D اندازه‌ی کریستالیت، β عرض پیک در نصف شدت بیشینه، θ زاویه‌ی براگ مربوط به پیک و λ طول موج پرتوی ایکس هستند.

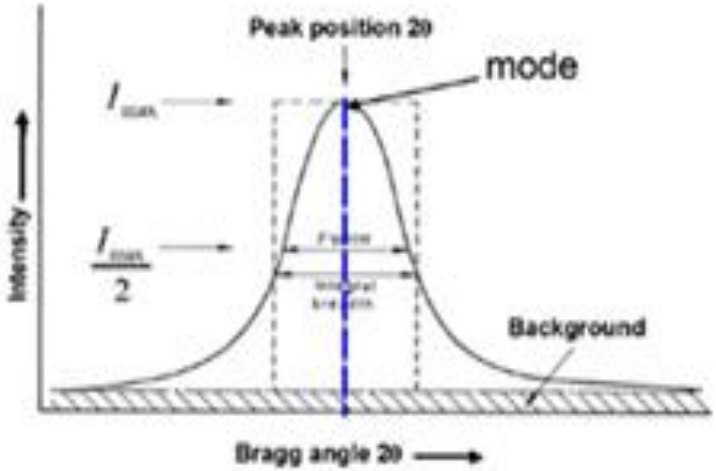

شکل 4: روش به دست آوردن FWHM

با توجه به رابطه ی شرر می‌توان دریافت که هرچه اندازه ی ذرات ماده کوچک تر باشد، FWHM بزرگتر است، یعنی پیک پهن‌تر و شدت آن کمتر است، یعنی پیک نانوذرات در مقایسه با مواد معمولی شدت کمتر و پهنای بیشتری دارند.

سوال: با توجه به داده‌های زیر و با استفاده از رابطه‌ی شرر اندازه‌ی کریستالیت را محاسبه کنید:

پاسخ: ابتدا β را به رادیان تبدیل می‌کنیم: $0.00872=360/(3.14\times2\times0.5)$

$D=(0.9\times0.154)/(0.00872\times\cos13.5)=16.33nm$

جذبهای مختلف

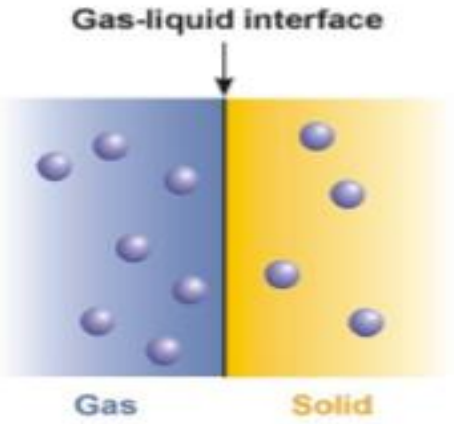

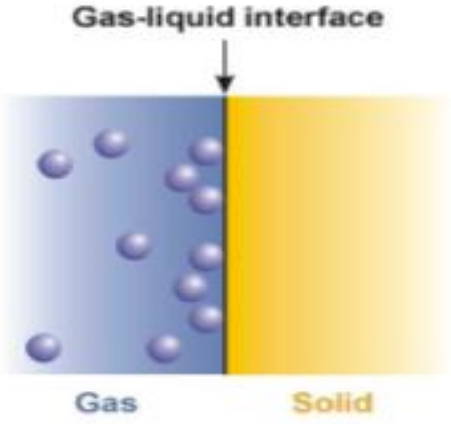

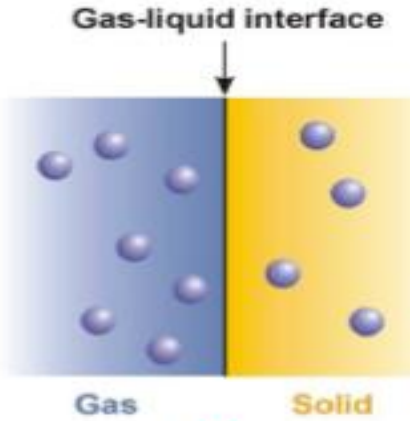

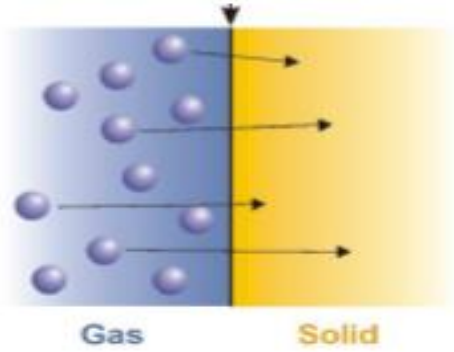

Adsorption

Absorption

Sorption

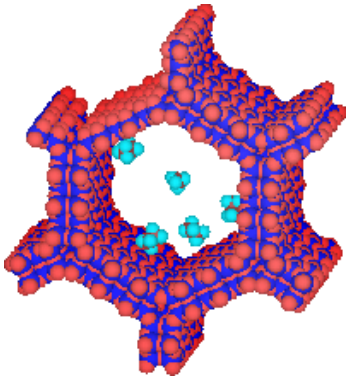

Planar, nonporous, macropores

mesoporous

microporous

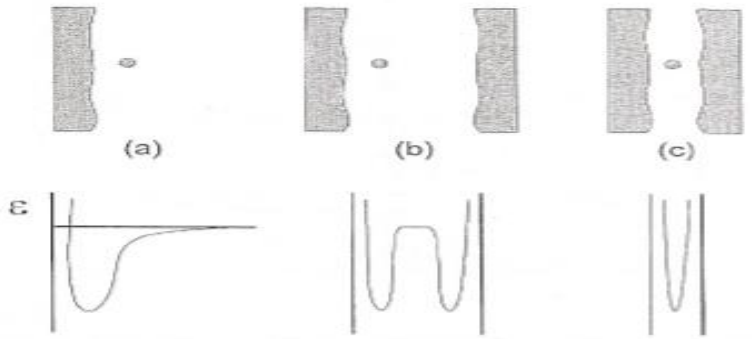

جذب شیمیایی

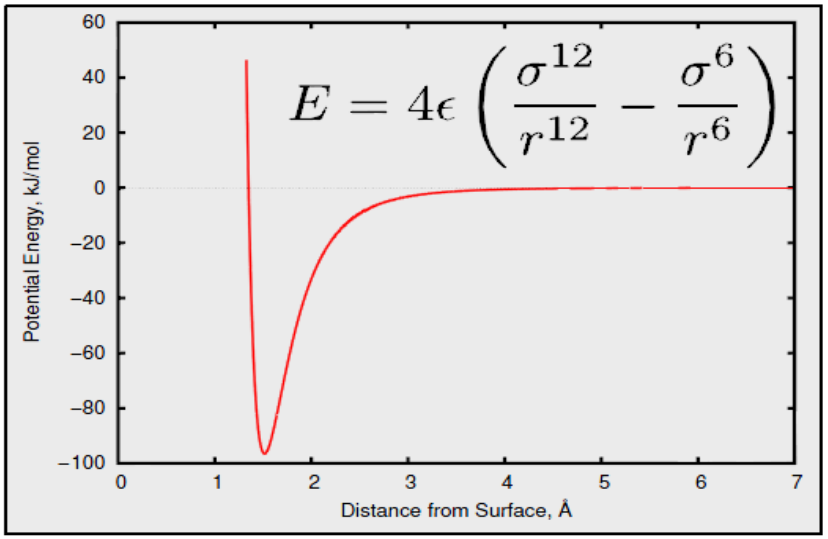

- May be activated
- Covalent, metallic, ionic
- Strong (> 35 kJ/mol)
- May be dissociative
- **Often irreversible**
- **Specific - surface symmetry**
- **Limited to a monolayer**
- Wide temperature range

Mainly used for;
- BET single point measurement.
- Chemisorption measurement.
  (TPD, TPR/TPO, Pulse chemisorption)

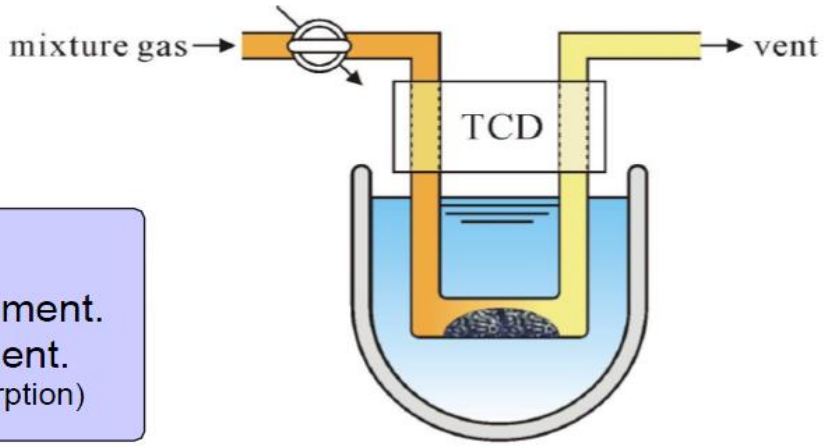

Dynamic flow method

جذب فیزیکی

- 1. Low heats of adsorption, no violent or disruptive structural changes.
- 2. Can involve multiple layers of adsorbate, thus allowing for pore measurements.
- 3. High temperatures tend to inhibit physical adsorption.
- 4. Adsorption equilibrium is achieved quickly since no activation energy is generally required.
- 5. Physical adsorption is fully reversible, allowing adsorbate to fully adsorb and desorb.

- Not activated (no barrier)
- Rapid
- Weak (< 38 kJ/mol)
- Atomic/Molecular
- **Reversible**
- **Non-specific**
- **May form multilayers**
- van der Waals/dipole interactions
- Often measured near the condensation temperature

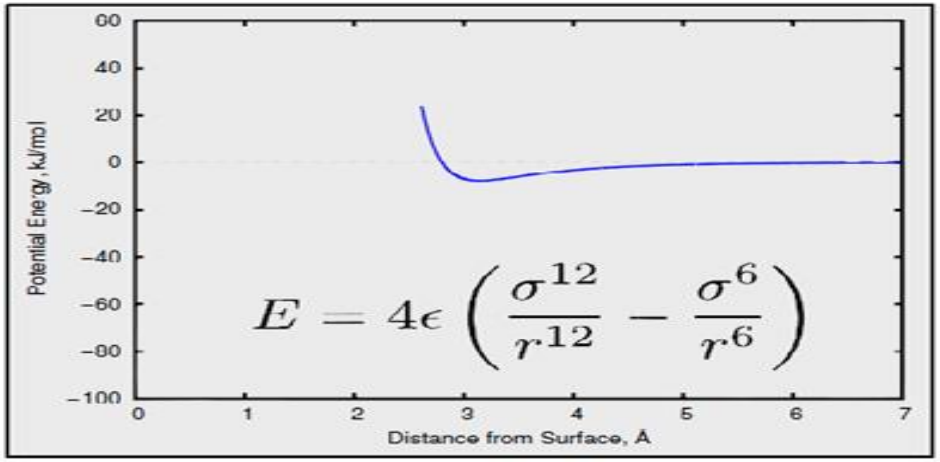


Quantachrome Instruments Gas Sorption Show

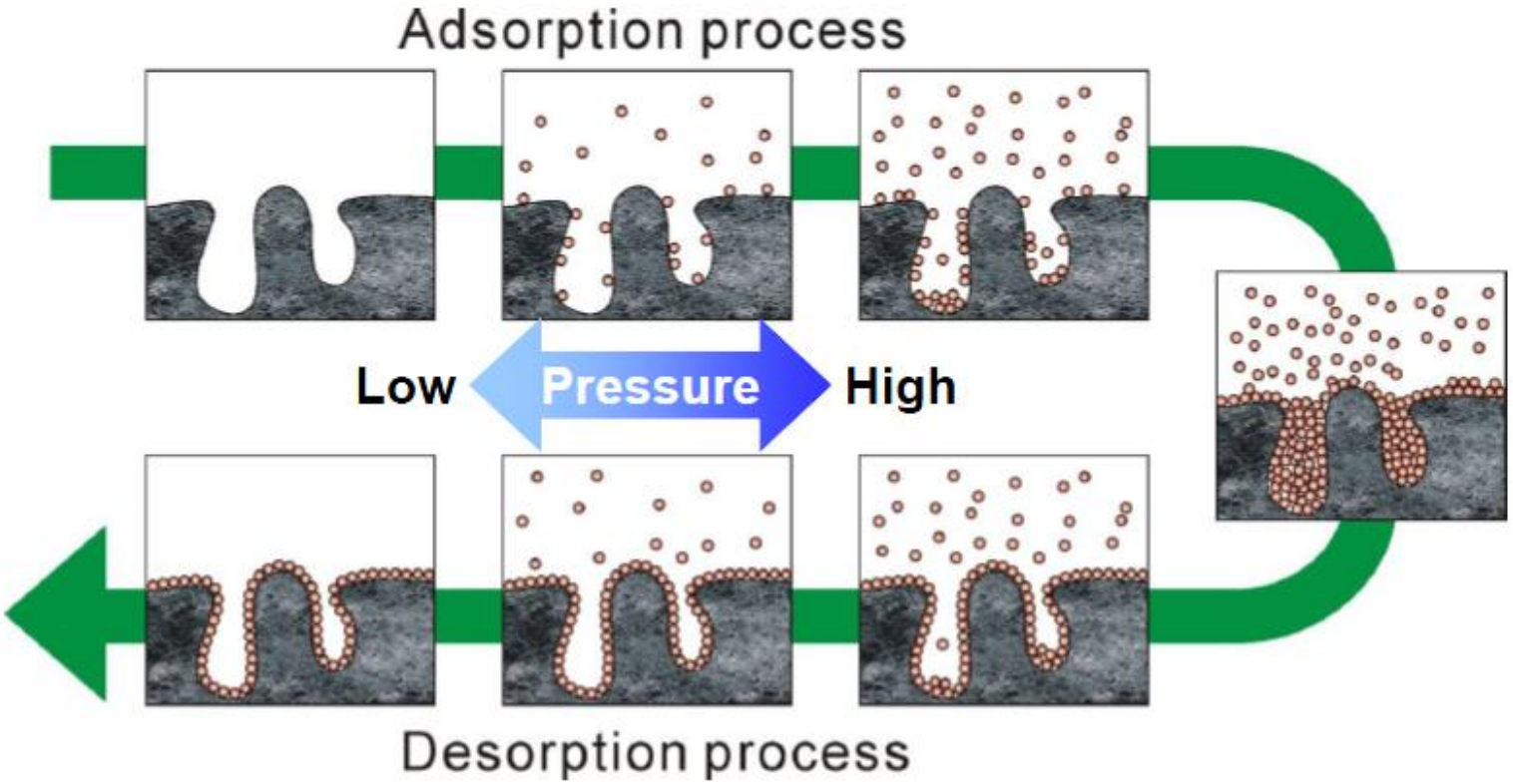
Adsorption process
Low
Pressure
High
Desorption process

- As pressure is further increased we may observe capillary condensation in mesopores.

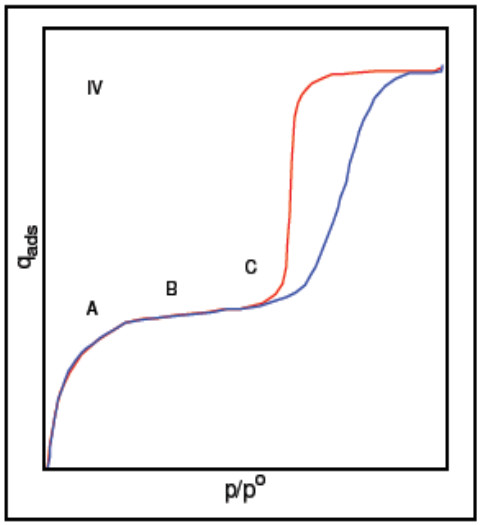

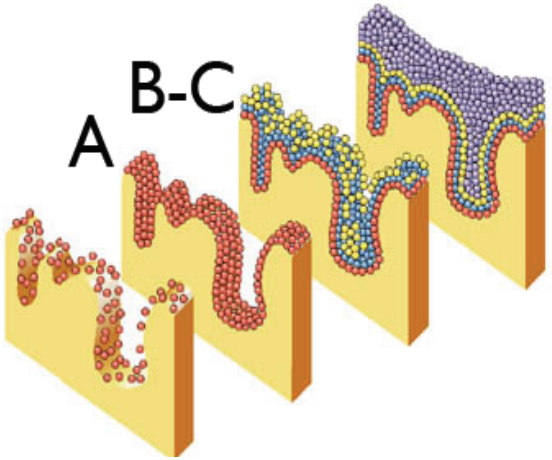

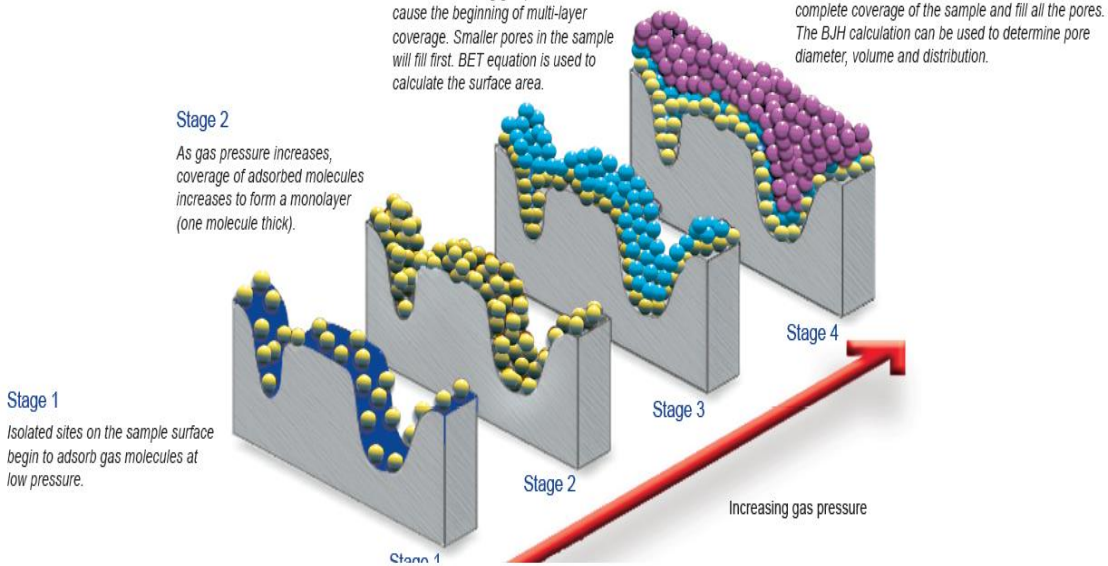

جذب گاز برای تعیین سطح

- The most common adsorbate used is Nitrogen, however, other adsorbates are used in some circumstances.

Gas	Temp (°C)	α factor x10^5 (1/mm Hg)	Cross Sectional Area (Å2/mol.)	Molecular weight (g/mol)
Ar	-195.8	11.4	14.2	39.948
	-183	3.94		
	-78	2.75		
CO_2	0	1.75	19.5	44.01
	25	1.55		
	-183	3.42		
CO	-195.8	6.58	16.3	28.01
N2	-183	3.78	16.2	28.0134
	-183	4.17		
O2	0	14.2		
C4H10	25	4.21	46.9	58.12
	-195.8	11.4		

The following sample information about surface areas and pores can be obtained from the measured data.

Name of analysis	Adsorptive	Analysis method	Primary data produced
Adsorption / desorption isotherm	Isotherms are displayed with this analysis. Judging from the shape of isotherm, the characteristic of the sample can be seen and appropriate method to analyze the isotherm can be chosen.		
PCT curve	H_2	Change in amount of hydrogen storage capacity	Amount of hydrogen storage capacity
BET plot	N_2, Ar, Kr, etc.	Evaluates a specific surface area for physical adsorption	Monomolecular layer adsorption
Langmuir plot	O_2, etc.	Evaluates the amount of chemical adsorption	Monomolecular layer adsorption
t plot	N_2	Evaluates micropores	Total specific surface area, external specific surface area, and pore volume
α_s plot	N_2	Evaluates micropores	Total specific surface area, external specific surface area, and pore volume
MP plot	N_2	Micropore distribution curve	Micropore distribution
BJH plot	N_2	Mesopore distribution curve	Mesopore distribution, volume and area
CI plot	N_2	Mesopore distribution curve	Mesopore distribution, volume and area
DH plot	N_2	Mesopore distribution curve	Mesopore distribution, volume and area
INNES plot	N_2	Mesopore distribution curve	Mesopore distribution, volume and area
DA plot	N_2, CO_2, C_6H_6, etc.	Evaluate the micropore volume	Micropore volume
HK plot	N_2, Ar	Micropore distribution curve	Micropore distribution (Pore shape: Slit)
SF plot	N_2, Ar	Micropore distribution curve	Micropore distribution (Pore shape: Cylinder)
Isosteric heat of adsorption	H_2O, etc.	Evaluates differential heat of adsorption	Differential heat of adsorption
Difference of adsorption isotherms	H_2O, NH_3 , etc.	Evaluates the amount of chemical adsorption	Difference adsorption isotherm
Metal dispersion	H_2, CO, etc.	Evaluates metal dispersion	Metal dispersion
Molecular probe	CO_2, C_2H_6, n-C_4H_{10}, iso-C_4H_{10} , etc.	Evaluate micropores	Micropore distribution curve

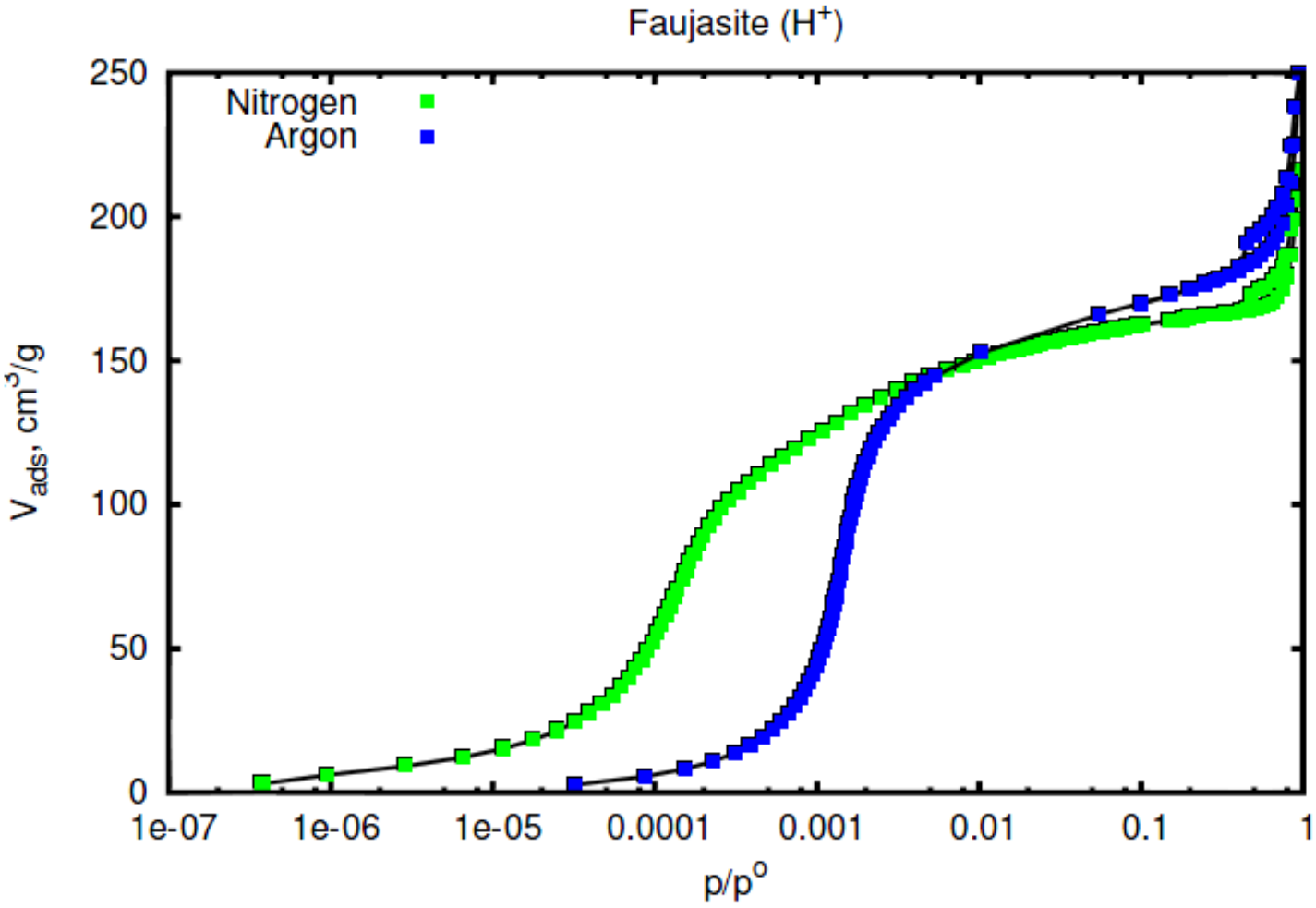

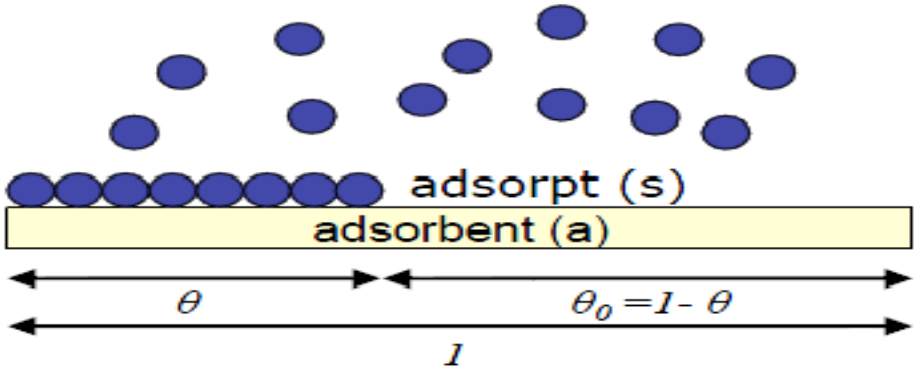

Fraction of occupied surface (coverage)

$\theta = \Gamma/\Gamma_m = \gamma/\gamma_m = N/N_m = W/W_m$

$$N_m \theta_1 \nu_1 e^{-E/RT} = kP\theta_0 A_1 \qquad \theta_1 = \frac{kPA_1}{N_m \nu_1 e^{-E/RT} + kPA_1}$$

$$\theta = \frac{N}{N_m} = \frac{K\ p}{1 + K\ p}$$

Linear plot

$$\frac{p}{N} = \frac{1}{KN_m} + \frac{p}{N_m}$$

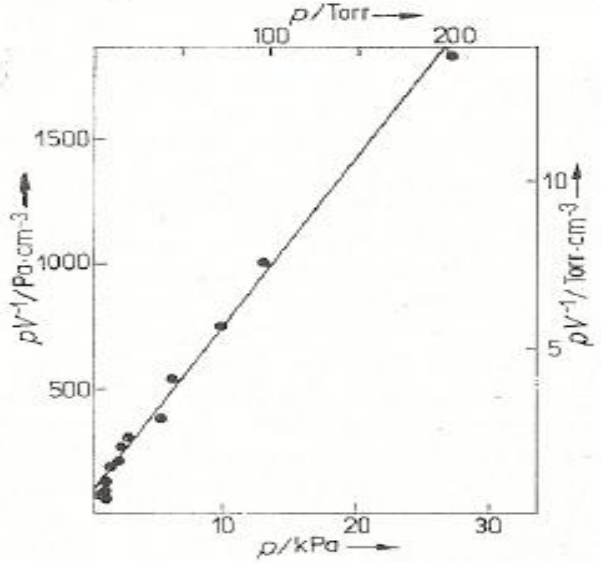

Abb. 6.47
Linearisierte Langmuirsche Adsorptionsisotherme für die Adsorption von Wasserstoff an Kupferpulver bei 25°C

$$n = \frac{N}{N_A} = \frac{m_m}{M_{asdorptive}}$$

$$S = N_m A_x = \frac{m_m N_A A_x}{M_{asdorptive}}$$

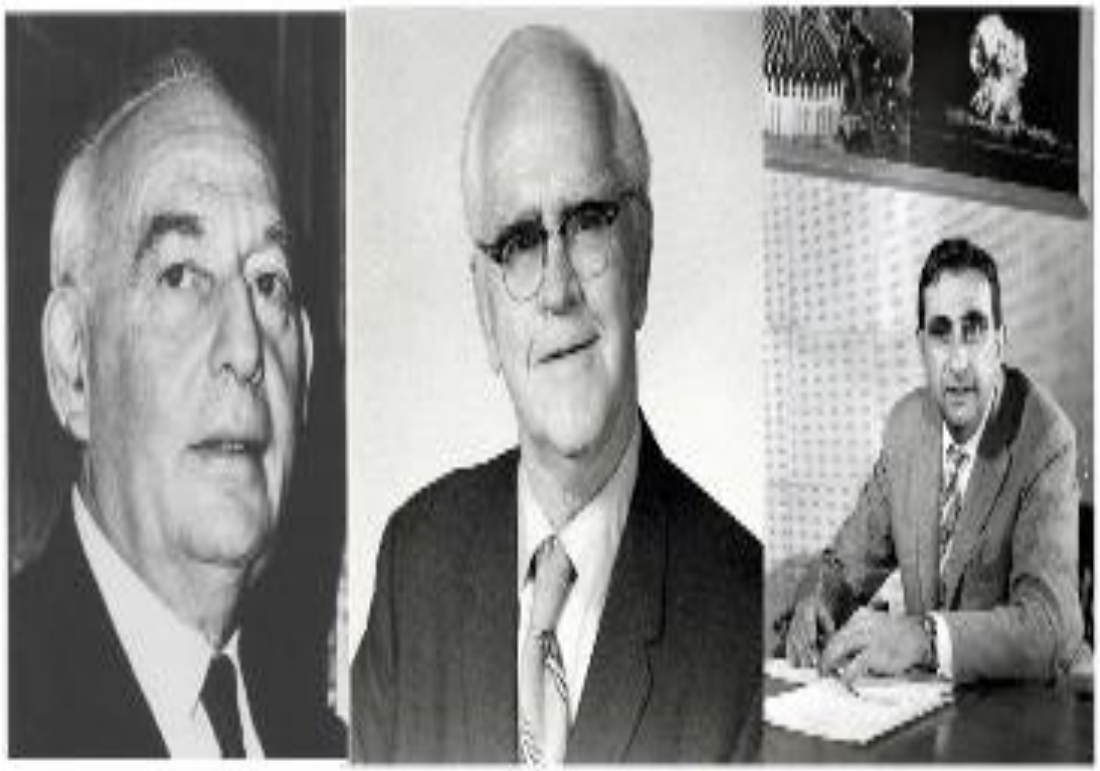

Named after Stephen Brunauer, P.H. Emmet and Edward Teller

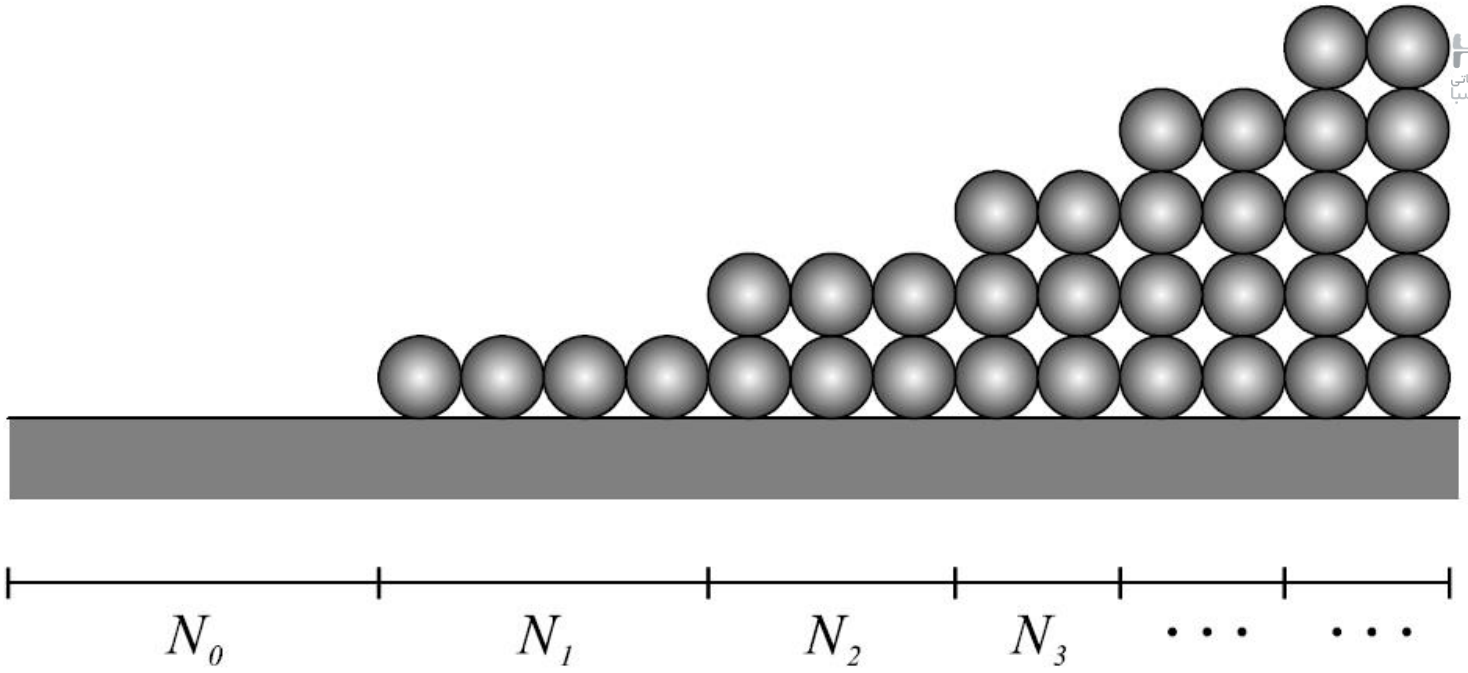

$$a_1 p N_0 + b_2 N_2 \exp\left(\frac{-E_2}{RT}\right) = a_2 p N_1 + b_1 N_1 \left(\frac{-E_1}{RT}\right)$$

$$N_i = \frac{a_i}{b_i} p N_{i-1} \exp\left(-\frac{E_i}{RT}\right)$$

$$N_i = \frac{a_1}{b_1} g \exp\left(\frac{E_1 - E_L}{RT}\right) x^i N_0 = c x^i N_0$$

$$\frac{V_a}{V_m} = \frac{c N_0 \sum_{i=1}^{\infty} i x^i}{N_0 + c N_0 \sum_{i=1}^{\infty} x^i}$$

$$\frac{V_a}{V_m} = \frac{cx}{(1-x)(1-x+cx)}$$

$$V_a = \frac{V_m c p}{(p_0 - p)\left\{1 + (c-1)\left(\frac{p}{p_0}\right)\right\}}$$

$$\frac{1}{W\left[p/p_0 - 1\right]} = \frac{1}{W_m C} + \frac{C-1}{W_m C}\left(\frac{p}{p_0}\right)$$

W ... mass of adsorbed N_2

Relative pressures near completed monolayers

$0.05 < p/p_0 < 0.3$

$$W_m = \frac{1}{s+i}$$

$$C = \frac{s}{i} + 1$$

$$S = \frac{W_m N_A A_x}{M_{adsorptive}}$$

$$S_{sp.} = \frac{S}{m}$$

$$s = \frac{C-1}{W_m C}$$

$$i = \frac{1}{W_m C}$$

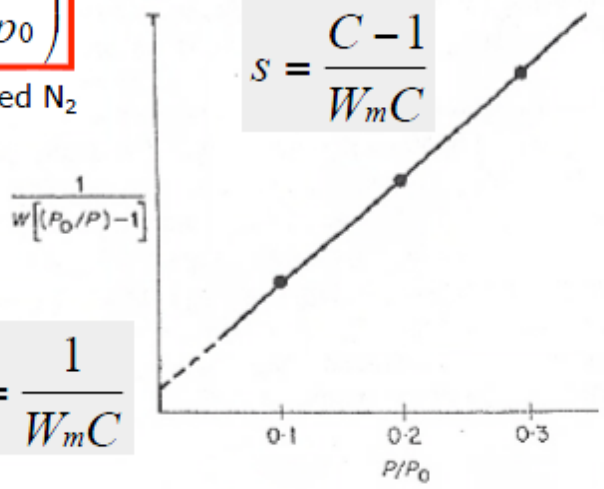

Single point BET

Assumption: For high values of C the intercept may be taken as zero

$$W_m = W\left(1 - \frac{p}{p_0}\right)$$

$$S = W\left(1 - \frac{p}{p_0}\right)\frac{N_A}{M_{adsorptive}} A_x$$

$$S_t = \frac{W_m \overline{N} A_x}{\overline{M}} \times 10^{-20}\, m^2$$

$$V_p = V/22414 \times M_g/\rho_a$$

$$d_p = \frac{4 \times V_p}{a_{S,BET}} \times 10^3$$

$$l = \frac{6}{\rho_S \times a_{S,BET}} \times 10^3$$

مقادیر ثابت c

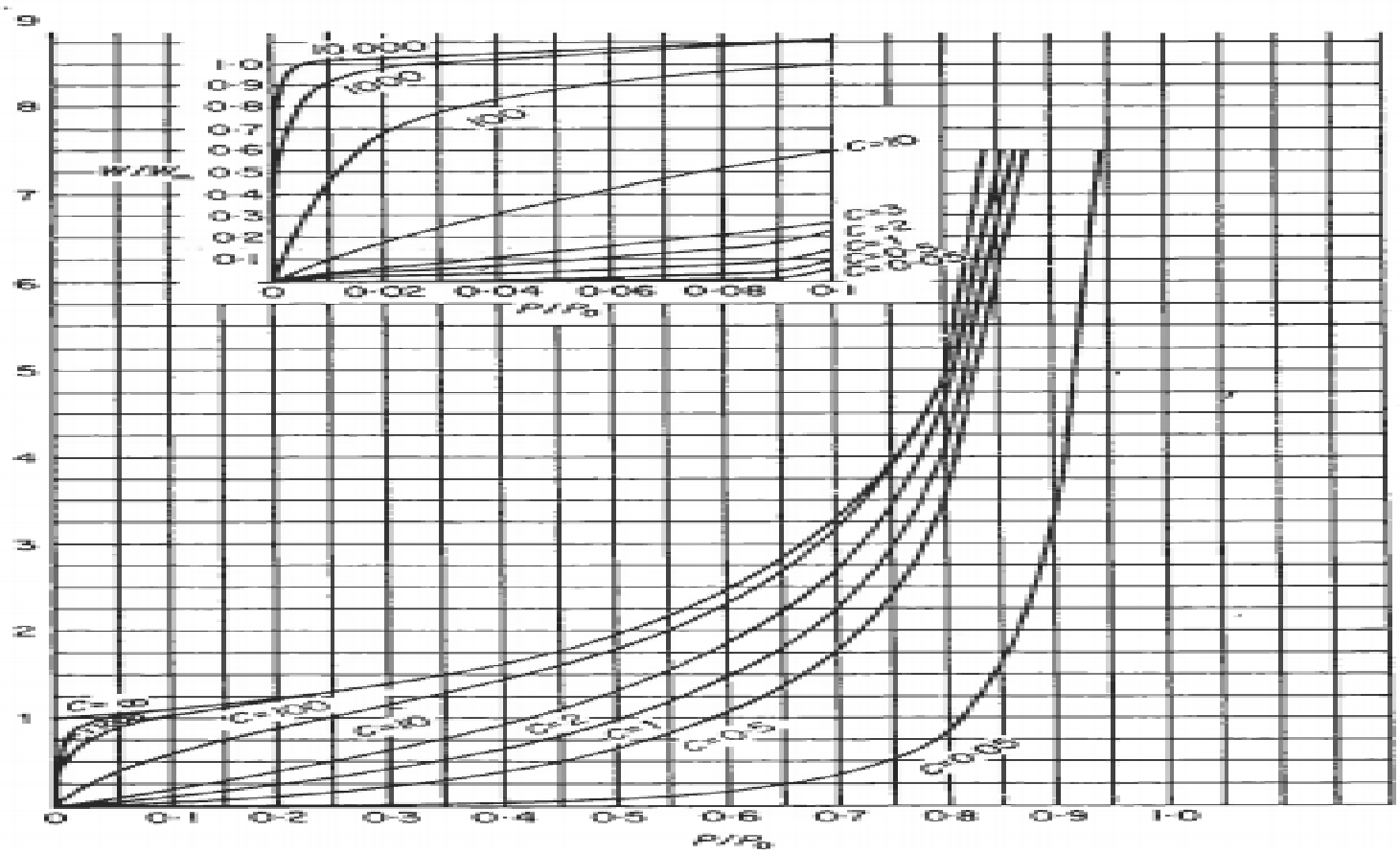

$$(\theta_i)_m = C\left(\frac{\sqrt{C}-1}{C-1}\right)^{i+1}$$

$$\left(\frac{P}{P_0}\right)_m = \frac{\sqrt{100}-1}{100-1} = 0.0909$$

$$(\theta_0)_m = \frac{\sqrt{C}-1}{C-1}$$

$$W_m = W_{0.3}(3.33-1)\left|\frac{1}{100}+\frac{100-1}{100}(0.3)\right| = 0.715W_{0.3}$$

3. Insert a funnel to the sample cell, and feed a sample through the funnel. Dry the sample before you use it. The sample should be around 0.2 g.

4. Remove the funnel with careful attention not to let the sample adhere to the inner wall of the sample cell, install the sample cell cap again, and measure the weight (sample + sample cell + sample cell cap) [2].

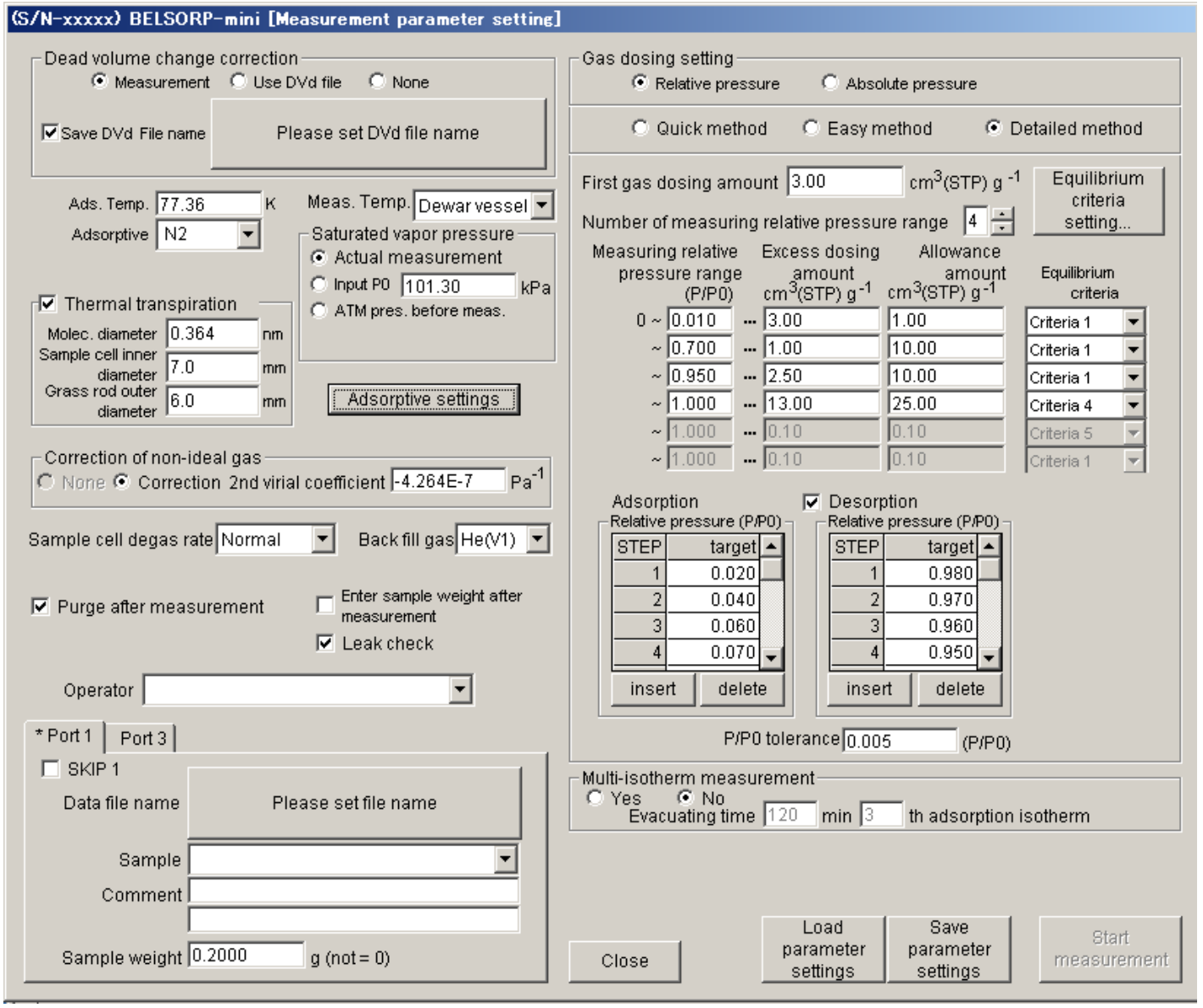
(S/N-xxxxx) BELSORP-mini [Measurement parameter setting]
Dead volume change correction
Measurement
Use DVd file
None
Save DVd File name
Please set DVd file name
Ads. Temp. 77.36 K
Meas. Temp. Dewar vessel
Adsorptive N2
Saturated vapor pressure
Actual measurement
Input P0 101.30 kPa
ATM pres. before meas.
Thermal transpiration
Molec. diameter 0.364 nm
Sample cell inner diameter 7.0 mm
Grass rod outer diameter 6.0 mm
Adsorptive settings
Correction of non-ideal gas
None
Correction 2nd virial coefficient -4.264E-7 Pa-1
Sample cell degas rate Normal
Back fill gas He(V1)
Purge after measurement
Enter sample weight after measurement
Leak check
Operator
* Port 1
Port 3
SKIP 1
Data file name
Please set file name
Sample
Comment
Sample weight 0.2000 g (not = 0)
Gas dosing setting
Relative pressure
Absolute pressure
Quick method
Easy method
Detailed method
First gas dosing amount 3.00 cm3(STP) g-1
Equilibrium criteria setting...
Number of measuring relative pressure range 4
Measuring relative pressure range (P/P0)
Excess dosing amount cm3(STP) g-1
Allowance amount cm3(STP) g-1
Equilibrium criteria
0 ~ 0.010 ... 3.00 1.00 Criteria 1
~ 0.700 ... 1.00 10.00 Criteria 1
~ 0.950 ... 2.50 10.00 Criteria 1
~ 1.000 ... 13.00 25.00 Criteria 4
~ 1.000 ... 0.10 0.10 Criteria 5
~ 1.000 ... 0.10 0.10 Criteria 1
Adsorption
Relative pressure (P/P0)
STEP target
1 0.020
2 0.040
3 0.060
4 0.070
insert
delete
Desorption
Relative pressure (P/P0)
STEP target
1 0.980
2 0.970
3 0.960
4 0.950
insert
delete
P/P0 tolerance 0.005 (P/P0)
Multi-isotherm measurement
Yes
No
Evacuating time 120 min 3 th adsorption isotherm
Close
Load parameter settings
Save parameter settings
Start measurement


BEL
BEL JAPAN, INC.
Belsorp

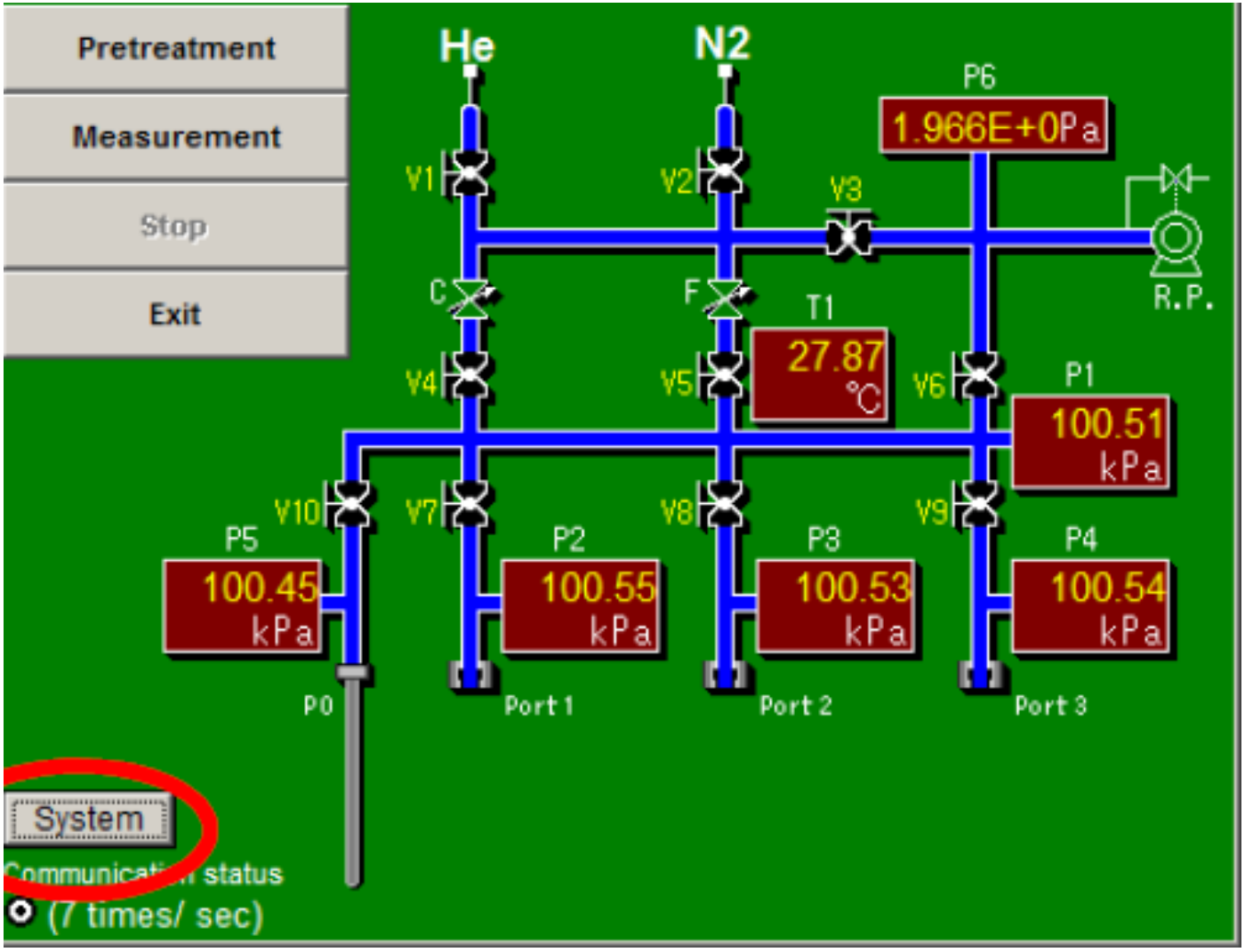
Pretreatment
Measurement
Stop
Exit
He
N2
P6
1.966E+0Pa
V1
V2
V3
C
F
T1
27.87
°C
R.P.
V4
V5
V6
P1
100.51
kPa
V10
V7
V8
V9
P5
100.45
kPa
P2
100.55
kPa
P3
100.53
kPa
P4
100.54
kPa
P0
Port 1
Port 2
Port 3
System
status
(7 times/ sec)

$$V1 = \frac{(P1_i(n) - P1_e(n)) \times Vs \times 273.15}{101.30 \cdot Ws \cdot T}$$

Ws is the mass of adsorbent, and T means the absolute tempe
before adsorption can be calculated using $P2_e(n\text{-}1)$ (the equilit

$$V2 = \frac{P2_e(n-1) \times Vd \times 273.15}{101.30 \cdot Ws \cdot T}$$

Furthermore, V3, amount of the gas that remains in Vd

$$V3 = \frac{P2_e(n) \times Vd \times 273.15}{101.30 \cdot Ws \cdot T}$$

The increased amount of adsorbed gas(ΔV) at n^{th} mea

$$\Delta V = V1 + V2 - V3$$

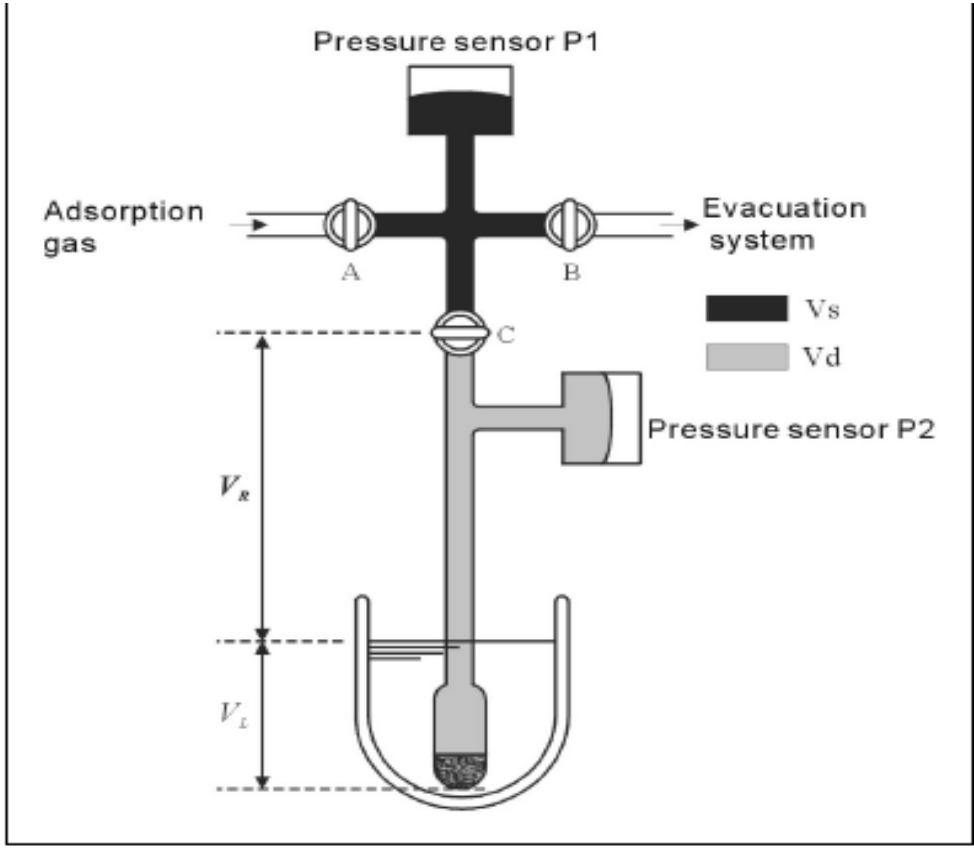

Analysis Specifications

Transducer Accuracy:	0.1% span (1000 torr transducer) each manifold/sample station 0.15% reading (1 torr transducer - KR/MP model) manifold
Pressure Resolution:	0.016 torr (1000 torr range) 0.000016 torr (1 torr range)
Ultimate Vacuum:	$<1 \times 10^{-2}$ torr achieved by dedicated 2 stage rotary, direct drive pump 1×10^{-9} torr achieved by turbo-molecular vacuum pump in QUADRASORB *SI* - KR/MP
Adsorbate:	Nitrogen or any other non-corrosive gas with appropriate coolant
Surface Area Range:	$0.01 m^2/g$ to no known upper limit (nitrogen) $0.0005 m^2/g$ to no known upper limit (krypton)KR/MP-model only
Minimum Pore Volume (liquid):	2×10^{-6} cc/g
(STP):	0.0001cc/g
Pore Size Range:	3.5 - 4000Å / 0.35 - 400 nm
Coolant Level:	Automatic compensation by RTD coolant level sensor
Minimum P/P_0 (N_2):	1×10^{-3} QUADRASORB *SI* 4×10^{-5} QUADRASORB *SI* -KR/MP

* Pressure transducer and vacuum pump specifications from their respective manufacturers.

مقایسه اندازه گیری Dead Volume

Dead volume ;

is the free space in the sample cell.

does not equal to the actual volume.
•It is the hypothetical value calculated assuming that whole system is kept at the same temperature at Vs to simplify the adsorption amount calculation.

is used for the adsorption amount calculation.

Dead volume evaluation is an important factor to obtain accurate adsorption isotherms.

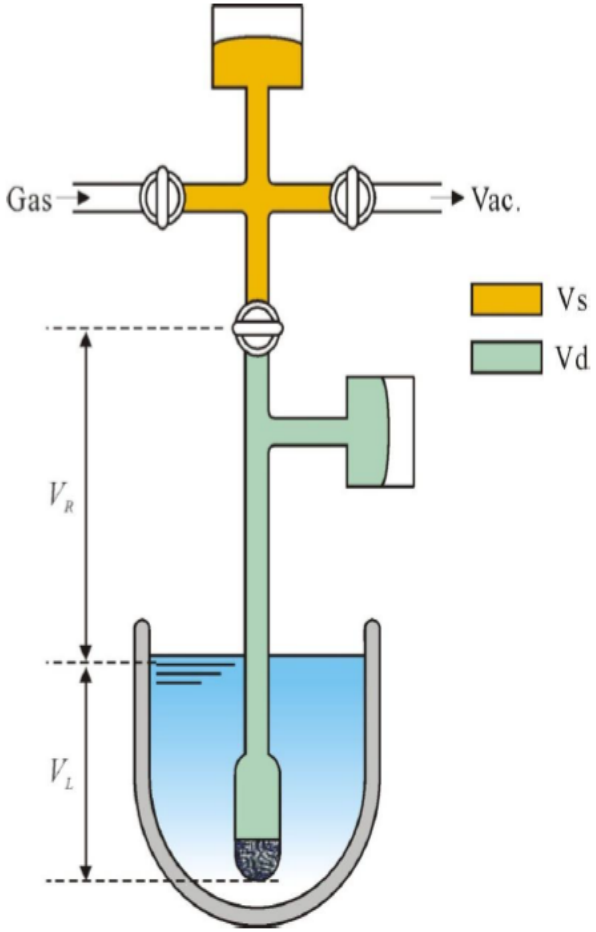

No	p_i /kPa	p_e /kPa	p_{e2} /kPa	p_0 /kPa	p/p_0	V_a/cm^3(STP) g^{-1}
ADS						
1	0	1.2084	0	88	0.013732	19.837
2	0	8.7916	0	88	0.099905	25.905
3	0	13.546	0	88	0.1539	27.811
4	0	18.22	0	88	0.207	28.965
5	0	22.722	0	88	0.2582	29.612
6	0	27.202	0	88	0.3091	30.142
7	0	31.668	0	88	0.3599	30.519
8	0	35.941	0	88	0.4084	30.639
9	0	40.329	0	88	0.4583	30.759
10	0	44.663	0	88	0.5075	30.896

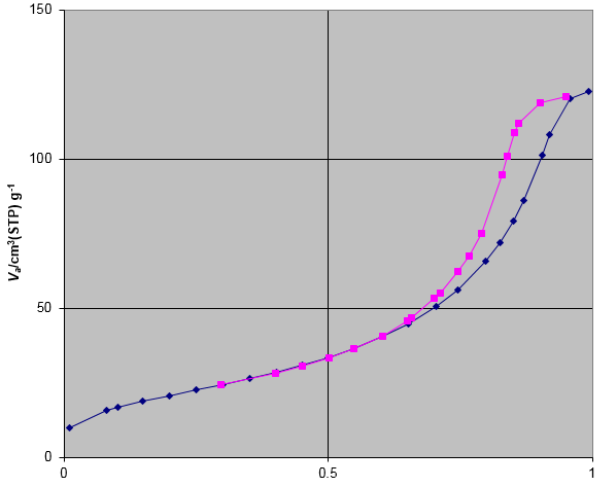

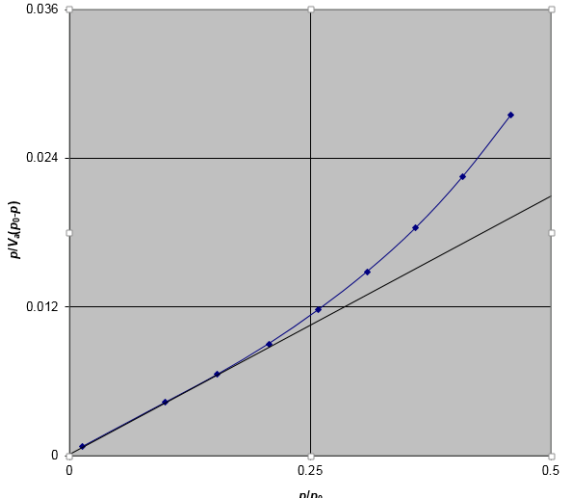

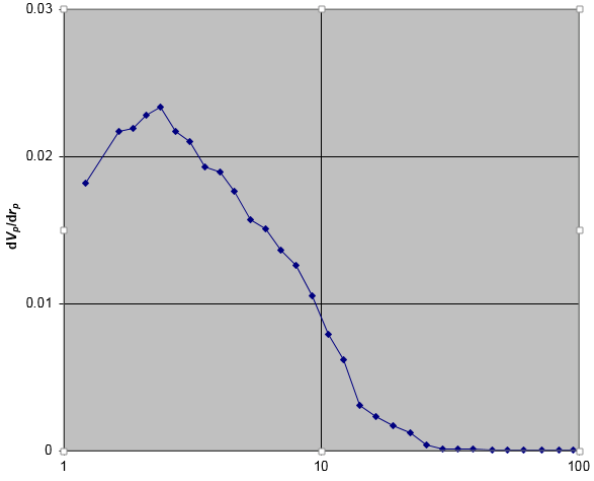

مقایسه اندازه گیری Dead Volume

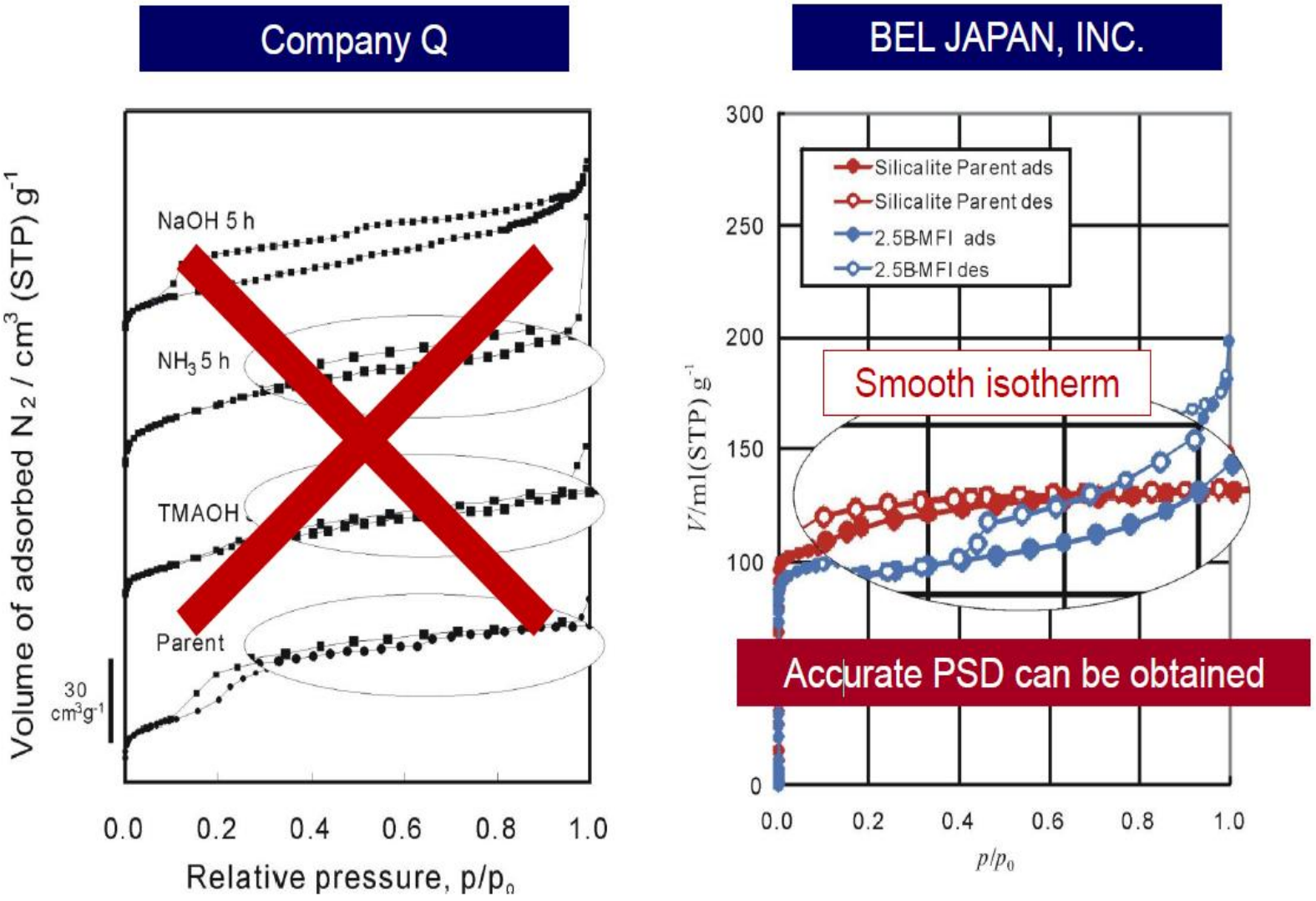

مقایسه اندازه گیری Dead Volume

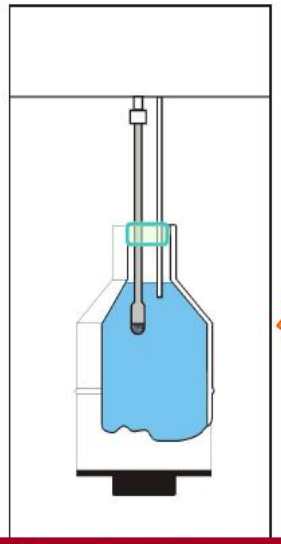

The Dewar moves up **discontinuously.**

Vd changes discontinuously.

Of course, not good for accurate measurements

Dead volume change

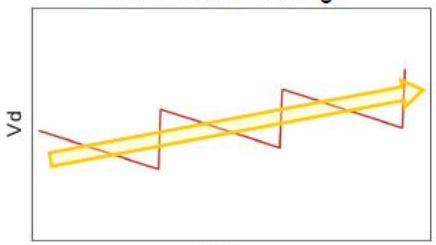

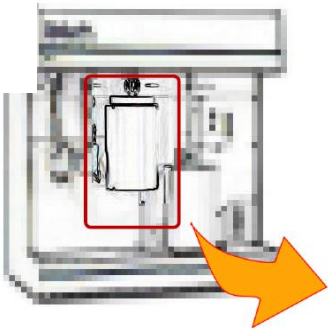

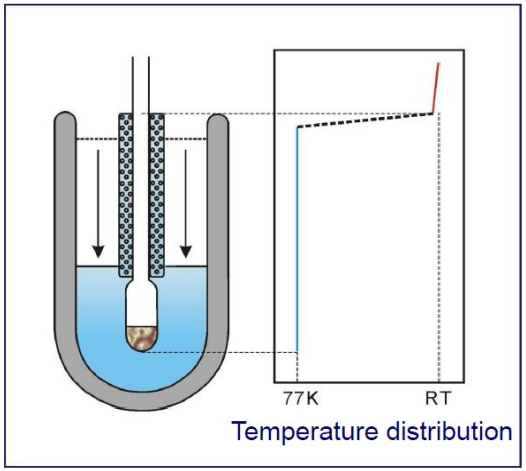

Temperature distribution

Company M insists that the isothermal jacket can keep the temperature distribution.

But...

Can such a tube keep the temperature condition?
Do you believe that?

مقایسه اندازه گیری Dead Volume

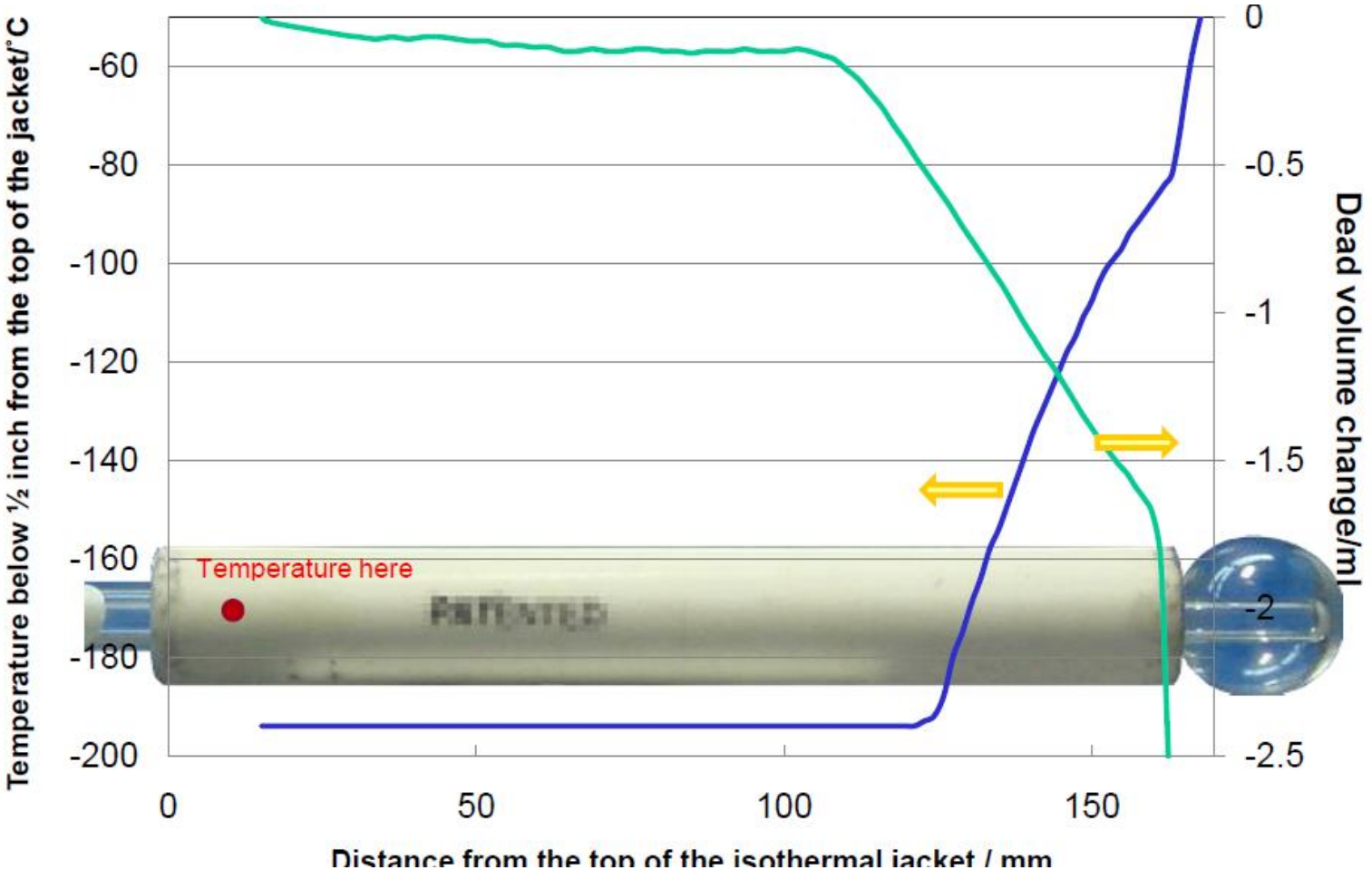

مقایسه اندازه گیری Dead Volume

AFSM

Advanced Free Space Measurement

- A dVd cell which has the same inner diameter as that of sample cell was adopted for measuring free space (Vd) change in the sample cell.

- Prior to the adsorption measurement, a certain pressure of gas is dosed to the dVd cell. During the adsorption measurement, the Vd change in sample cell can be corrected continuously from the pressure change in dVd cell.

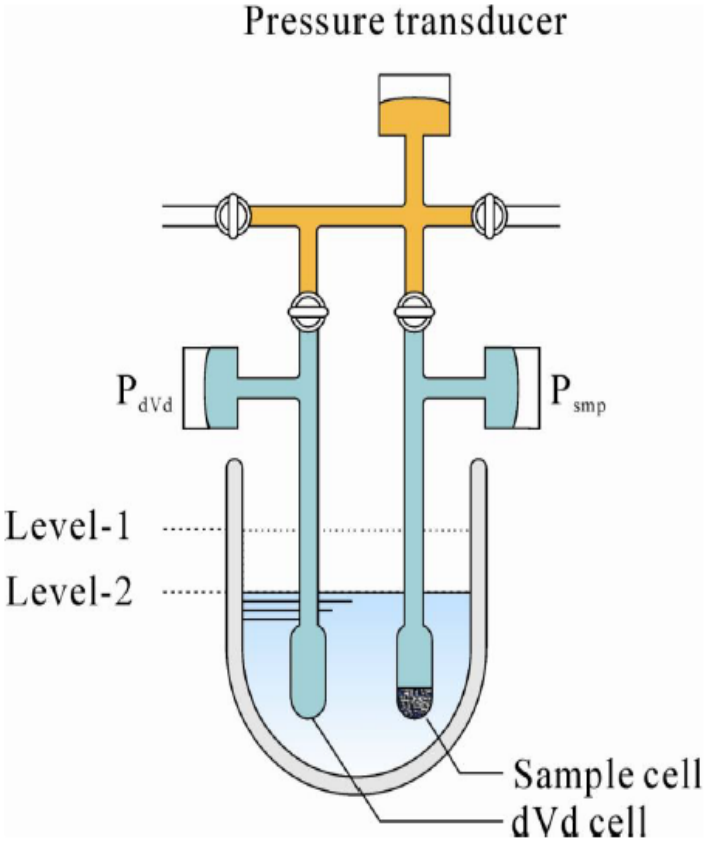

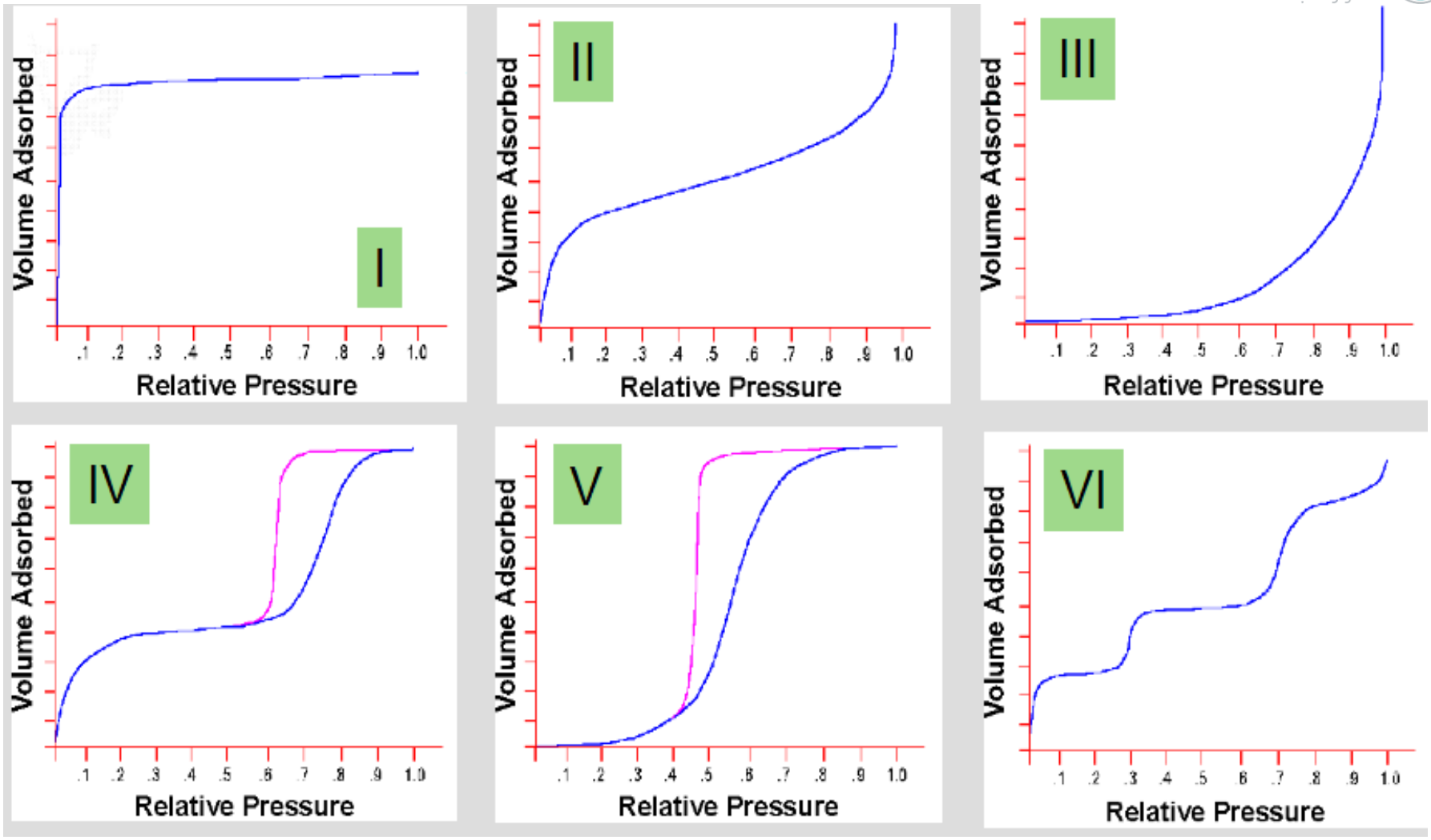
I
Volume Adsorbed
Relative Pressure
.1 .2 .3 .4 .5 .6 .7 .8 .9 1.0
II
Volume Adsorbed
Relative Pressure
.1 .2 .3 .4 .5 .6 .7 .8 .9 1.0
III
Volume Adsorbed
Relative Pressure
.1 .2 .3 .4 .5 .6 .7 .8 .9 1.0
IV
Volume Adsorbed
Relative Pressure
.1 .2 .3 .4 .5 .6 .7 .8 .9 1.0
V
Volume Adsorbed
Relative Pressure
.1 .2 .3 .4 .5 .6 .7 .8 .9 1.0
VI
Volume Adsorbed
Relative Pressure
.1 .2 .3 .4 .5 .6 .7 .8 .9 1.0

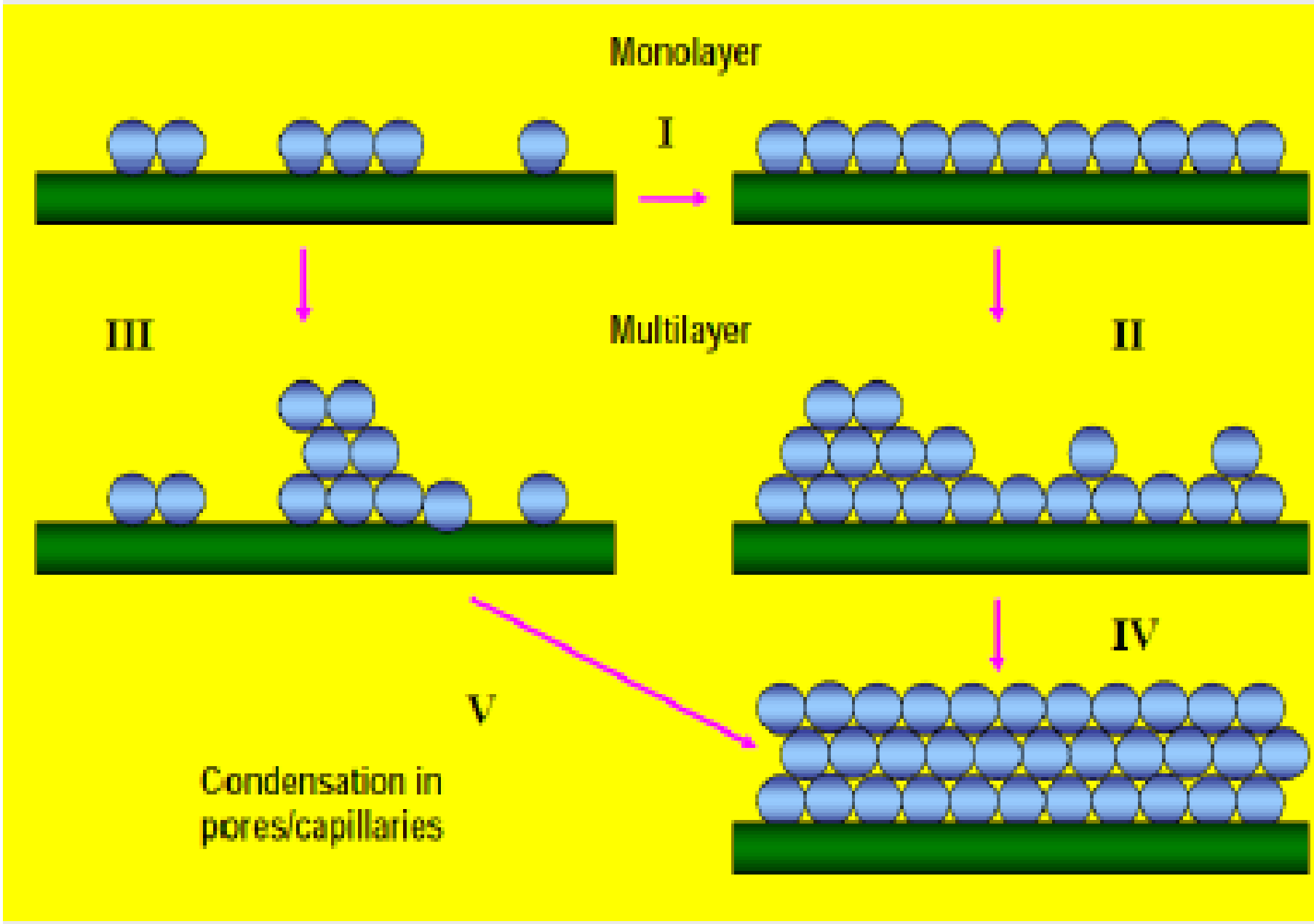
Monolayer
I
III
Multilayer
II
IV
V
Condensation in
pores/capillaries

ایزوترم نوع یک

Pores are typically microporus with the exposed surface residing almost exclusively inside the microspores, which once filled with adsorbate, leave little or no external surface for further adsorption.

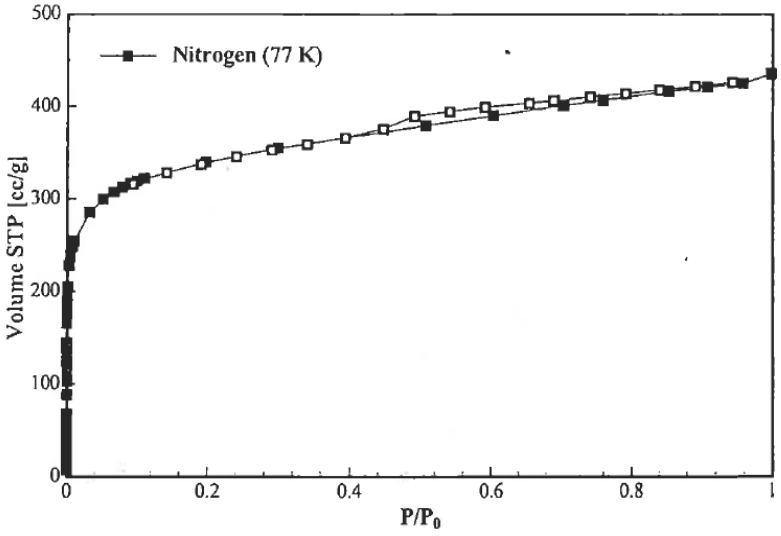

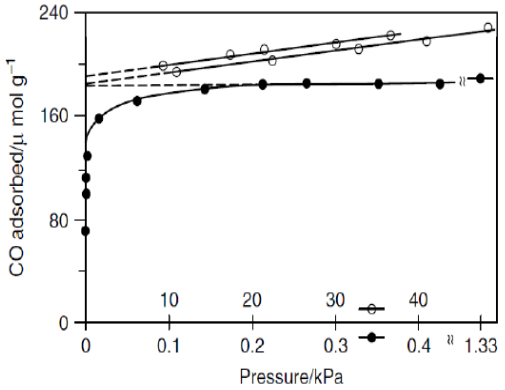

Fig. 4 Isotherms for the adsorption of CO on EUROPT-1 Pt/SiO_2 catalyst at room temperature from different laboratories for a pressure range 0–1.33 kPa (solid circles) and 10–50 kPa (open circles). (Adapted from Ref. [14].)

Linear extrapolation to p = 0 yields the volume of an adsorbed monolayer v_m

پهنای کم حفره وپتانسیل جذب بالا حجم میکرو حفره قابل دسترس میکرو حفره

IUPAC :

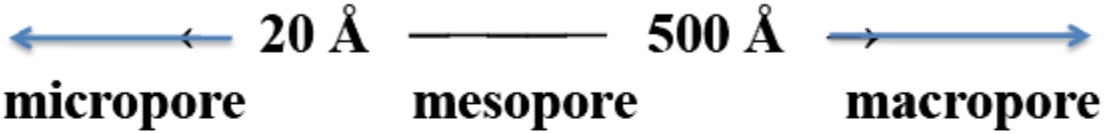

Langmuir eq. (Type I isotherm) can describe the adsorption on microporous materials, but may be only a correct mathematical description.

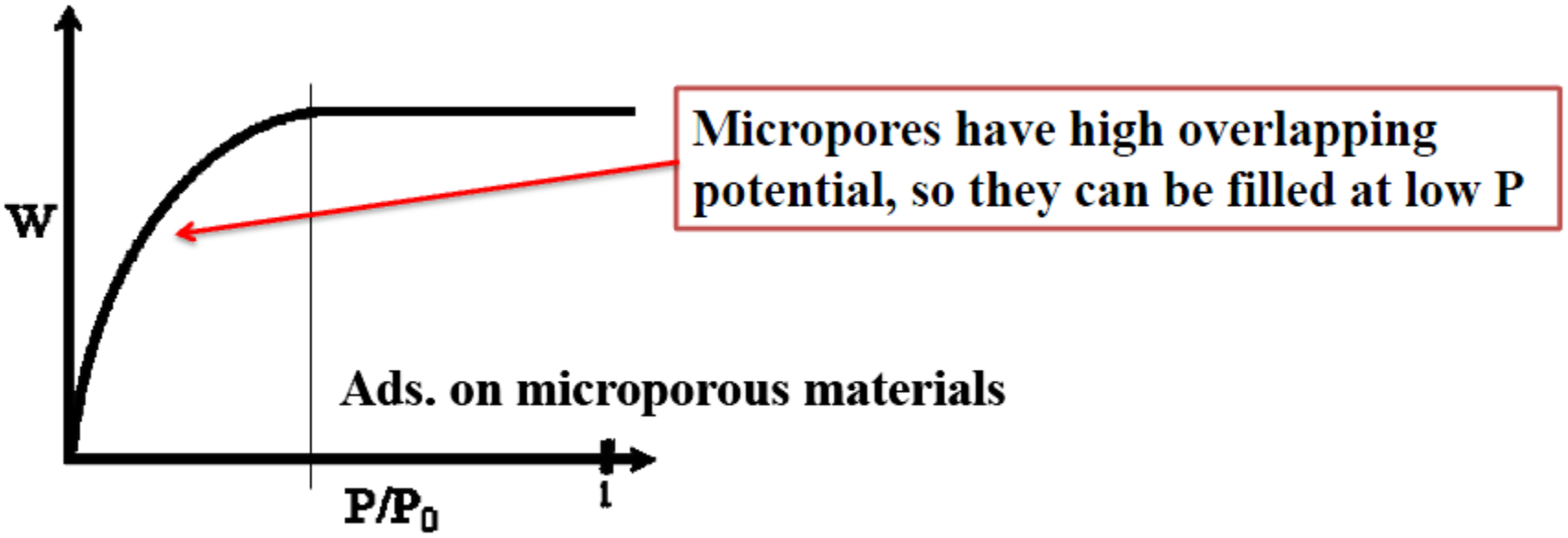

نوع اول

- ایزوترم نوع اول برگشت پذیر در برابر محور افقی مقعر است و میزان جذب‌شده به یک مقدار محدودکننده به عدد1 میل می‌کند. ایزوترم های نوع اول زمانی به دست می‌آیند که جذب، در بیشتر موارد، تنها به تعداد کمی از لایه‌های ملکولی محدود می‌شود. این شرایط در جذب شیمیایی باعث می‌شود که رویکرد مجانبی به یک مقدار محدود کننده نشان می‌دهد که تمام مناطق سطحی اشغال شده‌اند. در مورد جذب فیزیکی، ایزوترم های دفع حاصل شده بر مواد میکروحفره اغلب از نوع اول هستند. پر کننده میکروحفره و بنابرین جذب‌های بالا، به دلیل پهنای کم حفره و پتانسیل جذب بالا دردماهای نسبتاً پایین مشاهده می‌شوند. جذب محدود کننده با حجم میکروحفره قابل دسترسی بیش از ناحیه سطحی داخلی هدایت می‌شود

نوع دوم

- معمولادر مورد جاذب غیرمتخلخل یا حفره بزرگ به دست می‌آیند که جذب تک لایه ای-چند لایه‌ای نامحدود در آن‌ها صورت می‌گیرد. نقطه شکست یا زانوی ایزوترم نقطه B نام دارد. این نقطه مرحله‌ای را نشان می‌دهد که در آن پوشش تک لایه‌ای کامل است و جذب چندلایه‌ای شروع به وقوع می‌کند

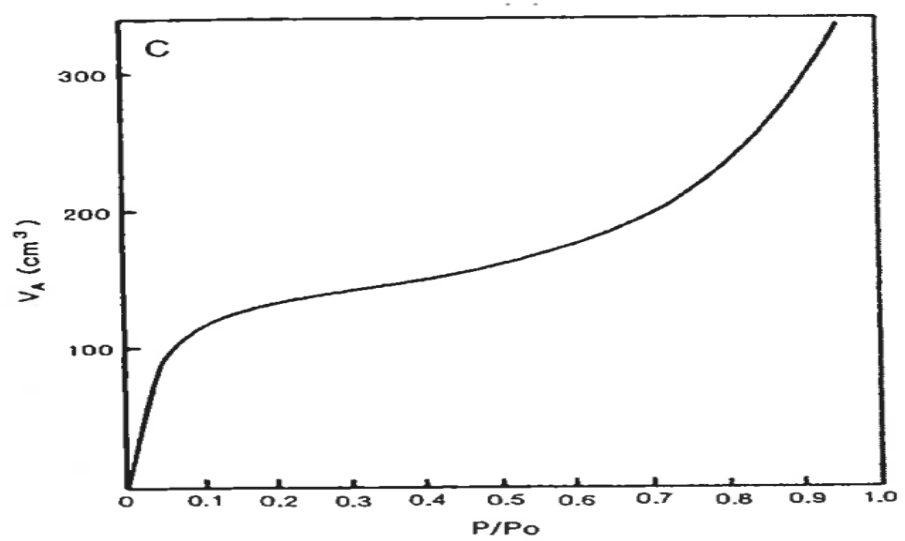

ایزوترم نوع سوم

Characterised by heats of adsorption less than the adsorbate heat of liquification, adsorption proceeds as the adsorbate interaction with an adsorbed layer is greater than the interaction with the adsorbent surface

بر هم کنش بسیار ضعیف جامد و گاز نمونه جذب گاز هیدروژن بر پلی اتیلن

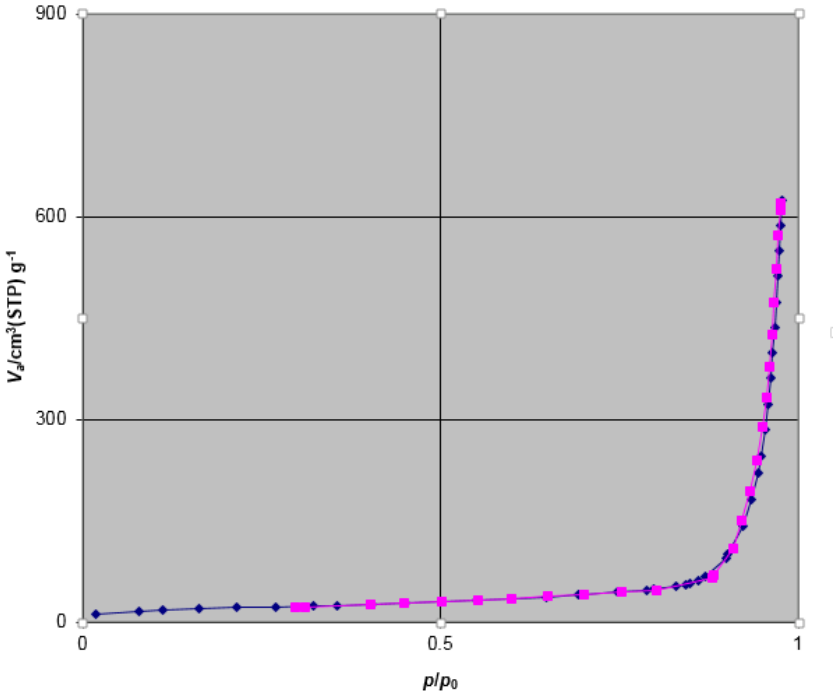

نوع سوم

- این منحنی ها در ایزوترم دفع،برگشت پذیر در برابر محور افقی در کل دامنه‌اش محدب است و بنابرین یک نقطه B را به نمایش نمی‌گذارد. این نشان می‌دهد که واکنش جذب شونده-جذب کننده نسبتاً ضعیف هستند و واکنش‌های جذب شونده-جاذب نقش مهمی دارند. ایزوترم های این نوع مشترک نیستند ولی یک نمونه جذب نیتروژن بر پلی اتیلن یا جذب بخار آب بر صفحه بازال تمیز گرافیت است

بر هم کنش بسیار ضعیف جامد و گاز
نمونه جذب گاز هیدروژن بر پلی اتیلن

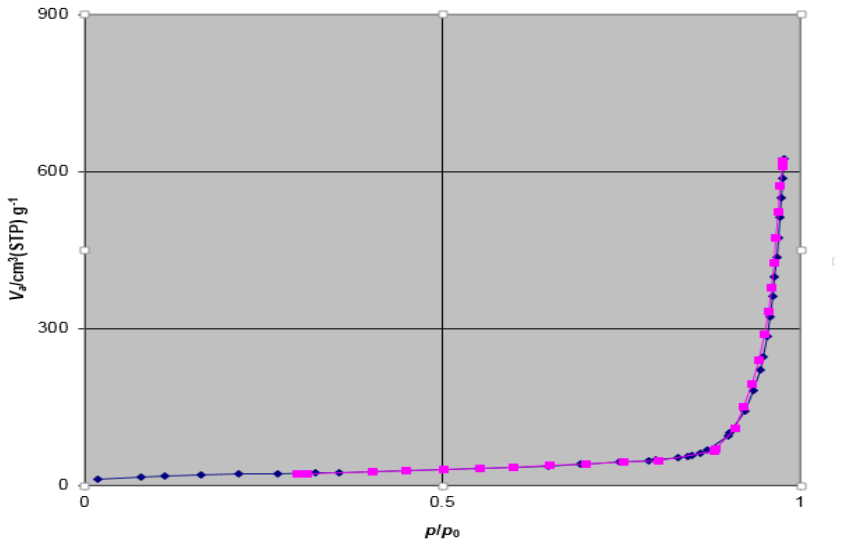

نوع چهارم

- ایزوترمهای که در این نوع رخ می‌دهد نشان می‌دهد که جذب سطحی در حفره‌هایی که در حد مزو یا حفره‌هایی در حد متوسط بین 1.5-100 نانومتر صورت می‌گیرد شیب تند در فشارهای بالا نشان می‌دهد که افزایش فشار باعث پر شدن حفره‌هامی‌شود این در حد تک لایه‌ها در فشار بالاتری رخ می‌دهد

تغلیظ حفره بخاطر پسماند

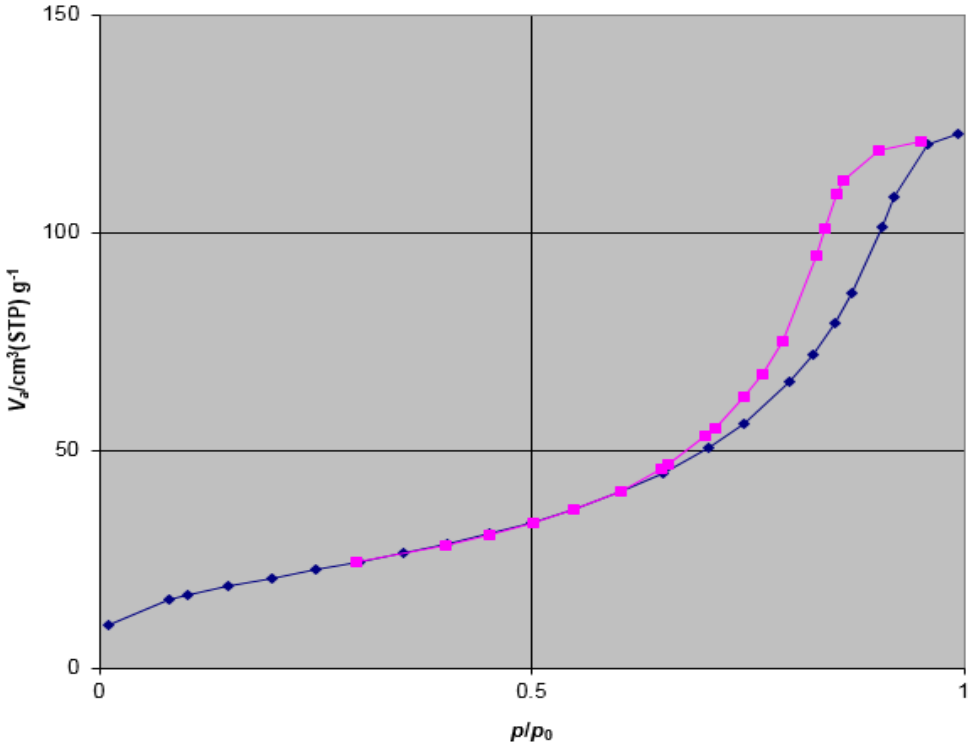

نوع پنجم

- برای مواد مزوحفره (حفره متوسط) معمول هستند.مشخص‌ترین ویژگی ایزوترم نوع پنجم چرخه پسماند است که با وقوع تغلیظ حفره همراه است. جذب محدود کننده در دامنه‌ای از نتایج بالا به صفحه‌ای از ایزوترم منجر می شودکه پر شدن حفره کامل را نشان می‌دهد. بخش ابتدایی نوع پنجم را می‌توان همانند مورد ایزوترم نوع دوم به جذب تک لایه‌ای- چند لایه‌ای نسبت داد.ایزوترم های نوع پنجم تغلیظ و پسماند حفره را نشان می‌دهند. هرچند، بر خلاف نوع چهارم و بخش اول این این دفع، ایزوترم با ایزوترم های جذب نوع سوم در ارتباط است که این از واکنش‌های جذاب نسبتاً ضعیف بین جاذب و جذب شونده حکایت دارد.

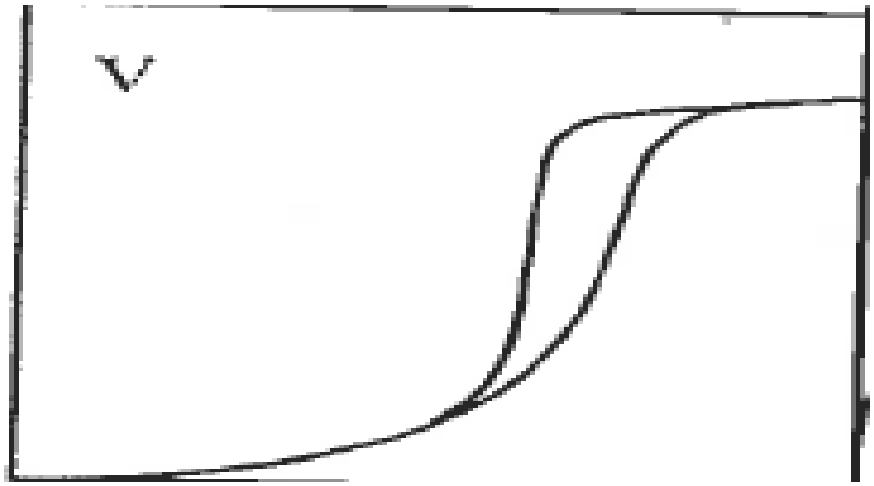

نسبتا ضعیف بین
جاذب و جذب شونده

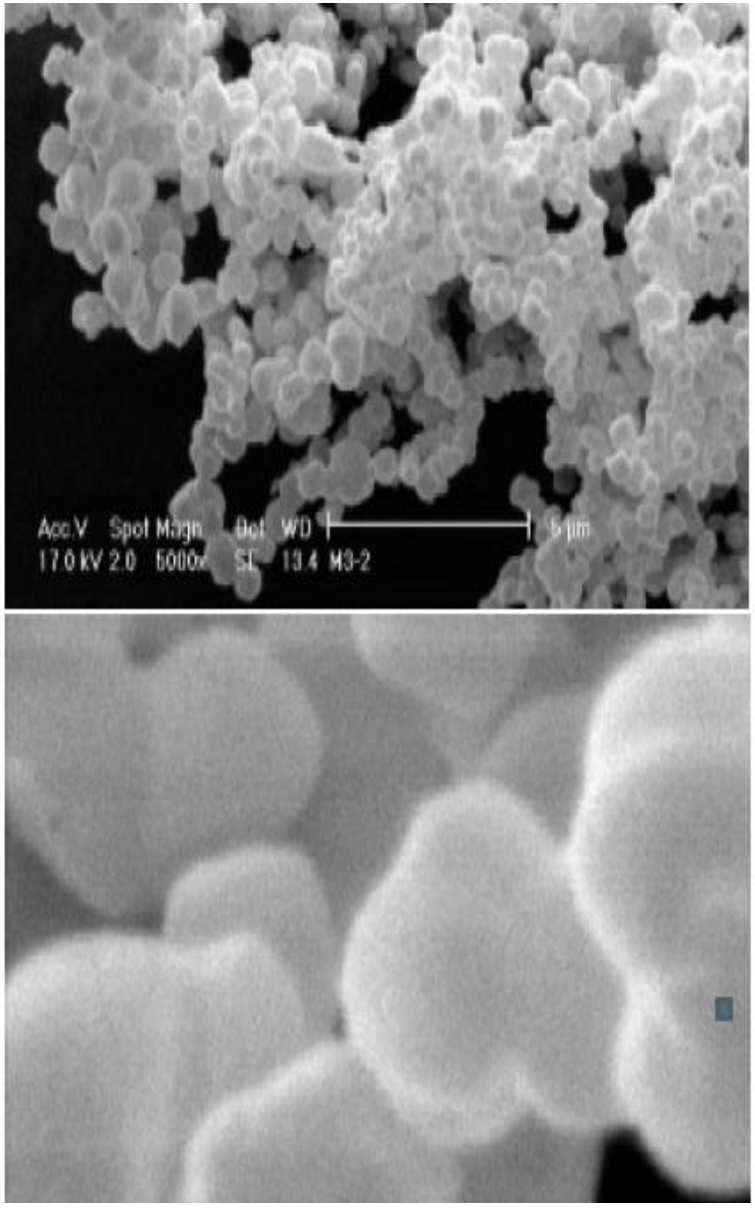

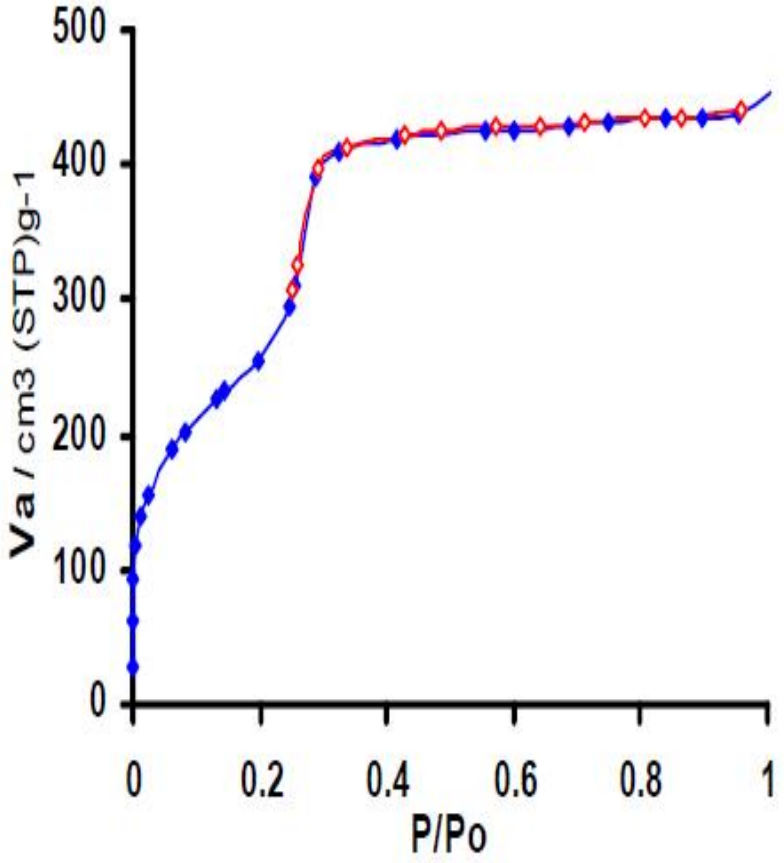

Fig. 3. Nitrogen isotherm of the calcined MCM-41 sapmle

نوع ششم

- یک مورد خاص است که جذب چند لایه‌ای گام به گام را بر یک سطح یکنواخت، غیرمتخلخل به خصوص با جذب کننده‌های متقارن کروی و غیرقطبی نشان می‌دهد. سختی مراحل به همگن بودن سطح جاذب، جذب کننده و دما بستگی دارد. ایزوترم های نوع ششم برای مثال با آرگون و کریپتون بر کربن‌های گرافیتی شده در دمای نیتروژن مایع به دست آمدند.

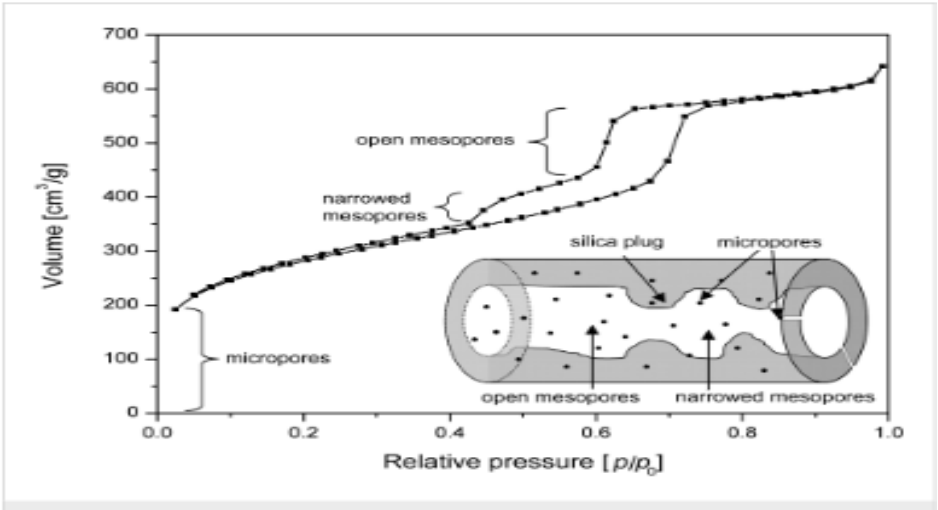

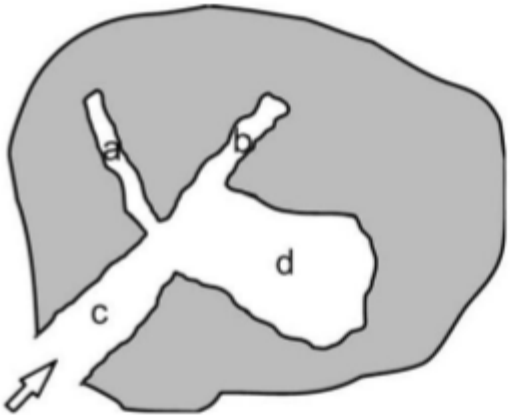

During desorption, the smaller pores a and b will empty at their corresponding pressure, being lower than that needed for emptying of pore c. How ever, pore d can only empty via pore c and accordingly will empty at lower pressure.

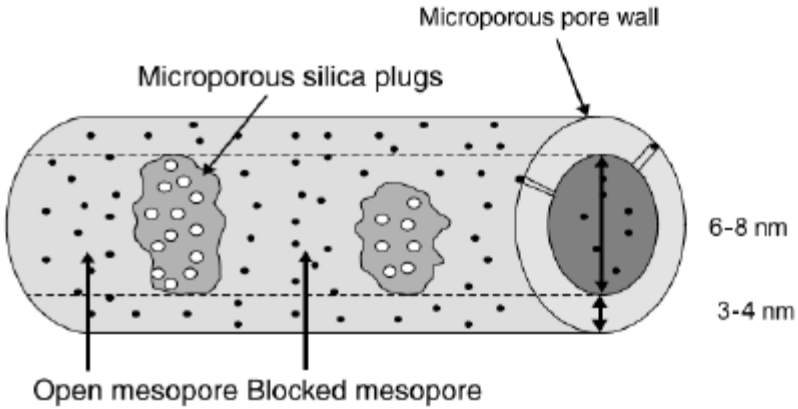

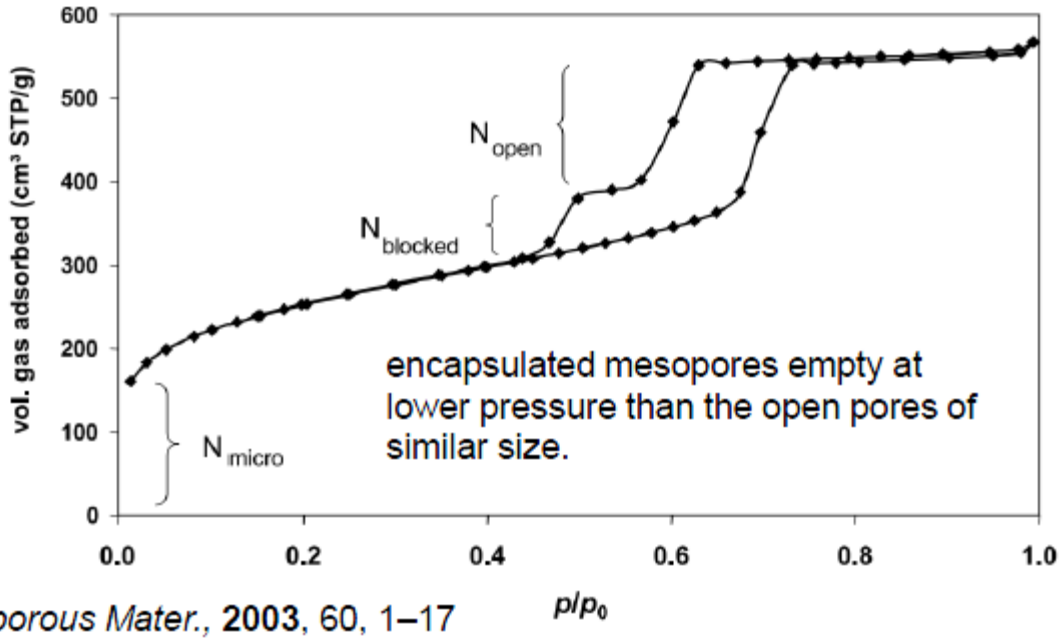

J.C. Groen et al., *Microporous and Mesoporous Mater.*, **2003**, 60, 1–17

Type	Features		Sample – Adsorptive example
	Interaction between sample surface and adsorbate	Porosity	
I	Relatively strong	Micropores	Activated carbon - Nitrogen
II	Relatively strong	Nonporous	Oxide - Nitrogen
III	Weak	Nonporous	Carbon – Water vapor
IV	Relatively strong	Mesopore	Silica – Nitrogen
V	Weak	Mesopore	
		Micropore	Activated carbon – Water vapor
VI	Relatively strong Sample surface has an even distribution of energy	Nonporous	Graphite - Krypton

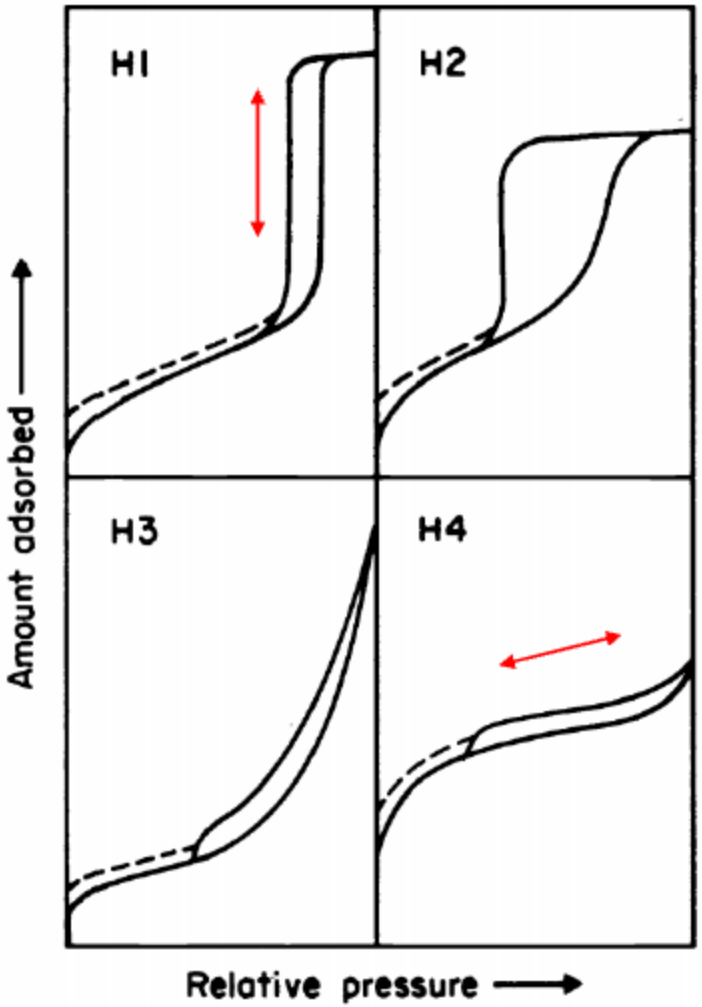

Steepness of the isotherms decreases from H1 to H4.

The hysteresis is usually attributed to the thermodynamic or network effects or the combination of these two effects.

H1: agglomerates or spherical particles arranged in a fairly uniform way, cylindrical pore geometry, indicating relatively high pore size uniformity and facile pore connectivity

H2: pores with narrow mouths (ink-bottle pores), relatively uniform channel-like pores, pore network (connectivity) effects

H3: aggregates (loose assemblages) of platelike particles forming slit-like pores

H4: narrow slit-like pores, particles with internal voids of irregular shape and broad size distribution, hollow spheres with walls composed of ordered mesoporous silica

Sing et.al, *Pure & Appl. Chem.*, **1985**, 57, 603-619

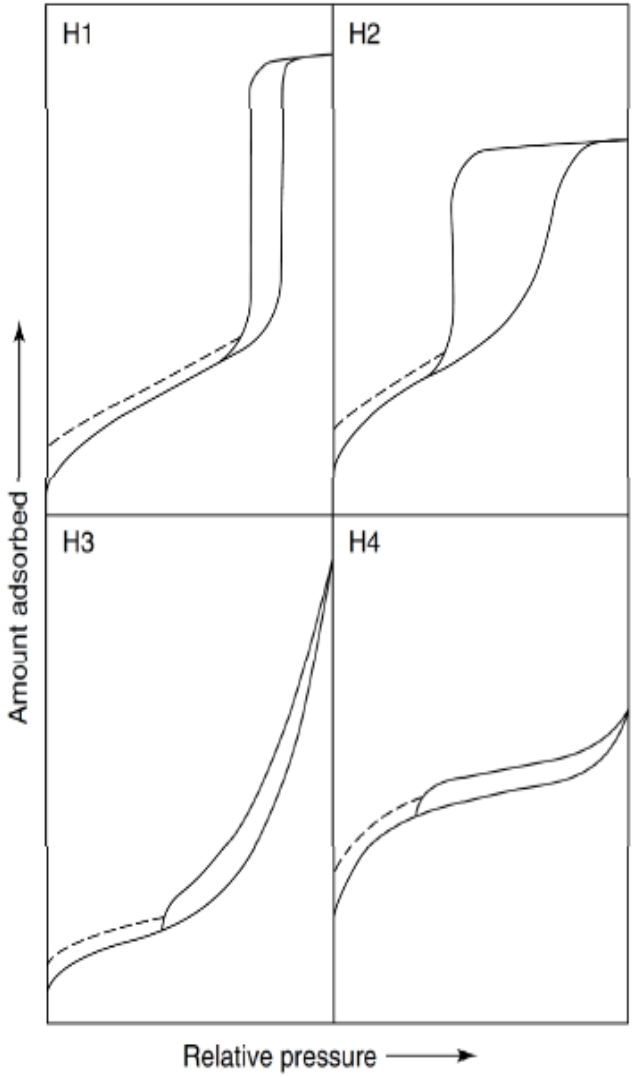

H1: narrow distribution of relatively uniform (cylindrical-like) pores
-delayed condensation and no network effects, analysis of the desorption branch

یکنواخت ضعیف

H2: complex pore structure, network effects are important, analysis of the adsorption branch

کمپلکس تاثیر شبکه مهم

H3: non-rigid aggregates of plate-like particles or assemblages of slit-shaped pores
- no saturation

منعطف – شیار باریک و ورقه ای

H4: complex materials containing both micropores and mesopores

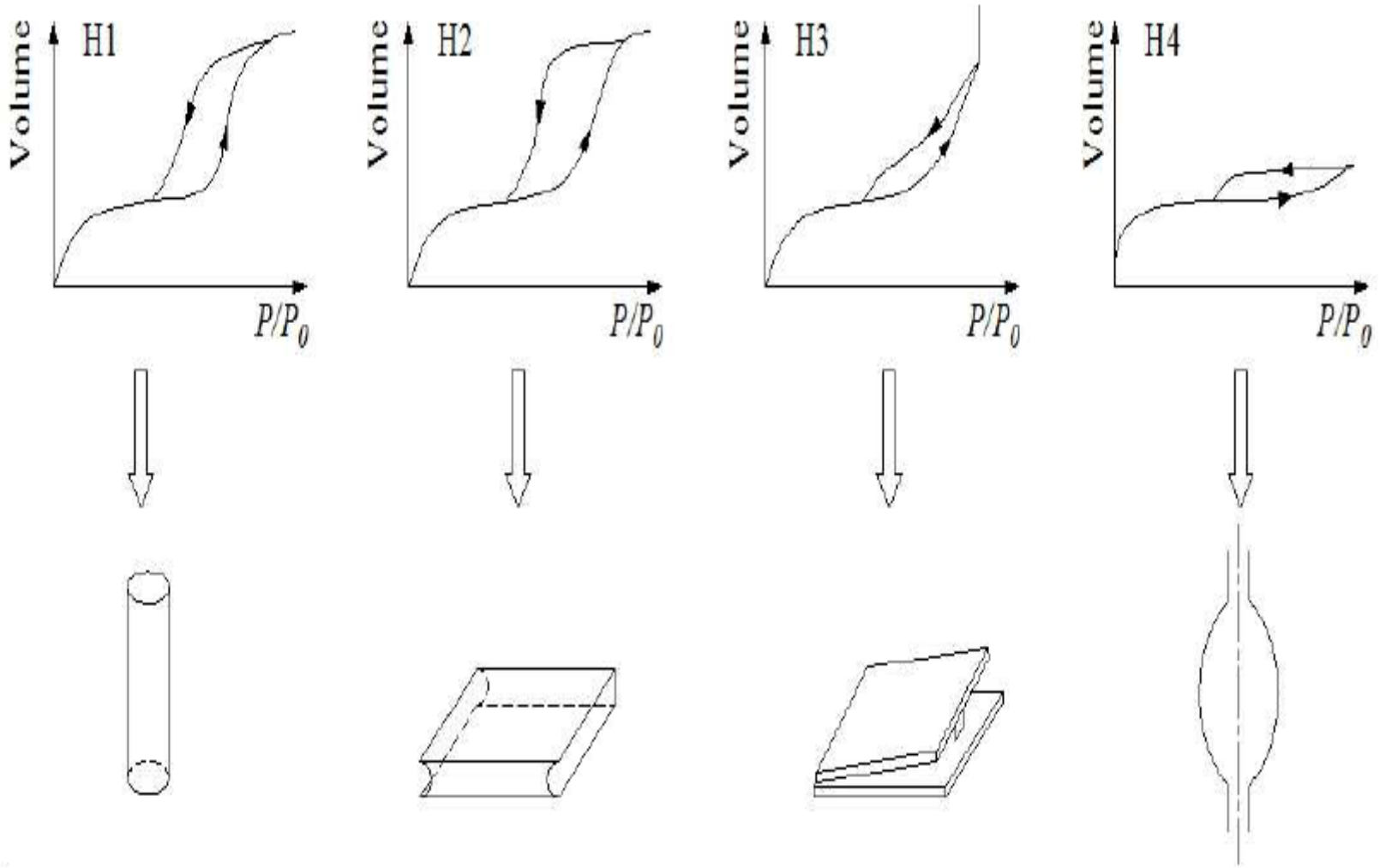

Fig. 10 Classification of hysteresis loops and pore types recommended by IUPAC

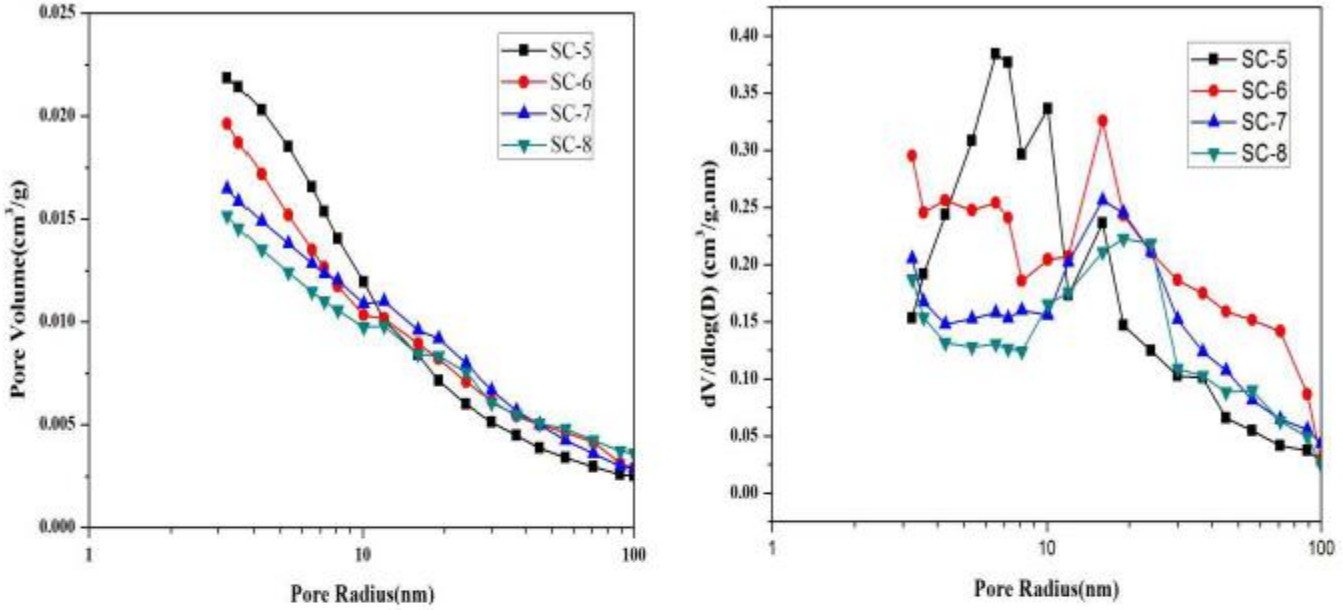

Fig. 8 Cumulative and incremental pore size plots from mercury intrusion data

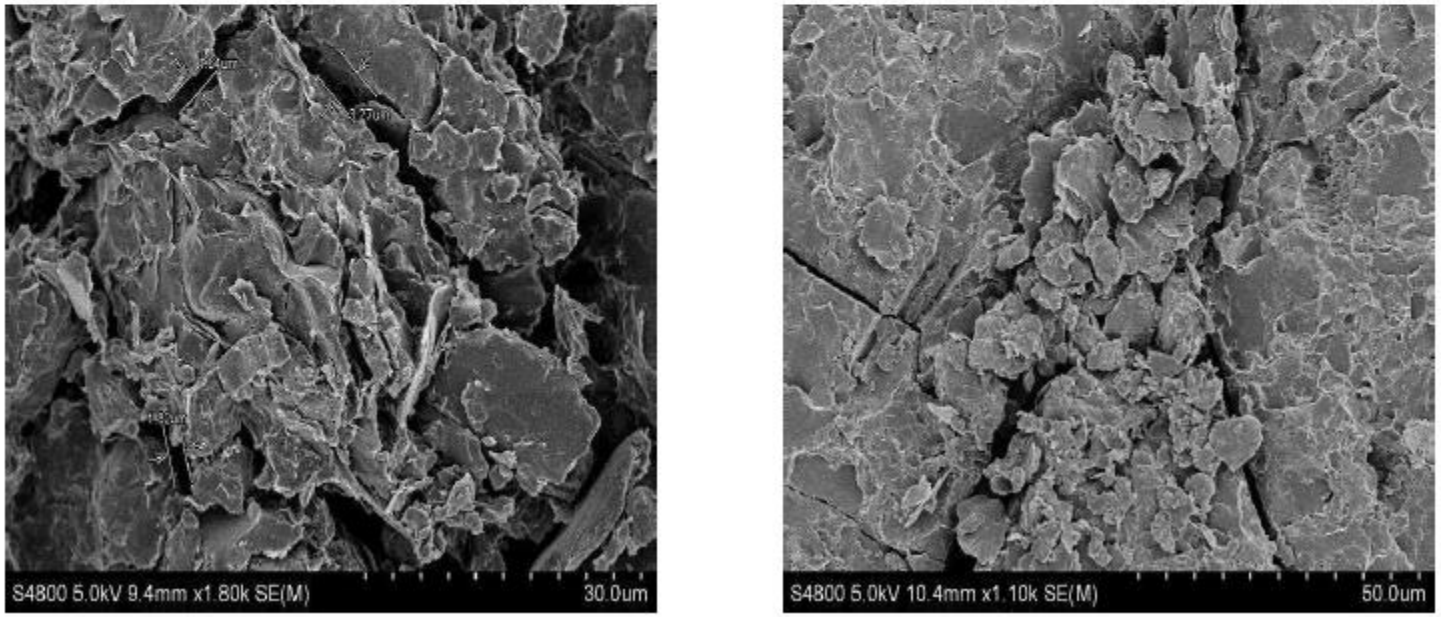

Fig. 9 The SEM photos of shale samples

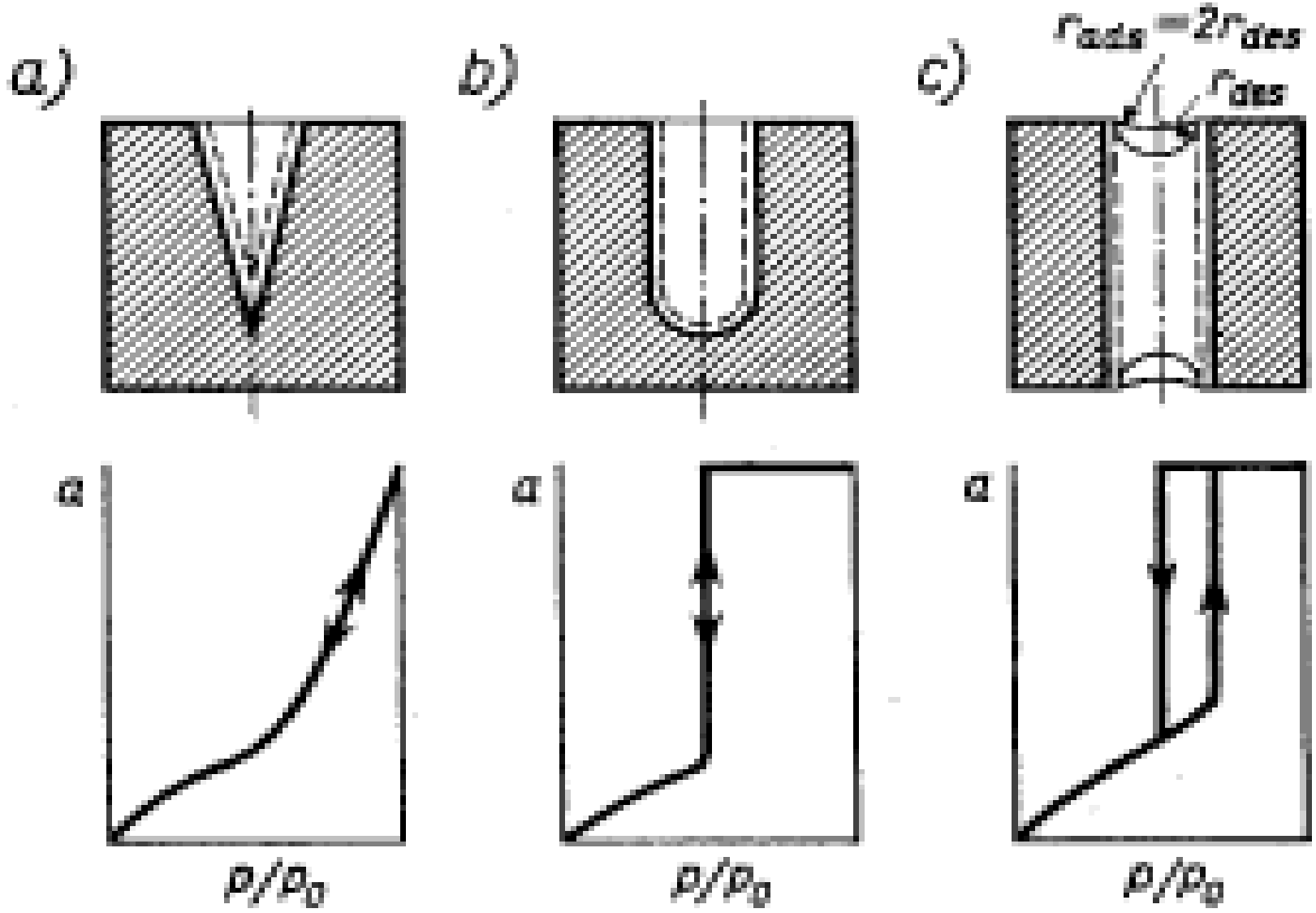
a)
b)
c)
$r_{ads} = 2r_{des}$
r_{des}
a
a
a
p/p_0
p/p_0
p/p_0

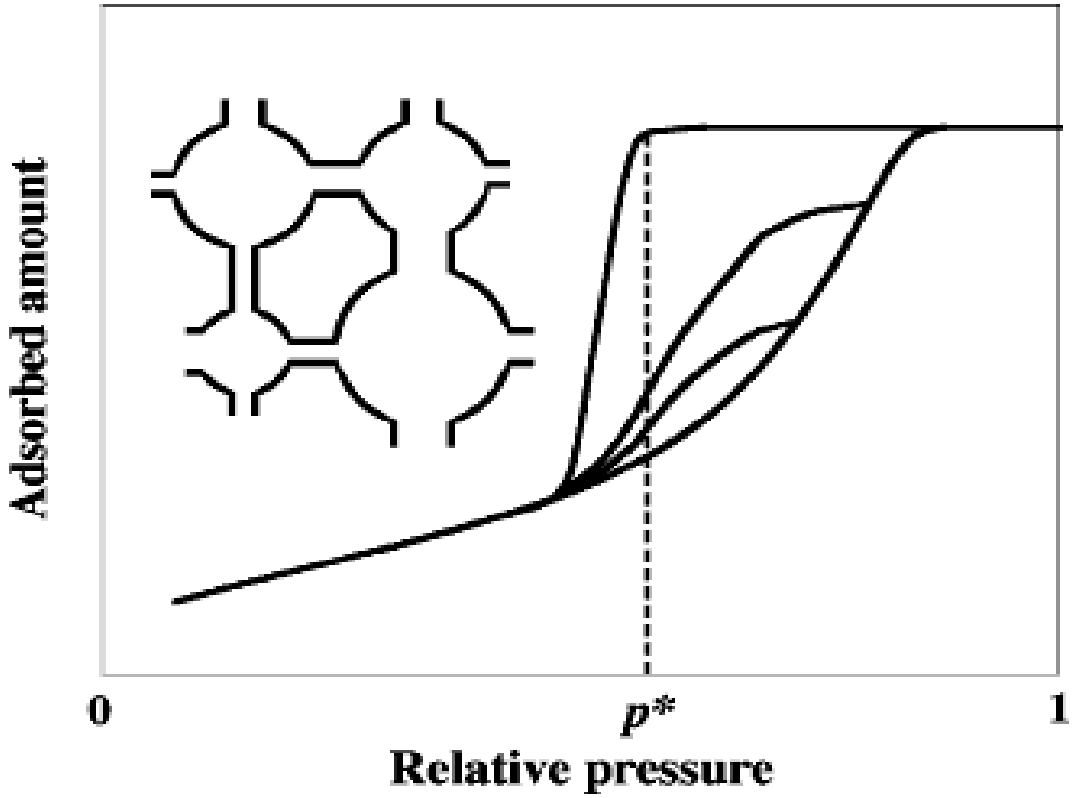

Figure 2. Schematic hysteresis loop of type H2 and PDSCs for porous glass, an assembly of cavities connected by constrictions as represented in the inset. According to the pore blocking/percolation model, evaporation along the PDSCs can occur at pressure higher than p^*, the evaporation pressure of the system when it is fully filled which is the signature of the occurrence of a percolation process.

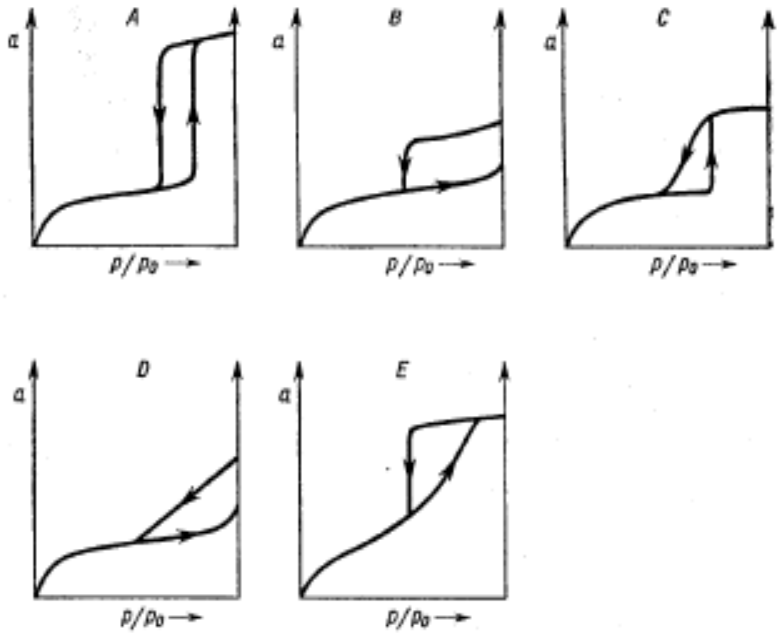

Rys.4. Classification of the capillary condensation hysteresis loops after De Boera.

According to de Boer:

- **Type A** – appears in double-open capillaries having shapes of regular or irregular cylinders prisms.
- **Type B** – appears In the presence of slit pores having paralel walls.
- **Type E** – such hysteresis appears in the case of ink-bottles shapes of the capillaries or deformed tubes with narrow outlets.
- **Types C** and **D** results from the pores shapes A and B which are partially

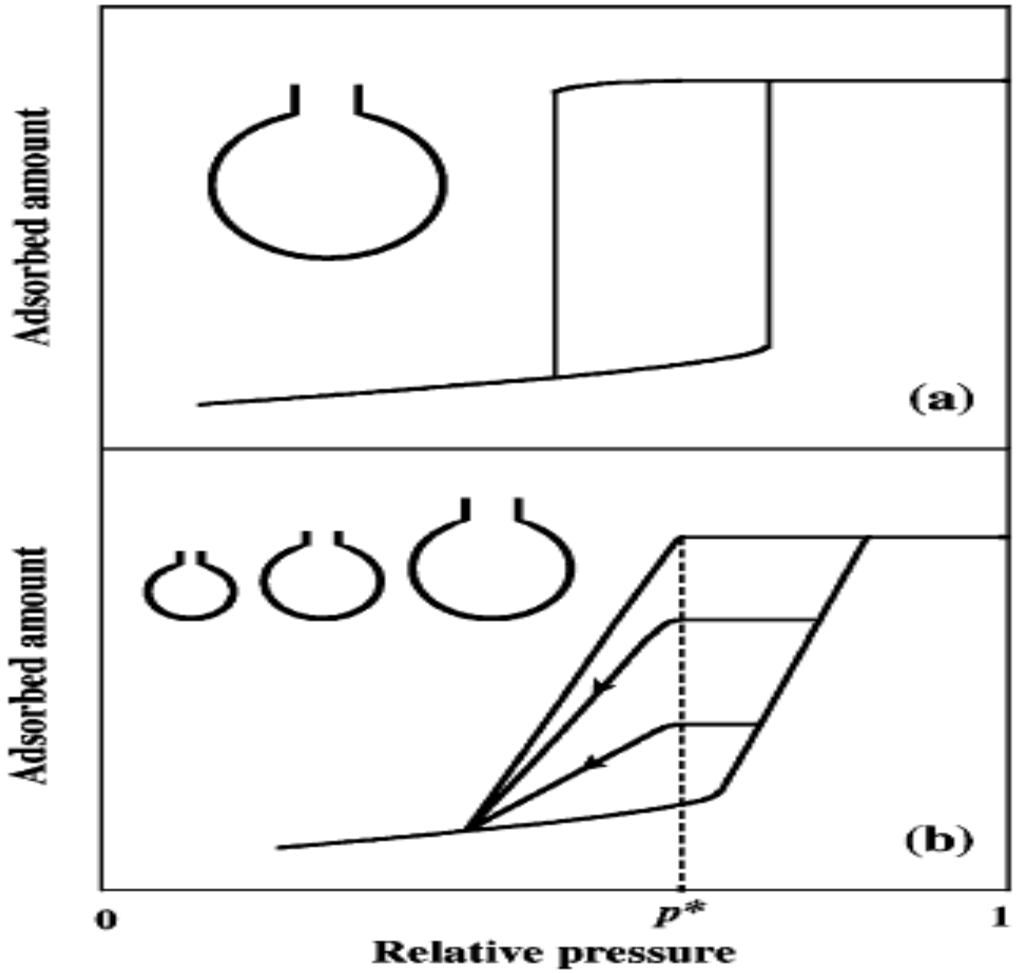

Figure 1. (a) Hysteresis loop for an ink-bottle pore. (b) Hysteresis loop for an assembly of non-interconnected ink-bottle pores with random size distributions of cavities and necks; two primary descending scanning curves (PDSCs) are represented. Along these PDSCs, none of pores can empty above p^*, the evaporation pressure of the largest necks.

منفذ و پسماند

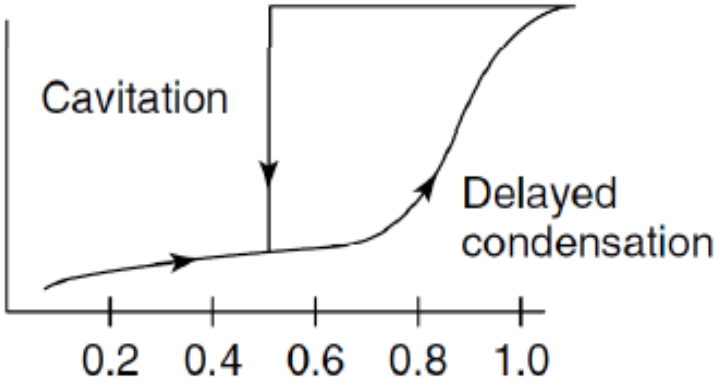

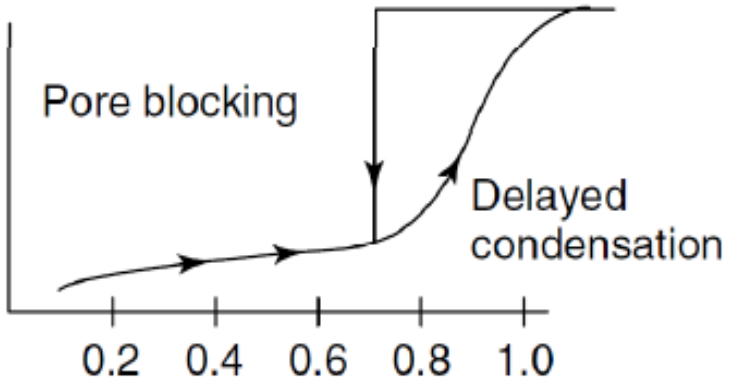

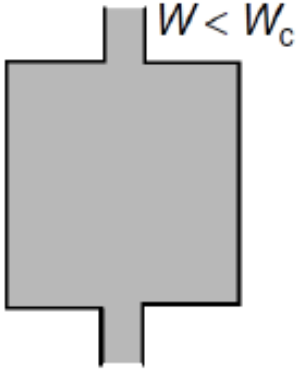

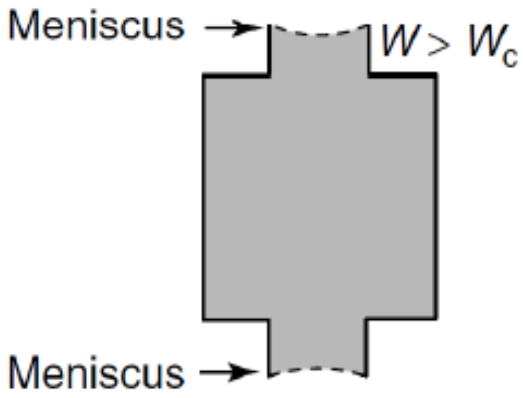

Often at p/p_0=0.42 for N_2
independent of the adsorbent

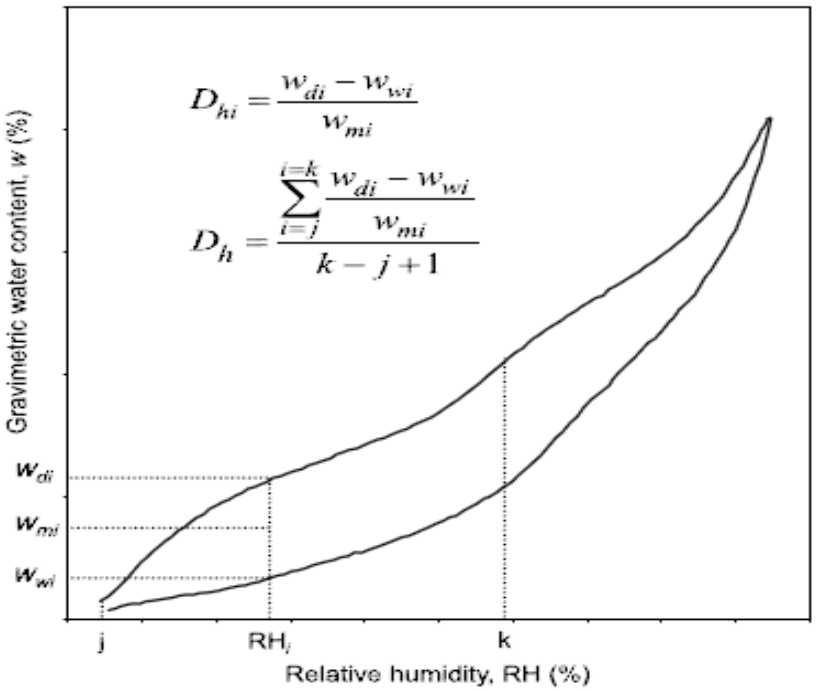

Fig. 5. Definition of the degree of hydraulic hysteresis

$$D_h = \frac{\sum_{i=j}^{i=k} \frac{w_{di} - w_{wi}}{w_{mi}}}{k - j + 1} \qquad (6)$$

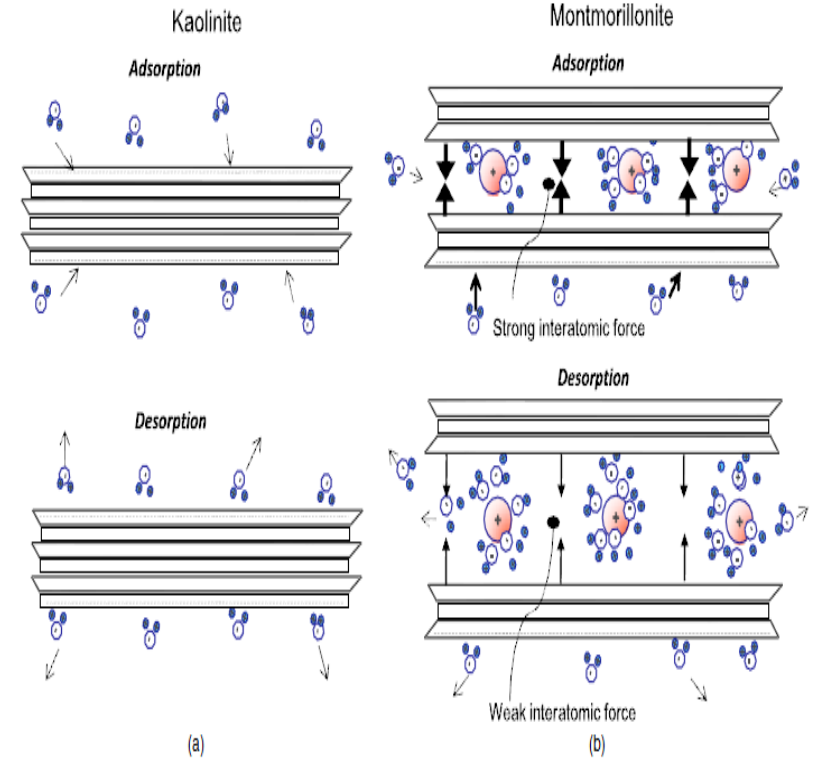

. Conceptual illustration of mechanism for hysteresis in the high suction range: (a) adsorption (wetting) path; (b) desorption (drying) path

Table 10. CPSM Fitting Parameters Referring to Hysteresis Loops of Figure 3(3-1a)−(3-2a)

specimen	V_{gmax}[a] ($cm^3(S^{TP})/g$)	N_S[b]	parameters of the intrinsic pore segment number distribution $F(D)$						Kelvin parameters[c]		adsorbed gas layer thickness parameters, eq 2	
			b_1	b_2	w_1	w_2	P_{ce}/P_0	$(P/P_0)_{max}$	$\cos\theta_c$	$\cos\theta_h$	m	n
dry lignite	12.876	3.3	−5400	−559	35	1000	0.25	0.9996	0.65	0.65	0.10	0.35
montmorillonite	48	2.90	−5000	−110	1	26	0.45	0.9980	0.60	0.60	0.10	0.35

[a] Measurement carried out in this work (Figure 3 (3-1a)−(3−2a)). [b] Pore cross-sectional variation number. [c] As defined by eq 11 (part 1 of this work).

Table 11. Surface Area (m^2/g) Data for Dry Lignite, Figure 3 (3-1e) and Montmorillonite Figure 3(3-2e)

specimen	S_{BET}	C (BET parameter)	$S_{Rb(co)}$	$S_{Rb(ev)}$	S_{CPSM}	$(S_{Rb(co)}-S_{BET})/S_{BET}$ (%)	$(S_{Rb(ev)}-S_{BET})/S_{BET}$ (%)	$(S_{CPSM}-S_{BET})/S_{BET}$ (%)
dry lignite	5.3	103	3.4	7.4	5.3	−35.8	+39.6	0
montmorillonite	20.4	72	10.0	23.0	20.4	−51.0	+12.7	−1.2

Table 3. Summary of Porous Materials Studied in This Work (Using the CPSM Model To Simulate Nitrogen Sorption Hysteresis Data)

hysteresis loop type	description of material
H_1-type (IUPAC)	**Anodic oxide film** Preparation (Salmas Doctoral Thesis, under preparation[13]). Porosimetry measurements, this work.[a]
H_2-type (IUPAC)	**HDS catalysts** Commercial grades, Table 7. Porosimetry measurements, this work.[a]
H_3-type (IUPAC)	**Dry lignite** Sample preparation and porosimetry measurements, this work.[a] **Montmorillonite** Literature data.[8]
H_4-type (IUPAC)	**Pillared clays** Literature data[18,19]
novel nanoporous materials (mesoporous molecular sieves)	**MCM-41** Literature data[5,6]

[a] A Sorptomatic, Carlo Erba, Model 1800, has been used to carry out the porosimetry measurements.

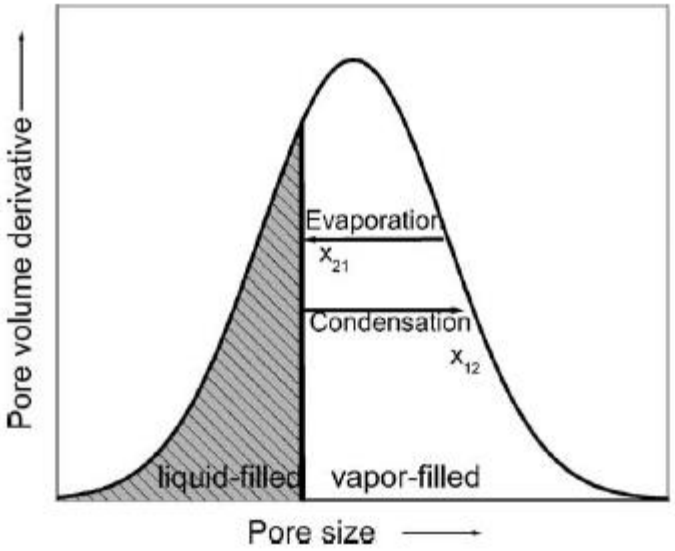

Fig. 1. Domain complexion diagram related to capillary condensation and evaporation in a system formed by straight, non-intersecting cylindrical capillaries.

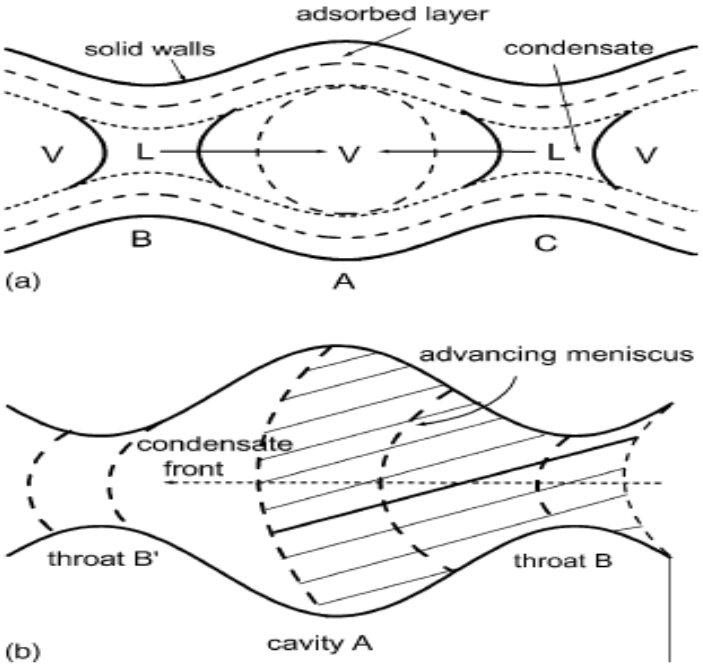

Fig. 2. Schematic representation of advanced condensation inside an undulated cylindrical pore: (a) the liquid (L)–vapor (V) menisci first appearing at necks B and C advance toward bulge A, replenishing it completely with condensate. (b) A L–V meniscus is first formed at throat B, then moving into cavity A and throat B′.

Table 2. Calculated Parameters for Various Soils Based on the BET Model

Soil	X_m (mg H_2O/g soil)	c	Highest total suction (kPa)	Specific surface area by BET (m^2/g)	Degree of hysteresis
100% GaK–0% NaS	6.14	5.95	4.7×10^5	22.14	0.12
90% GaK–10% NaS	11.08	6.75	4.8×10^5	39.96	0.59
80% GaK–20% NaS	17.87	4.55	5.2×10^5	64.44	0.76
70% GaK–30% NaS	21.92	7.52	5.5×10^5	79.05	0.82
60% GaK–40% NaS	26.97	9.22	5.5×10^5	97.26	0.76
50% GaK–50% NaS	32.41	8.45	5.0×10^5	116.89	0.81
40% GaK–60% NaS	37.37	9.34	6.1×10^5	134.79	0.88
30% GaK–70% NaS	41.17	9.30	5.9×10^5	148.48	0.96
20% GaK–80% NaS	51.26	6.84	5.4×10^5	184.88	0.92
10% GaK–90% NaS	57.11	7.05	5.7×10^5	205.96	0.95
0% GaK–100% NaS	69.60	6.19	6.1×10^5	251.03	0.90
100% CaS–0% Cs	109.98	20.98	9.7×10^5	396.66	0.28
90% CaS–10% Cs	98.66	27.84	1.1×10^6	355.82	0.25
80% CaS–20% Cs	93.43	22.64	9.7×10^5	336.95	0.29
70% CaS–30% Cs	75.01	16.28	8.0×10^5	270.55	0.41
60% CaS–40% Cs	67.71	13.87	7.7×10^5	244.19	0.35
50% CaS–50% Cs	56.32	14.75	7.6×10^5	203.14	0.49
40% CaS–60% Cs	48.49	13.83	7.1×10^5	174.90	0.43
30% CaS–70% Cs	42.63	14.16	7.0×10^5	153.76	0.52
20% CaS–80% Cs	34.16	15.53	7.5×10^5	123.19	0.48
10% CaS–90% Cs	29.77	26.64	1.2×10^6	107.39	0.52
0% CaS–100% Cs	22.98	19.48	8.2×10^5	82.86	0.52
Bonny silt	16.13	18.66	7.9×10^5	58.19	0.19
BALT silt I	15.72	22.25	8.8×10^5	56.69	0.22
BALT silt II	14.13	16.34	7.7×10^5	50.98	0.24
Hopi silt I	18.20	32.73	1.1×10^6	65.63	0.14
Hopi silt II	18.19	32.53	1.2×10^6	65.61	0.19
Iowa silt I	17.69	13.62	7.4×10^5	63.79	0.14
Iowa silt II	16.22	12.76	7.3×10^5	58.51	0.21

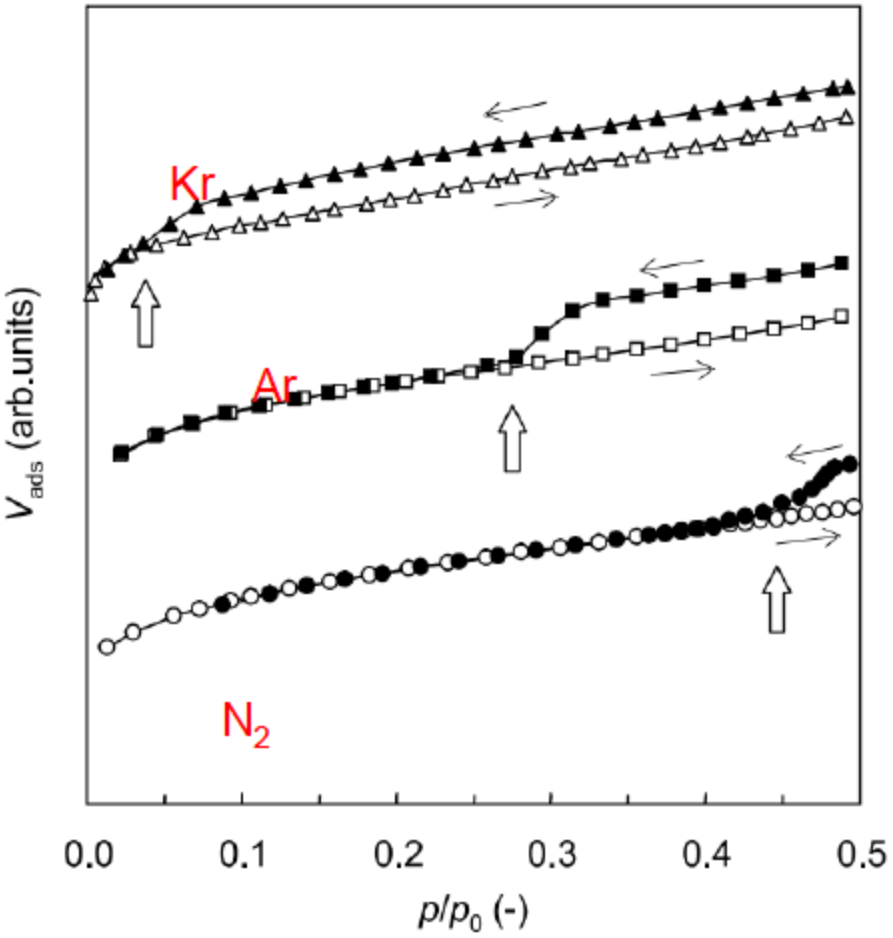

Adsorption (open symbols) and desorption (solid symbols) isotherms at 77 K of alkaline-treated ZSM-5

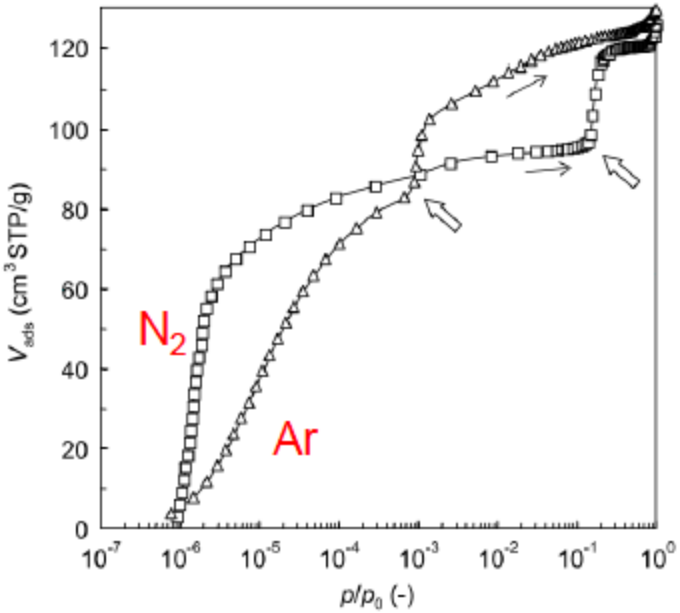

High-resolution N_2 and Ar adsorption isotherms of silicalite-1

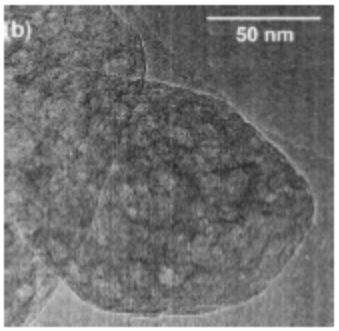

ZSM-5

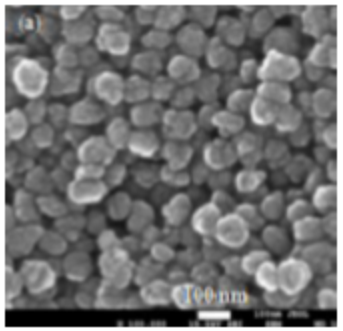

silicalite-1

J.C. Groen et al., *Microporous and Mesoporous Mater.*, **2003**, 60, 1–17

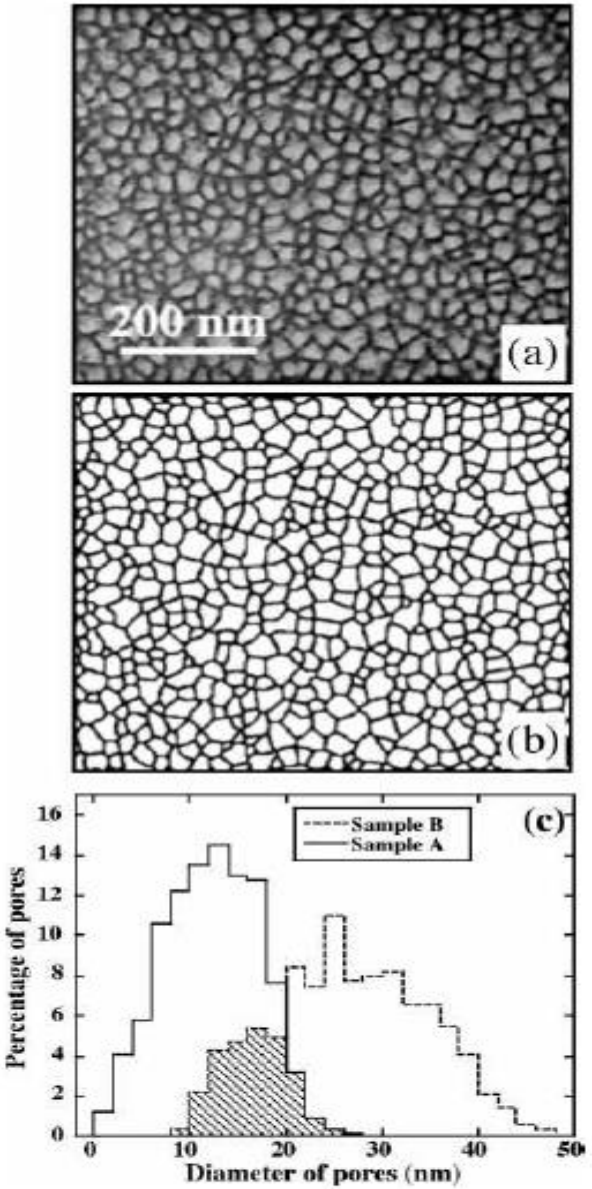

Figure 5. (a) Bright field TEM plane view of a porous Si layer, 70% porosity (sample B), prepared from a p^+-type (100) Si substrate. Observation axis [100]. (b) The corresponding binary image which reproduces both the porosity deduced by weighing and the consistancy in the Si wall thickness. (c) The PSDs, corresponding to cylindrical pores having the same cross section area as the polygonal pores, for samples A and B. The hatched region represents the overlap of the two PSDs.

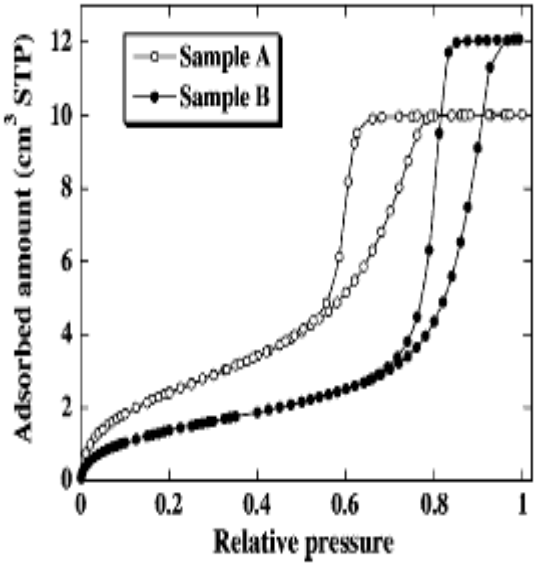

Figure 6. Nitrogen adsorption isotherm at 77.4 K for porous silicon samples A and B, which are composed of pores closed at one end.

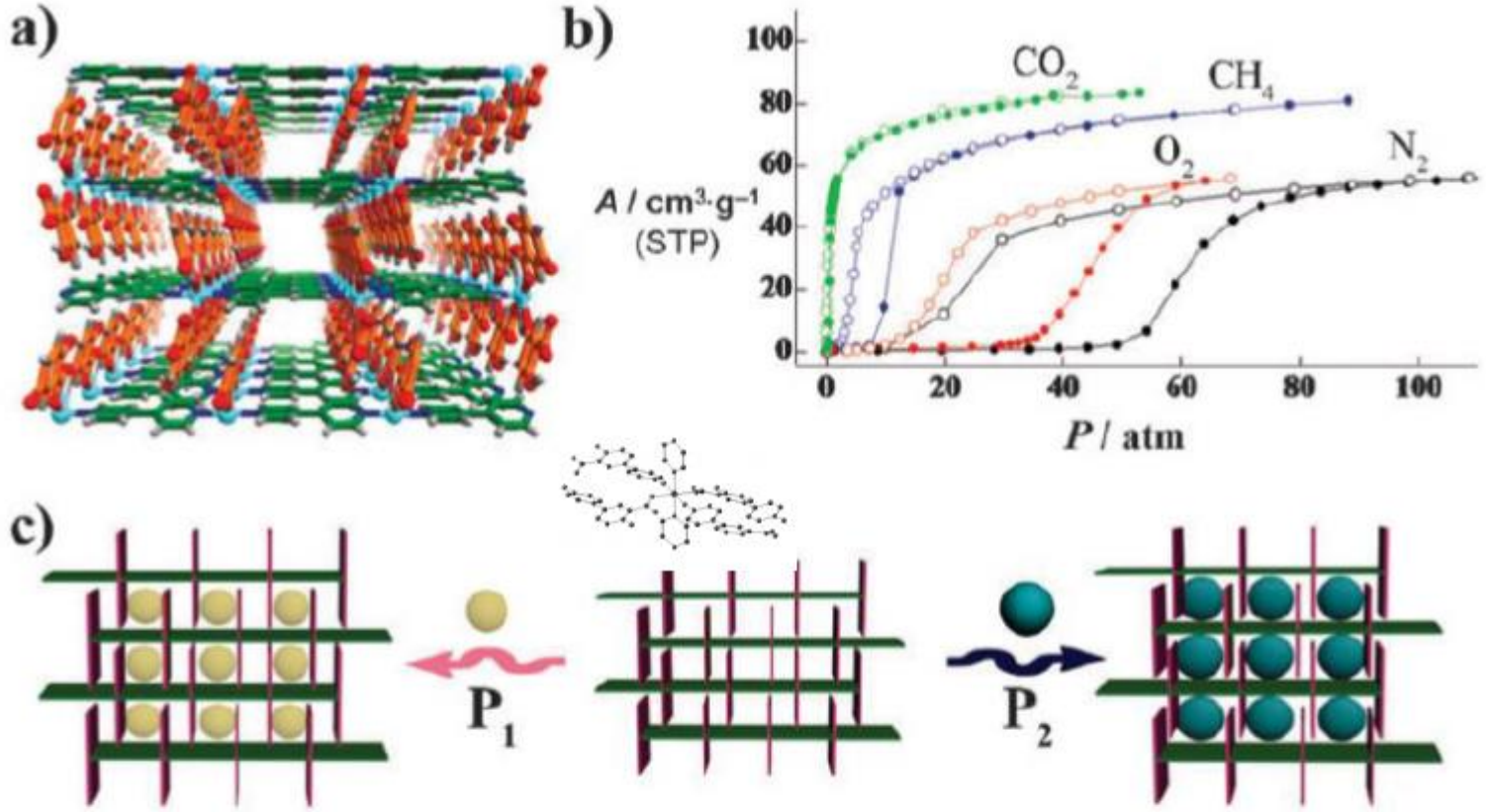

3D π-stacked pillared layer structure of $Cu(dhbc)_2(4,4'\text{-bpy})$. (b) Gas adsorption (filled circles) and desorption (open circles) isotherms at 298 K. (c) Schematic representation of the gas selective adsorptions in the dynamic framework $Cu(dhbc)_2(4,4'\text{-bpy})$ whose gap open size depends on the guest molecules at special pressure.

Kitaura et.al, *Angew. Chem., Int. Ed.*, **2003**, 42, 428–431

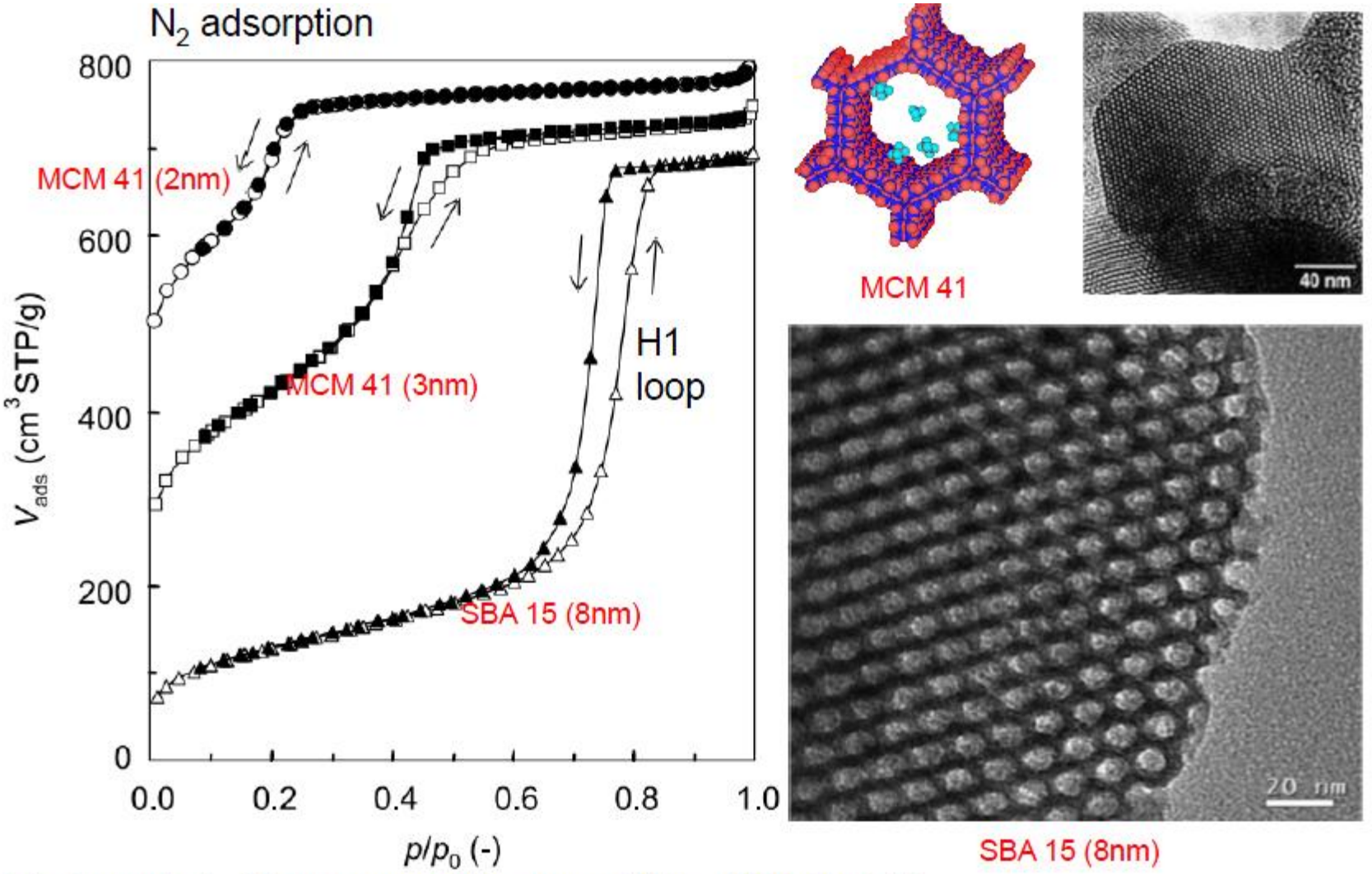

J.C. Groen et al., *Microporous and Mesoporous Mater.*, **2003**, 60, 1–17

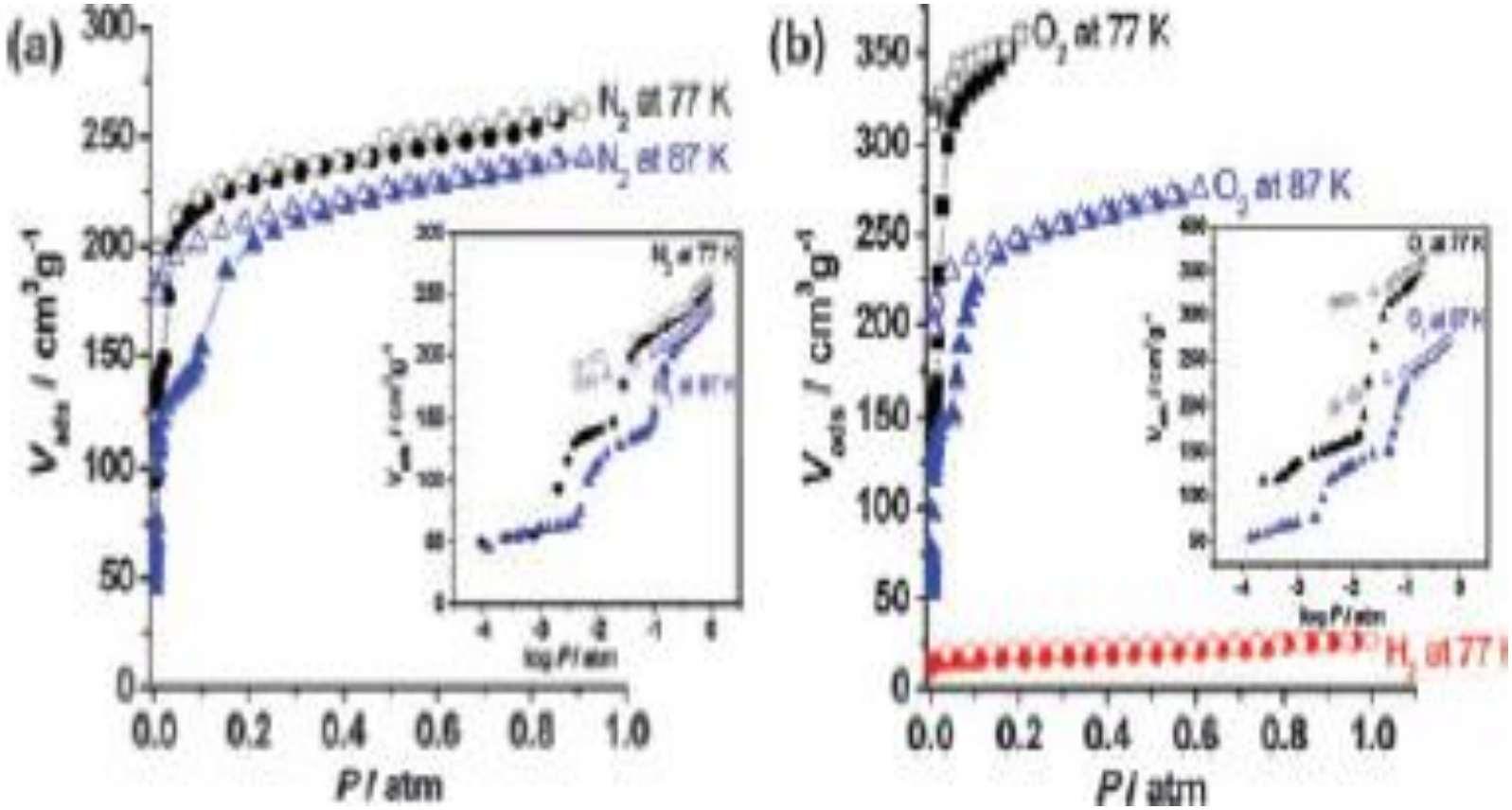
(a)
N_2 at 77 K
N_2 at 87 K
V_{ads} / cm^{3}g^{-1}
P / atm
(b)
O_2 at 77 K
O_2 at 87 K
H_2 at 77 K
V_{ads} / cm^{3}g^{-1}
P / atm

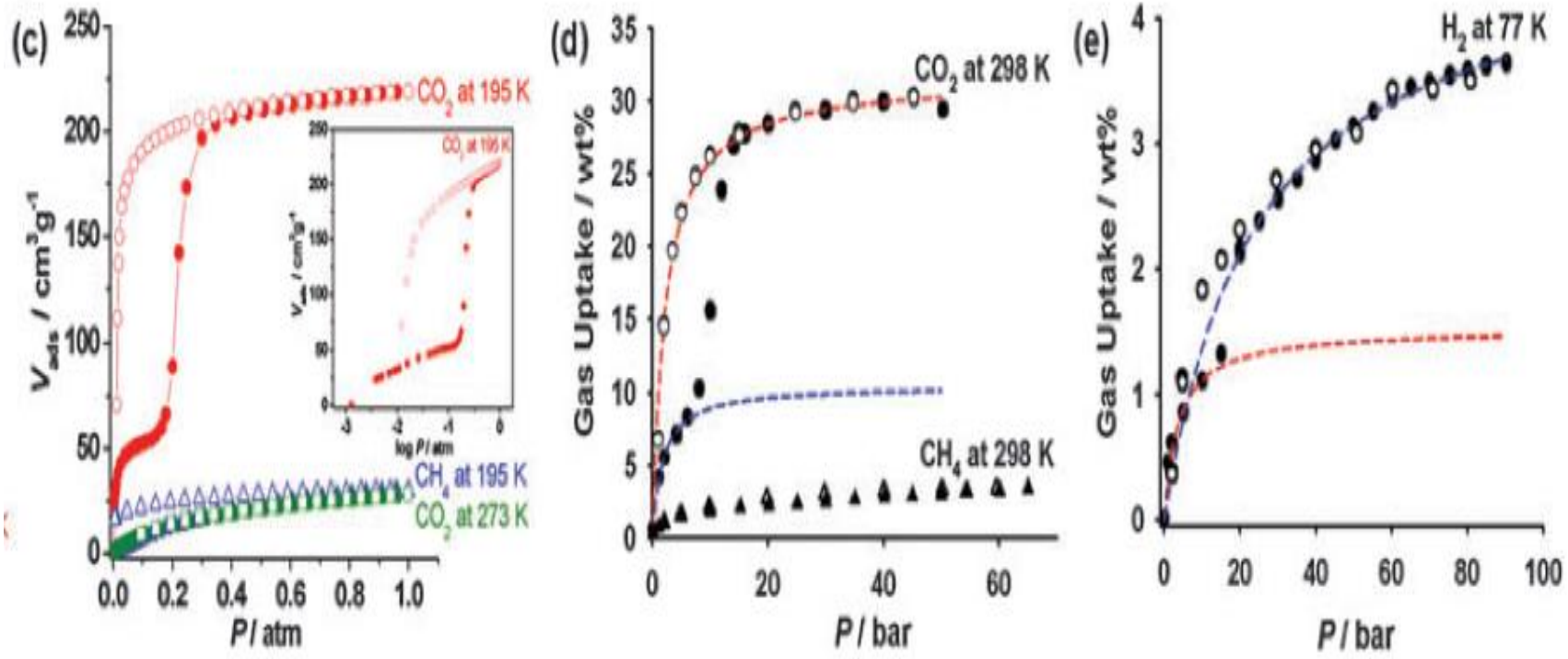
(c)
V_{ads} / cm^{3}g^{-1}
P / atm
CO$_2$ at 195 K
CH$_4$ at 195 K
CO$_2$ at 273 K
log P / atm
(d)
Gas Uptake / wt%
P / bar
CO$_2$ at 298 K
CH$_4$ at 298 K
(e)
Gas Uptake / wt%
P / bar
H$_2$ at 77 K

8. Pore analysis by adsorption

8.1. Kelvin equation

Adsorption data → pore size or pore size distribution

$$\ln\left(\frac{P}{P_0}\right) = -\frac{2}{r}\frac{\gamma \bar{V}}{RT}\cos\theta$$

$$\Rightarrow \ln\left(\frac{P}{P_0}\right) = -\frac{2}{r}\frac{\gamma \bar{V}}{RT} \quad if\ \theta = 0$$

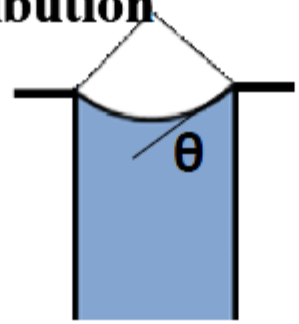

P : equilibrium P in pores with a radius r.
P_0 : equilibrium P_0 on planar surface.

r : pore radius
γ : surface tension
$\bar{V}$: molar volume of liquid

In a pore, the overlapping potential of the wall can overcome the translational energy of an adsorbate molecule. So that condensation will occur at a lower pressure. Thus, as the relative pressure is increased, condensation will occur first in pores of smaller radii and will progress into larger pores.

As explained in part 1 of this work (eq 11), the Kelvin equation assumes the form

$$D_K = \frac{4 V_L \gamma \cos\theta}{\ln(P_0/P) RT} \Rightarrow D_K = \frac{1.906}{\ln(P_0/P)} \cos\theta \qquad (3)$$

that is valid for an l/v interface geometry varied between a hemispherical ($\cos\theta \equiv \cos\theta_h = 1$) and a cylindrical one ($\cos\theta \equiv \cos\theta_c = 0.5$) while the numerator is computed by $(2 V_L \gamma / RT) = 1.906$ where $V_L = 34.517$ cm^3/gmol, $\gamma = 8.88$ mN/m, $R = 1.987$ cal/(gmol K), and $T = 77.35$ K for $[D_K]$ = nm.

8.2. Adsorption hysteresis

Hysteresis:
two relative pressures corresponding to a given quantity:
$(P/P_0)_{ads} > (P/P_0)_{des}$

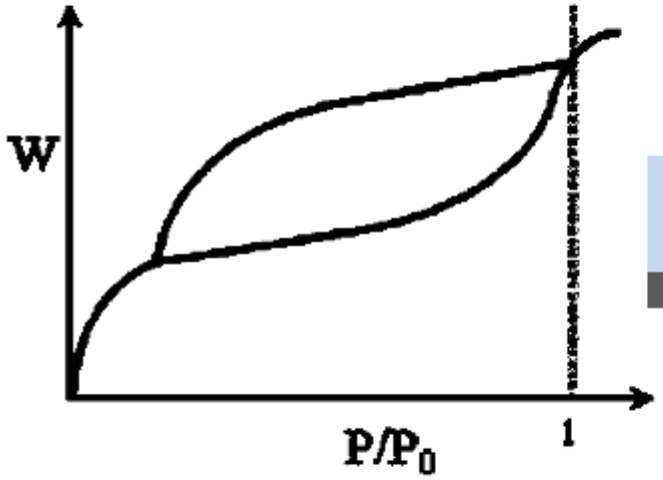

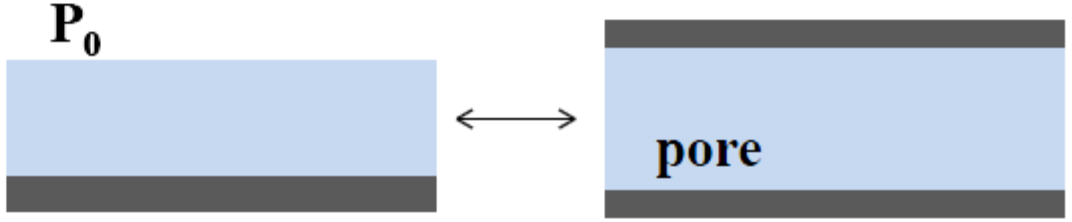

$$\Delta G_{ads} = RT\left(\ln P_{ads} - \ln P_0\right)$$

$$\Delta G_{des} = RT\left(\ln P_{des} - \ln P_0\right)$$

$$\because P_{des} < P_{ads} \quad \Rightarrow \quad \Delta G_{des} < \Delta G_{ads}$$

∴ desorption value corresponds to the more stable condition

→ desorption isotherm should be used for pore analysis.

Theories for hysteresis:

Zsigmondy : different contact angles during adsorption and desorption.

McBain : bottle neck

Cohan : adsorption on a cylindrical meniscus
desorption from a hemispherical meniscus.

8.3. Total Pore Volume

Gurvitsh rule:

At saturation ($P/P_0 \approx 1$) the liquid volume of different adsorbates, when measured on porous adsorbents, is essentially constant and is independent of adsorbate.

This constancy of adsorbed liquid at saturation provides direct evidenc that the pores are filled.

$\therefore$ **at** $P/P_0 \approx 1$

The amount of adsorption can be used to calculate total pore volume.

For example

At $P/P_0 = 0.99$ W_a gram of N_2 are adsorbed

$$V_p = \frac{W_a}{\rho}$$ **, ρ = liquid density**

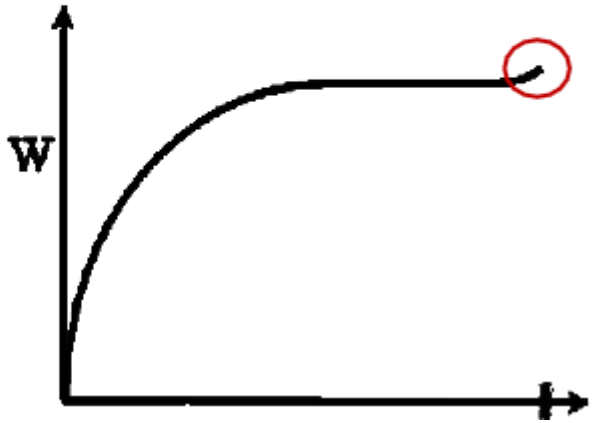

Based on Kelvin eq., the largest pore radii are given by

$$r_\kappa = \frac{-2\gamma \bar{V}}{RT\ln(\frac{P}{P_0})} = \frac{-2\left(8.85\,\frac{erg}{cm^2}\right)\left(34.6\,\frac{cm^2}{mol}\right)}{\left(8.314\times10^7\,\frac{erg}{K\cdot mol}\right)(77K)(\ln 0.99)} = 950\times10^{-8}\,cm = 950\ \text{Å}$$

$\therefore V_p$ represents the pore volume of all the pores up to 950Å.

An implicit assumption: no surface other than the inner walls of the pores exists.

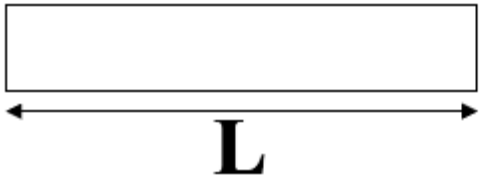

$$V_p = \pi \bar{r}_p^2 \cdot L$$

$$S_{BET} = 2\pi \bar{r}_p \cdot L$$

Average pore size = $2 \cdot \bar{r}_p$

$$\bar{r}_p = \frac{2V_p}{S_{BET}}$$

Porous materials: most of the surface area is contributed by the pore wall

8.4. Pore Size Distribution (PSD)

PSD is usually measured using the desorption isotherm.

N_2 as the adsorbate

$$r_k = \frac{4.15}{\log(P_0/P)} \quad [\text{Å}]$$

r_k : Kevin radius or critical radius

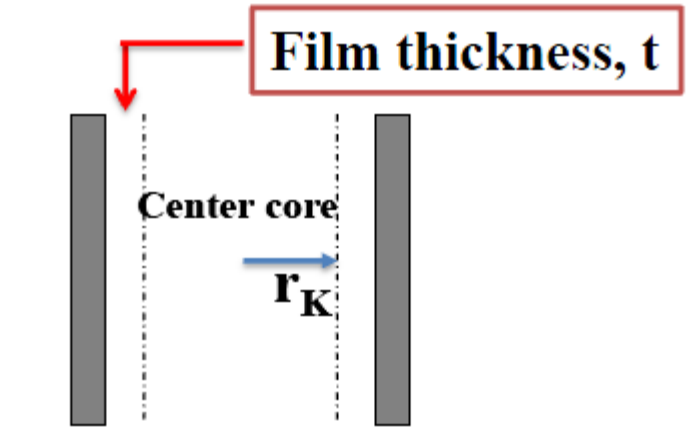

Pore radius, $r_p = r_K + t$

It is difficult to estimate film thickness over the inner walls.

Assumptions for adsorption in pores.

1. A planar surface

2. Adsorbate evenly distributed over surface.

$$t = \left(\frac{W_a}{W_m}\right)\tau$$

W_a : weight adsorbed

W_m : weight for monolayer coverage.

τ : thickness of one layer

For liquid N_2

One mole of molecules spread on surface

$$S = (16.2\ \text{Å}^2)(6.02\cdot 10^{23}) = 97.5\cdot 10^{23}\ \text{Å}^2/\text{gmol}$$

$$\bar{V} = 34.6\cdot 10^{24}\ \text{Å}^3/\text{gmol}$$

$$\tau = \frac{\bar{V}}{S} = 3.54\text{Å} \qquad t = \left(\frac{W_a}{W_m}\right)\cdot 3.54\text{Å}$$

On nonporous surface, it has been shown that when W_a/W_m is plotted vs. P/P_0, the data all approximately fit a common Type II curve as $P/P_0 > 0.3$ regardless of the adsorbent used.

This is an implication of even distribution of the adsorbate.

ie. When $W_a/W_m = 3$ $\Rightarrow t = (3\times 3.54) = 10.62$ Å

Halsey equation for N_2 adsorption on planar surface to predict t.

Halsey equation for N_2 adsorption on planar surface to predict t.

$$t = 3.54\left(\frac{5}{2.303 \cdot \log\left(P_0/P\right)}\right)^{\frac{1}{3}}$$

Table 8.1 (Next page)

consider both the layering and condensation.

◆ **Similar to the BJH method (Barrett, Joyner and Halenda), only for mesopores**

◆ **BJH takes into account the film thickness change after each decrement of P/Po.**

Three conditions Kelvin eq. analysis should be terminated

1. **$P/P_0 < 0.3$, adsorption in micropore range**

   The validity of Kelvin eq. becomes questionable, because the uncertain -ty regarding molar volume and surface tension when only one or two molecular diameters are involved.

2. **When $\Delta t \sum S \approx \Delta V_{liq}$, represents the absence of evaporation from center cores**

3. **Hysteresis loop closes,**

   Micropore vol. = total pore vol. – $\sum V_p$ (BJH, column 12)

$$\frac{Wa/_{P/P0} = 0.99}{\rho_l}$$

$\sum S$ **= 212.1 m^2g^{-1} (in Table 8.1) ←does not include micropore S.A.**

(∵ $\sum S$ should be smaller than BET area)

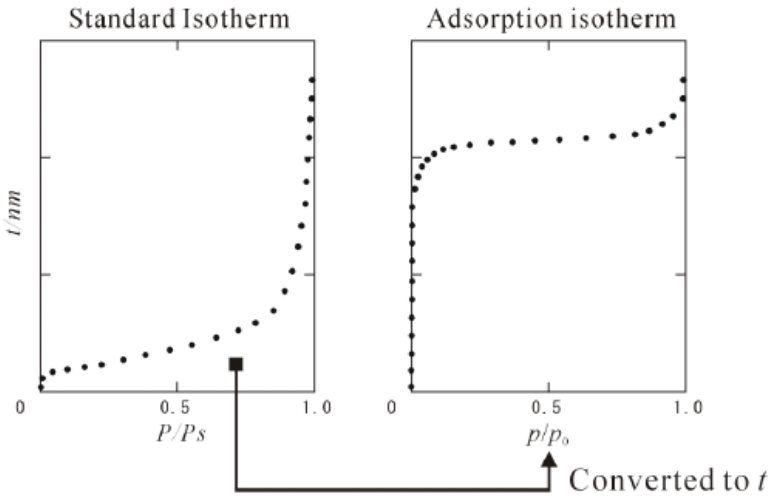

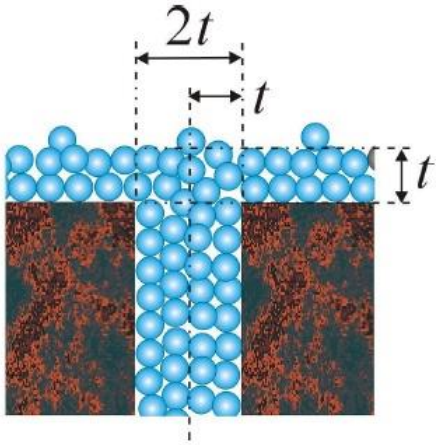

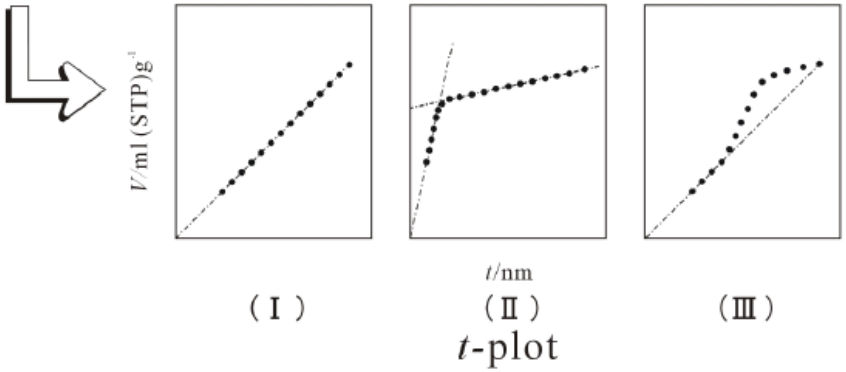

$$t = \frac{V_a}{V_m} \times 0.354[\text{nm}]$$

$$a_s = \frac{s \times 0.354}{22414} \times L \times \sigma = 1.541 \times s$$

Halsey equation for N_2 adsorption on planar surface to predict t.

$$t = 3.54\left(\frac{5}{2.303 \cdot \log\left(P_0/P\right)}\right)^{\frac{1}{3}}$$

Table 8.1 (Next page)

consider both the layering and condensation.

◆ **Similar to the BJH method (Barrett, Joyner and Halenda), only for mesopores**

vin equation provides a correlation between pore diameter and pore condesa
e

otions

of cylindrical shape
d-wall interactions

$$\ln\frac{p}{p_0} = \frac{-2\gamma V_l}{r_p RT}$$

γ surface tension of liquid n
V_l liquid molar volume
r_p pore radius
r_k critical radius
R universal gas constant
t statistical thickness

eration of fluid-wall interactions (modified Kelvin equation):

$$\frac{4.15}{\log(p_0/p)}\ \text{Å} \qquad (N_2,\ 77\ K)$$

$$+ t$$

$$4\left[\frac{5}{\ln(p/p_0)}\right]\ \text{Å}$$

$$\Delta V_{liq} = \frac{\Delta V_{gas}}{22.4\times10^{3}}\times 34.6 = \Delta V_{gas}\left(1.54\times10^{-3}\right)\ \text{cm}^3$$

$$\Delta V_{liq} = \pi \bar{r}_k^{\,2}\ell + \Delta t \Sigma S$$

$$V_p = \pi \bar{r}_p^{\,2}\ell$$

$$V_p = \left(\frac{\bar{r}_p}{\bar{r}_k}\right)^2\left[\Delta V_{liq} - \left(\Delta t \Sigma S\times10^{-4}\right)\right]\ \text{cm}^3$$

$$S = \frac{2V_p}{\bar{r}_p}\times10^{4}\ \text{m}^2$$

$$t = 3.54\left(\frac{5}{\ln(P_0/P)}\right)^{1/3}\ \text{Å} \qquad r_k = \frac{4.15}{\log(P_0/P)}$$

1	2	3	4	5	6	7	8	9	10	11	12	13	14
$\frac{P}{P_0}$	V_{gas} STP (cm^3/g)	r_k (Å)	T (Å)	r_p (Å)	$\bar{r}_k$ (Å)	$\bar{r}_p$ (Å)	Δt (Å)	ΔV_{gas} STP (cm^3/g)	$\Delta V_{liq}\times10^3$ (cm^3/g)	$\Delta t\Sigma S\times10^3$ (cm^3/g)	$V_p\times10^3$ (cm^3/g)	S (m^2/g)	ΣS (m^2/g)
0.99	161.7	950	28.0	978									
0.98	161.5	473	22.2	495	711	737	5.8	0.2	0.31	0.00	0.33	0.01	0.01
0.97	161.0	314	19.4	333	394	414	2.8	0.5	0.77	0.00	0.85	0.04	0.05
0.95	160.2	186	16.3	202	250	268	3.1	0.8	1.23	0.02	1.40	0.10	0.15
0.90	158.8	90.7	12.8	104	138	153	3.5	1.4	2.16	0.05	2.59	0.34	0.49
0.85	157.2	58.8	11.1	69.9	74.8	87.0	1.7	1.6	2.46	0.08	3.22	0.74	1.23
0.80	155.2	42.8	10.0	52.8	50.8	61.4	1.1	2.0	3.08	0.14	4.30	1.40	2.63
0.77	152.9	36.6	9.5	46.1	39.7	49.5	0.5	2.3	3.54	0.13	5.30	2.14	4.77
0.75	148.9	33.2	9.2	42.4	34.9	44.3	0.3	4.0	6.16	0.14	9.70	4.38	9.15
0.73	145.1	30.4	8.9	39.3	31.8	40.9	0.3	3.8	5.85	0.27	9.22	4.51	13.66
0.71	140.9	27.9	8.7	36.6	29.2	38.0	0.2	4.2	6.47	0.27	10.49	5.52	19.18
					26.9	35.4	0.3	5.0	7.70	0.58	12.34	6.97	26.15

0.69	135.9	25.8	8.4	34.2						
0.67	130.0	23.9	8.2	32.1	24.9	33.2	.2	5.9	9.09	0.52	15.23	9.17	35.32
0.65	123.9	22.2	8.0	30.2	23.1	31.2	.2	6.1	9.39	0.71	15.84	10.15	45.47
0.63	117.3	20.7	7.8	28.5	21.5	29.4	.2	6.6	10.16	0.91	17.30	11.77	57.24
0.61	110.1	19.3	7.7	27.0	20.0	27.8	.1	7.2	11.09	0.57	20.32	14.62	71.86
0.59	102.6	18.1	7.5	25.6	18.7	26.3	.2	7.5	11.55	1.44	20.00	15.21	87.07
0.57	95.0	17.0	7.3	24.3	17.6	25.0	.2	7.6	11.70	1.74	20.09	16.07	103.1
0.55	86.9	16.0	7.2	23.2	16.5	23.8	.1	8.1	12.47	1.03	23.80	20.00	123.1
0.53	78.8	15.1	7.0	22.1	15.6	22.7	.2	8.1	12.47	2.46	21.19	18.67	141.8
0.51	71.5	14.2	6.9	21.1	14.7	21.6	.1	7.3	11.24	1.42	21.21	19.64	161.4
0.49	65.4	13.4	6.8	20.2	13.8	20.7	.1	6.1	9.39	1.61	17.50	16.90	178.3
0.45	57.3	12.0	6.5	18.5	12.7	19.4	.3	8.1	12.47	5.35	16.62	17.13	195.4
0.40	51.7	10.4	6.2	16.6	11.2	17.6	.3	5.6	8.62	5.86	6.81	7.74	203.1
0.35	47.4	9.1	6.0	15.1	9.8	15.9	.2	4.3	6.62	4.06	6.73	8.47	212.1

[1] $\Sigma V_p = 0.28\,cm^3g^{-1}$; [1] $\Sigma S = 212.1\,m^2g^{-1}$

Table 8.1 shows that : the pore volume = 0.28 cm^3g^{-1} for $r_p > 15.1$ Å

Table 8.1

Table 8.1 Pore size distribution work table

1	2	3	4	5	6	7	8	9	10	11	12	13	14
$\frac{P}{P_0}$	V_{gas} STP ($cm^3 g^{-1}$)	r_k (Å)	t (Å)	r_p (Å)	$\bar{r}_k$ (Å)	$\bar{r}_p$ (Å)	Δt (Å)	ΔV_{gas} STP ($cm^3 g^{-1}$)	$\Delta V_{liq} \times 10^3$ ($cm^3 g^{-1}$)	$\Delta t \Sigma S \times 10^3$ ($cm^3 g^{-1}$)	$V_p \times 10^3$ ($cm^3 g^{-1}$)†	S (m^2)	ΣS (m^2)‡
0.99	161.7	950	28.0	978									
					711	737	5.8	0.2	0.31	0	0.33	0.01	0.01
0.98	161.5	473	22.2	495									
					394	414	2.8	0.5	0.77	0.00	0.85	0.04	0.05
0.97	161.0	314	19.4	333									
					250	268	3.1	0.8	1.23	0.02	1.40	0.10	0.15
0.95	160.2	186	16.3	202									
					138	153	3.5	1.4	2.16	0.05	2.59	0.34	0.49
0.90	158.8	90.7	12.8	104									
					74.8	87.0	1.7	1.6	2.46	0.08	3.22	0.74	1.23
0.85	157.2	58.8	11.1	69.9									
					50.8	61.4	1.1	2.0	3.08	0.14	4.30	1.40	2.63
0.80	155.2	42.8	10.0	52.8									
					39.7	49.5	.5	2.3	3.54	0.13	5.30	2.14	4.77
0.77	152.9	36.6	9.5	46.1									
					34.9	44.3	.3	4.0	6.16	0.14	9.70	4.38	9.15
0.75	148.9	33.2	9.2	42.4									
					31.8	40.9	.3	3.8	5.85	0.27	9.22	4.51	13.66
0.73	145.1	30.4	8.9	39.3									
					29.2	38.0	.2	4.2	6.47	0.27	10.49	5.52	19.18
0.71	140.9	27.9	8.7	36.6									
					26.9	35.4	.3	5.0	7.70	0.58	12.34	6.97	26.15

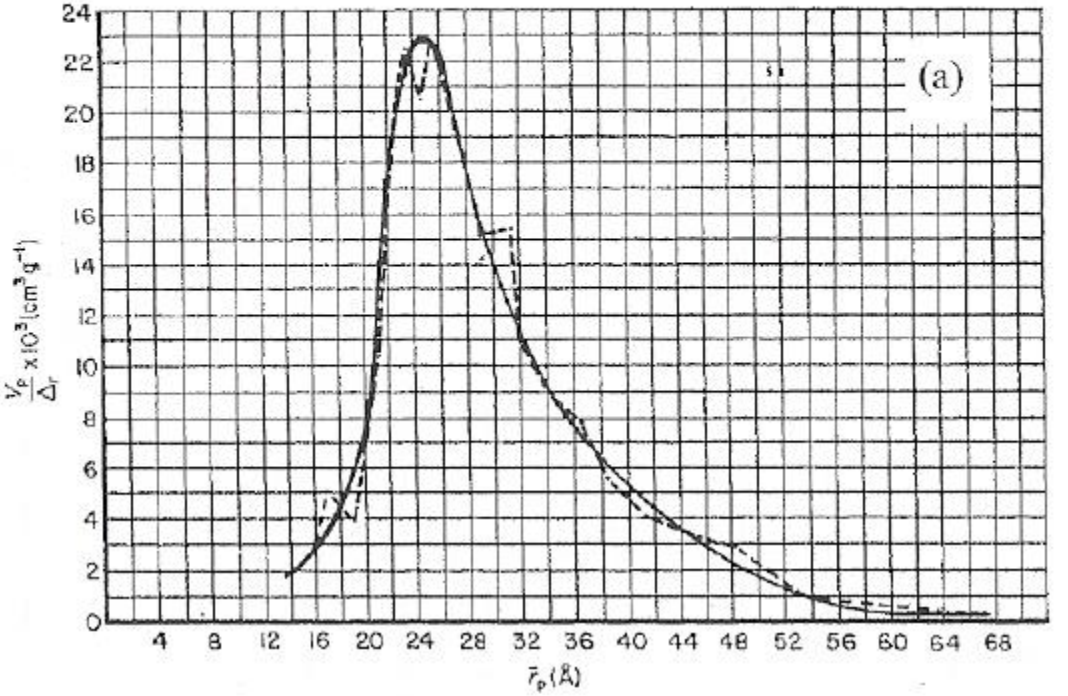
(a)
$\frac{V_p}{\Delta r} \times 10^3 (cm^3 g^{-1})$
$\bar{r}_p$ (Å)

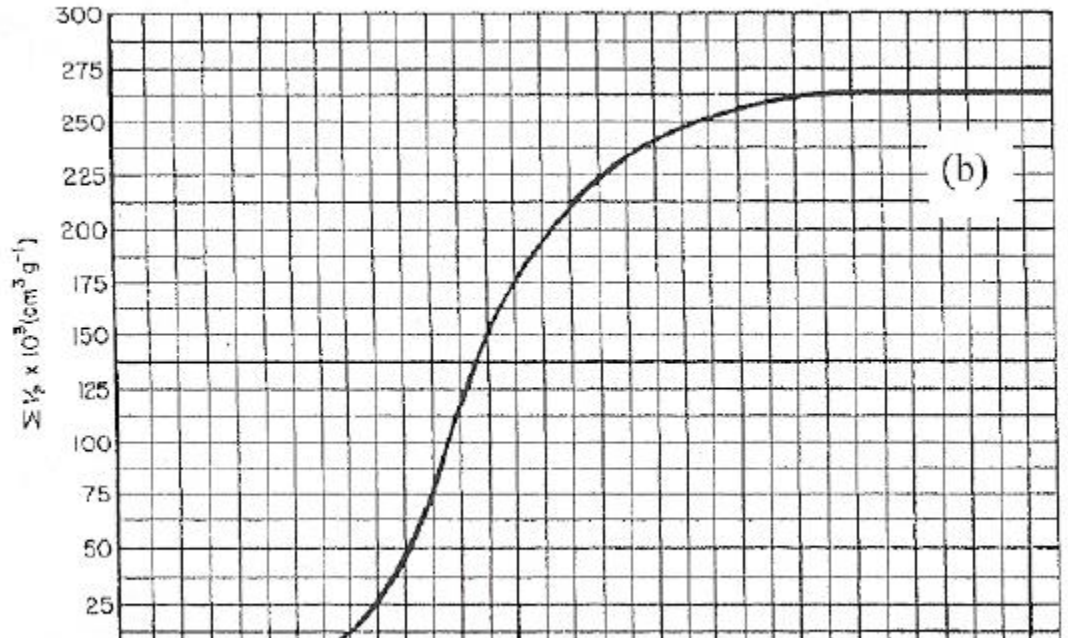
(b)
$\Sigma V_p \times 10^3 (cm^3 g^{-1})$

Why hysteresis? Which branch to use?

The shape of the isotherm does not depend only on the texture of the porous material, but also on the differences of the thermodynamic states between the confined fluid and the bulk fluid

H1 - independent cylindrical pores (MCM-41, SBA-15)

„Independent pore model“

- Pore condensation is associated with metastable states of the pore fluid in ordered materials
- The **desorption branch** of the hysteresis loop reflects the equilibrium phase transition
- Methods, which describe the equilibrium phase transition (**BJH**) have to be applied to the desorption branch
- (Applicable also to three-dimensional network of pores)

H2, H3 – disordered, connected pores

Origin of hysteresis not yet completely understood

- Pore blocking (inkbottle pores) associated with the desorption process
- Analysis of the **adsorption branch** (**NLDFT**-spinodal condensation method, Kelvin equation based approach calibrated for the adsorption branch)

Micropores	Width* [nm]	Pore filling governed by
Supermicropores	0.7 ~ 2	Gas-solid interactions Cooperative mechanism
Ultramicropores	< 0.7	Bilayer thickness of the N_2 molecule! Gas-solid interaction

Micropore filling is a continuous process and different from pore condensation in mesopores

Adsorption potential theories (0.4 nm ~)

Classical methods based on macroscopic, thermodynamic assumptions

- Polanyi
- Dubinin (DR method)
- Stoeckli
- Horvath-Kawazoe

Density Functional Theory

Monto Carlo simulations

Empirical methods (0.7~2nm)

t-method

MP-method

α_s-method

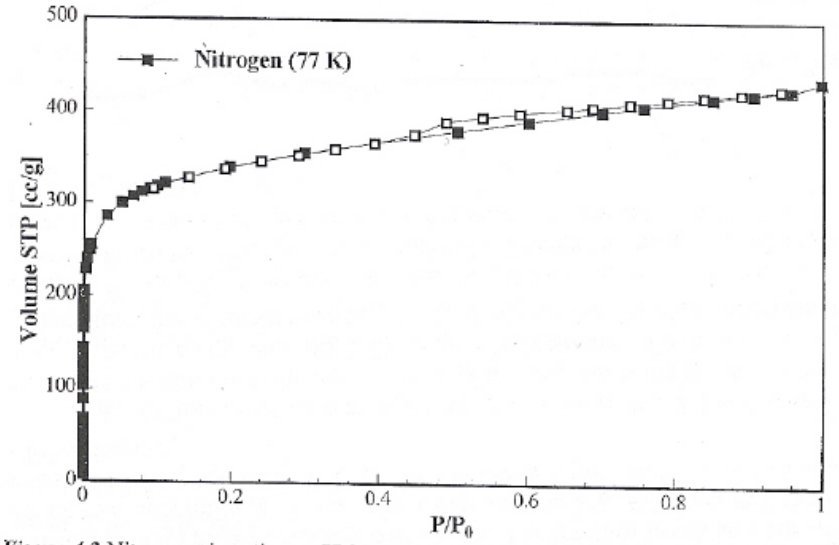

Figure 4.2 Nitrogen adsorption at 77.35 K on an active carbon sample, which contains, in addition to its microporosity, some mesoporosity indicated by the occurrence of hysteresis and the fact that the adsorption isotherm does not reveal a truly horizontal plateau at relative pressures > 0.1; the observed slope being associated with the filling of mesopores.

Assumption

The thickness of the absorbed film on pore walls is uniform → statistical thickness *t*

$$t = 3.54 \frac{W_a}{W_m} \text{Å} = \frac{V_{liq}}{S} \times 10^4 \text{ Å} \qquad (N_2, 77 \text{ K})$$

It has been shown for type II isotherms that a plot of the volume adsorbed versus t gives a staight line throug the origin

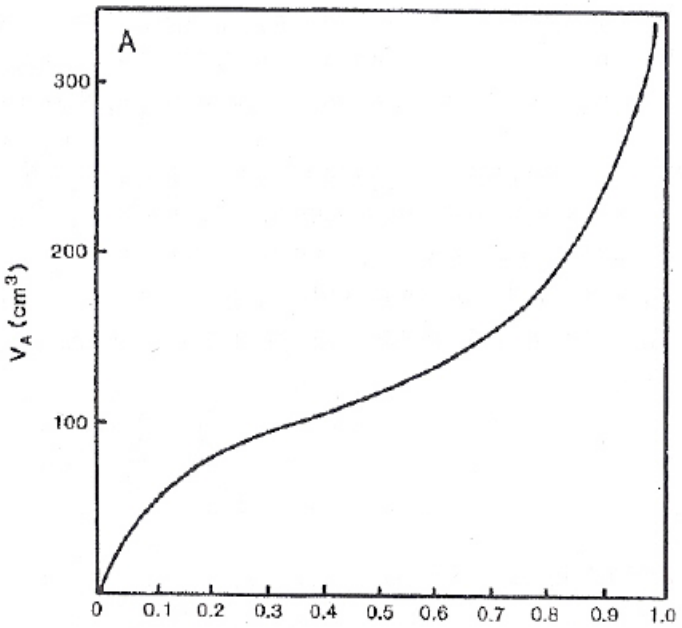

V-t curve

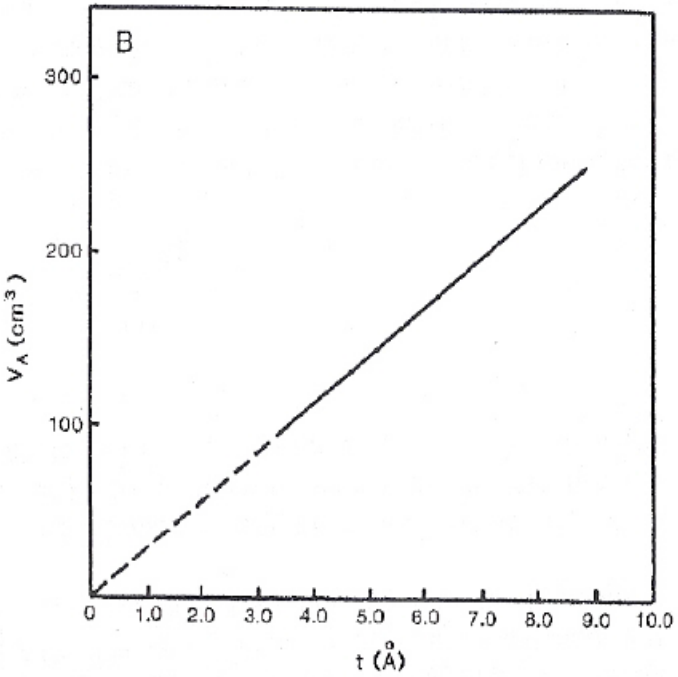

In absence of micropores surface areas calculated from the slope comparable to BET values

rinciple

Comparing an isotherm of a microporous material with a standard type II isotherm of a onporous absorbent with BET C constants similar to that of the microporous sample

Plot of the reference isotherm as a t-curve: $V_{ads}=f(t)$

The t values are in practice calculated with the help of thickness equations that desribe the articular standard reference curve

Siliceous materials

$$t = \left[\frac{13.99}{\log(p/p_0) + 0.034}\right]^{\frac{1}{2}} \text{Å}$$

.H.De Boer *et al.*, J. Colloid Interface Sci. 21 (1966) 405.

C-like materials

$$t = 0.88(p/p_0)^2 + 6.45(p/p_0) + 2.98 \text{ Å}$$

STM standard D-6556-01

Intercept: Volume of micropores

$V_{micro} = i \times 0.001547\ cm^3$

Slope: Surface area of micropores

$$t = \frac{V_{liq}}{S} \times 10^4\ \text{Å}$$

$S_t = s \times 15.47\ m^2/g$

nonporous material: $S_t = S_{BET}$
microporous material: $S_t = S_{ext}$

$S_{micro} = S_{BET} - S_{ext}$

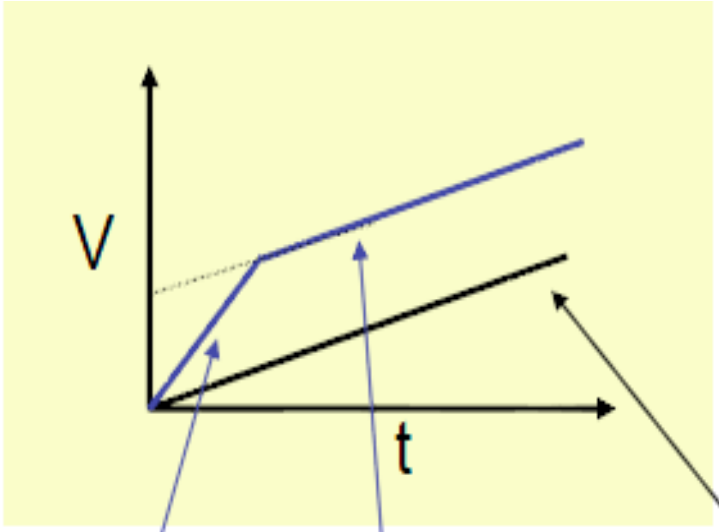

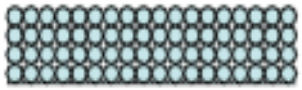

no micropores

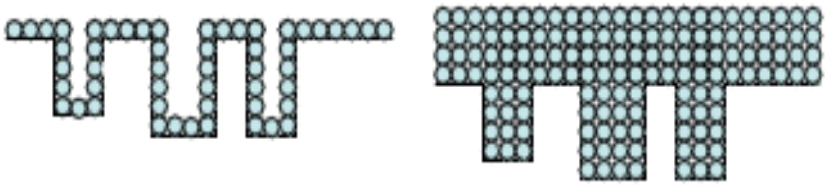

with micropores

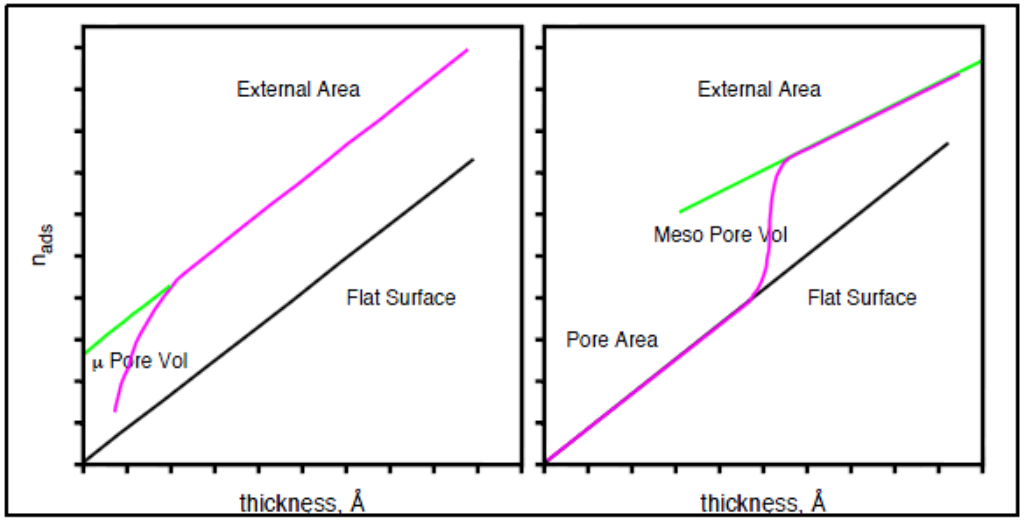

- Low ”t” slope is area
- Intercept is meso pore volume
- High ”t” slope is external area

- Slope of a linear region corresponds to area
- Intercept from a linear region is a pore volume
- Based on BET surface area

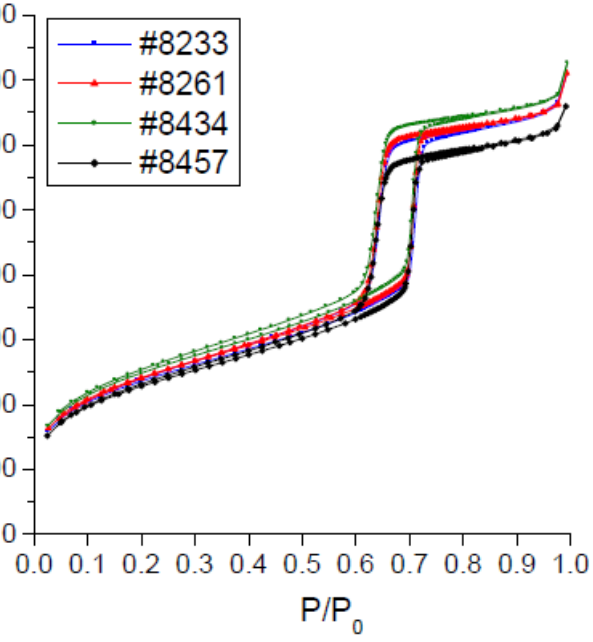
#8233
#8261
#8434
#8457
0.0 0.1 0.2 0.3 0.4 0.5 0.6 0.7 0.8 0.9 1.0
P/P0

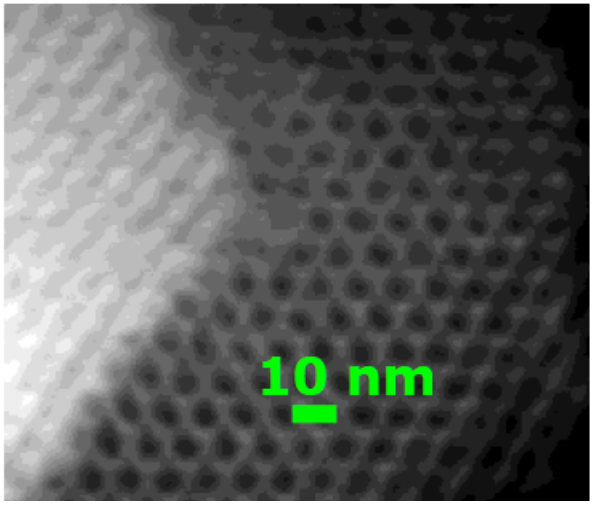
10 nm

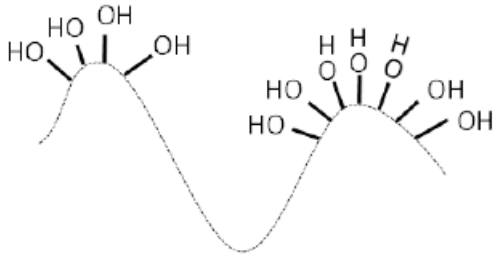
HO
OH
HO
OH
H
O
H
O
H
O
HO
HO
OH
OH

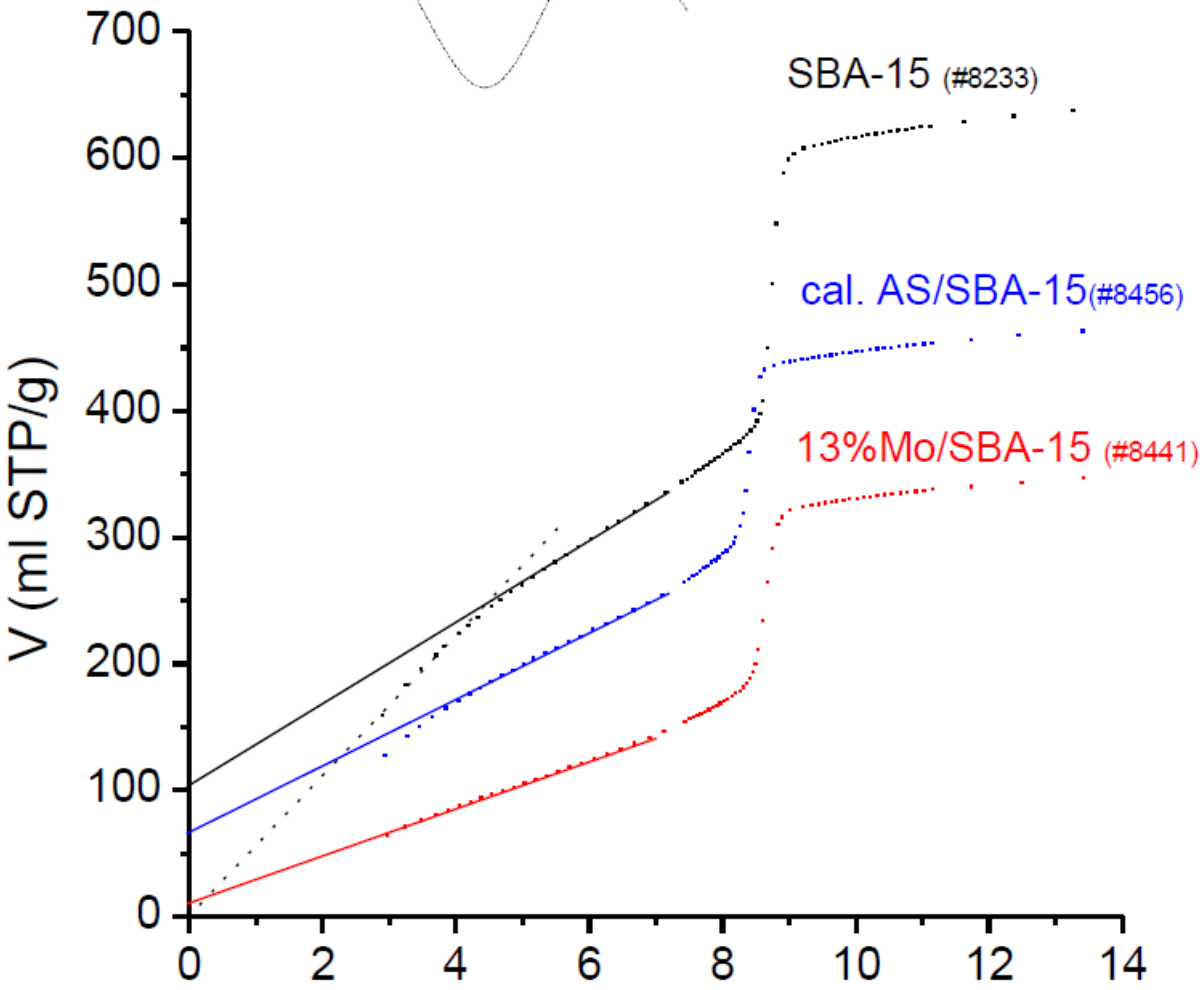
V (ml STP/g)
0
100
200
300
400
500
600
700
0
2
4
6
8
10
12
14
SBA-15 (#8233)
cal. AS/SBA-15(#8456)
13%Mo/SBA-15 (#8441)

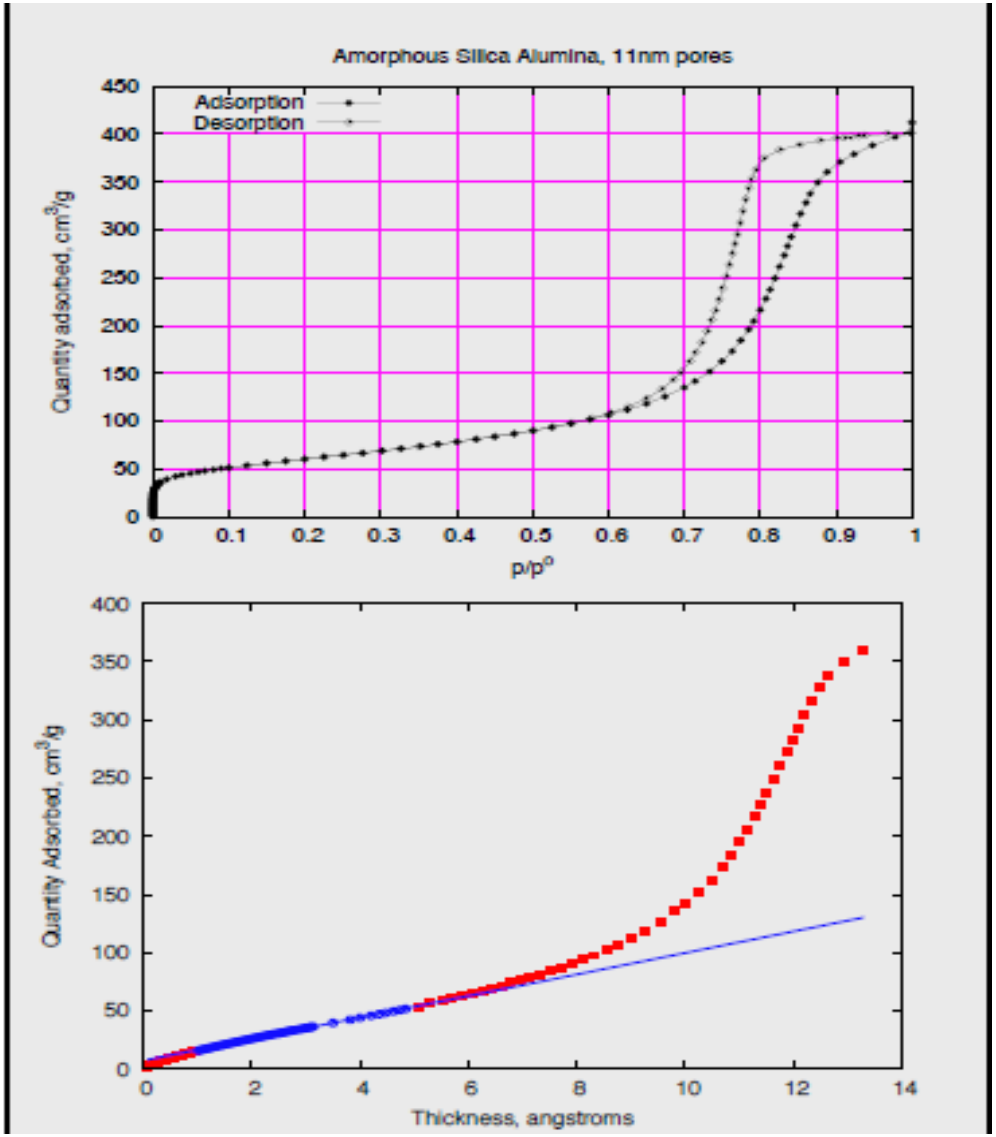
Amorphous Silica Alumina, 11nm pores
Adsorption
Desorption
Quantity adsorbed, cm3/g
p/p°
Quantity Adsorbed, cm3/g
Thickness, angstroms

α_s plot

$$\alpha_s = \frac{n_a}{n_{0.4}} \qquad t = \frac{V_a}{V_m} \times 0.354[\text{nm}]$$

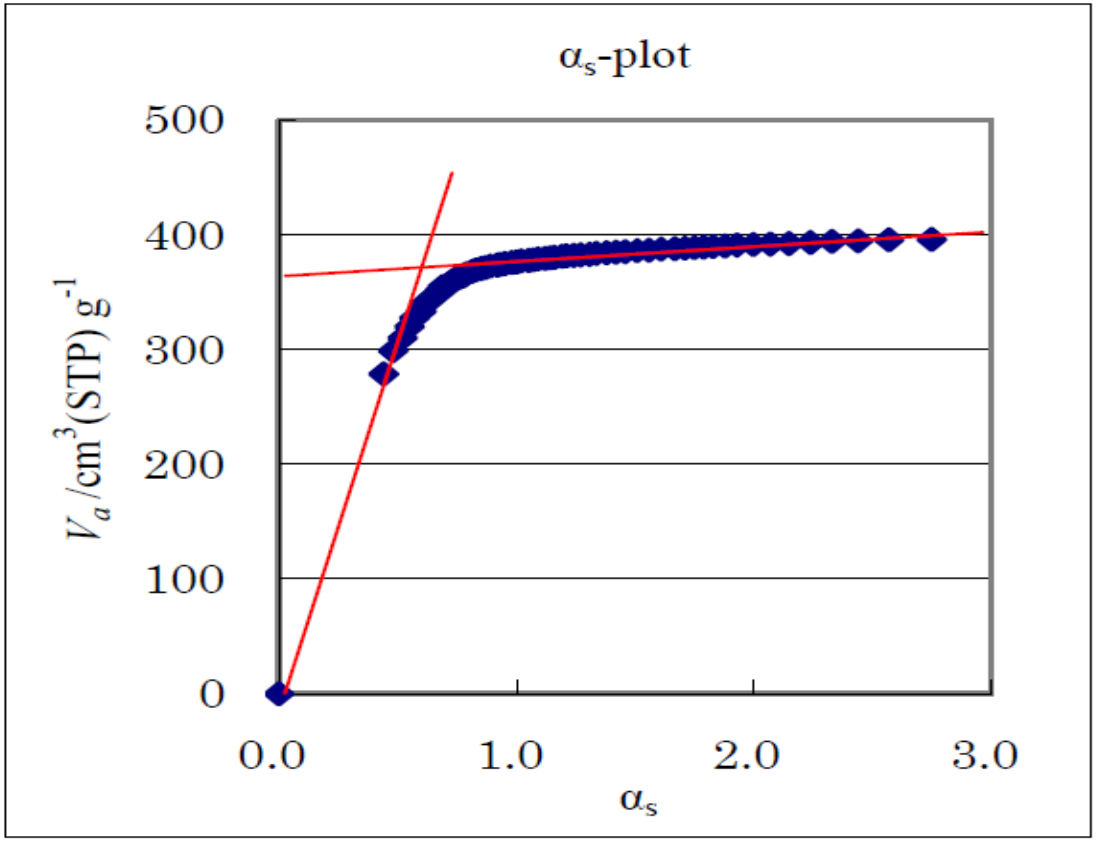

براورد حجم و محیط میکرو حفره بدون داشتن ضخامت آماری

Properties of MoO_x/SBA-15

Mo loading [a] (wt%)	Surface Mo density (nm^{-2})		A_s (m^2/g)	A_μ [e] (m^2/g)		V_p [g] (ml/g)	d_p [h] (nm)
	Mo [b] (nm^{-2})	Isolated SiOH [c, d] (nm^{-2})			($\%$) [f]		
0	0	1.6 [c]	859	261	36	1	7.5
2.1	0.21	1.1 [d]	637	164	31	0.79	7.1
5.1	0.58	0.88 [d]	554	127	28	0.71	7.1
6.6	0.85	0.68 [d]	490	135	28	0.61	7.1
9.7	1.09	0.39 [d]	556	96	21	0.78	7.2
13.3	2.51	0.07 [d]	332	36	13	0.55	7.4

[a] by XRF, [b] Mo loading (at%) divided by A_s, [c] by TG, [d] by IR at the dehydrated state using relative heights of the silanol peak at 3745cm^{-1}, [e] micropore (< ~0.9 nm of width) surface estimated by *t*-plot method, [f] A_μ divided by A_S, [g] at $P/P_0 = 0.95$, [g] at the dehydrated state; [h] estimated by NLDFT approach.

α_s plot

- رفتار متقابل بین جذب و جاذب زیرفشار 0.4 میباشد
- ار تئوری اثبات شده که حلقه پسماند زیر این فشار بسته میشود
- اگر اندازه ذرات زیر 3.5 نانومتر باشد t جواب نمیدهد
- S بدون دیمانسیون است
- سطح وی ه داخلی حفره از کم کردن حجم سطح خارجی از حجم کل بدست میاید

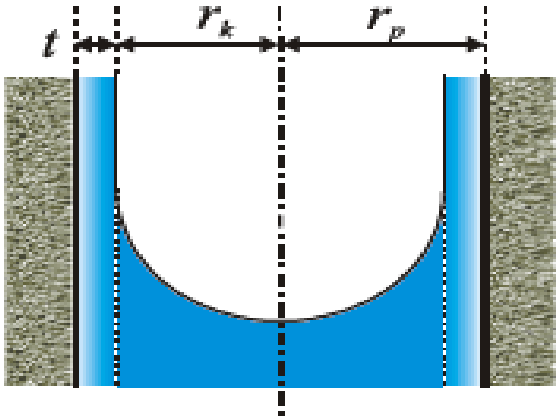

In the area where capillary condensation is in presence, radius of cyrinder shaped pore is sum of the thickness of adsorption layer at the arbitrary pressure (t) and core radius (r^k) of meniscus part.

$$r_p = t + r_k \tag{18.1}$$

Thickness of adsorption layer can be calculated from t curve of standard sample, and core radius can be calculated by Kelvin equation (18.2).

$$\ln\frac{p}{p_0} = -\frac{2\gamma V_L}{RT}\frac{1}{r_m} \tag{18.2}$$

Here, r_m is meniscus radius, γ is surface tension, V_L is molar volume of liquid adsorptive, R is gas constant and T is absolute temperature. In mesopore with cyrinder shape, suppose menisucus radius at desorption is equal to core radius (r_k), and if γ and V_L of nitrogen at liquid nitrogen temperature (77 K) are applied, the following equation can be obtained.

$$r_m = 0.953/\ln(p_0/p) \tag{18.3}$$

$$\Delta V_{liq} = \frac{\Delta V_{gas}}{22.4\times10^{3}}\times 34.6 = \Delta V_{gas}\left(1.54\times10^{-3}\right)\ \text{cm}^3$$

$$\Delta V_{liq} = \pi \bar{r}_k^{\,2}\ell + \Delta t \Sigma S$$

$$V_p = \pi \bar{r}_p^{\,2}\ell$$

$$V_p = \left(\frac{\bar{r}_p}{\bar{r}_k}\right)^2\left[\Delta V_{liq} - \left(\Delta t \Sigma S\times10^{-4}\right)\right]\ \text{cm}^3$$

$$S = \frac{2V_p}{\bar{r}_p}\times10^{4}\ \text{m}^2$$

$$t = 3.54\left(\frac{5}{\ln(P_0/P)}\right)^{1/3}\ \text{Å} \qquad r_k = \frac{4.15}{\log(P_0/P)}$$

1	2	3	4	5	6	7	8	9	10	11	12	13	14
$\frac{P}{P_0}$	V_{gas} STP (cm^3/g)	r_k (Å)	T (Å)	r_p (Å)	$\bar{r}_k$ (Å)	$\bar{r}_p$ (Å)	Δt (Å)	ΔV_{gas} STP (cm^3/g)	$\Delta V_{liq}\times10^3$ (cm^3/g)	$\Delta t\Sigma S\times10^3$ (cm^3/g)	$V_p\times10^3$ (cm^3/g)	S (m^2/g)	ΣS (m^2/g)
0.99	161.7	950	28.0	978									
0.98	161.5	473	22.2	495	711	737	5.8	0.2	0.31	0.00	0.33	0.01	0.01
0.97	161.0	314	19.4	333	394	414	2.8	0.5	0.77	0.00	0.85	0.04	0.05
0.95	160.2	186	16.3	202	250	268	3.1	0.8	1.23	0.02	1.40	0.10	0.15
0.90	158.8	90.7	12.8	104	138	153	3.5	1.4	2.16	0.05	2.59	0.34	0.49
0.85	157.2	58.8	11.1	69.9	74.8	87.0	1.7	1.6	2.46	0.08	3.22	0.74	1.23
0.80	155.2	42.8	10.0	52.8	50.8	61.4	1.1	2.0	3.08	0.14	4.30	1.40	2.63
0.77	152.9	36.6	9.5	46.1	39.7	49.5	0.5	2.3	3.54	0.13	5.30	2.14	4.77
0.75	148.9	33.2	9.2	42.4	34.9	44.3	0.3	4.0	6.16	0.14	9.70	4.38	9.15
0.73	145.1	30.4	8.9	39.3	31.8	40.9	0.3	3.8	5.85	0.27	9.22	4.51	13.66
0.71	140.9	27.9	8.7	36.6	29.2	38.0	0.2	4.2	6.47	0.27	10.49	5.52	19.18
					26.9	35.4	0.3	5.0	7.70	0.58	12.34	6.97	26.15

$$V = \frac{Ad}{4}$$

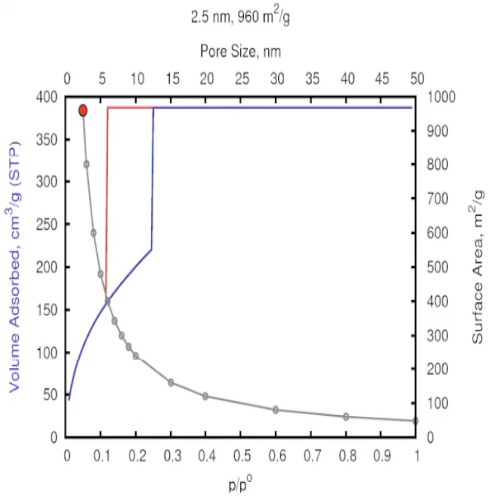

$$A = \frac{4V}{d}$$

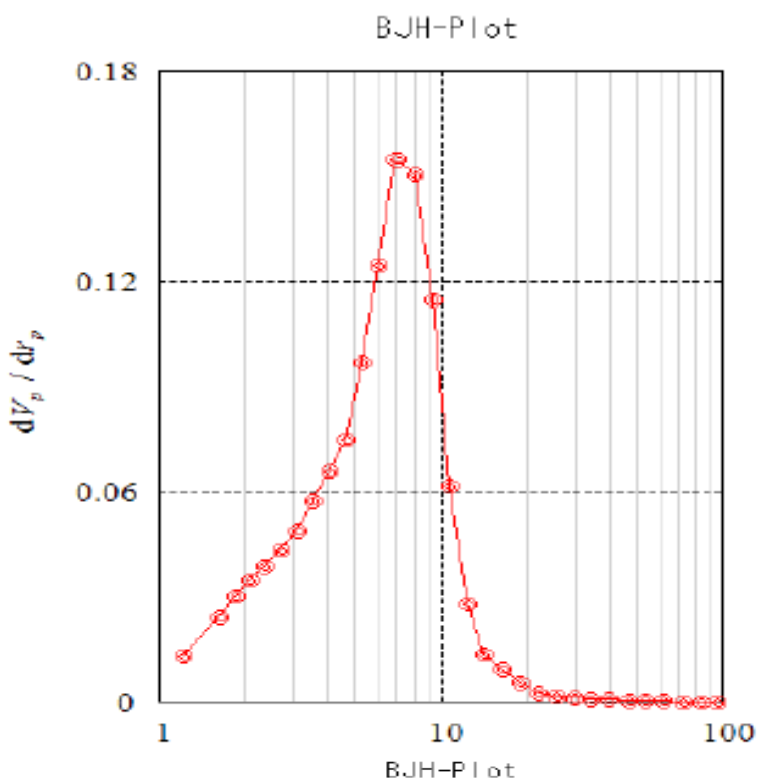

SAMPLE03.DAT(ADS)

V_p [cm³ g⁻¹]	1.0640
$r_{p,peak}$(Area) [nm]	7.99
a_p [m² g⁻¹]	338.88

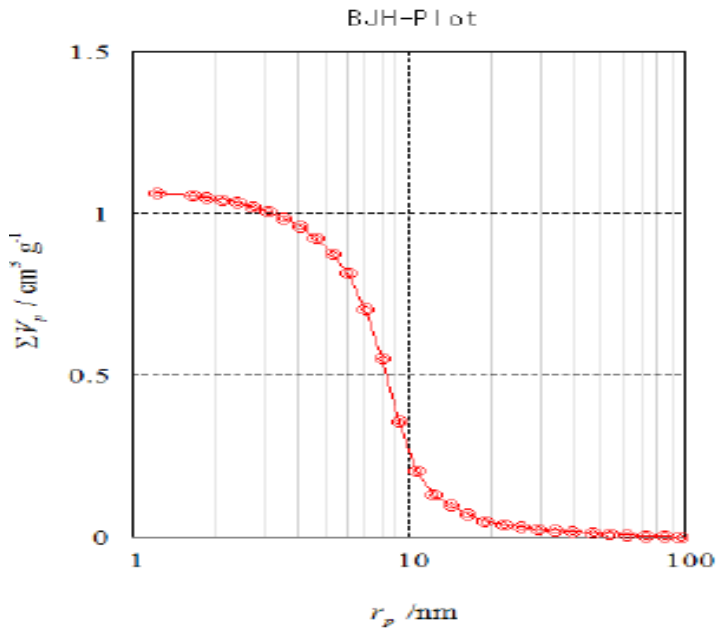

SAMPLE03.DAT(ADS

V_p [cm³ g⁻¹]	1.0640
a_p [m² g⁻¹]	338.88

Amorphous Silica-alumina

- BJH
- From Δpore volume and calculated diameter, we can estimate surface area for a cylinder
- Common to observe the BJH estimate of area is greater than the BET estimate

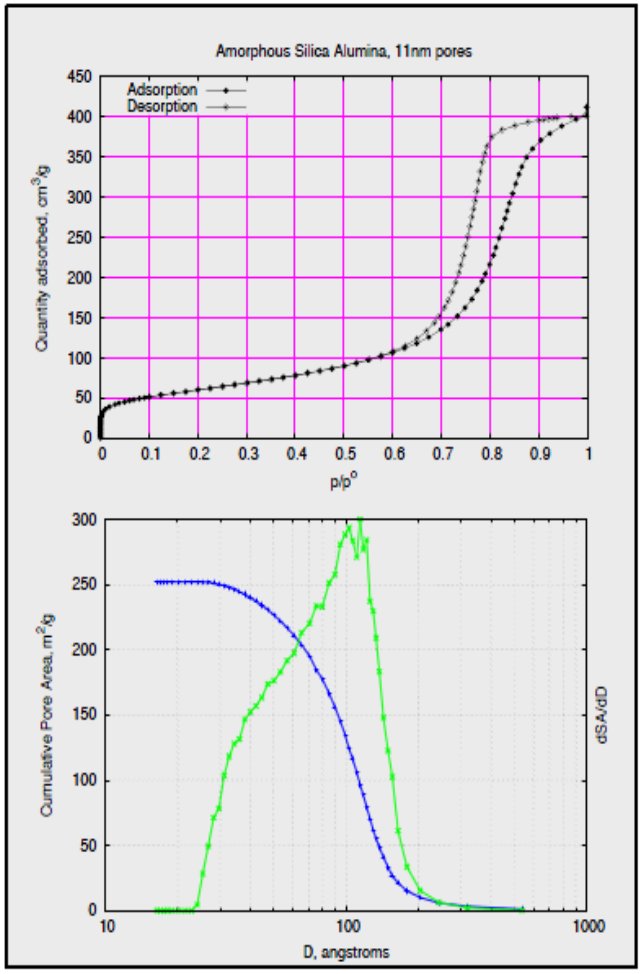

BJH - PVD
Pt/Al_2O_3

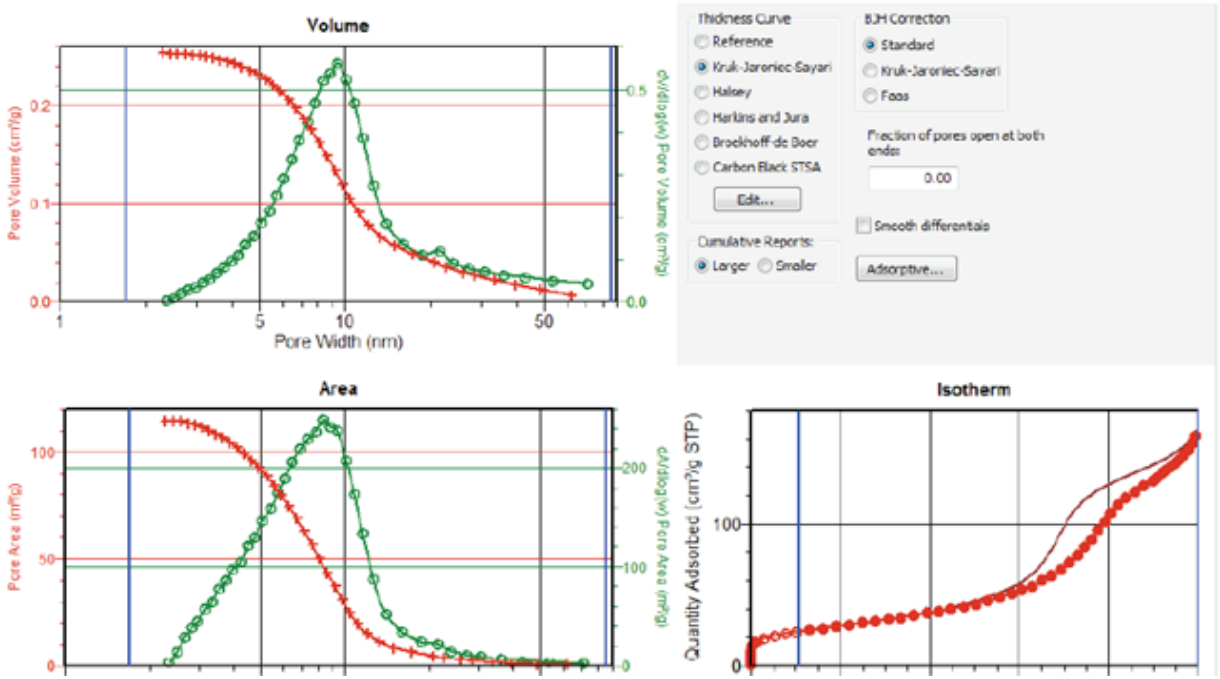

Amorphous Silica-Alumina

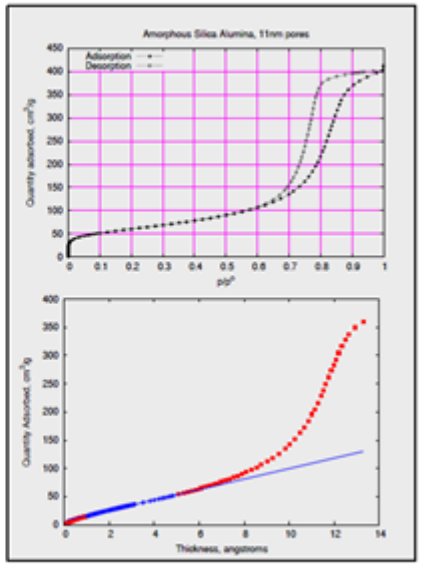

- Negligible micro-pore volume
- Capillary condensation at large “t” values

t-Plot for 13X

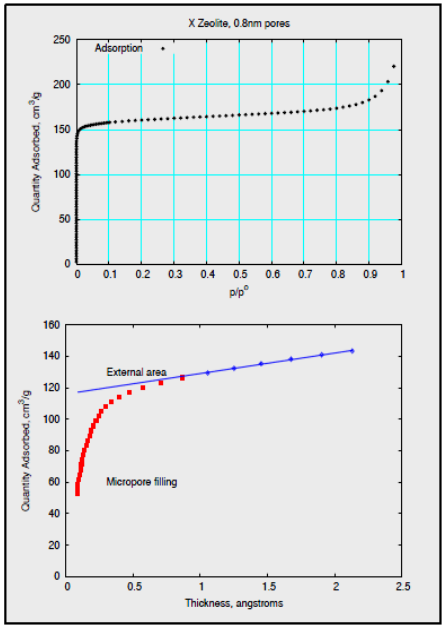

- Reference curve
- “0” intercept

مقایسه بین ایزوترم

SiO_2	SiO_2-Al_2O_3	MCM-41
100 nm pores	11 nm pores	4 nm pores
25.7 m^2/g	215.5 m^2/g	926.8 m^2/g

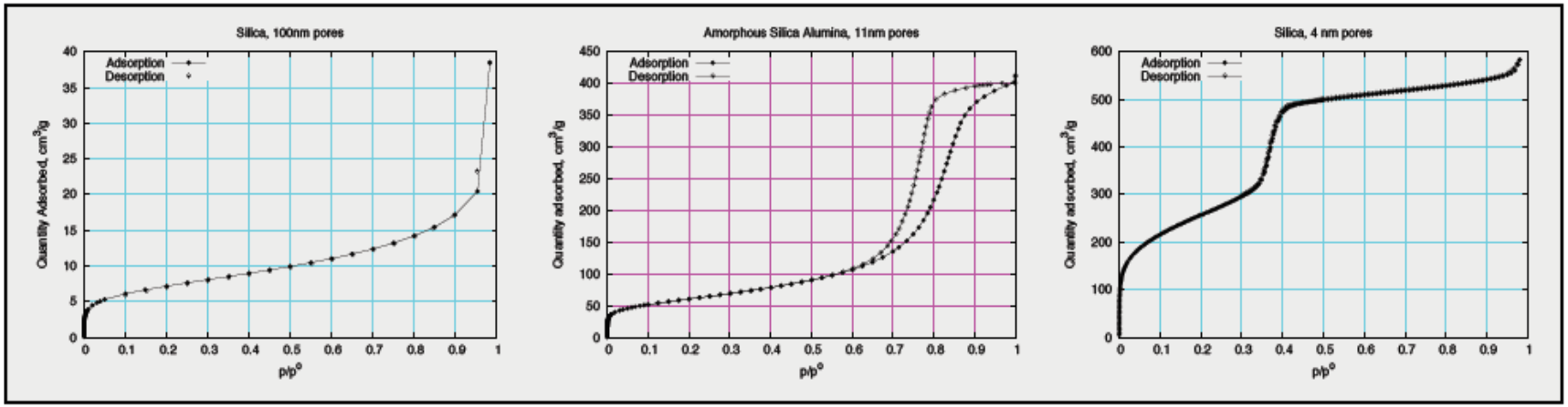

منفذو پسماند

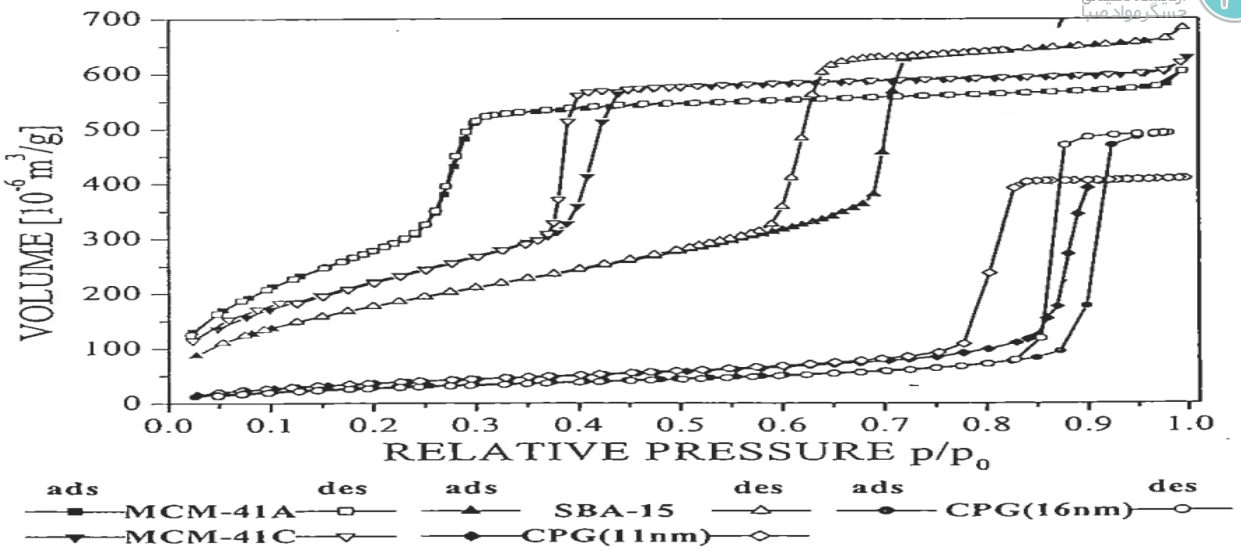

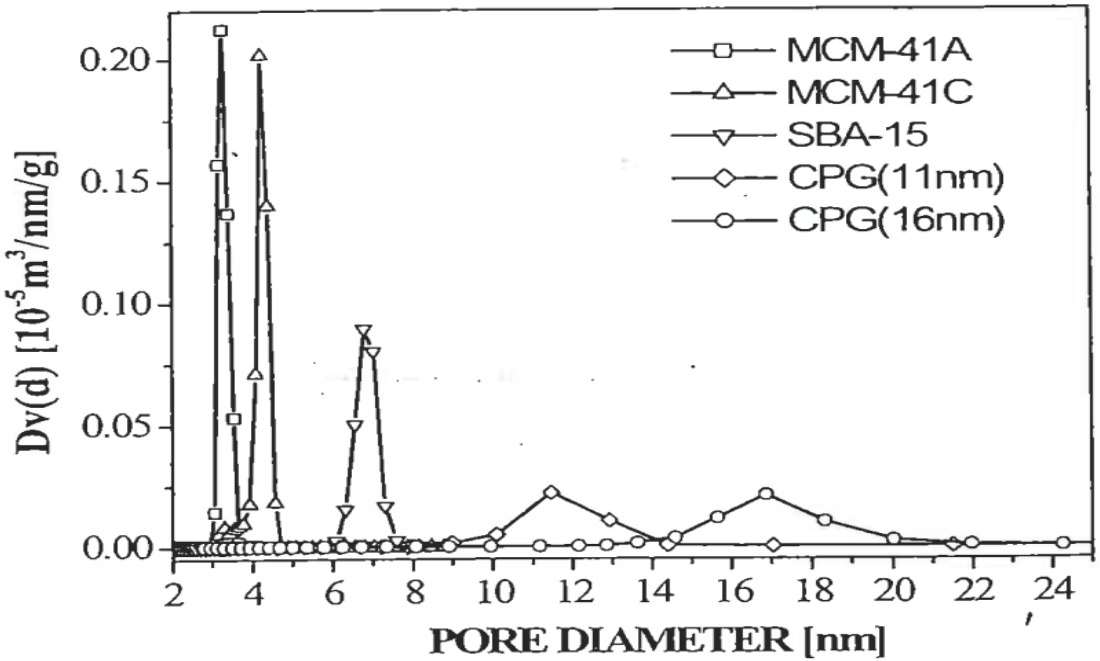

رابطه پسماند با اندازه منفذ

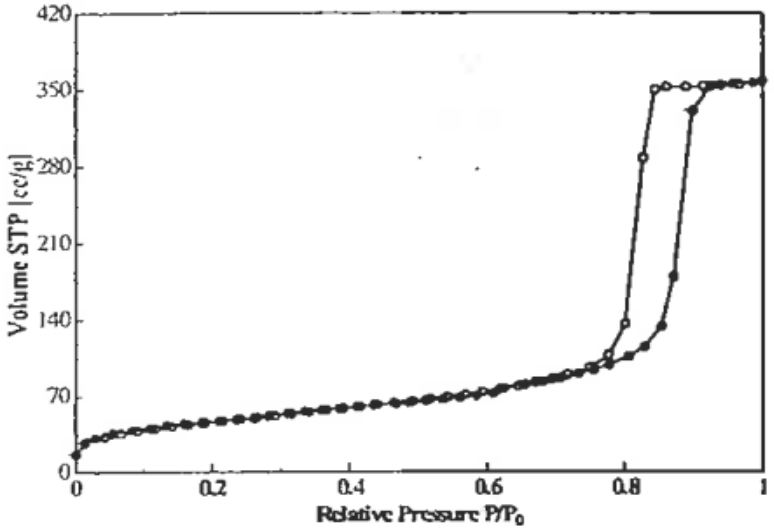

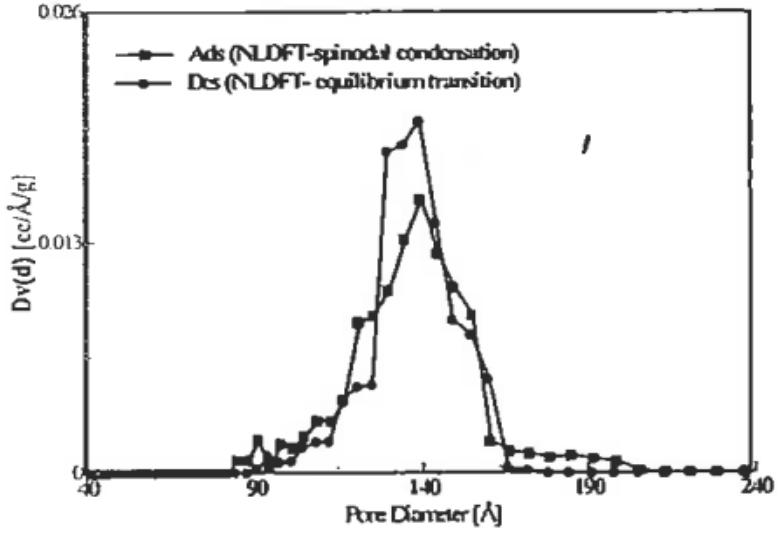

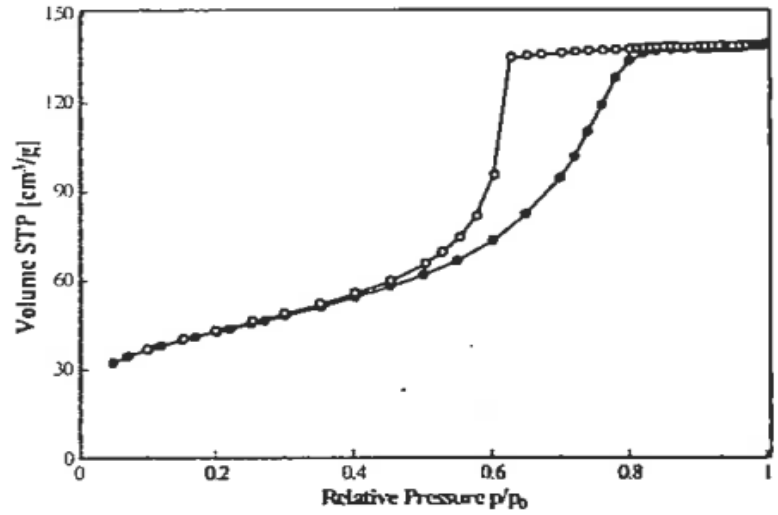

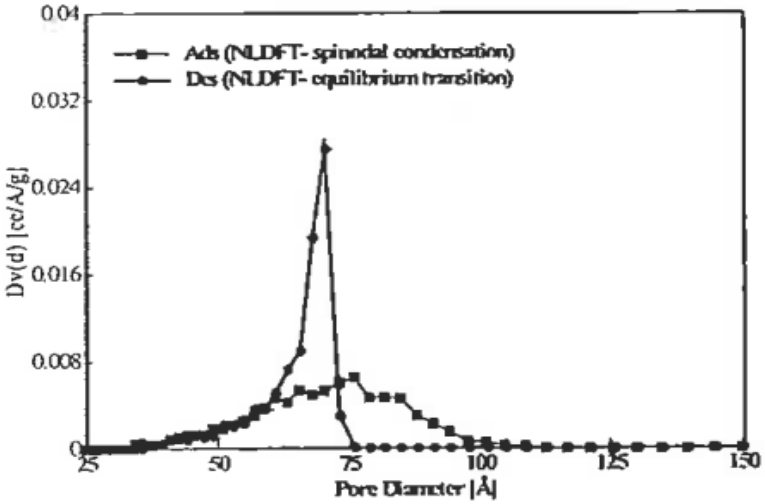

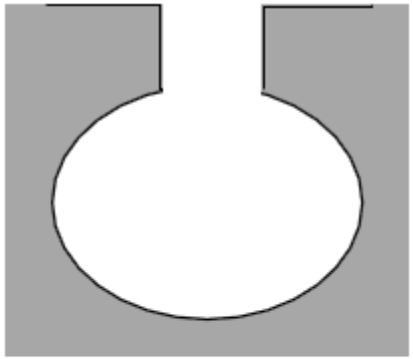

But in some cases, you obtain $\sum S >$ BET S.A, indicating the presence of ink-bottle pores.

You use a small r and a correct ΔV_{liq} to estimate the surface area, $S = \frac{2 \cdot \Delta V}{r}$

(you should use the adsorption isotherm to calculate pore size distribution)

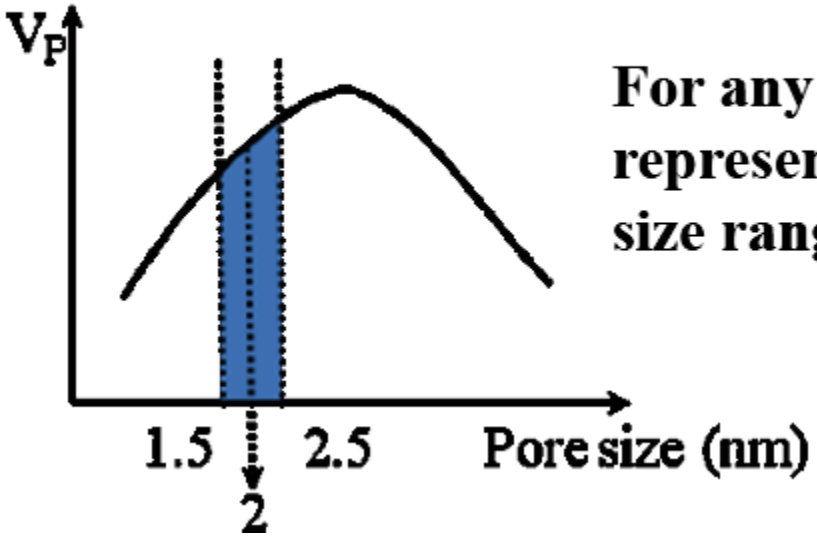

For any distribution, the integrated area represents the volume within the pore size range.

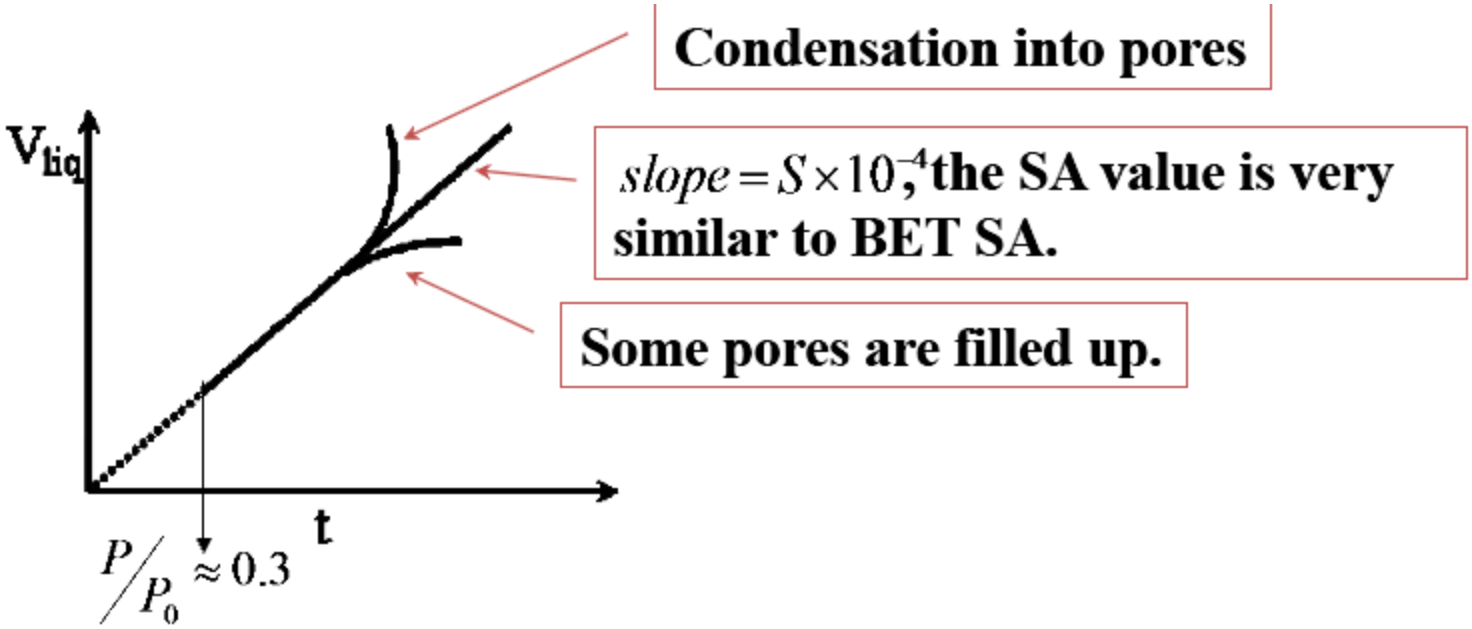

9. Microporosity

9.1. Introduction

Pore diameter analyzed by Kelvin eq. 15-1000 Å

Dubinin's definition:

Pore diameter > 1000 Å macropores

15–1000 Å transitional (Kelvin)

< 15 Å micropores

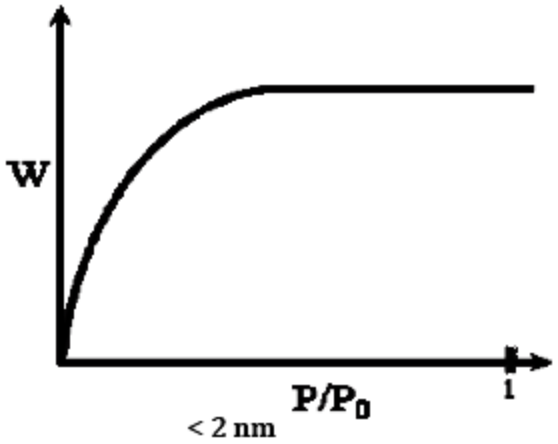

∴ in micropore regime, pore filling starts from the pores with larger over potentials (or adsorption energy).

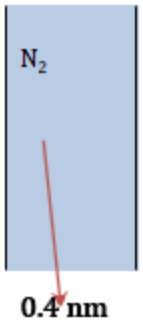

Because the pore size is so small, once a molecule is attached to the pore wall, the pore size reduction will initiate the filling of the pore. (no layering behavior in micropores.)

9.2. Langmuir Plots for Microporous Surface Area

∵ adsorption in micropores belongs to Type I, Langmuir equation can describe the isotherm.

$$\frac{P}{W} = \frac{1}{KW} + \frac{P}{W} \qquad \frac{P}{W} \text{ vs. P} \rightarrow \frac{1}{W_m} \Rightarrow St = \frac{W_m \bar{N} A}{\bar{M}}$$

In reality, adsorption in micropores is not monolayer, and Langmuir usually over estimates the S.A.

9.3. Polanyi's Theory for Micropore Volume and Area

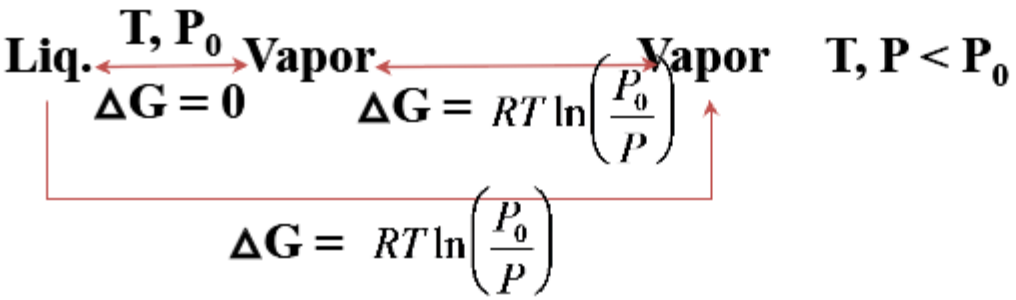

Polanyi's potential theory of adsorption

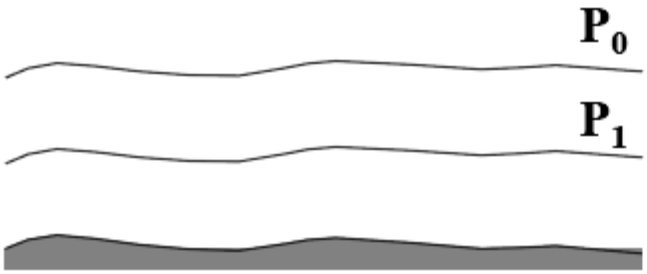

Adsorption represents that adsorbates can be trapped on surfaces with energies between E_n and E_s

$P\uparrow \Rightarrow$ adsorption potential required $\downarrow$

$P = P_0 \Rightarrow$ adsorption potential required = 0

P is very small $\Rightarrow$ required potential is large

Let adsorption vol. $\tilde{V} = \frac{W}{\rho}$ **W= f(P/P$_0$)**
E = f(P/P$_0$)

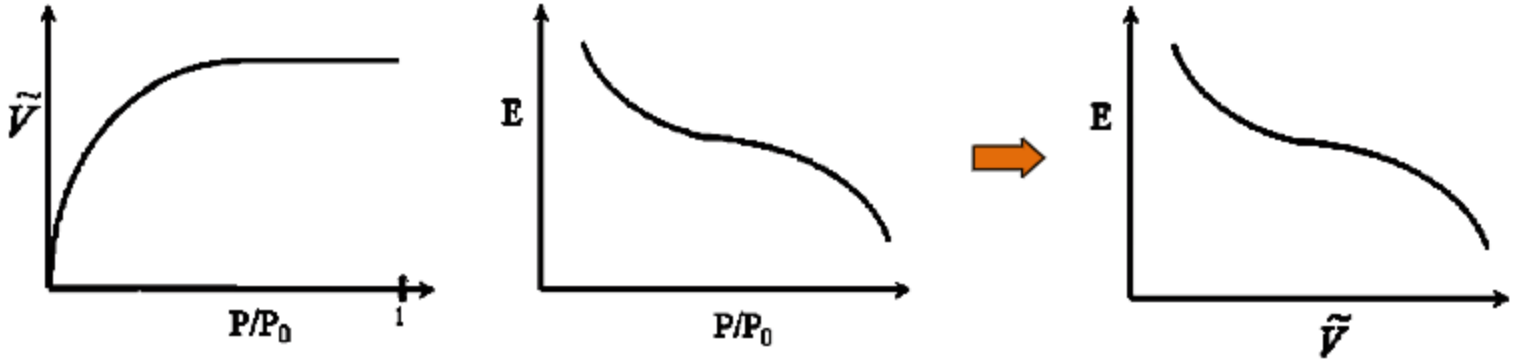

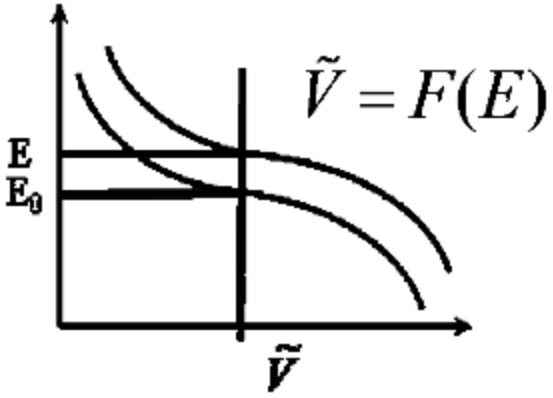

Characteristic curve for different adsorbates.

At the same $\tilde{V}$ **value,** $\frac{E}{E_0}$ **represents the relative affinity**

Dubinin assumed that E/E$_0$ are constant at different $\tilde{V}$ **values,**

$$\frac{E}{E_0} = \beta = affinity\ coefficient$$

log(W) vs. $[\log(P_0/P)]^2$ $\xrightarrow{\text{intercept}}$ $\log(W_0)$ → $\tilde{V}_0 = \dfrac{W_0}{\rho}$

at $P/P_0 = 10^{-5} \sim 10^{-1}$, give good linear fit for DR eq.

$$\tilde{V} = \tilde{V}_0 \cdot e^{-KE_0^2}$$

Let $K = \left(\dfrac{1}{\varepsilon_0}\right)^2$

When $E_0 = \varepsilon_0$ => $\tilde{V} = \tilde{V}_0 \cdot e^{-1} = 0.368 \cdot \tilde{V}_0$

ε_0 is called the characteristic adsorption energy.

For slit-like micropores

Stoeckli:

$$L(nm) = \frac{10.8}{\varepsilon_0(kJ \cdot mol^{-1}) - 11.4}, \quad S_{mi}(m^2 g^{-1}) = \frac{2000 \cdot \tilde{V}_0(cm^3 g^{-1})}{L(nm)}$$

9.4 The t-method

de Boer et al. used microporous material isotherm and standard type II isotherm

t-method to determine micropore vol. and surface area

de Boer equation

$$t(\text{Å}) = \left(\frac{13.99}{\log \frac{P_0}{P} + 0.034} \right)^{\frac{1}{2}}$$

, standard t curve for N_2 adsorption

t: statistical thickness on nonporous materials, but with C value close to that of microporous materials

for the standard sample

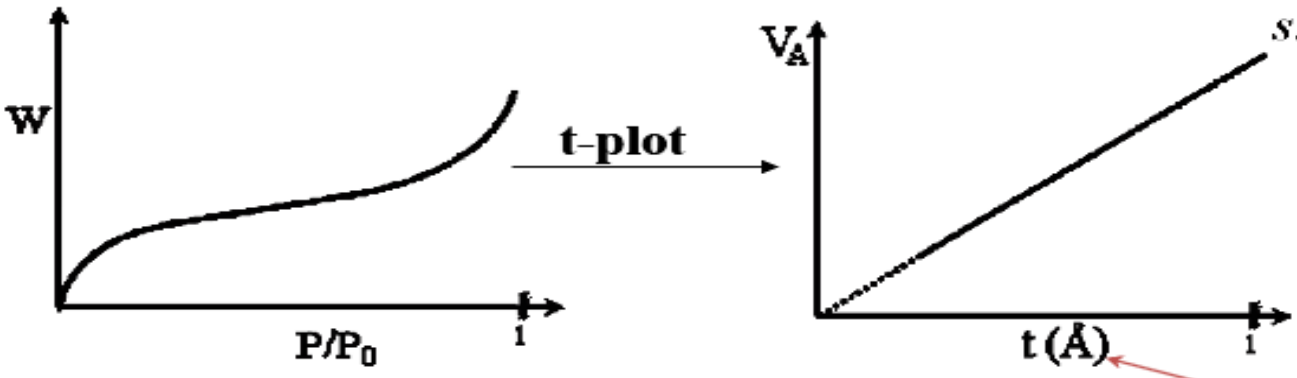

$$slope = \frac{S_t(m^2)}{10^4}$$

$$S_t(m^2) = \frac{V_{liq}(cm^3)}{t(\text{Å})} \times 10^4$$

de Boer

$$t = n\left(\frac{5}{\ln(P_0/P)}\right)^{1/3}(P/P_0)^m \qquad (2)$$

Parameter n is expected to vary between 0.35 and 0.45[8] while m is in the range 0–0.28.

Intercept: Volume of micropores

$V_{micro} = i \times 0.001547\ cm^3$

Slope: Surface area of micropores

$$t = \frac{V_{liq}}{S} \times 10^4\ \text{Å}$$

$S_t = s \times 15.47\ m^2/g$

nonporous material: $S_t = S_{BET}$
microporous material: $S_t = S_{ext}$

$S_{micro} = S_{BET} - S_{ext}$

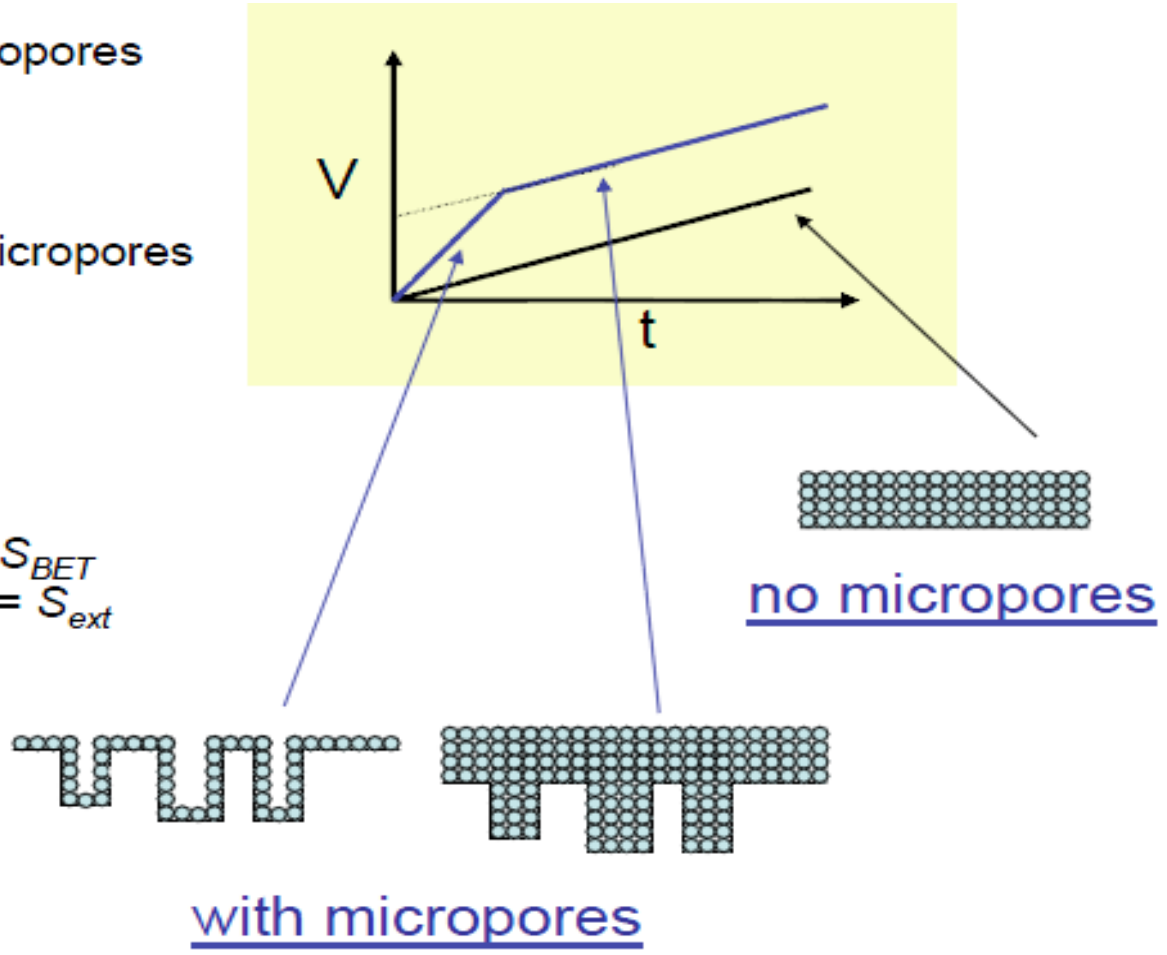

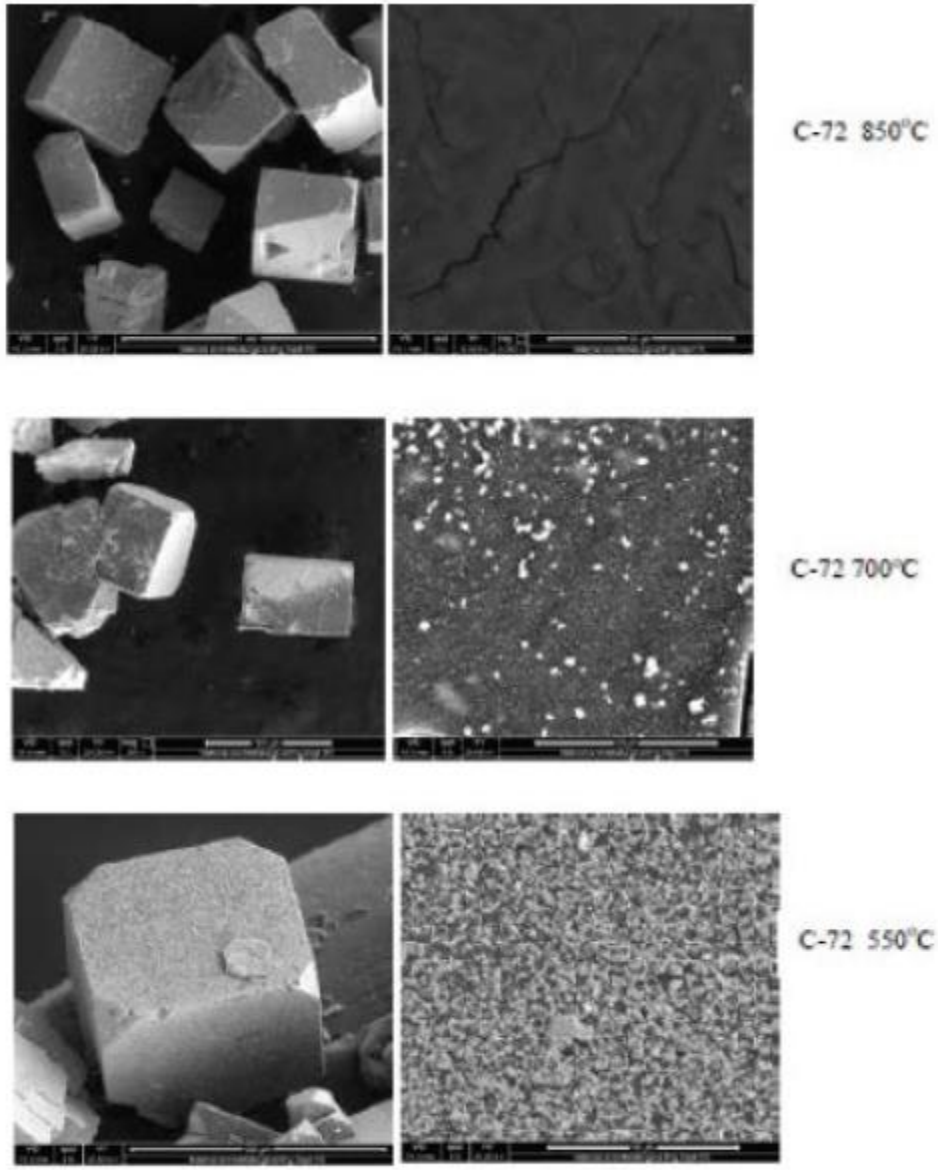

Figure 8. Micrograph of C-72 at various carbonation temperature

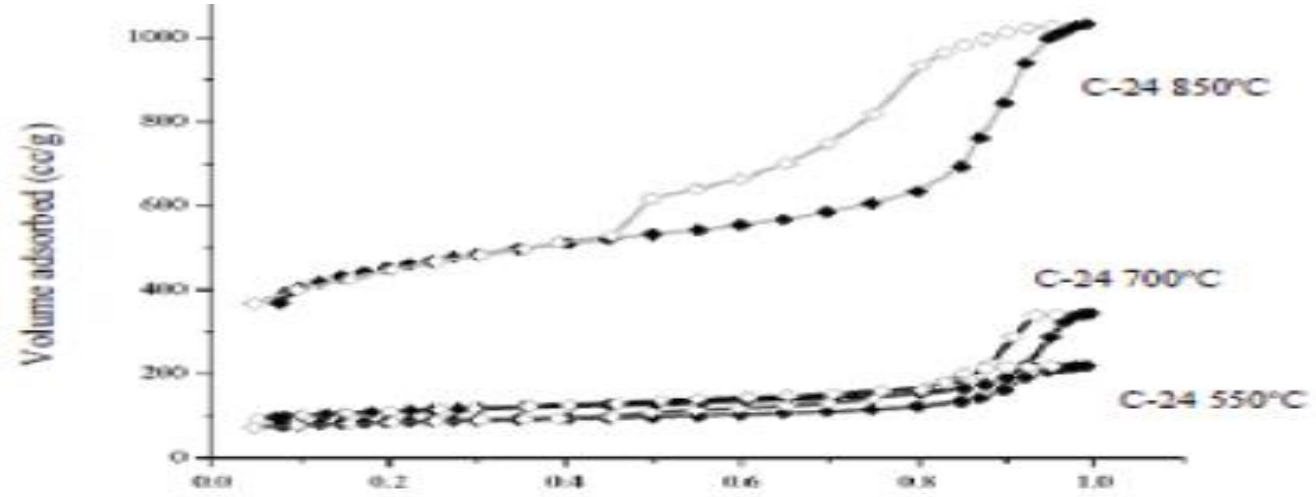

Figure 9. Isothermal adsorption-desorption C-24

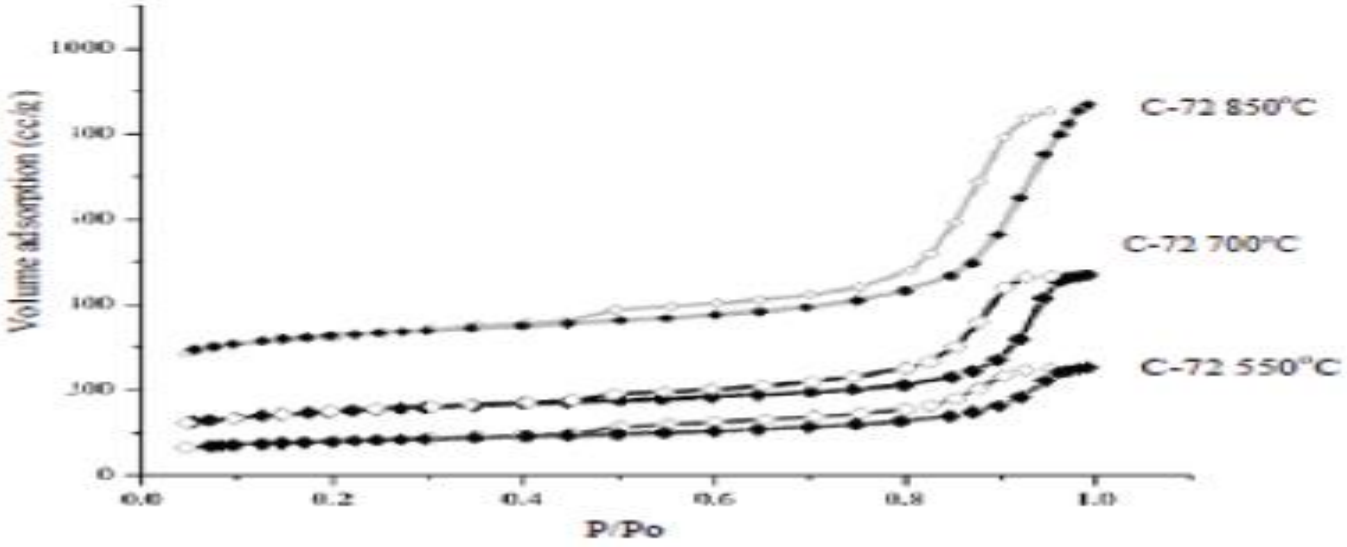

Figure 10. Isothermal adsorption-desorption C-72

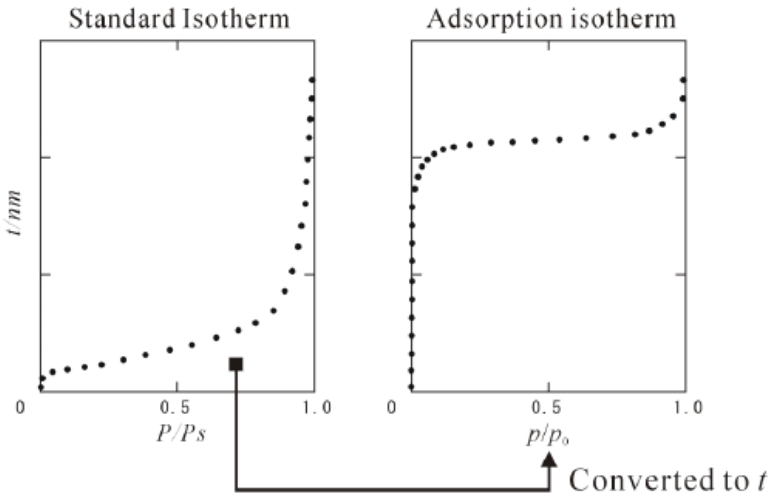

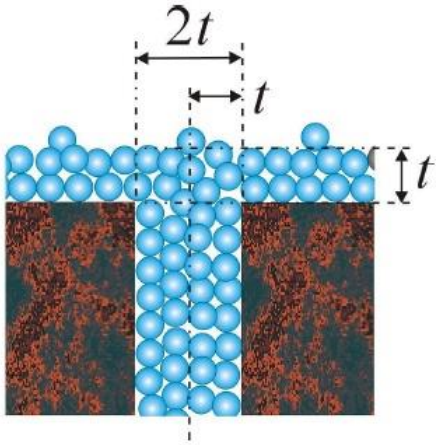

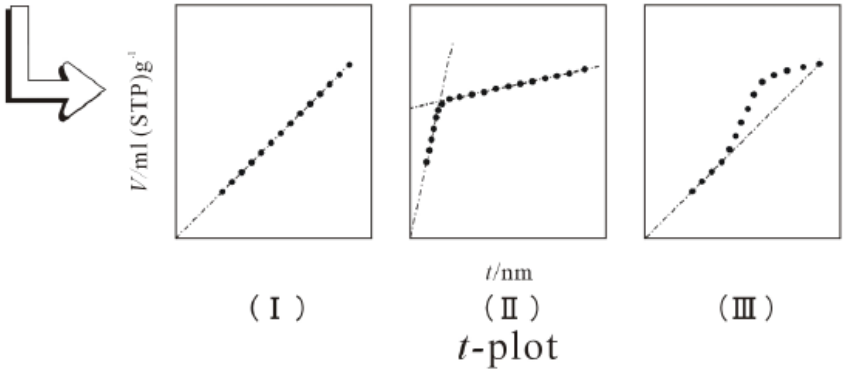

$$t = \frac{V_a}{V_m} \times 0.354[\text{nm}]$$

$$a_s = \frac{s \times 0.354}{22414} \times L \times \sigma = 1.541 \times s$$

Microporous + standard

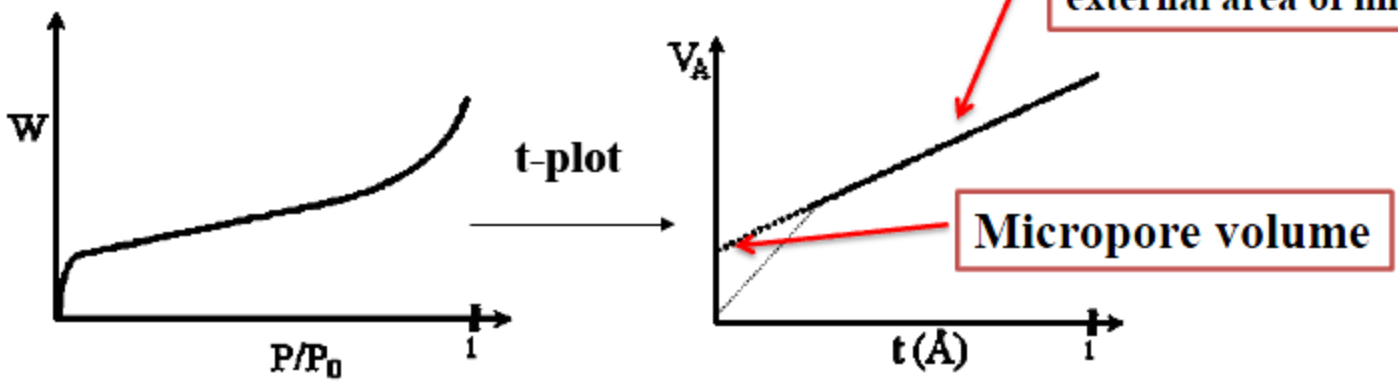

Microporous

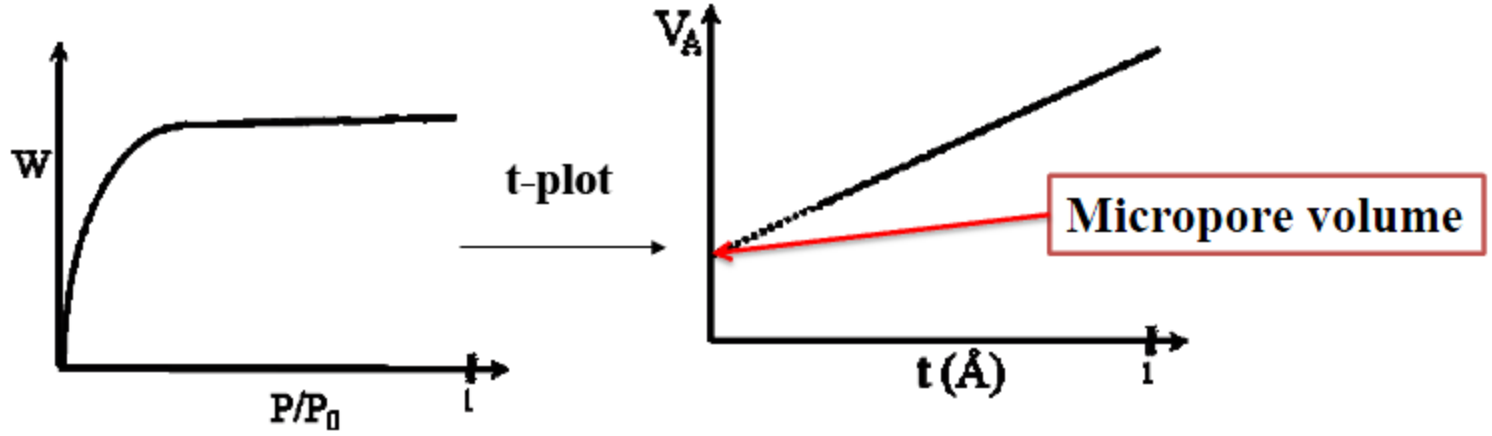

Mesoporous + standard

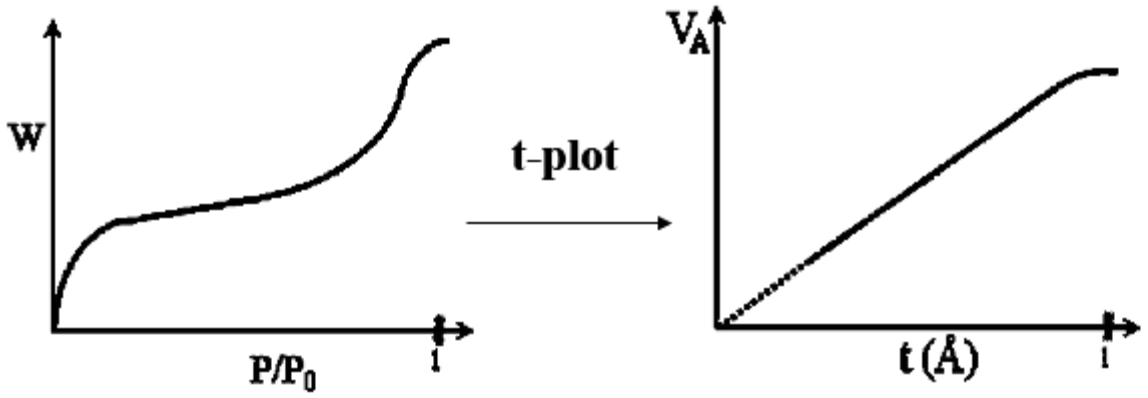

Micro+Meso

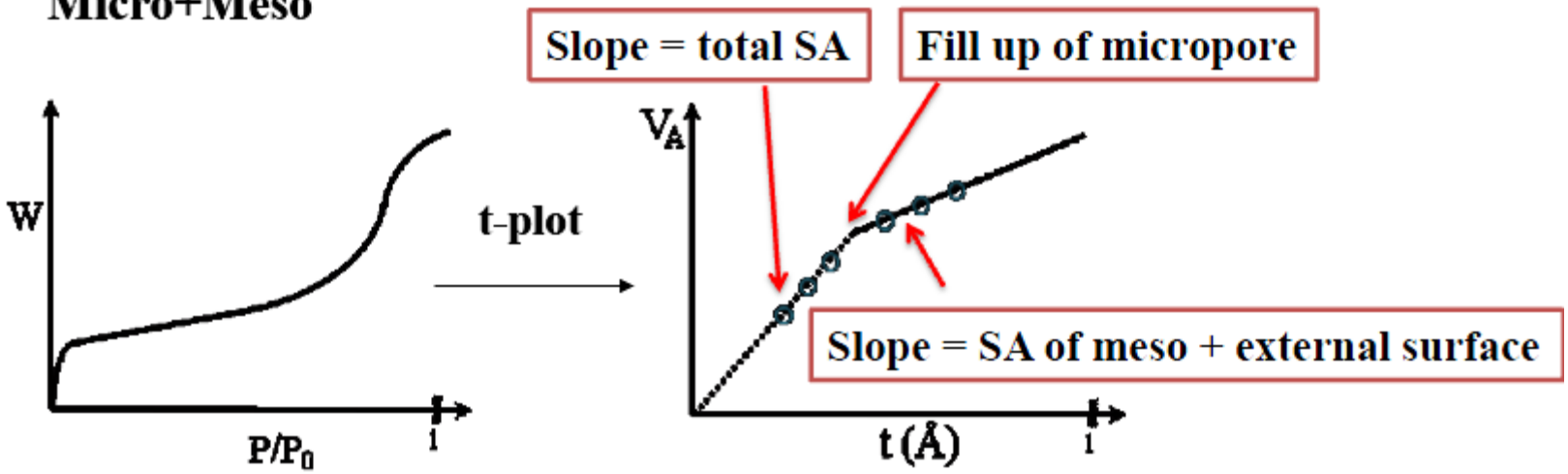

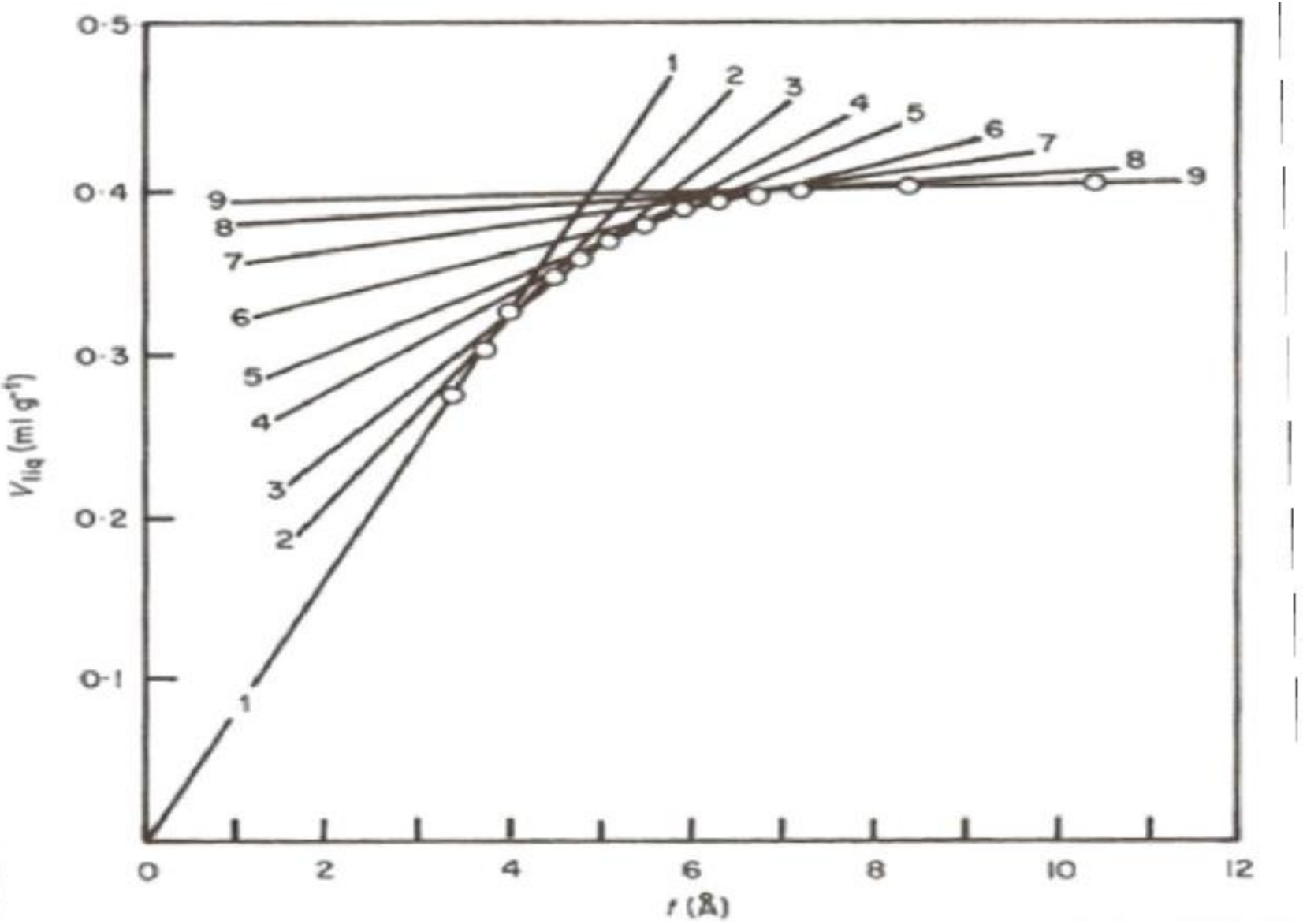
0·5
0·4
0·3
0·2
0·1
V_{liq} (ml g^{-1})
0
2
4
6
8
10
12
t (Å)
1
2
3
4
5
6
7
8
9

Slope of line 1 → S=792 m^2/g
0.0792 (>4Å)

Slope of line 2 → S=520 m^2/g
0.0520 (>4.5Å)

Slope of line 3 → S=360 m^2/g
0.0360 (>5Å)

$\Delta S = 160$, pores of 4.5~5Å are filled up

$\overline{r} = 4.75\text{Å}$, $V = \Delta S \cdot \overline{r} \times 10^4 \; cm^3/g = 0.076 \; cm^3/g$

The calculation is continued in this manner until there is no further decrease in the slope. $S_{min} = S_{ext}$

$\sum\Delta S$ = micropore SA $\sum V$ = micropore vol.

Table 9.1

Pore group	S_{i+1} (m^2/g)	$S_i - S_{i+1}$† (m^2/g)	mean r_h (Å)	V_i (cm^3/g)
1	520	272	4.25	0.1156
2	360	160	4.75	0.0760
3	280	80	5.25	0.0420
4	200	80	5.75	0.0460
5	140	60	6.25	0.0375
6	80	60	6.75	0.0405
7	20	60	7.25	0.0435
8	10	10	7.75	0.0077
		$\Sigma S_i = 782$		

BET area = 793 m^2/g
V–t area 782 m^2/g
Total Pore volume = 0.4034
MP pore volume = 0.4088

The authors attributed the difference between the V-t and BET areas to surfaces that did not lie within pores.

Slope of line 1 → S=792 m^2/g
0.0792 (>4Å)

Slope of line 2 → S=520 m^2/g
0.0520 (>4.5Å)

Slope of line 3 → S=360 m^2/g
0.0360 (>5Å)

ΔS = 160, pores of 4.5~5Å are filled up

$$\overline{r} = 4.75\text{Å}, \quad V = \Delta S \cdot \overline{r} \times 10^4 \; cm^3/g = 0.076 \; cm^3/g$$

The calculation is continued in this manner until there is no further decrease in the slope. $S_{min} = S_{ext}$

$\sum\Delta S$ = micropore SA $\sum V$ = micropore vol.

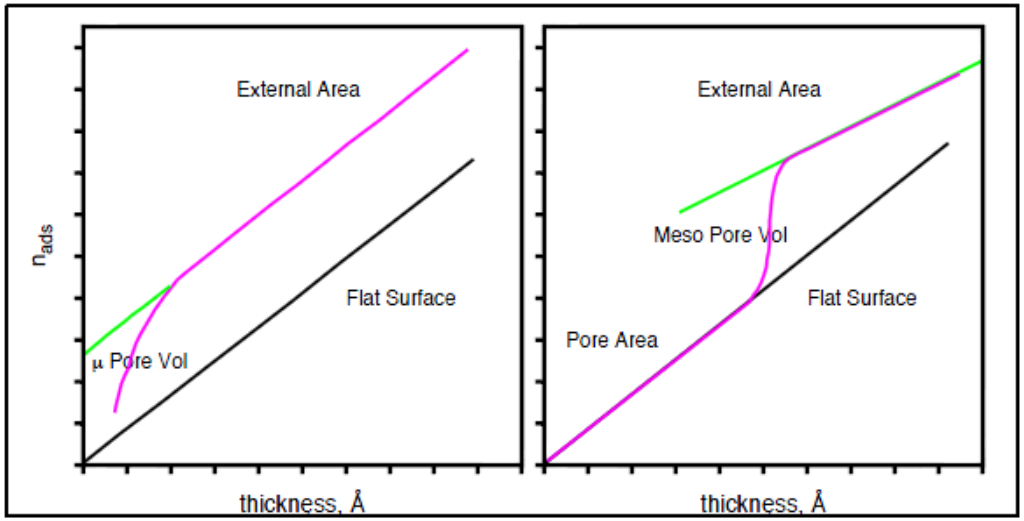

- Low ”t” slope is area
- Intercept is meso pore volume
- High ”t” slope is external area
- Slope of a linear region corresponds to area
- Intercept from a linear region is a pore volume
- Based on BET surface area

$$S_{micro} = \left[\left(\frac{V_{liq}}{t} \right)_{lower} - \left(\frac{V_{liq}}{t} \right)_{upper} \right] \times 10^4$$

or

$$S_{micro} = S_{BET} - \left(\frac{V_{liq}}{t} \right)_{upper} \times 10^4$$

9.6 The micropore analysis method (MP method)

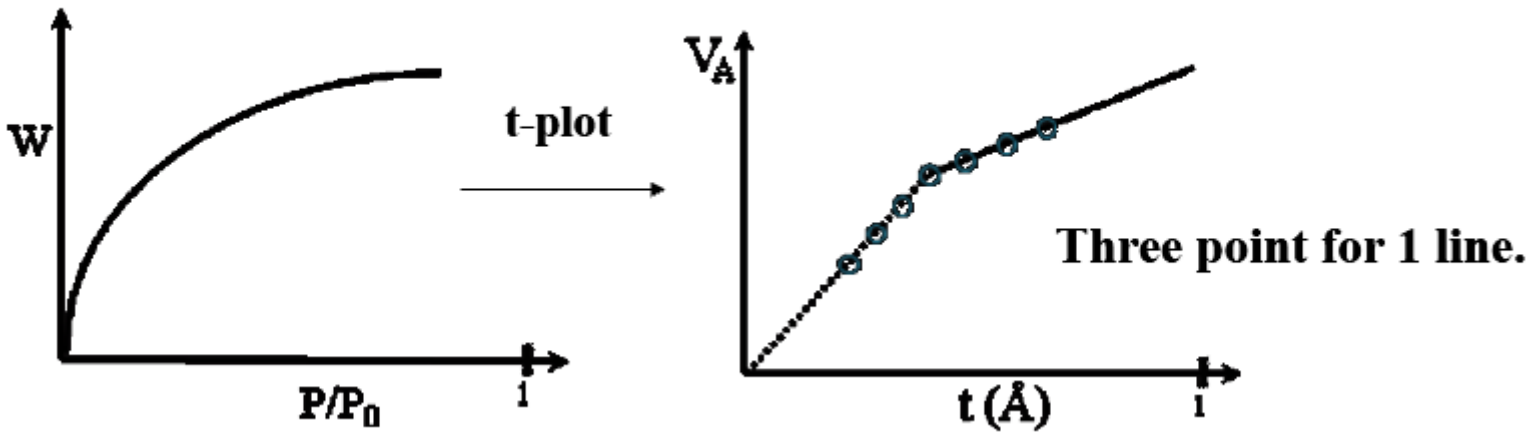

Amorphous Silica-Alumina

- Negligible micro-pore volume
- Capillary condensation at large “t” values

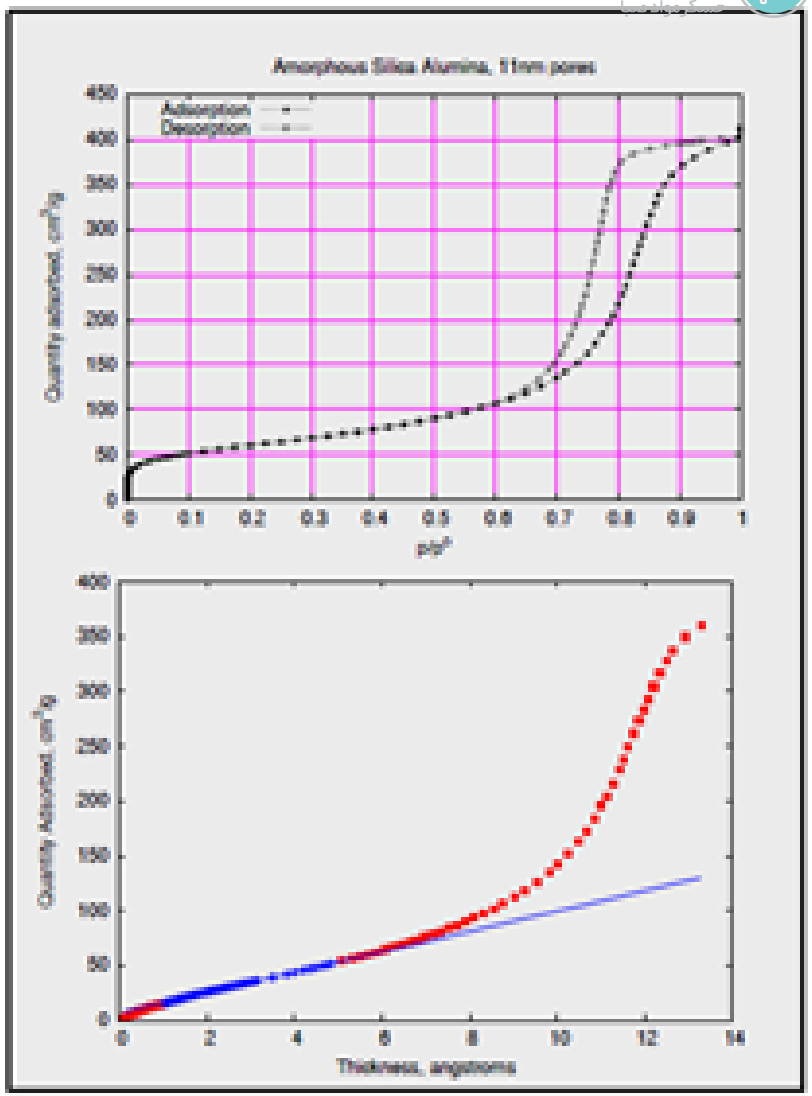

t-Plot for 13X

- Reference curve
- “0” intercept

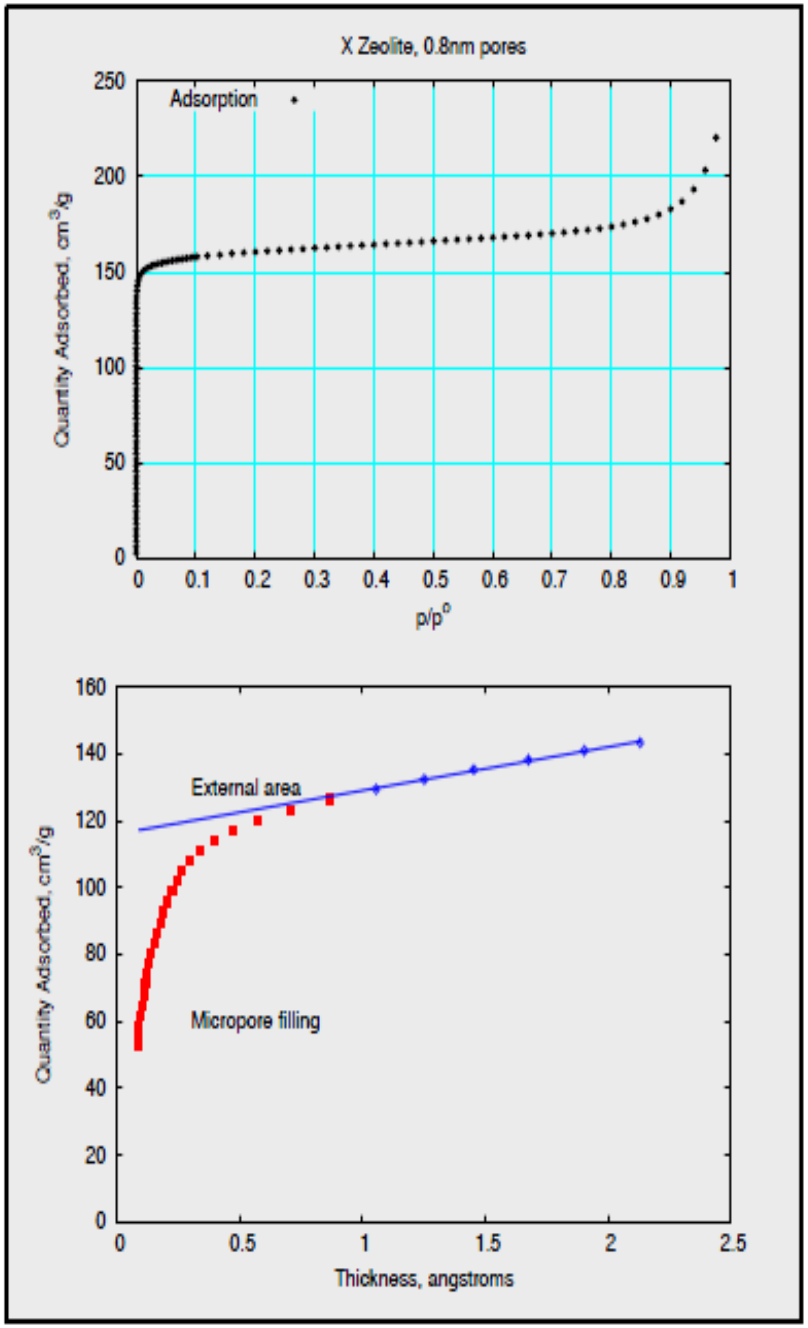

α_s plot

$$\alpha_s = \frac{n_a}{n_{0.4}} \qquad t = \frac{V_a}{V_m} \times 0.354[\text{nm}]$$

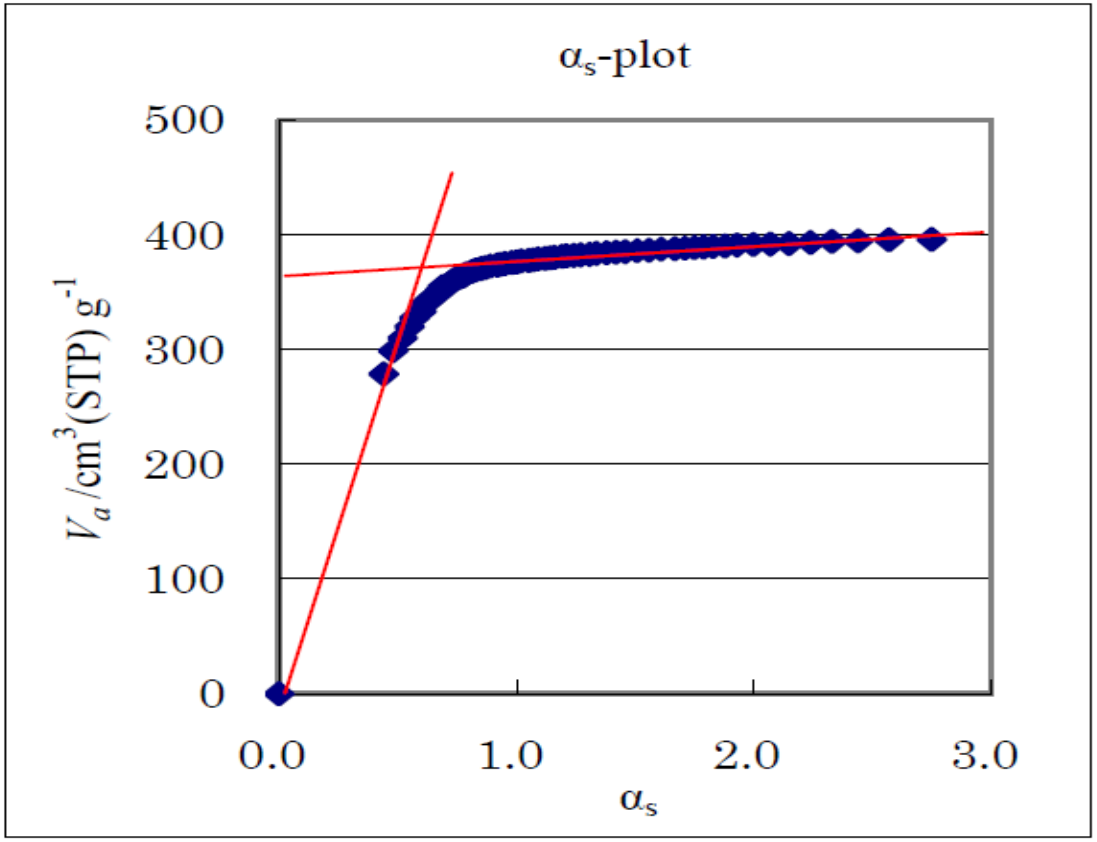

براورد حجم و محیط میکرو حفره بدون داشتن ضخامت آماری

α_s plot

- رفتار متقابل بین جذب و جاذب زیرفشار 0.4 میباشد
- ار تئوری اثبات شده که حلقه پسماند زیر این فشار بسته میشود
- اگر اندازه ذرات زیر 3.5 نانومتر باشد t جواب نمیدهد
- S بدون دیمانسیون است
- سطح داخلی حفره از کم کردن حجم سطح خارجی از حجم کل بدست میاید

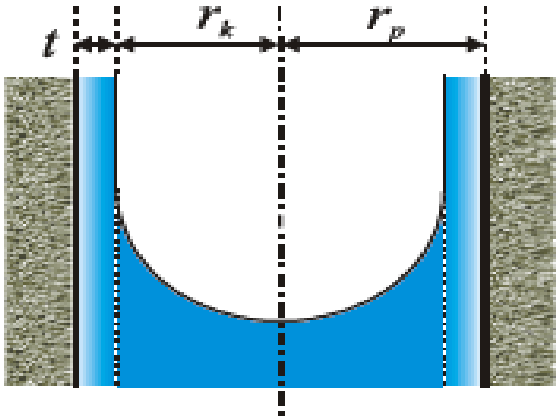

In the area where capillary condensation is in presence, radius of cyrinder shaped pore is sum of the thickness of adsorption layer at the arbitrary pressure (t) and core radius (r^k) of meniscus part.

$$r_p = t + r_k \tag{18.1}$$

Thickness of adsorption layer can be calculated from t curve of standard sample, and core radius can be calculated by Kelvin equation (18.2).

$$\ln\frac{p}{p_0} = -\frac{2\gamma V_L}{RT}\frac{1}{r_m} \tag{18.2}$$

Here, r_m is meniscus radius, γ is surface tension, V_L is molar volume of liquid adsorptive, R is gas constant and T is absolute temperature. In mesopore with cyrinder shape, suppose menisucus radius at desorption is equal to core radius (r_k), and if γ and V_L of nitrogen at liquid nitrogen temperature (77 K) are applied, the following equation can be obtained.

$$r_m = 0.953/\ln(p_0/p) \tag{18.3}$$

BJH pore size distribution

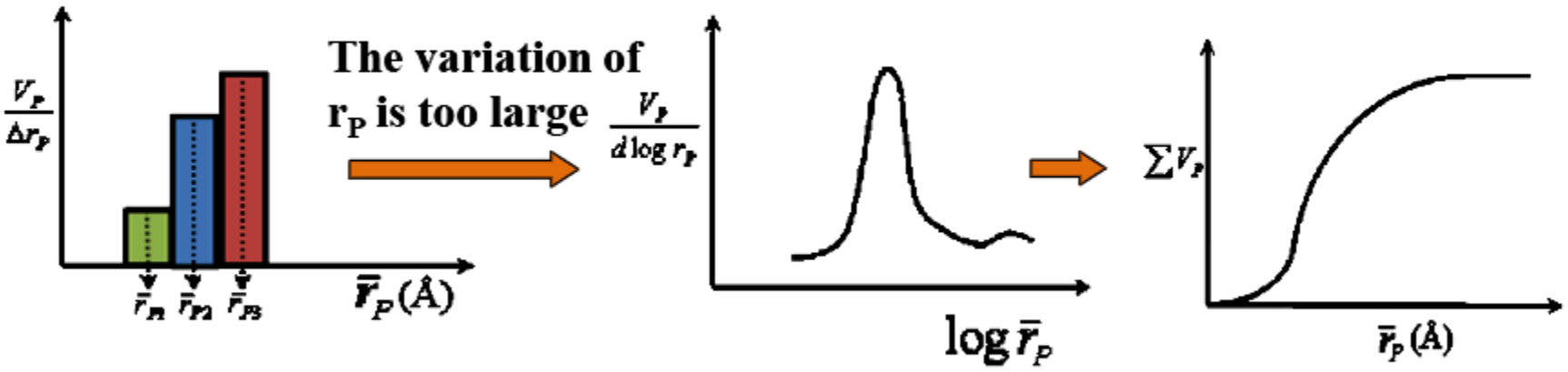

8.7. V-t curves

Adsorption on nonporous materials

If plot W_a/W_m vs. P/P_0

The data fit a common Type II curves, especially for $P/P_0 > 0.3$ and

$t = (W_a/W_m)\cdot 3.54$Å is used (t : statistical depth)

$\therefore$ t vs. P/P_0 should show Type II curves.

$$t = \frac{V_{liq}}{S} \times 10^4 (\text{Å}),\ V_{liq} = [\text{cm}^3],\ S = [\text{m}^2]$$

$$V = \frac{Ad}{4}$$

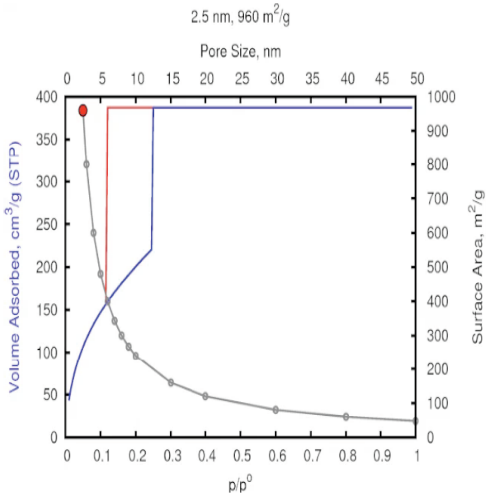

$$A = \frac{4V}{d}$$

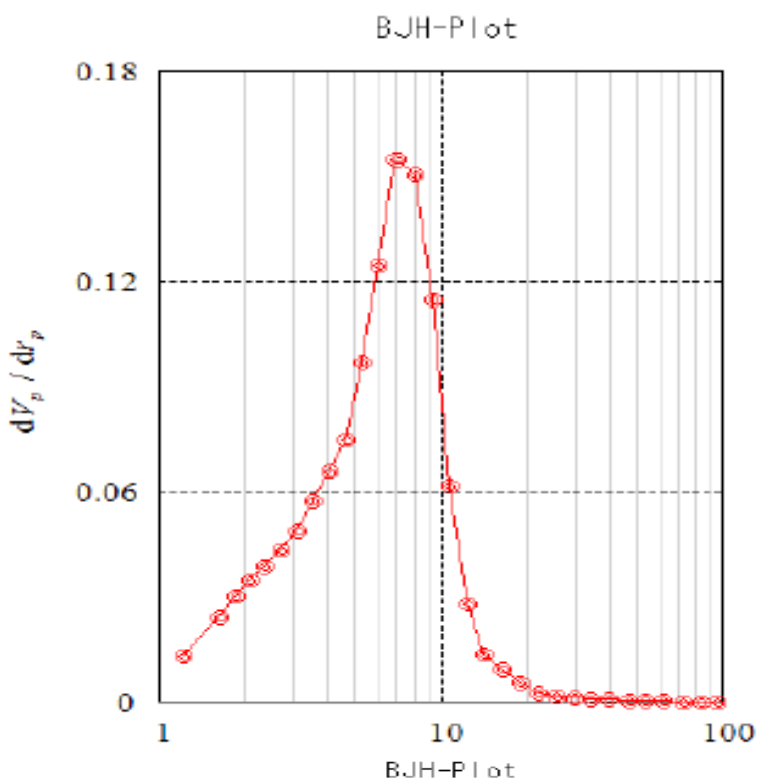

SAMPLE03.DAT(ADS)

V_p [cm³ g⁻¹]	1.0640
$r_{p,peak}$(Area) [nm]	7.99
a_p [m² g⁻¹]	338.88

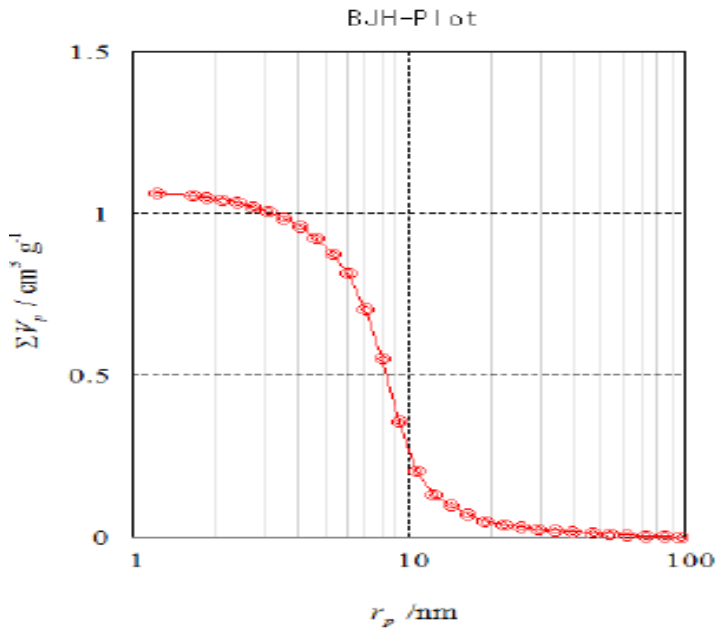

SAMPLE03.DAT(ADS

V_p [cm³ g⁻¹]	1.0640
a_p [m² g⁻¹]	338.88

Amorphous Silica-alumina

- BJH
- From Δpore volume and calculated diameter, we can estimate surface area for a cylinder
- Common to observe the BJH estimate of area is greater than the BET estimate

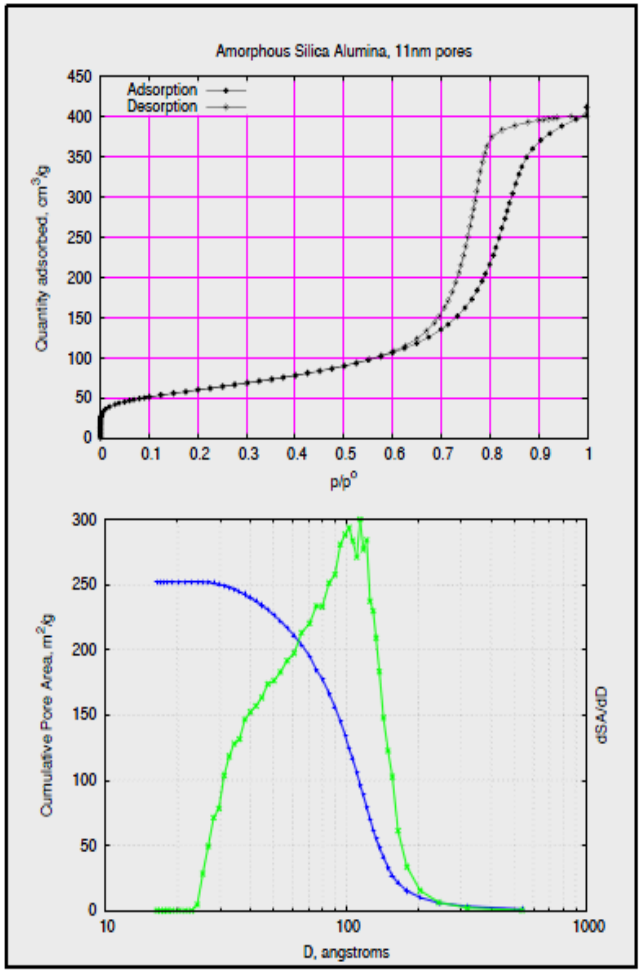

BJH - PVD
Pt/Al_2O_3

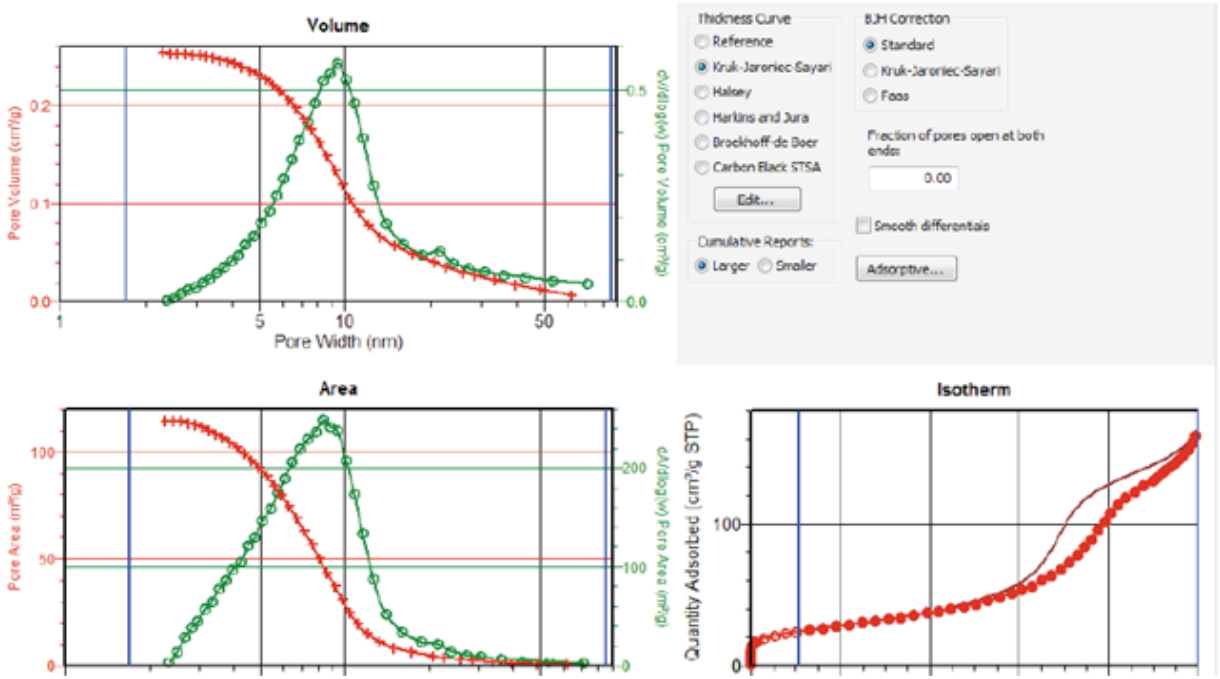

مقایسه بین ایزوترم

SiO_2	SiO_2-Al_2O_3	MCM-41
100 nm pores	11 nm pores	4 nm pores
25.7 m^2/g	215.5 m^2/g	926.8 m^2/g

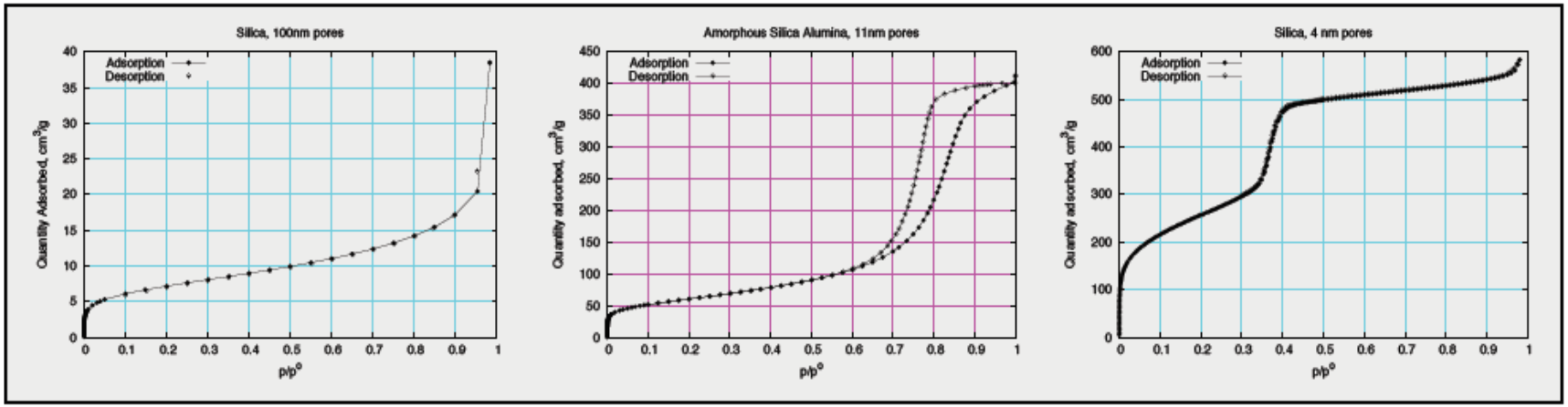

Figure 2

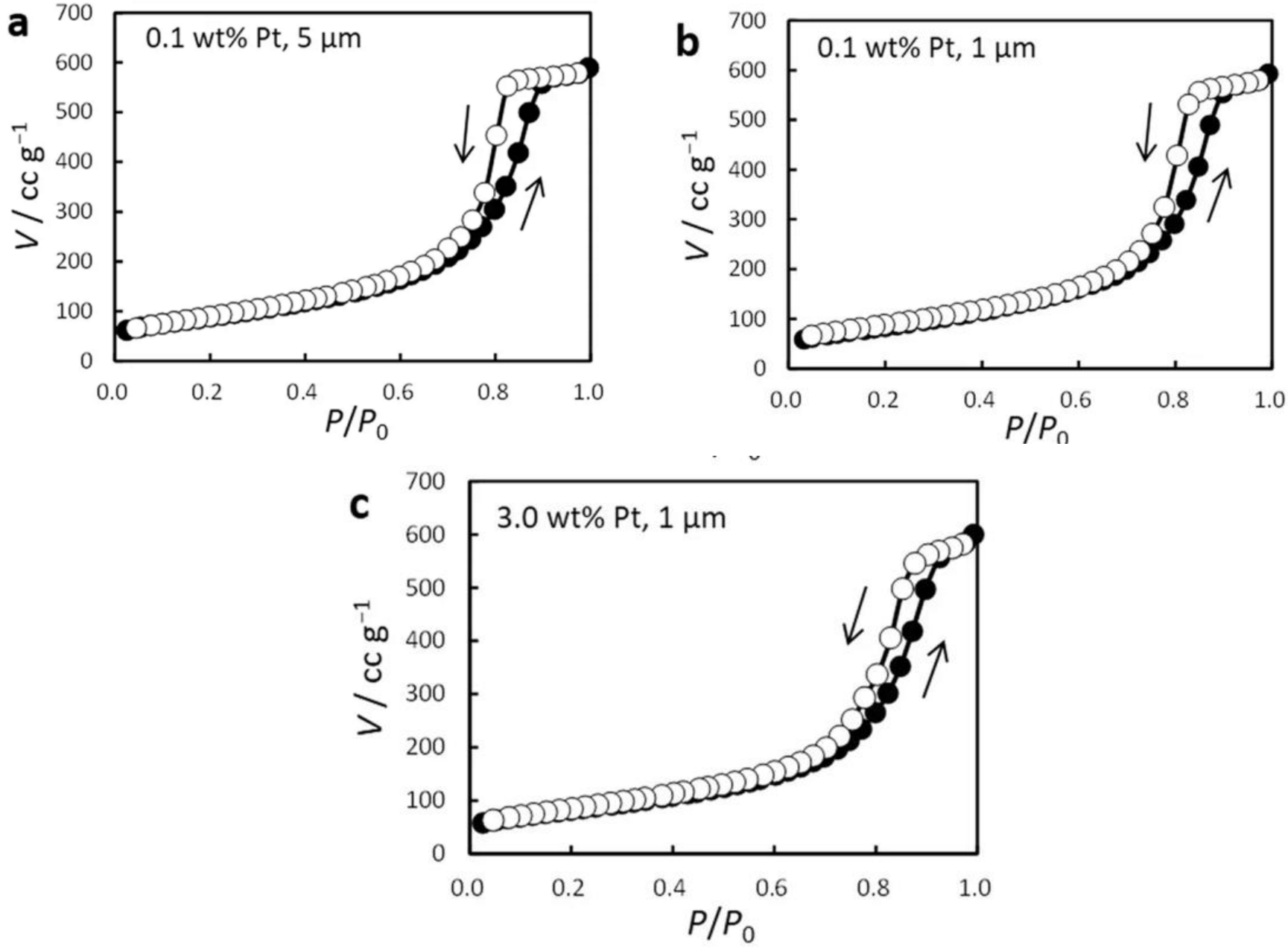
a
0.1 wt% Pt, 5 µm
b
0.1 wt% Pt, 1 µm
c
3.0 wt% Pt, 1 µm
V / cc g⁻¹
P/P0
0
100
200
300
400
500
600
700
0.0
0.2
0.4
0.6
0.8
1.0

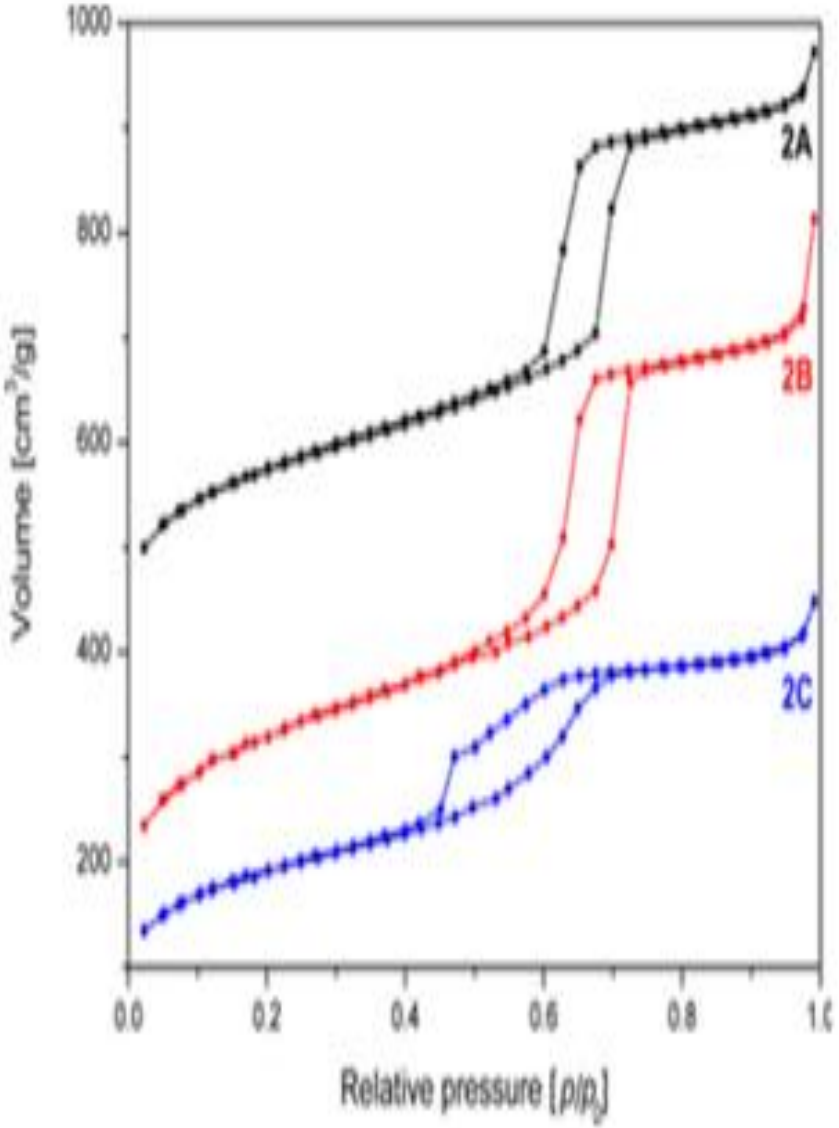

Pore structure and surface area of silica SBA-15: influence of washing and scale-up

Jörg P. Thielemann, Frank Girgsdies, Robert Schlögl et al.

Beilstein J. Nanotechnol. **2011,** 2, 110–118.

doi:10.3762/bjnano.2.13

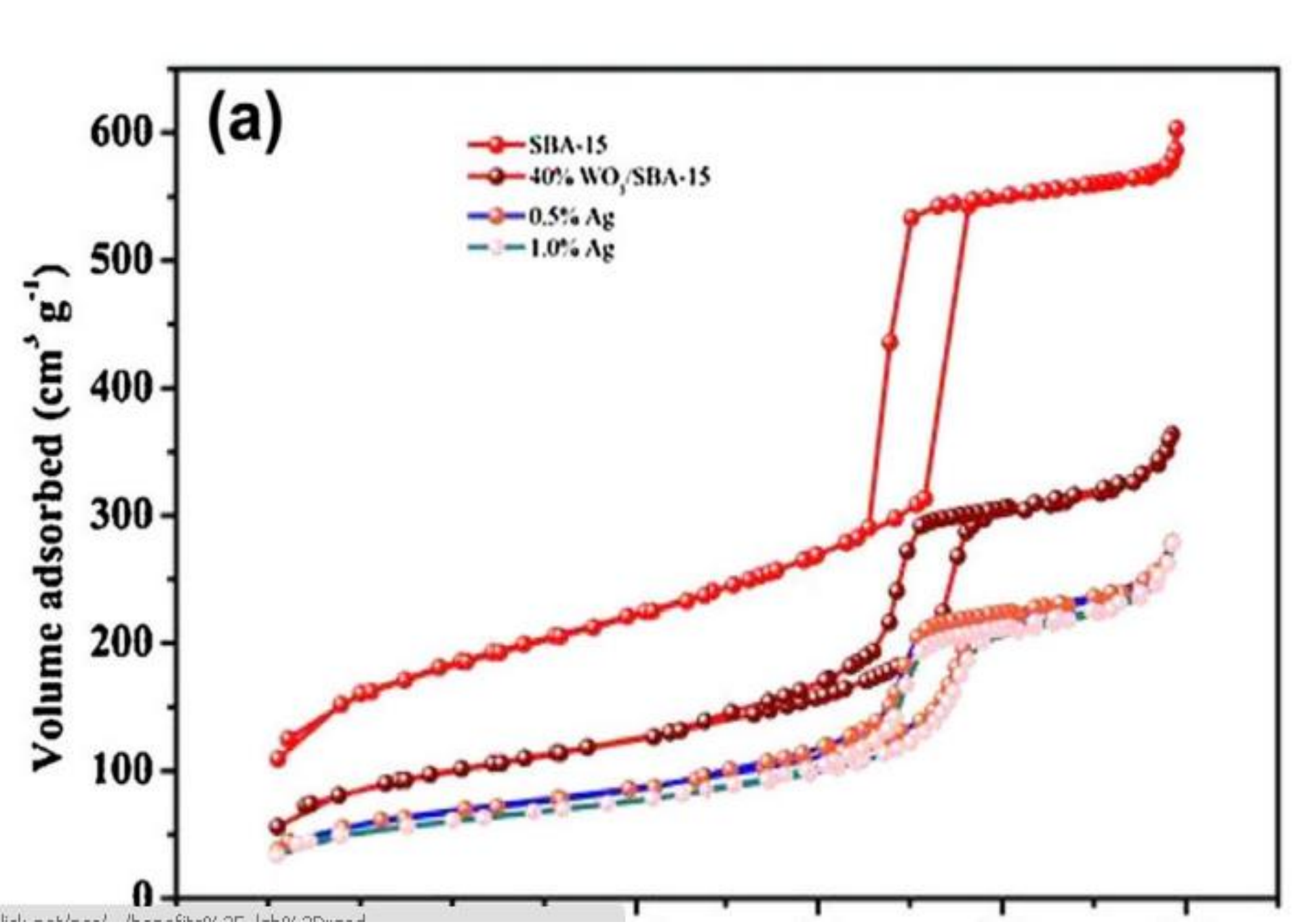
(a)
SBA-15
40% WO3/SBA-15
0.5% Ag
1.0% Ag
Volume adsorbed (cm3 g-1)
0
100
200
300
400
500
600

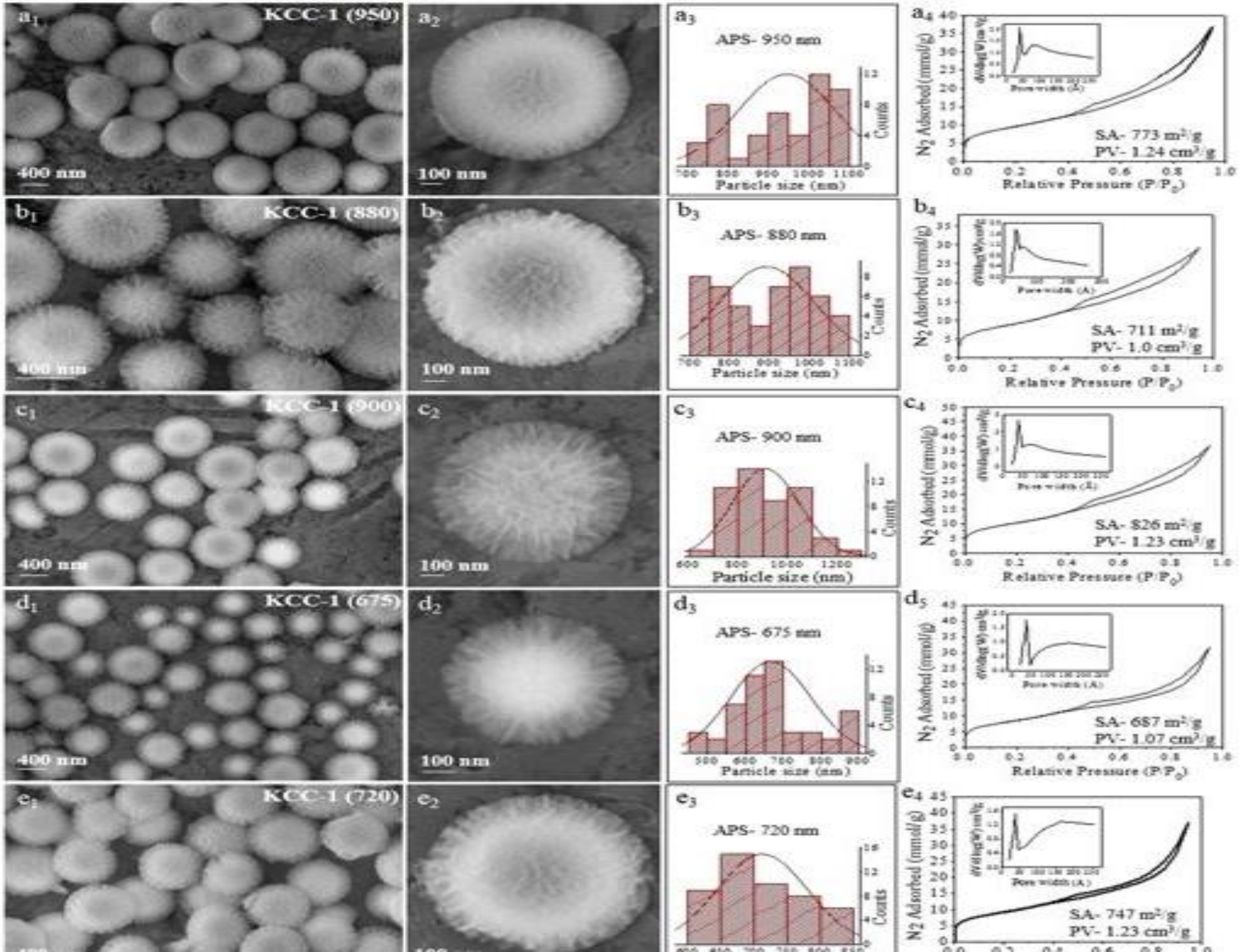
a1
KCC-1 (950)
400 nm
a2
100 nm
a3
APS- 950 nm
Particle size (nm)
Counts
a4
N2 Adsorbed (mmol/g)
SA- 773 m²/g
PV- 1.24 cm³/g
Relative Pressure (P/P0)
b1
KCC-1 (880)
400 nm
b2
100 nm
b3
APS- 880 nm
Particle size (nm)
Counts
b4
N2 Adsorbed (mmol/g)
SA- 711 m²/g
PV- 1.0 cm³/g
Relative Pressure (P/P0)
c1
KCC-1 (900)
400 nm
c2
100 nm
c3
APS- 900 nm
Particle size (nm)
Counts
c4
N2 Adsorbed (mmol/g)
SA- 826 m²/g
PV- 1.23 cm³/g
Relative Pressure (P/P0)
d1
KCC-1 (675)
400 nm
d2
100 nm
d3
APS- 675 nm
Particle size (nm)
Counts
d5
N2 Adsorbed (mmol/g)
SA- 687 m²/g
PV- 1.07 cm³/g
Relative Pressure (P/P0)
e1
KCC-1 (720)
e2
e3
APS- 720 nm
Counts
e4
N2 Adsorbed (mmol/g)
SA- 747 m²/g
PV- 1.23 cm³/g

Figure 3

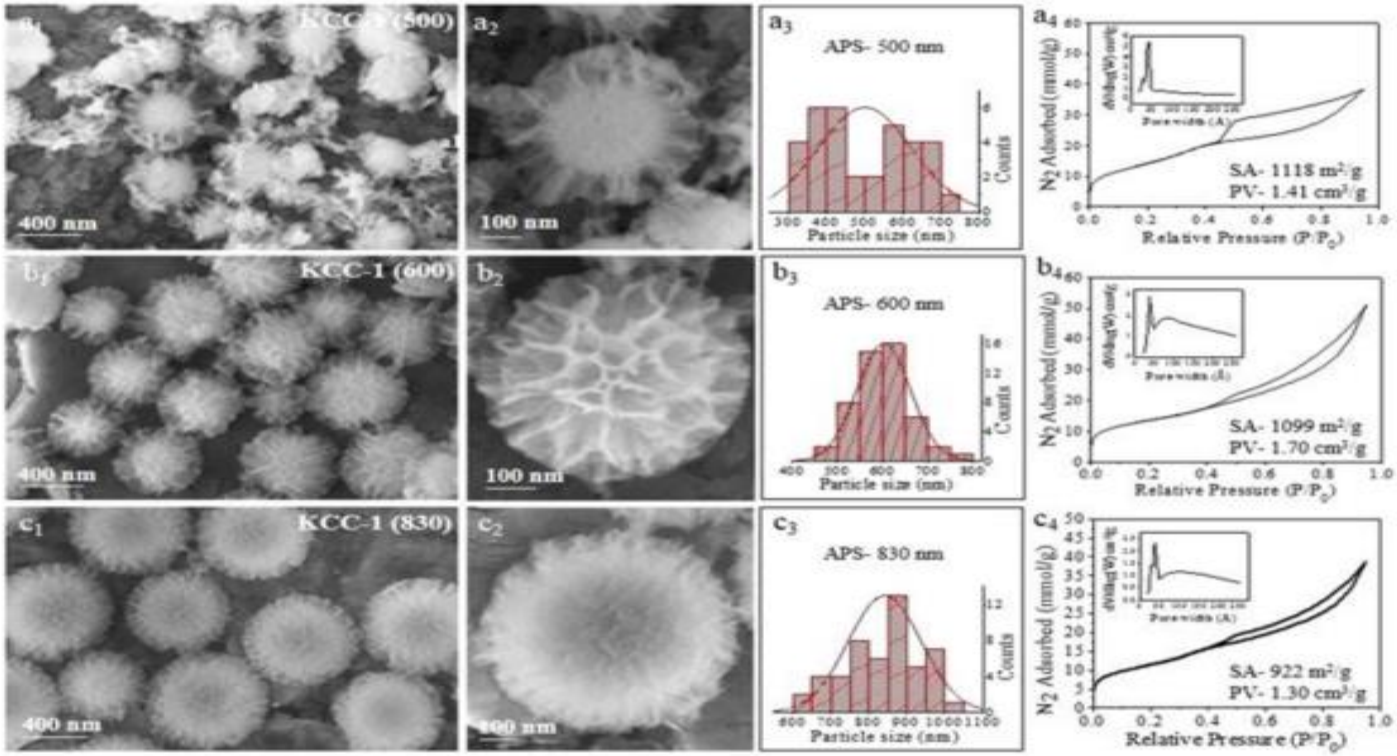

SEM images, particle size distribution, and N_2 sorption isotherm (pore size distribution in inset) with CTAB concentrations of (**a**) 1.5 g, (**b**) 3 g and (**c**) 6 g. *Other synthesis conditions were kept the same as given in* Table S1.

منفذو پسماند

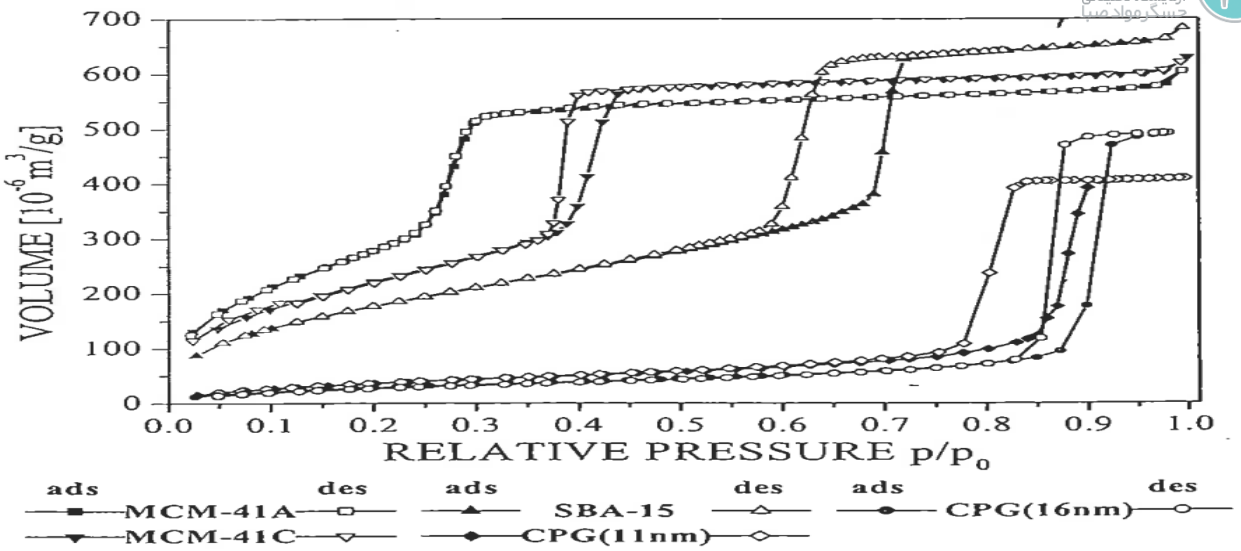

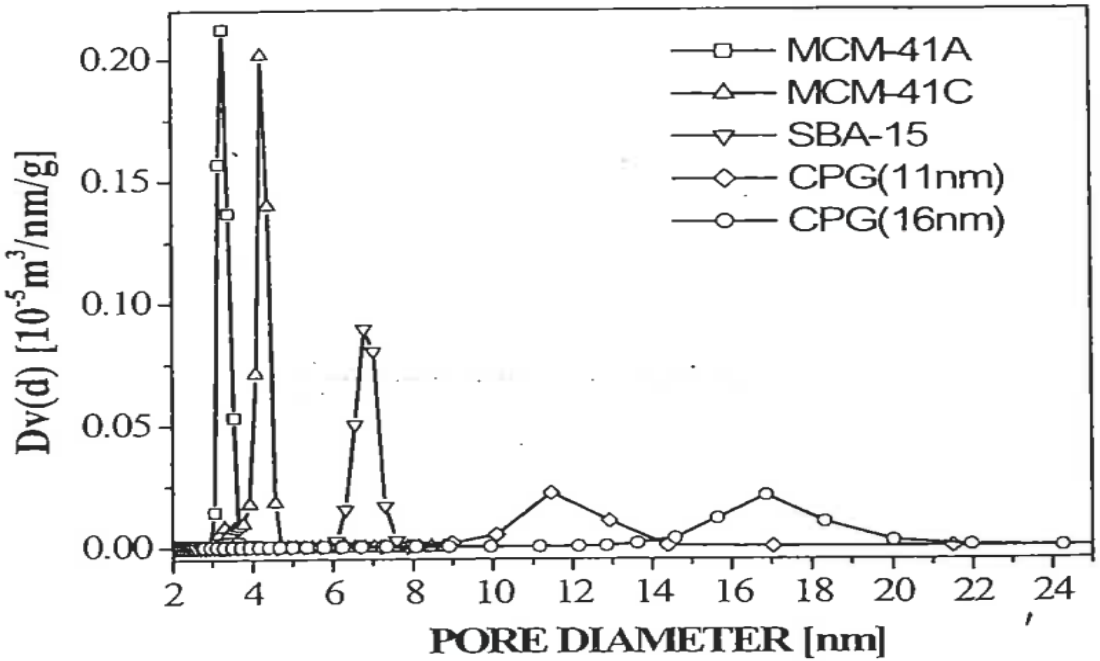

رابطه پسماند با اندازه منفذ

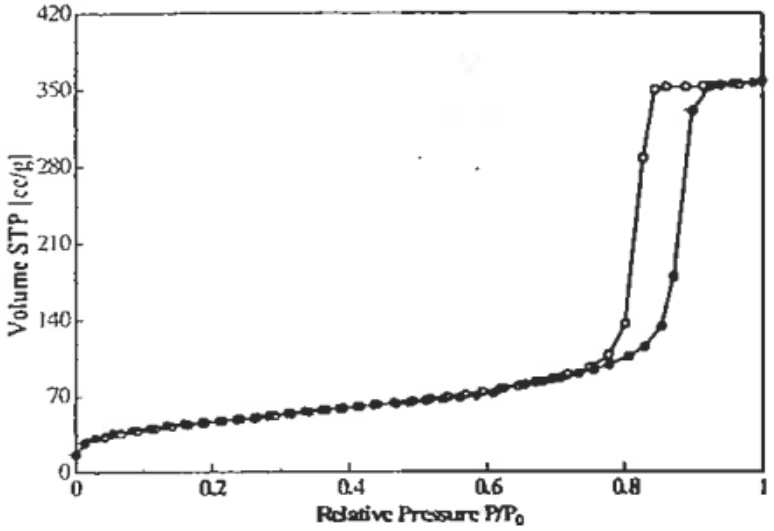

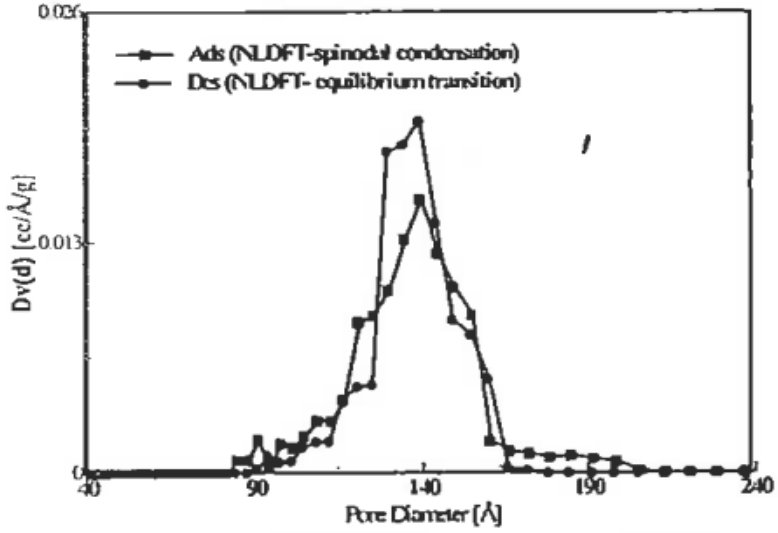

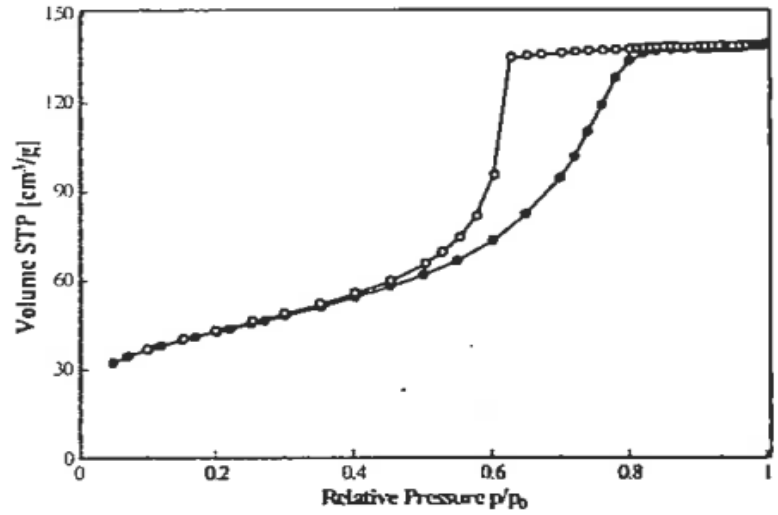

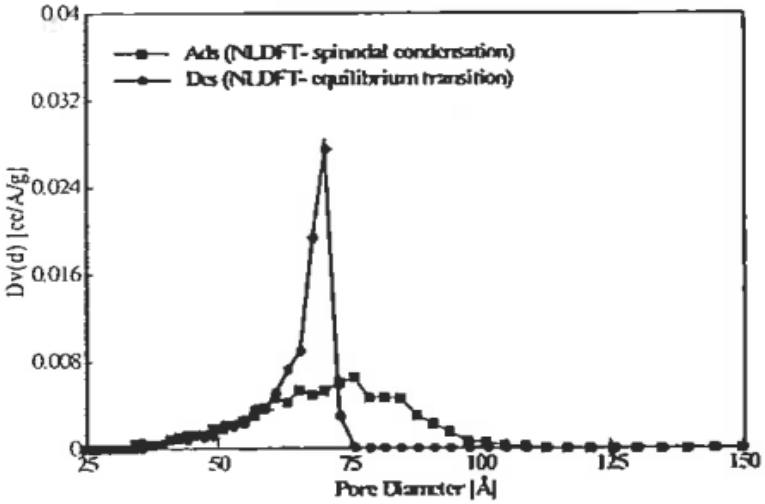

Material	Bezeichnung	Bezugs-quelle	Spezifische Oberfläche[a] m^2g^{-1}
Silica[b]	BAM-PM-101	BAM	0,177
Alpha-Alumina	BAM-PM-102	BAM	5,41
Alumina	BAM-PM-103	BAM	156
Alumina	BAM-PM-104	BAM	79,8
Alpha-Alumina	BCR-169	IRMM	0,104
Alpha-Alumina	BCR-170	IRMM	1,05
Alumina	BCR-171	IRMM	2,95
Quartz	BCR-172	IRMM	2,56
Titania-Rutile	BCR-173	IRMM	8,23
Tungsten	BCR-175	IRMM	0,181
Carbon black	LGC2101	LGC	10,5
Carbon black	LGC2102	LGC	69
Silica (nonporous)	LGC2103	LGC	142
Silica (mesoporous)	LGC2104	LGC	247
Silica/Alumina	SRM 1897	NIST	258,32
Silicon nitride	SRM 1899	NIST	10,52
Silicon nitride	SRM 1900	NIST	2,85

[a] Die spezifische Oberfläche ist mit dem Stickstoffadsorptionsverfahren bei 77 K gemessen worden (Ausnahmen sind besonders gekennzeichnet).

[b] Gemessen mit Krypton bei 77 K.

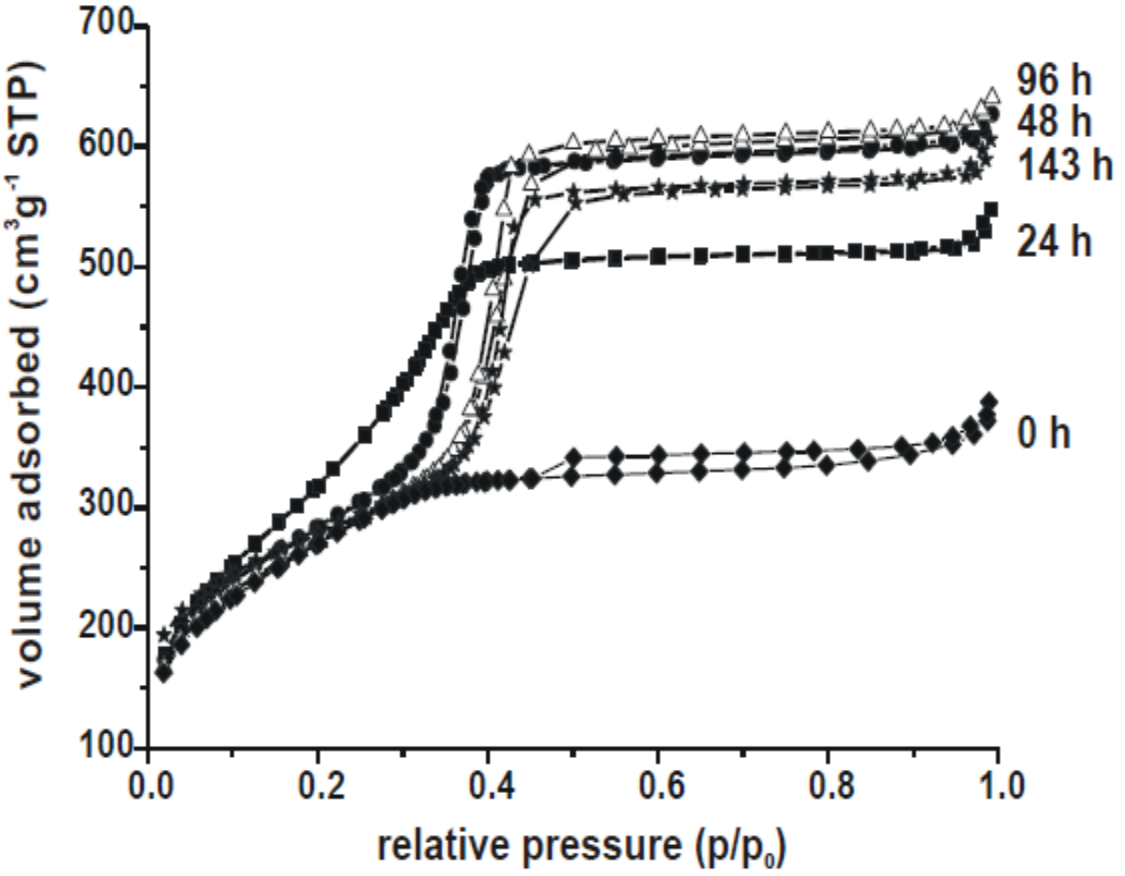

Figure 4.4 N_2 isotherms of the samples of series 1. Time labels indicate the duration of the steam treatment at 150 °C.

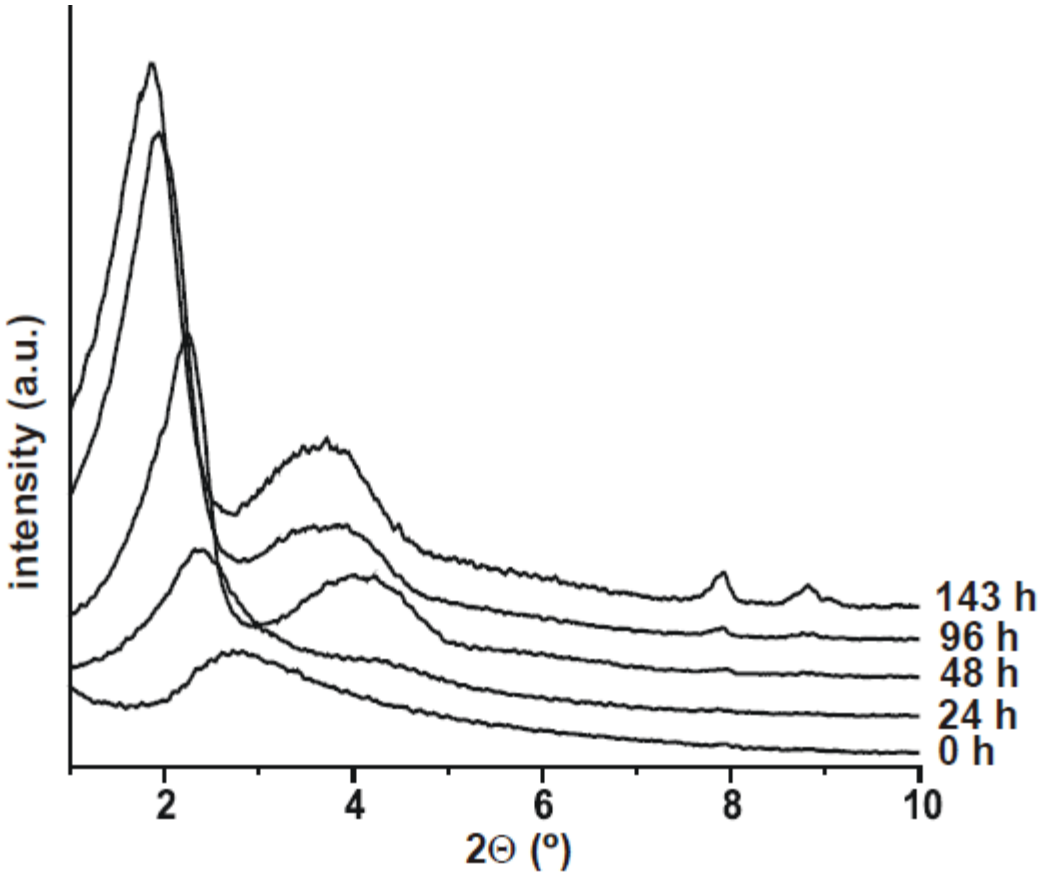

Figure 4.5 XRD powder patterns of calcined samples of series 1 measured at low 2 theta angles. Time labels indicate the duration of the steam treatment at 150 °C.

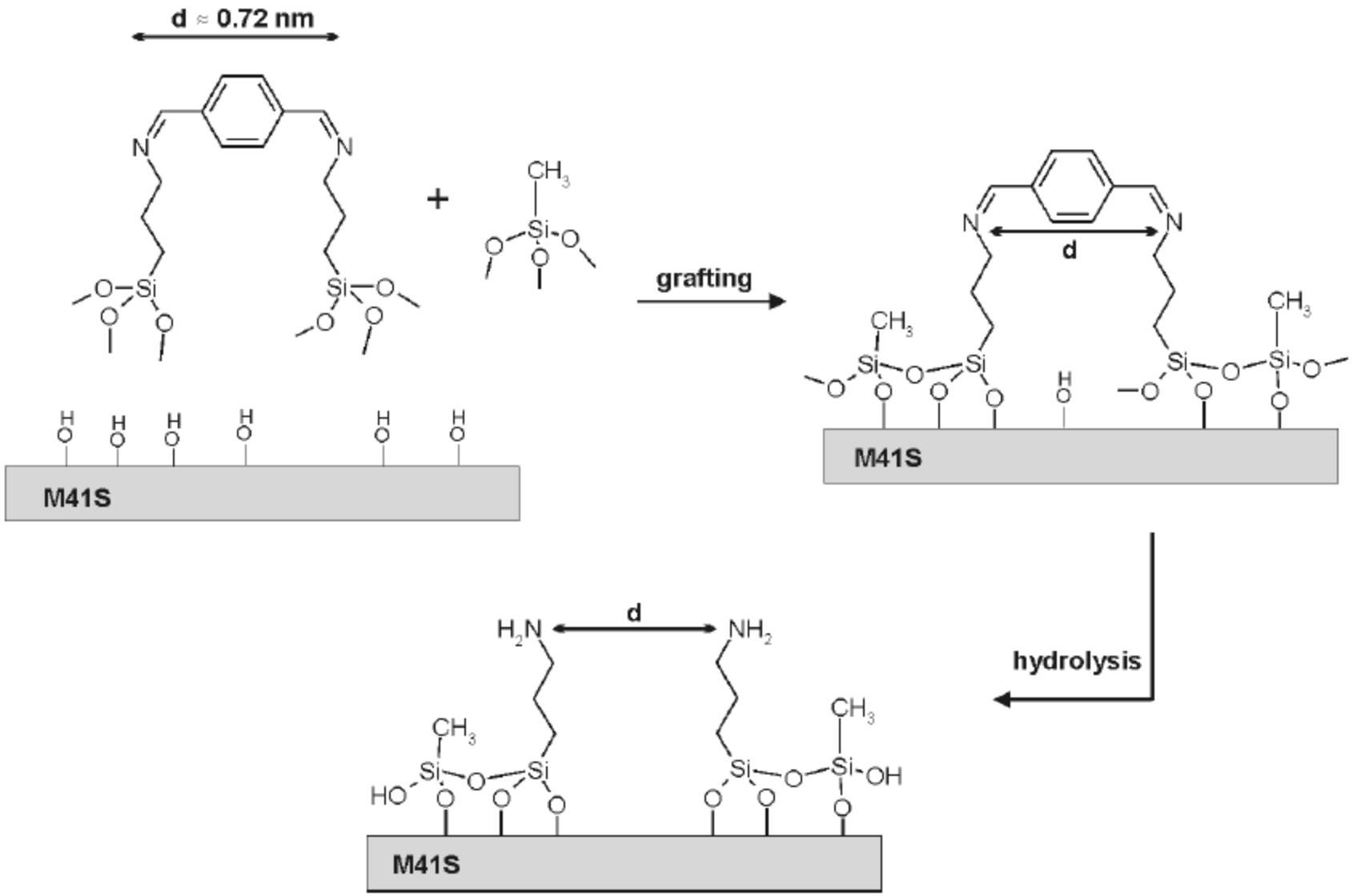

Scheme 5.3 Procedure for a distance controlled pair-wise functionalization of M41S with 3-aminopropyl and methyl groups.

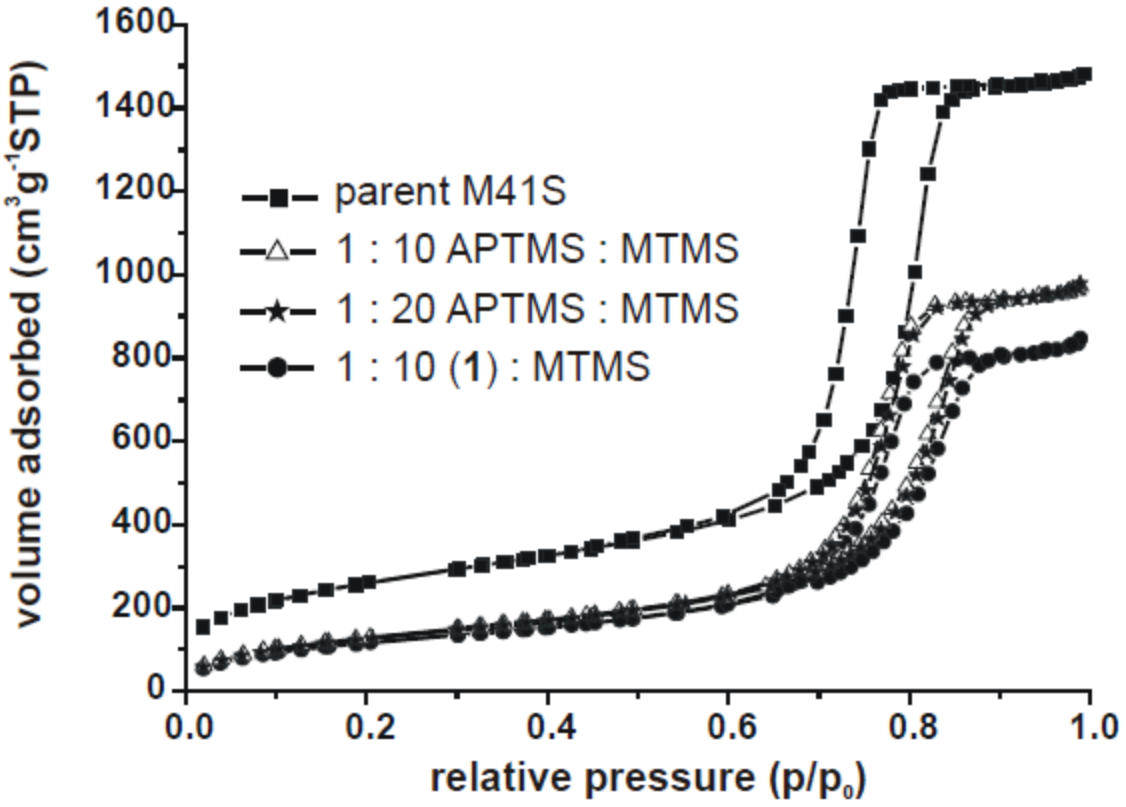

Figure 5.1 N_2 isotherms of M41S (squares) and three samples treated with different functionalization mixtures.

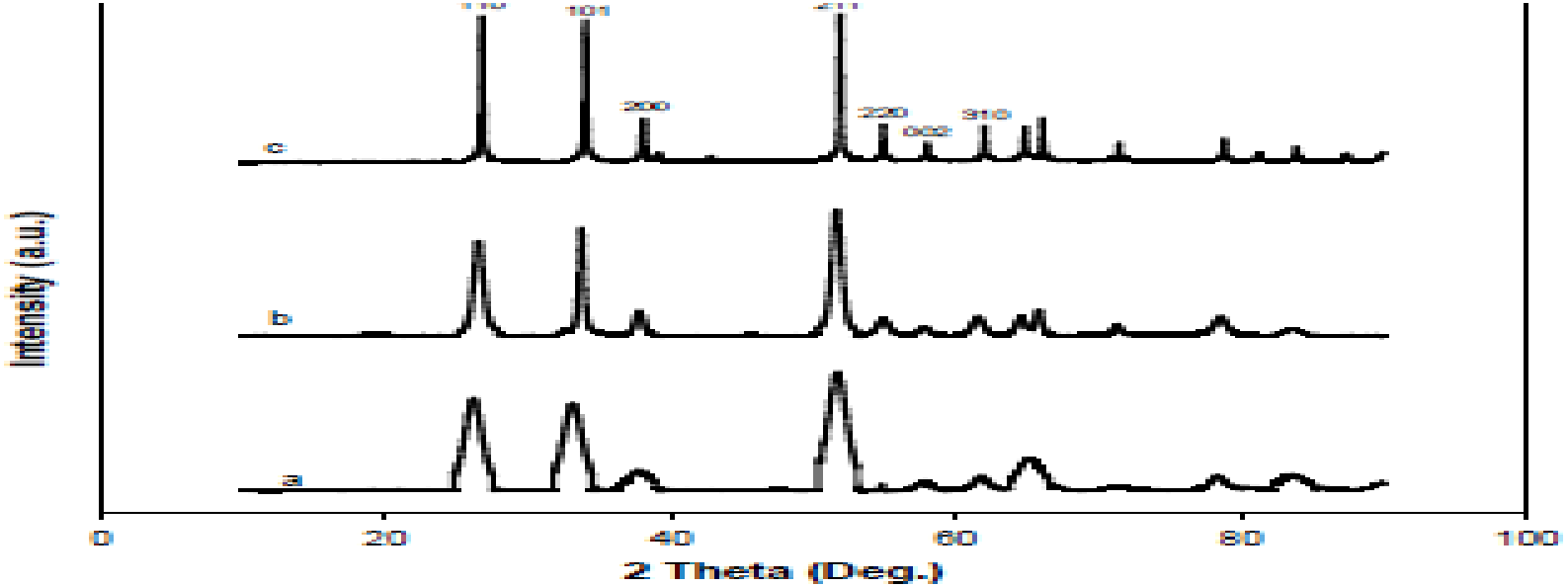

Figure 2. XRD patterns of Sn-400 (a), Sn-500 (b), and Sn-C (c)

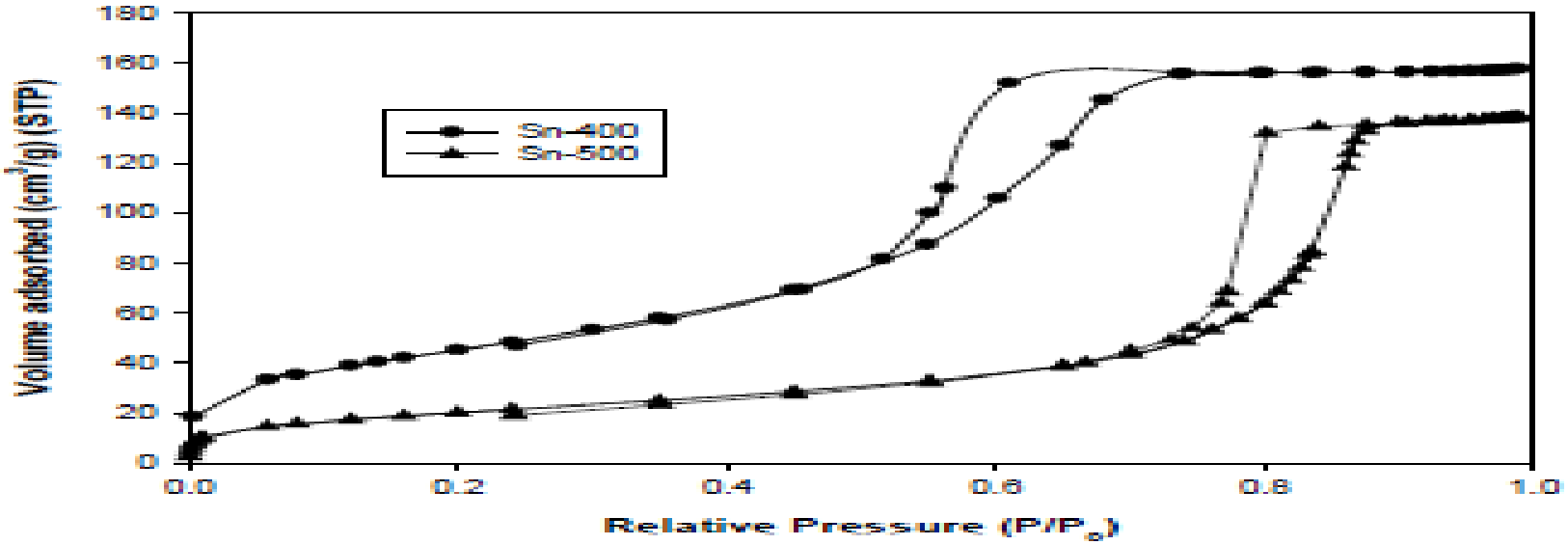

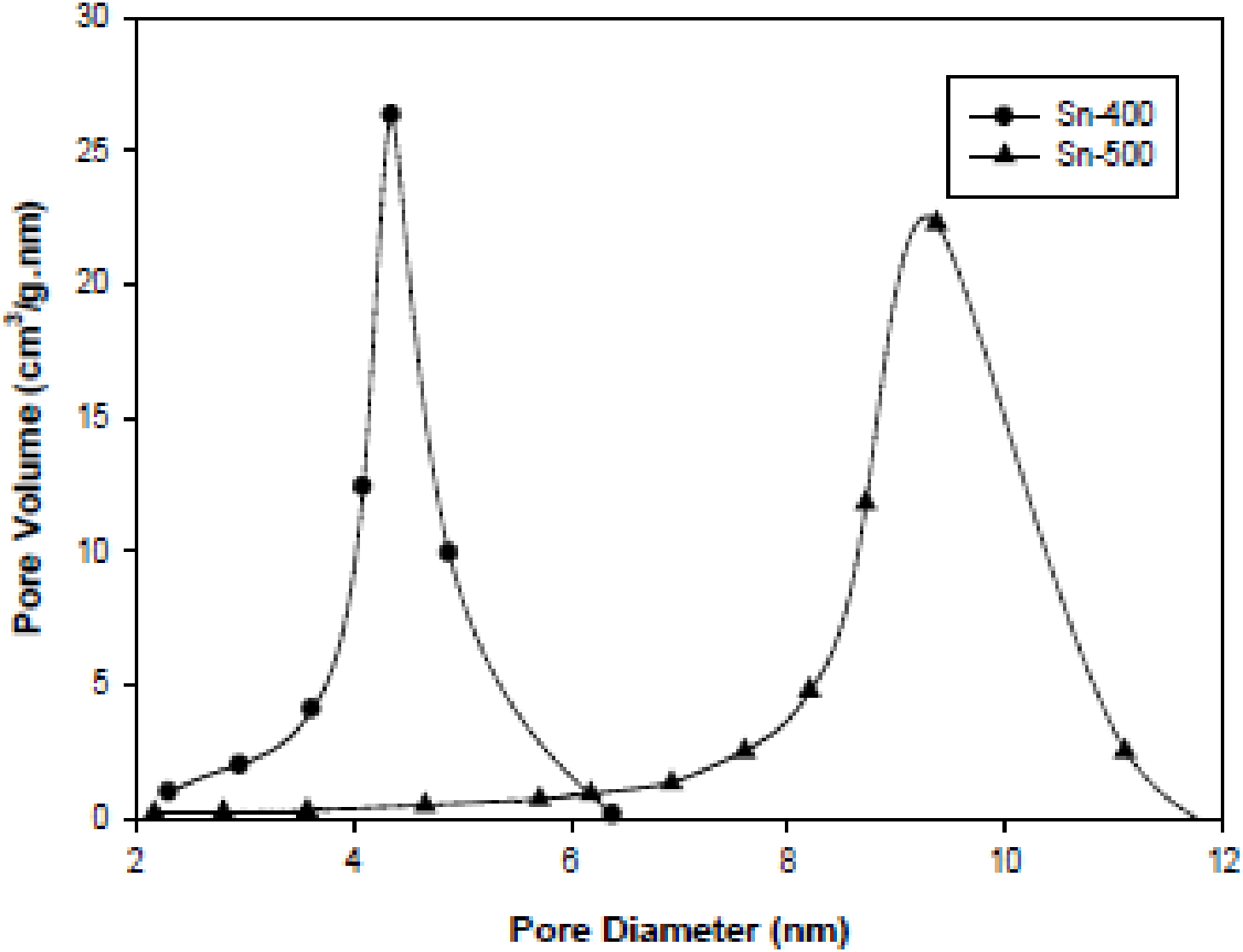

Figure 4. Pore size distribution of mesoporous SnO_2

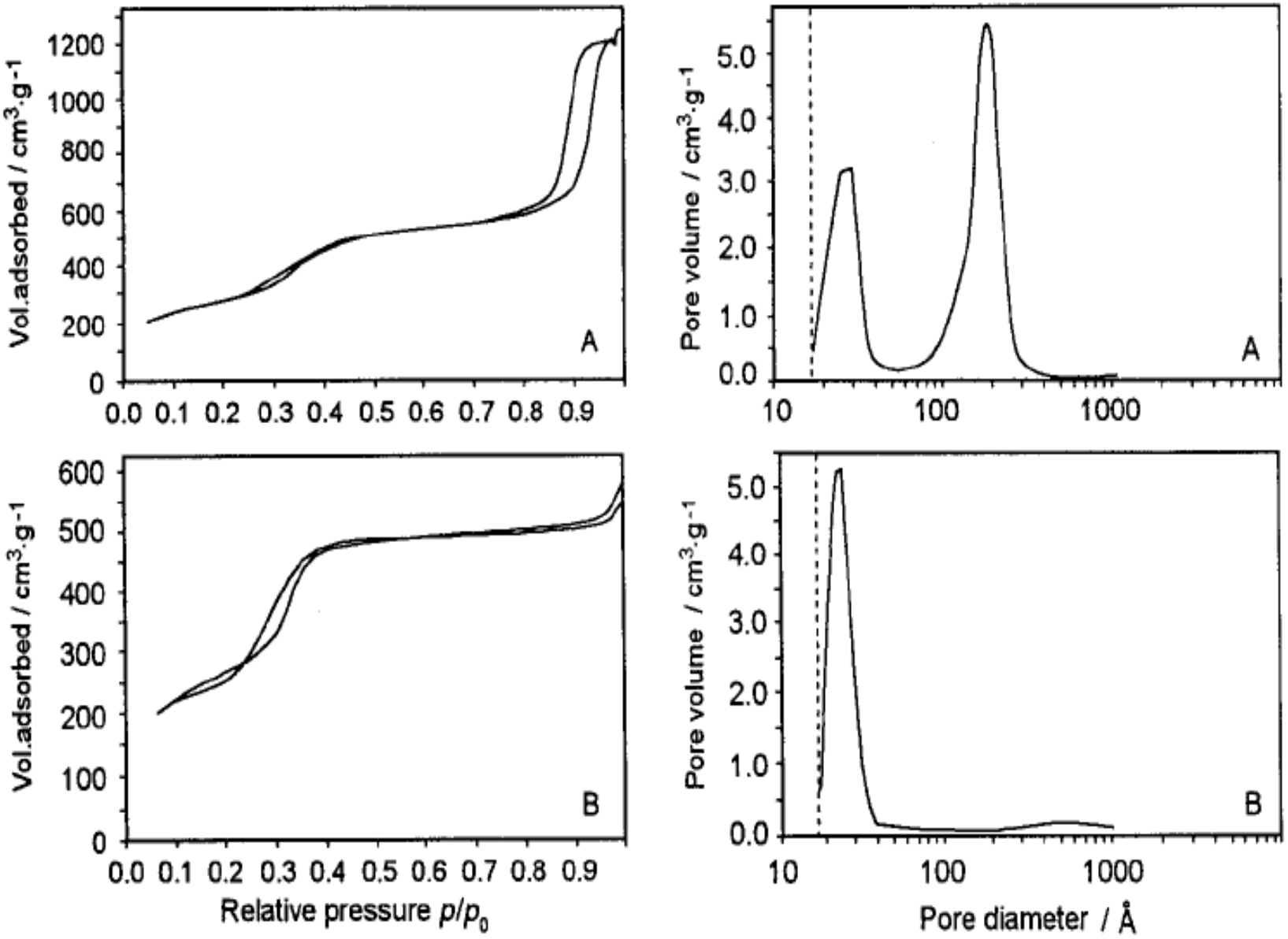

Fig.2 N_2 adsorption-desorption isotherms and corresponding pore size distribution curves of

Table 2 Sorption properties of the calcined double-mesopore and hexagonal mesopore silicas

Sample	Primary mesopore				Secondary mesopore			
	p/p_0	S_{BET} m^2/g	V_p cm^3/g	D_p nm	p/p_0	S_{BET} m^2/g	V_s cm^3/g	D_s nm
Double-mesopore	0.24~0.34	1064.6	0.66	2.6~3.0	0.85~1.0	243.1	1.18	19.0
Hexagonal mesopore	0.25~0.34	1046.8	0.87	2.2~2.5				

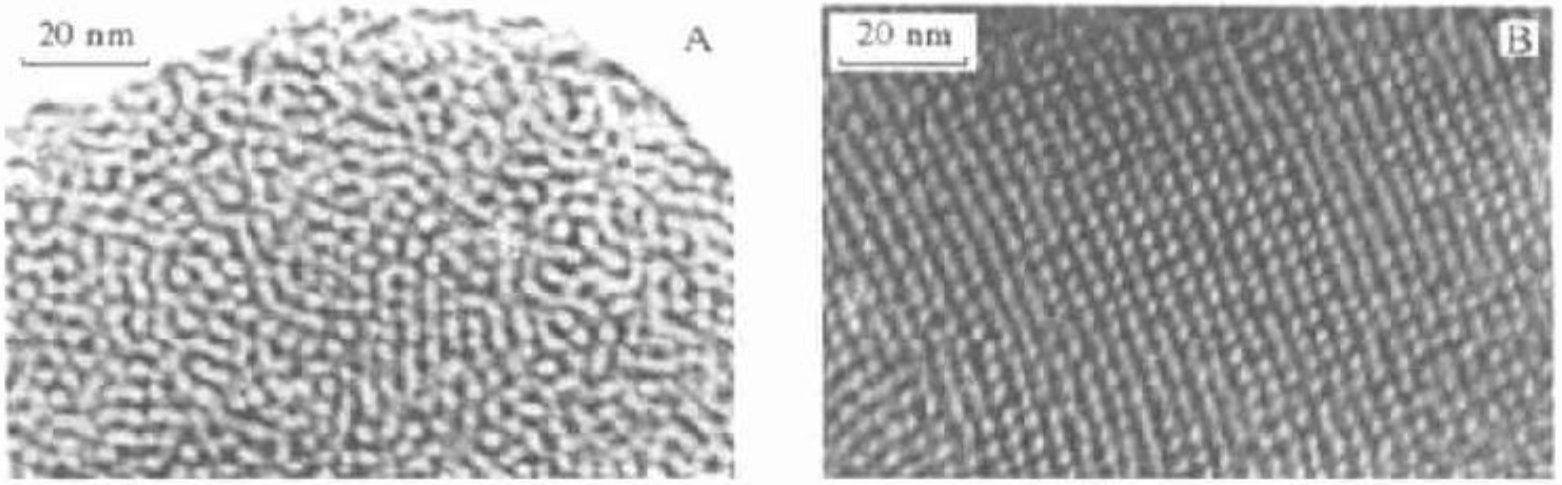

Fig.3 Transmission electron micrographs of the double-mesopore silica (A) and the hexagonal mesopore silica (B)

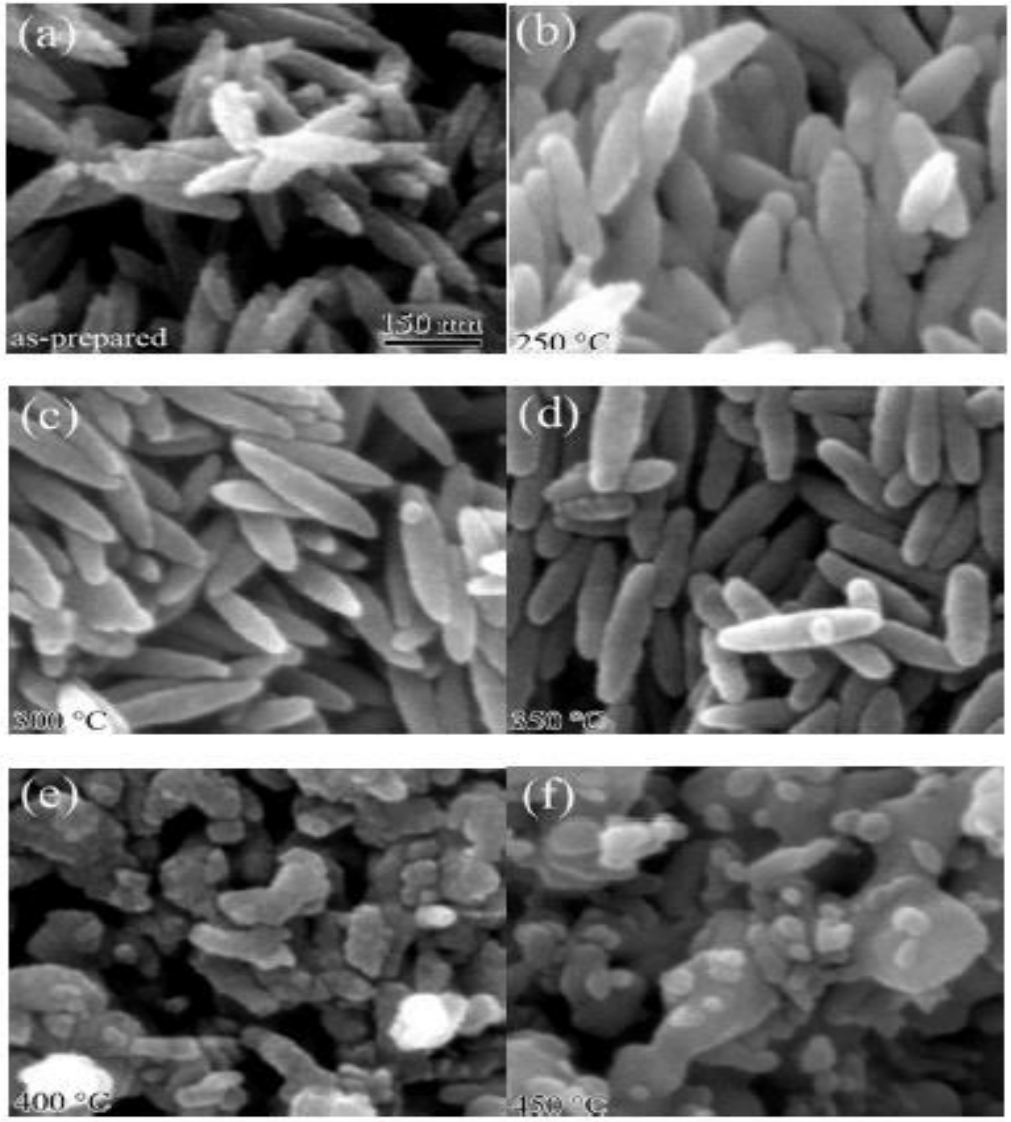

Figure 2 SEM images of the samples S1 (a), S2 (b), S3 (c), S4 (d), S5 (e), and S6 (f).

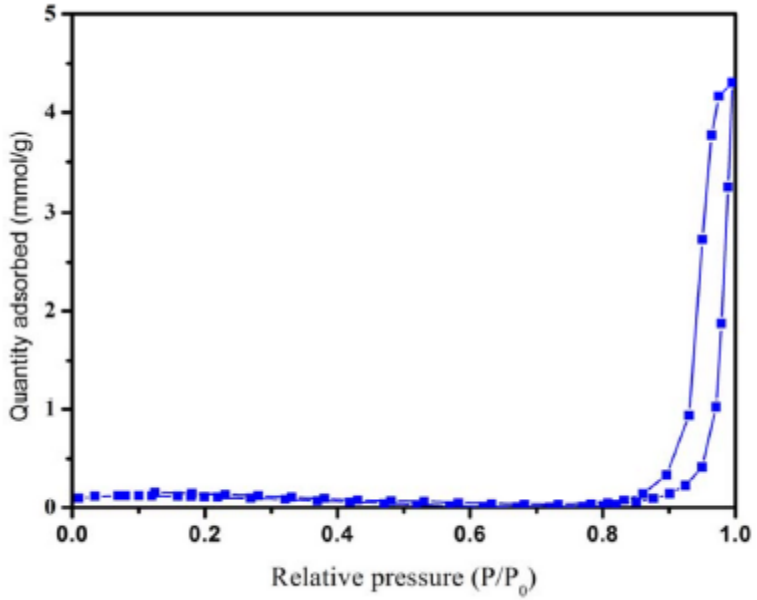

Figure 5 N_2 adsorption and desorption isotherms of Fe_3O_4 NPs.

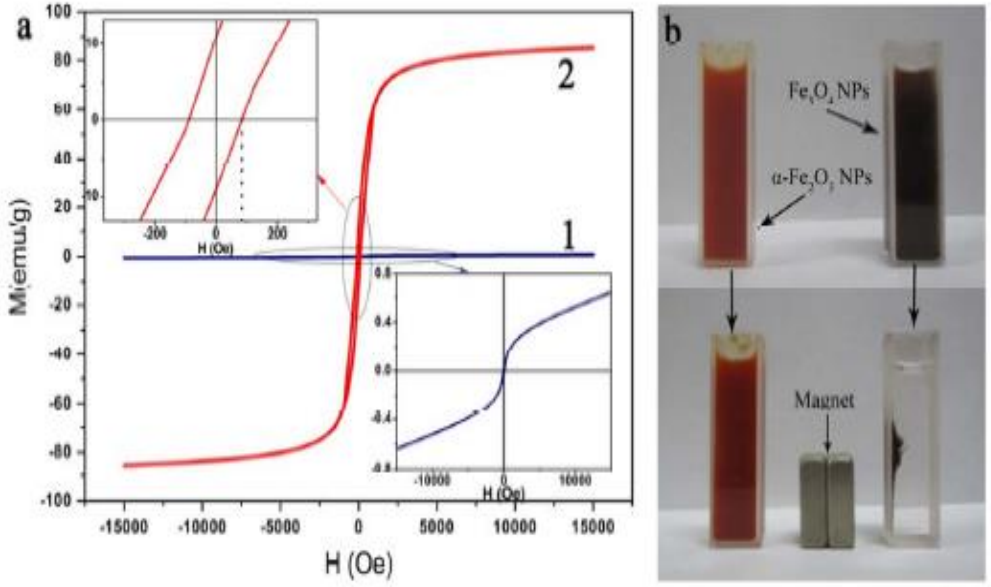

Figure 6 Magnetic hysteresis loops of α-Fe_2O_3 NPs (curve 1) and Fe_3O_4 NPs (curve 2) (a); photographs of α-Fe_2O_3 NPs and Fe_3O_4 NPs before and after magnetic separation with an external magnetic field (b).

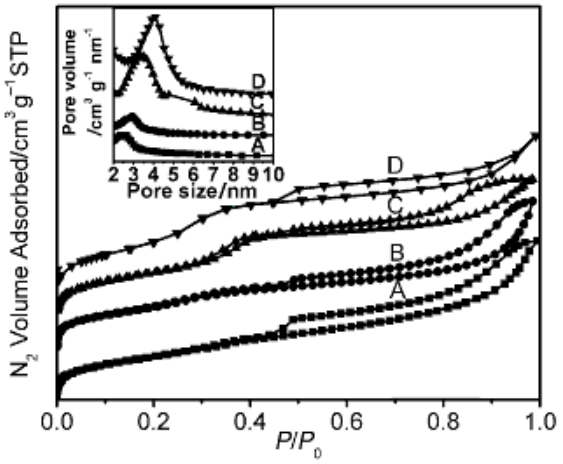

Figure 2. The N_2 adsorption–desorption isotherms and po size distribution curve of (A) Fe_3O_4@MSPC-1, (B) Fe_3O_4 MSPC-2, (C) Fe_3O_4@MSPC-3, and (D) Fe_3O_4@MSPC-4.

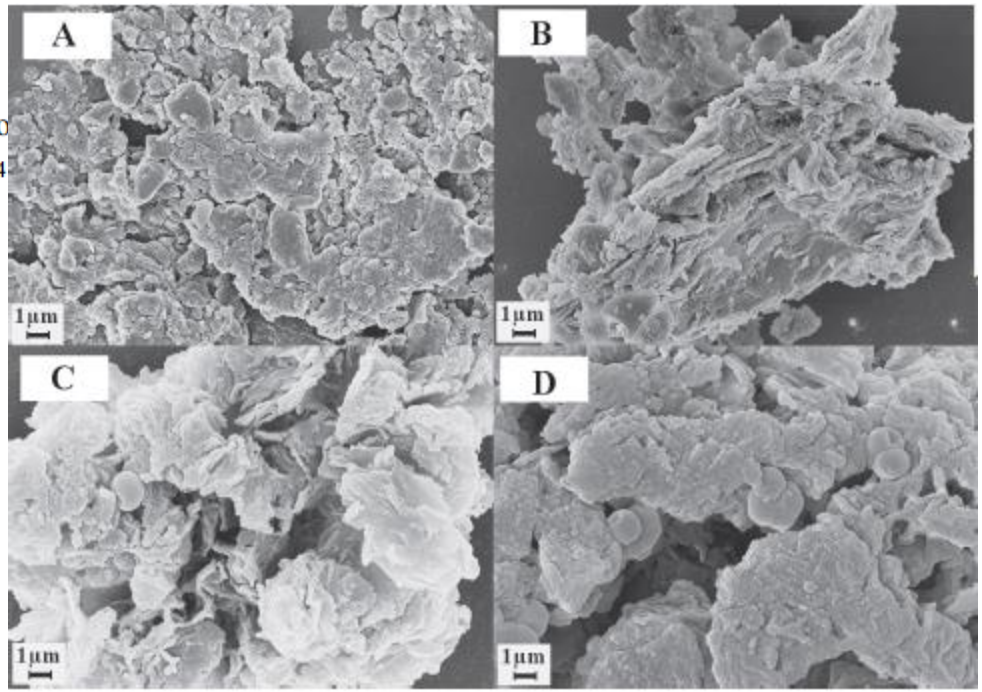

Figure 4. Scanning electron microscope micrograph of (A) Fe_3O_4@MSPC-1, (B) Fe_3O_4@MSPC-2, (C) Fe_3O_4@MSPC-3, and (D) Fe_3O_4@MSPC-4.

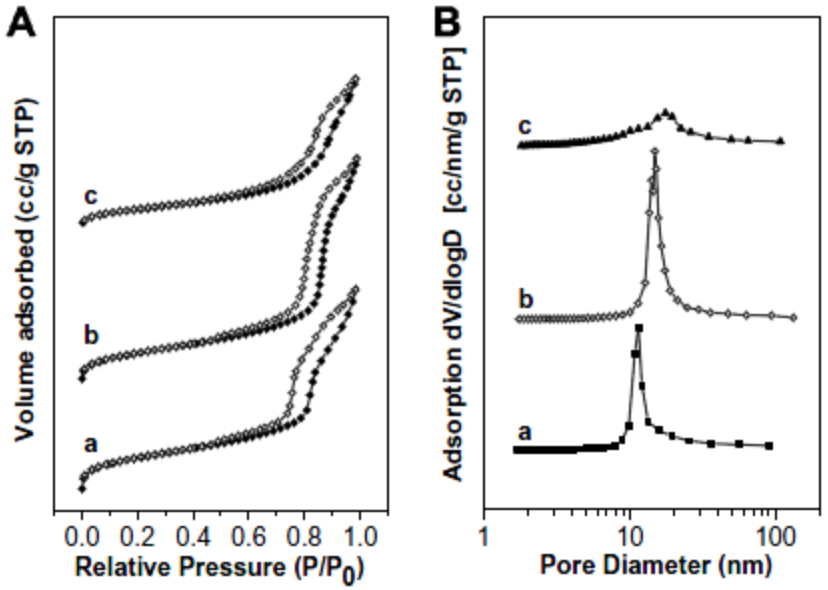

Fig. 6. Nitrogen adsorption (●) and desorption (○) isotherm curves (A) and pore size distribution curve (B) of mesoporous silicas synthesized with different molar ratio of ethanol/P123: (a) $(NaSi)_{50}E_{50}^{*}$, (b) $(NaSi)_{50}E_{50}$, (c) $(NaSi)_{50}E_{50}^{**}$.

Table 2
Physicochemical properties of $(NaSi)_{50}E_{50}$

Sample	d_{100} (nm)	BET surface area ($m^2\ g^{-1}$)	Pore diameter[a] (nm)	Total pore volume ($cm^3\ g^{-1}$)
$(NaSi)_{50}E_{50}^{*}$[b]	11.0	662	11	1.5
$(NaSi)_{50}E_{50}$	12.0	577	15	1.6
$(NaSi)_{50}E_{50}^{**}$[c]	–	403	18	1.1

[a] Calculated using the Barrett–Joyner–Halenda (BJH) model based on the adsorption branch of the isotherm.
[b] Synthesized without addition of ethanol.
[c] Synthesized with ethanol/P123 molar ratio of 426.

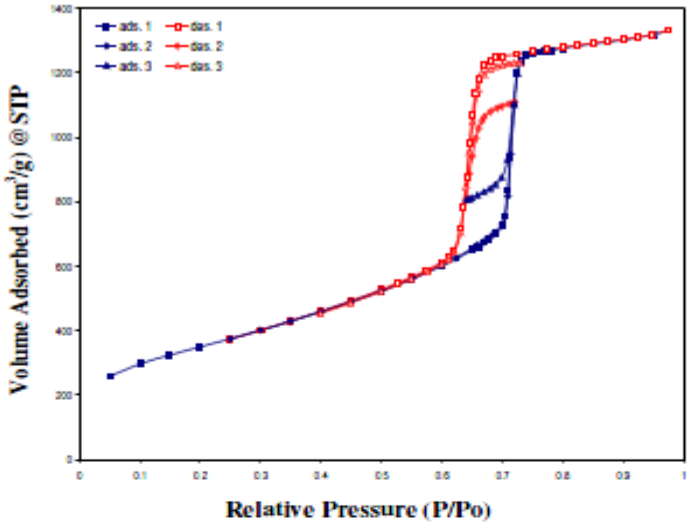

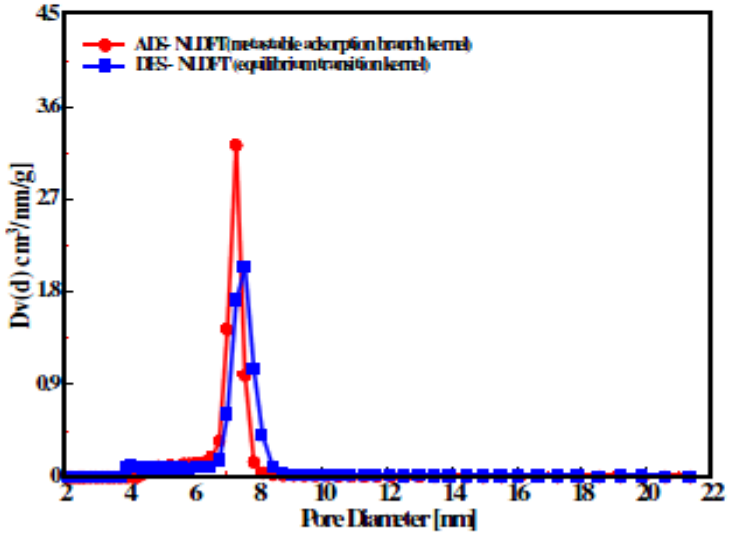

Fig.2 *(a) Nitrogen (77.4 K) sorption isotherms in SBA-15 silica and corresponding hysteresis scanning isotherms ; (b) NLDFT pore size distribution (cylindrical pore model) from adsorption by applying the so-called metastable adsorption branch kernel and desorption (by applying an equilibrium*

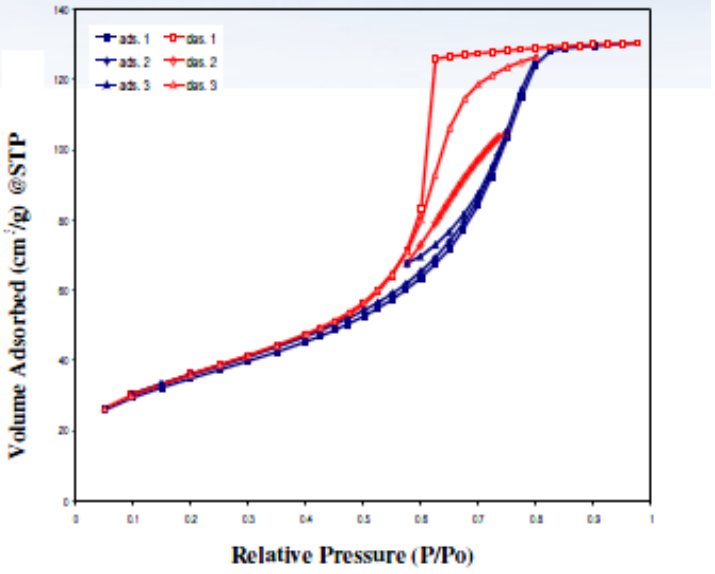

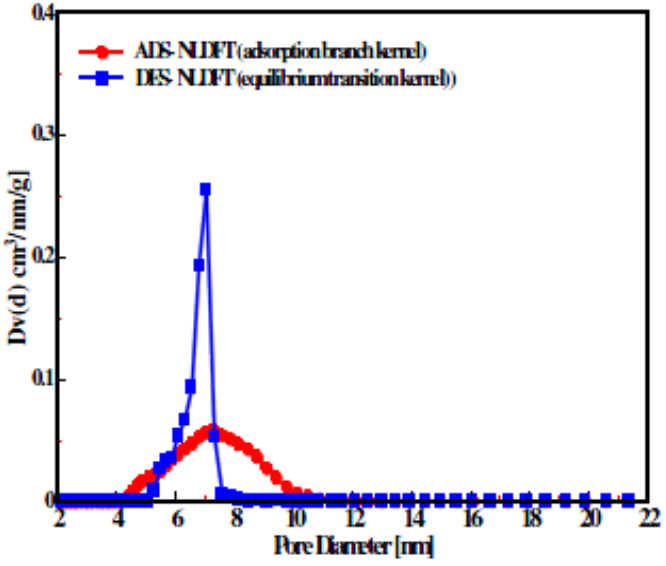

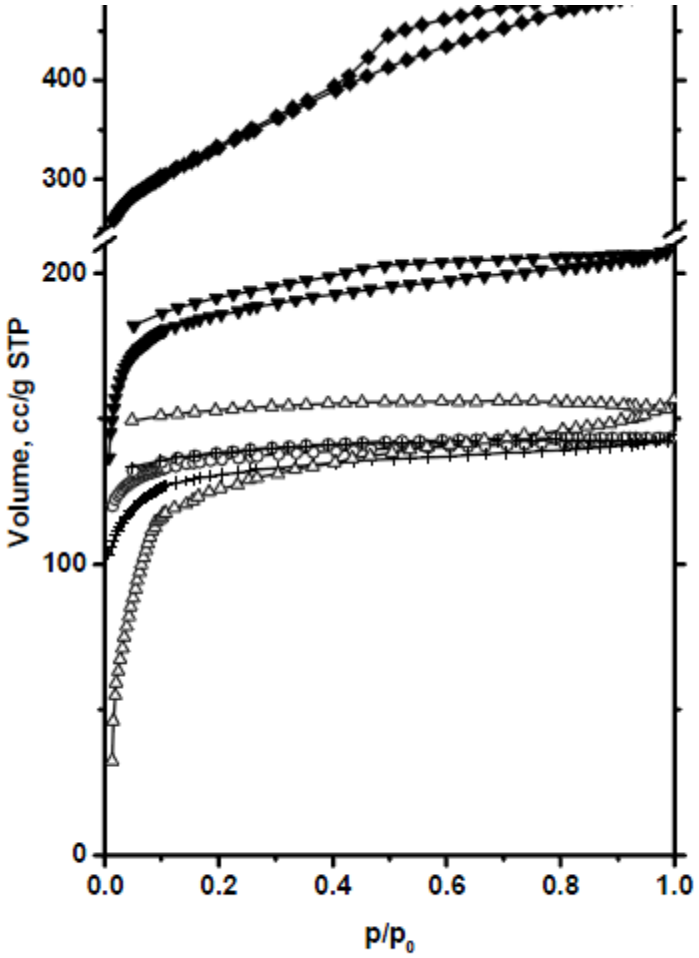

Figure 1. N_2 adsorption isotherms of the carbon samples (77 K).
O: PS600, +: PS700, △: PS800, ▼: PS900, ◆: PS1000.

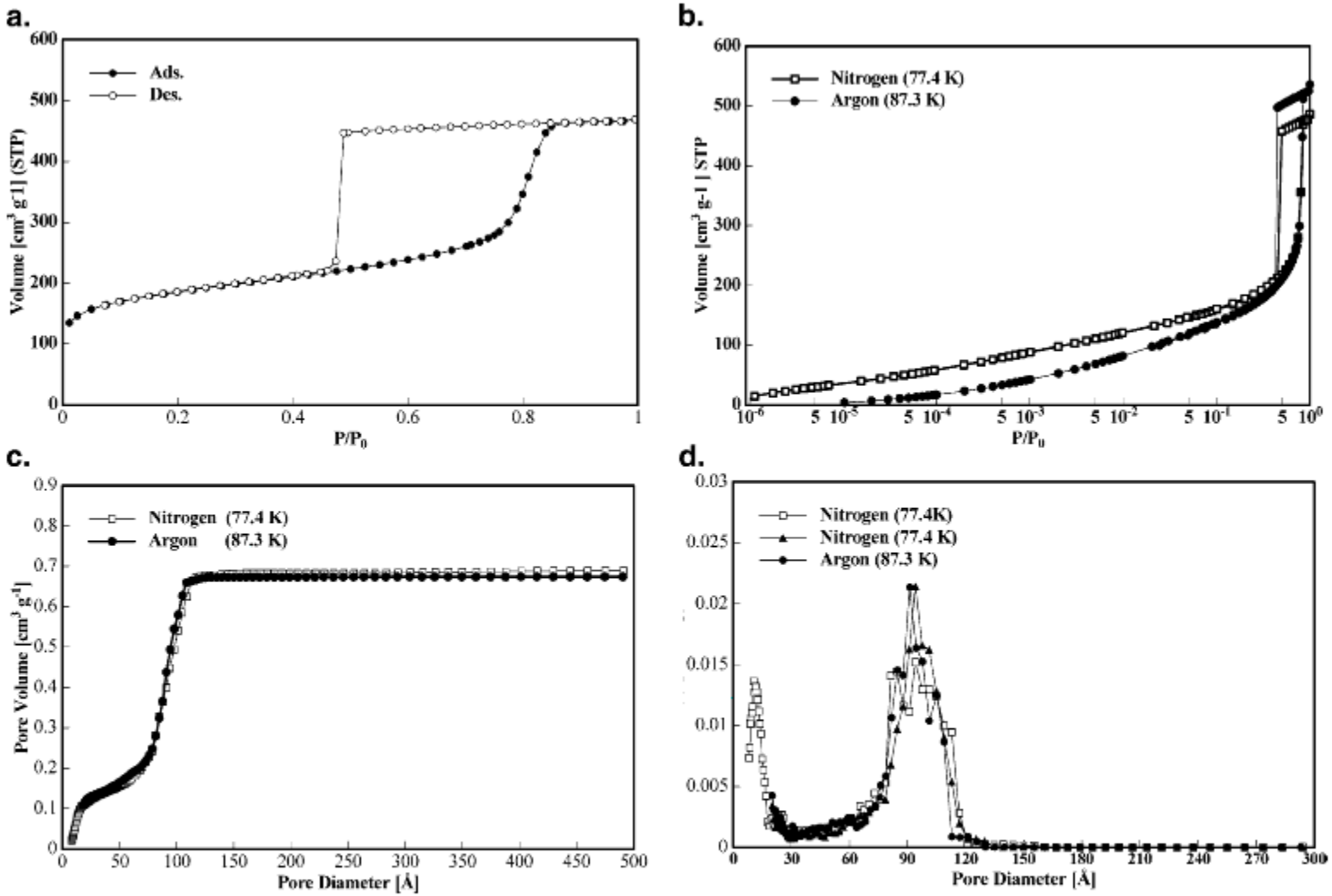

Figure 2. (a) High-resolution nitrogen (77.4 K) adsorption/desorption isotherm on SE3030 silica. (b) Nitrogen (77.4 K) and argon (87.3 K) adsorption/desorption on SE3030 silica (semilogarithmic plot). (c) NLDFT cumulative pore volume plots calculated from the adsorption branch of the adsorption/desorption isotherms shown in b by applying the kernel of metastable adsorption isotherms based on a cylindrical pore model for the systems nitrogen (77.4 K)/silica and argon (87.3 K)/silica. (d) NLDFT differential pore size distribution for SE3030 silica from nitrogen (77.4 K) and argon (87.3 K) adsorption data (see b and c).

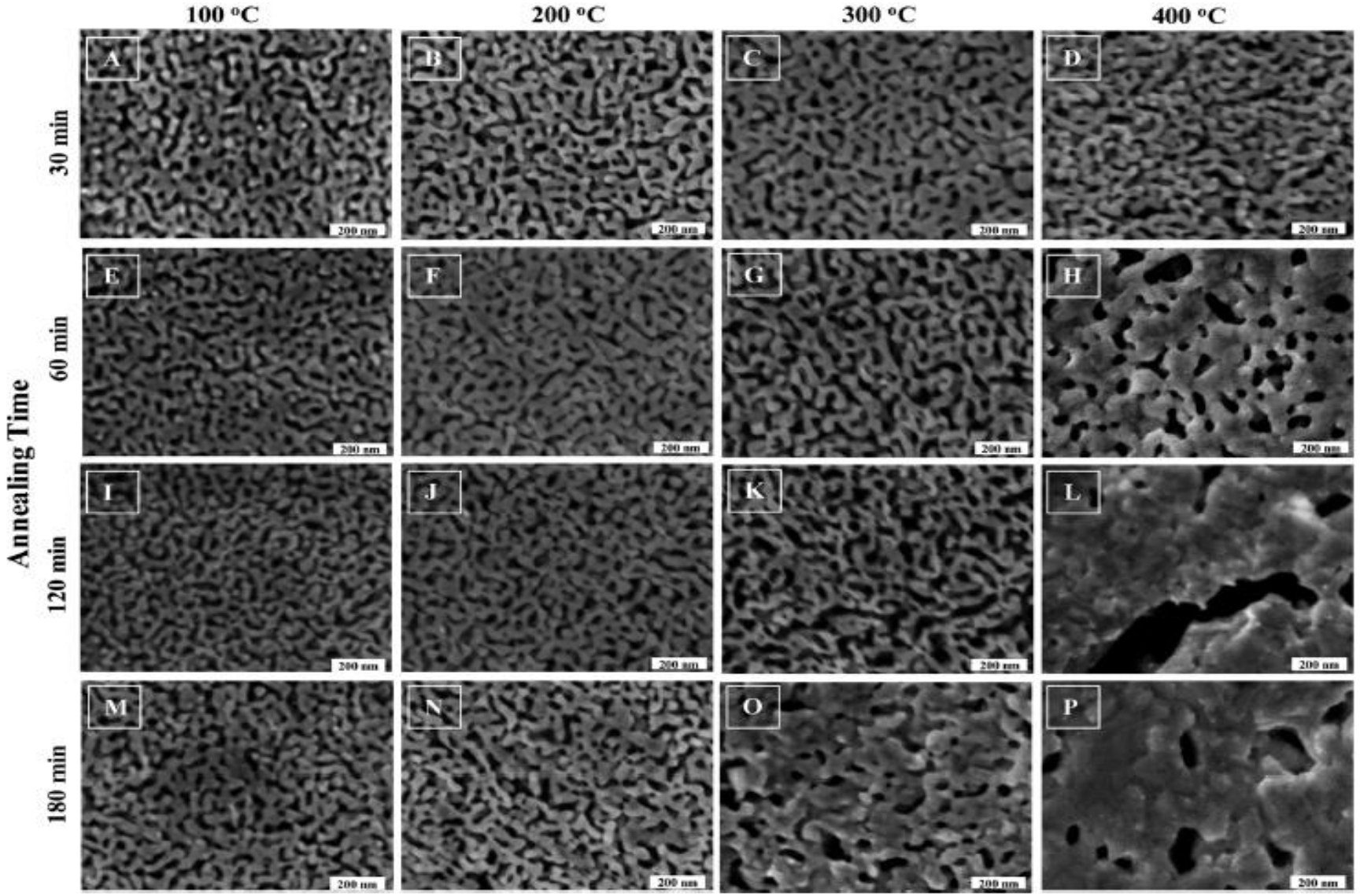

Fig. 1 SEM images of the exterior of thermally annealed nanoporous gold. Nitric acid dealloyed np-Au plates were subjected to the indicated annealing temperatures and times. Gradual and small morphology changes for np-Au were observed for annealing temperatures of 100 °C and 200 °C. More noticeable changes were observed at 300 °C. Drastic changes in np-Au morphology were apparent for np-Au annealed at 400 °C. The first observation of np-Au fusion/nucleation begins at 400 °C at 60 min annealing time. The SEM image for un-annealed np-Au was very similar to A above, and is not shown.

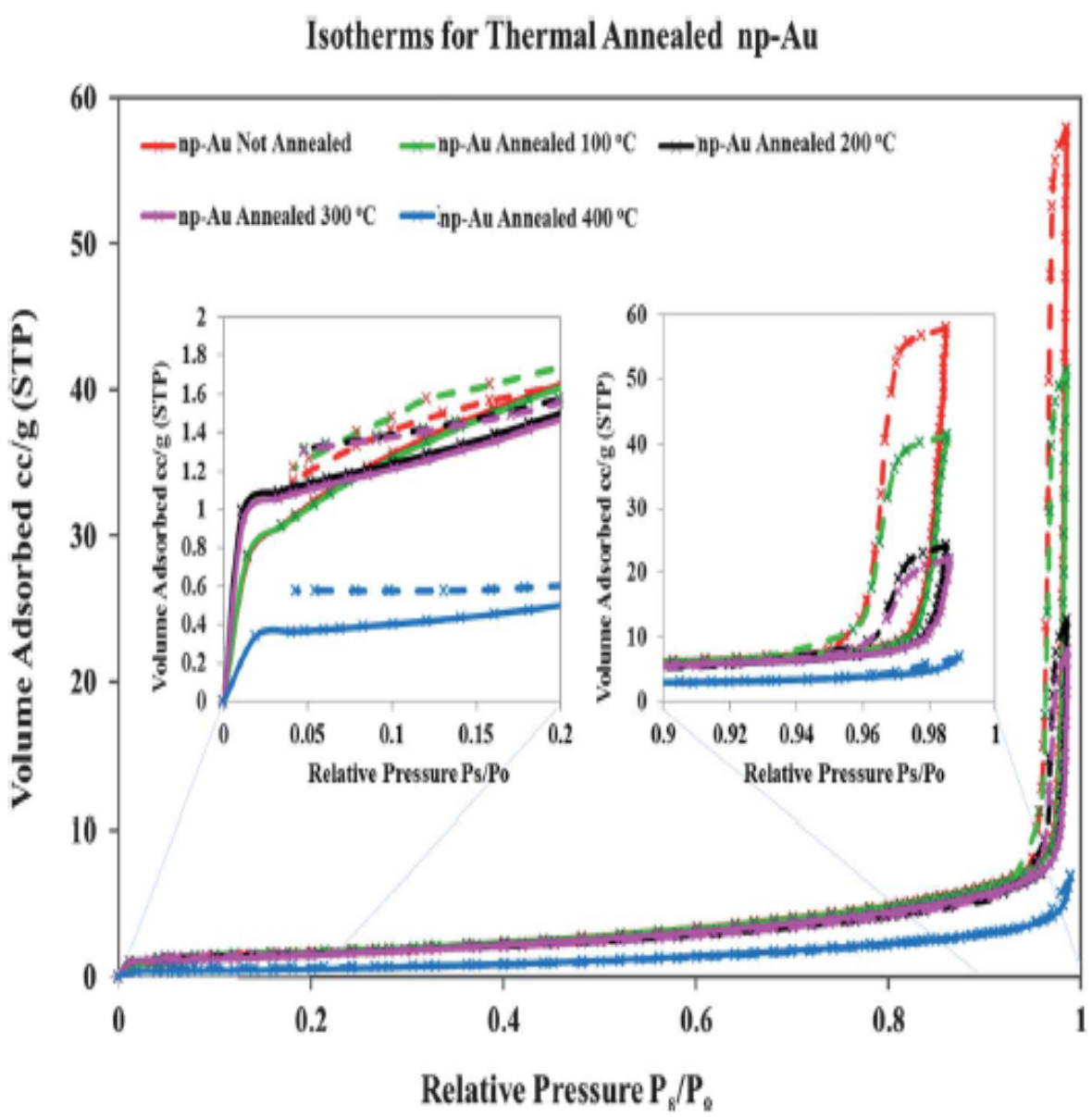

Fig. 2 Nitrogen adsorption and desorption isotherms for thermally annealed np-Au samples. The sorption isotherms for the un-annealed np-Au (red), and thermally annealed np-Au at 100 °C (green), 200 °C (black), 300 °C (pink), and 400 °C (blue) are shown. The isotherm of each substrate shows a distinct sharp "knee" point near P_s/P_o around 0.01–0.02. The np-Au isotherms present a steep adsorption/desorption at very high relative pressures

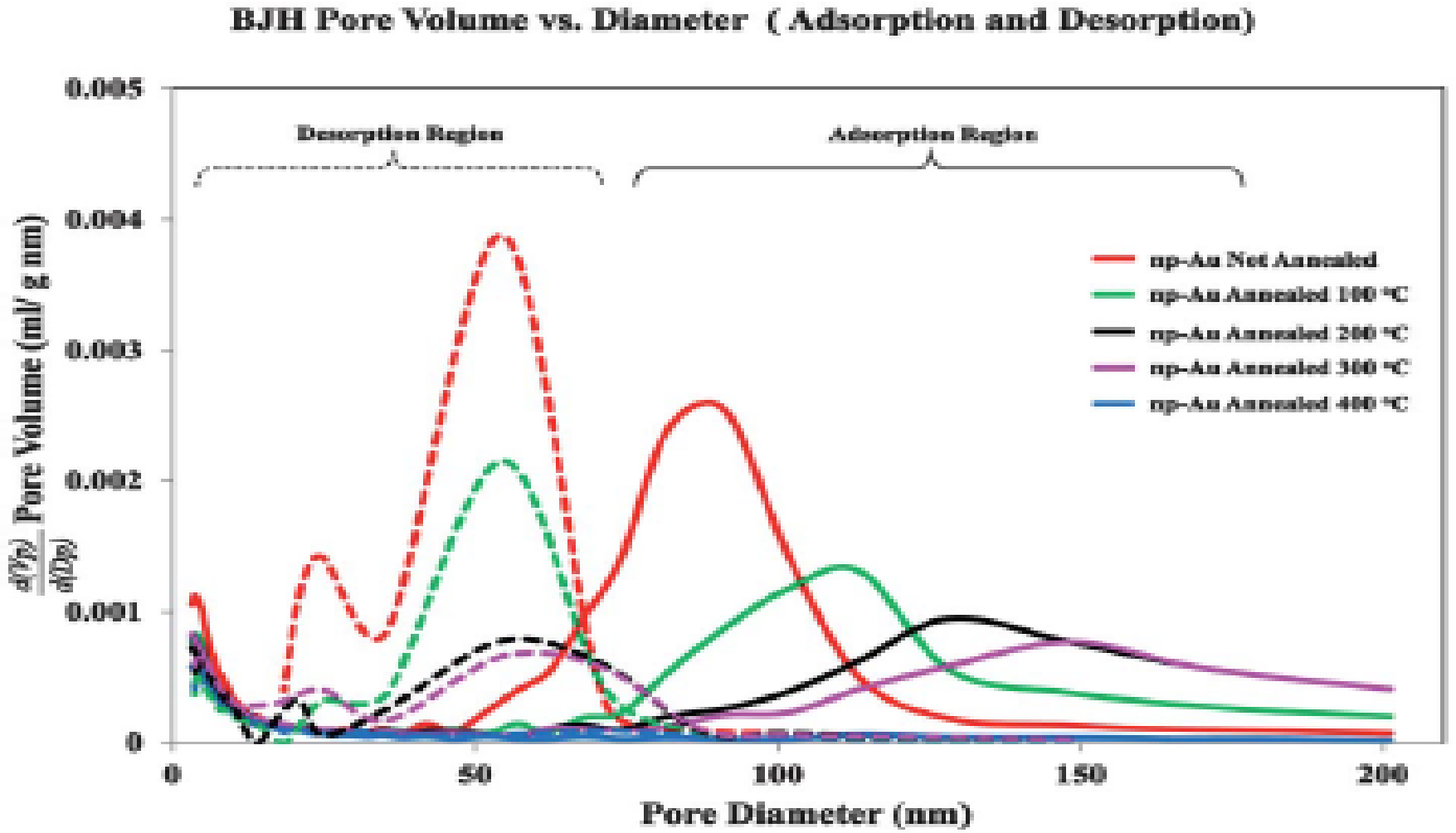

Fig. 3 Barrett-Joyner-Halenda (BJH) pore-size distribution and nitrogen adsorption-desorption isotherms for np-Au that was not annealed and for np-Au annealed at 100 °C, 200 °C, 300 °C, and 400 °C. The area under the pore size distribution curves decreases with annealing temperature, consistent with the decrease in total surface area.

No.	Catalyst Metal/Support	Metal content wt%	Volumetric adsorption H/M	O/M	CO/M[b]	TPR H/M	TEM $\bar{d}_{VA}$(Å)	D[c] from TEM
1	Pt / ALO-1	0.50[d]	1.25 (0.41)	0.55	1.22 (0.60)	0.98	10	1.14
2	Pt / ALO-4	0.50[d]	1.25 (0.43)	0.57	1.25 (0.52)	1.06	10	1.14
3	Pt / ALO-4	5.1[d]	1.14 (0.37)	0.48	0.72 (0.15)	0.83	18	0.63
4	Pt / SIO-2	0.50[d]	0.28 (0.10)	0.13	0.19 (0.026)	0.33	72	0.16
5	Pt / SAH	0.64[e]	0.76 (0.25)	0.36	0.82 (0.33)	0.68	18	0.63
6	Pt / SAL	0.72[e]	0.60 (0.22)	0.34	0.73 (0.30)	0.56	21	0.54
7	Pt / Z-1	0.50[d]	0.13[f] (0.07)	0.08[f]	0.29 (0.15)	0.04	82	0.14
8	Pd / ALO-4	0.50[e]	0.91 (0.28)	0.40	0.82 (0.27)	0.90	9	1.26
9	Rh / ALO-4	0.50[e]	0.92 (0.46)	0.91	1.29 (0.30)	0.79	9	1.22

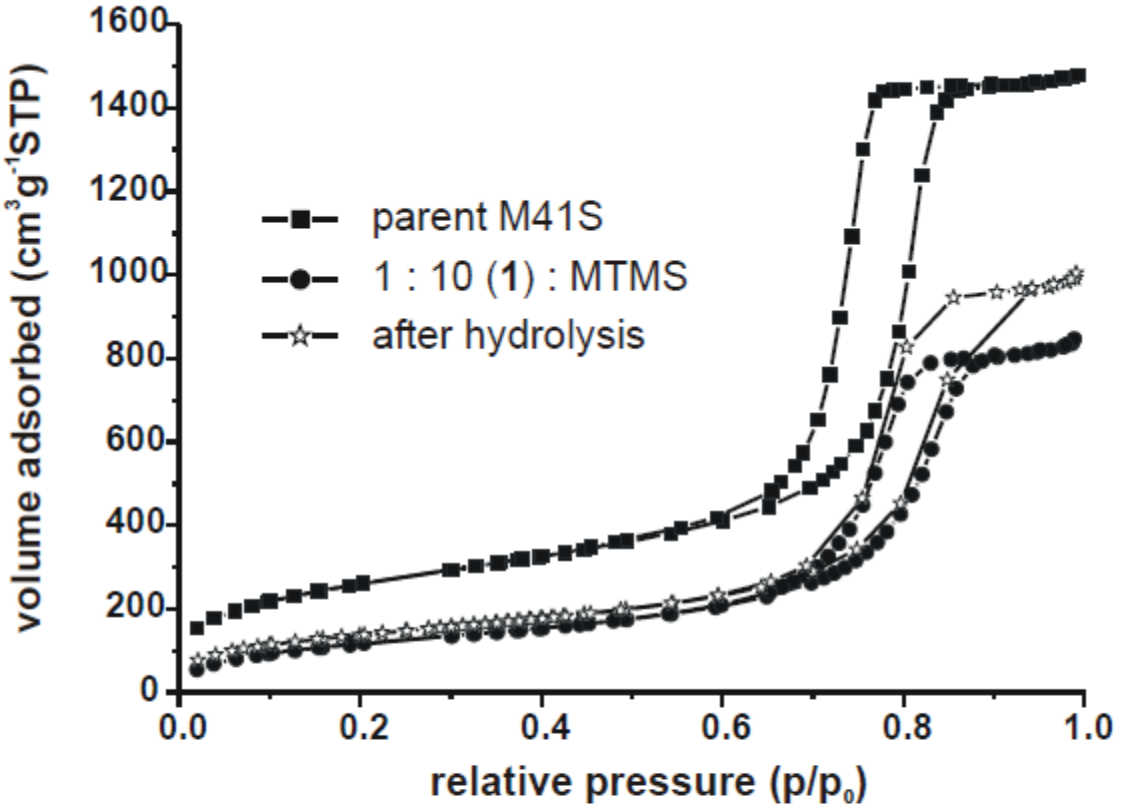

Figure 5.2 N_2 isotherms of the parent M41S sample (squares), of a M41S material functionalized with (**1**) : MTMS 1 : 10 (circles) and of the same sample after hydrolysis (stars).

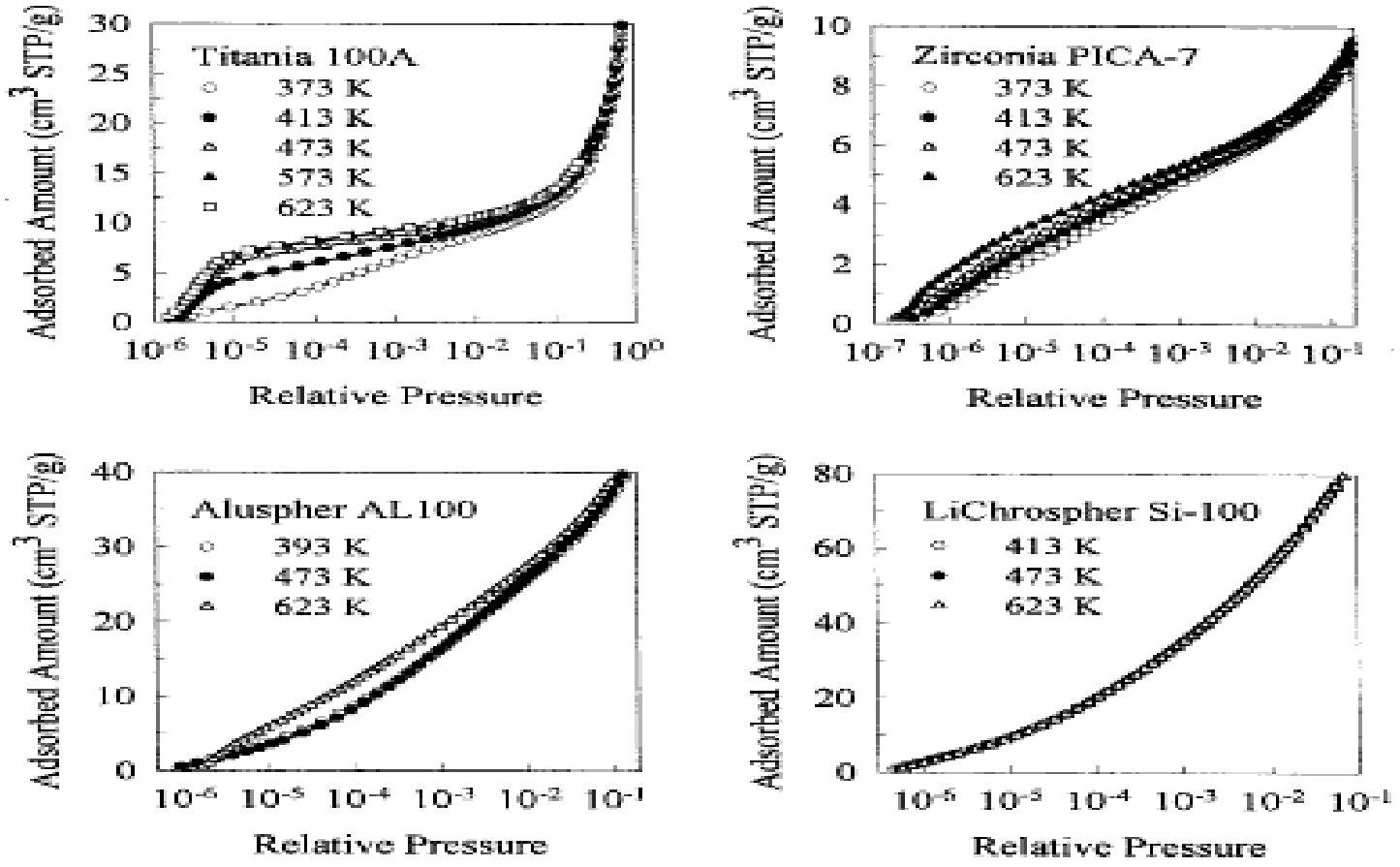

Fig. 3. Comparison of low-pressure nitrogen adsorption isotherms for the porous oxides thermally treated at different temperatures in the range from 373 to 623 K.

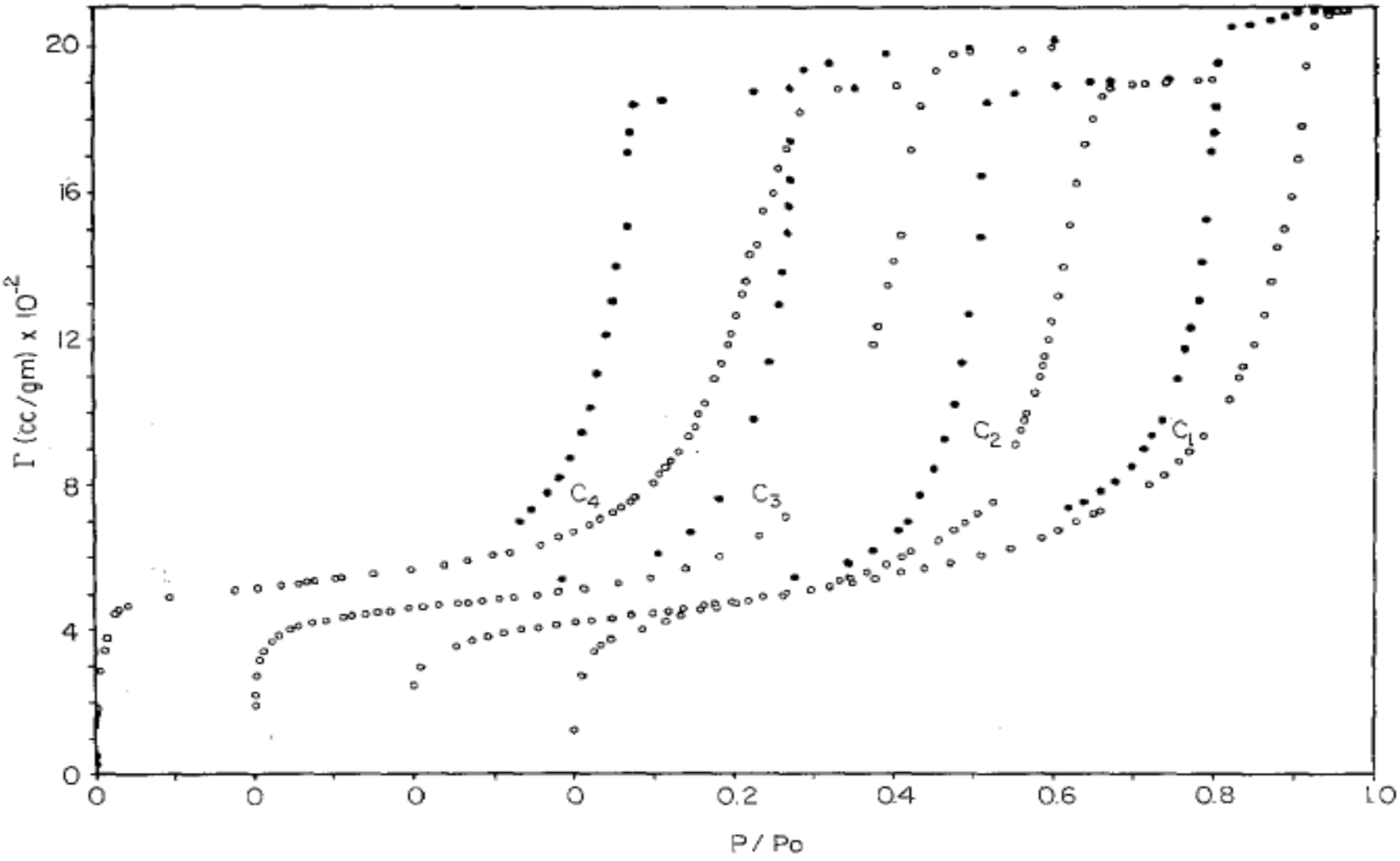

FIG. 1. The measured isotherms for the four alcohols as indicated

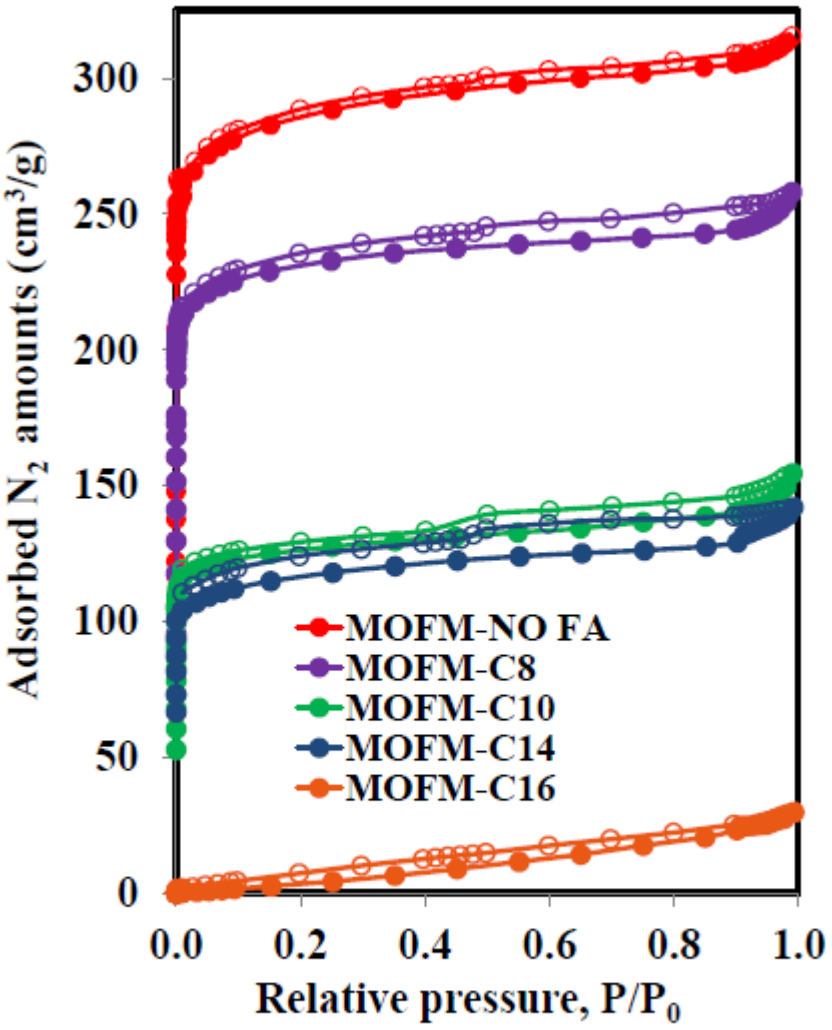

Fig. 3. Nitrogen N_2 adsorption-desorption isotherms of MOF-199 samples

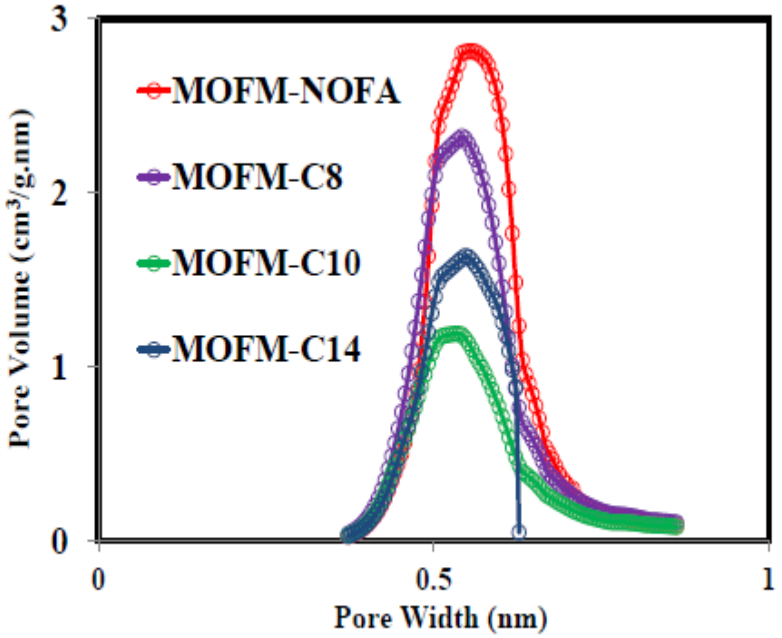

Fig.5. Nitrogen N_2 adsorption-desorption isotherms of MOF-199 samples

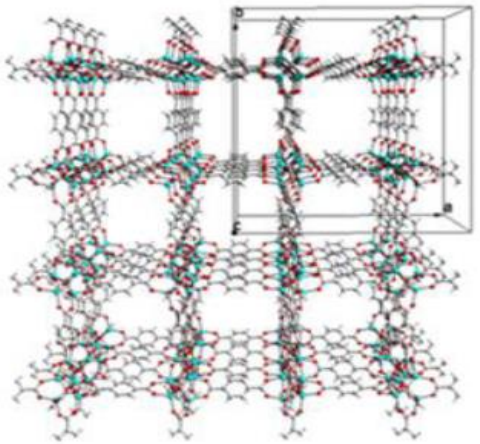

Fig. 2. Crystal structure of MOF-5 [7].

- پایان BET

FT_IR 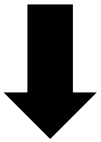

FT_IR

اینکه ما روی علم و فنّاوری تکیه میکنیم، فقط به خاطر این نیست که میخواهیم نِصاب علمی خودمان را بالا ببریم؛ پیشرفت علم و فنّاوری به پیشرفت اقتصاد کمک میکند؛ بنگاه‌هایی که دانش‌بنیان هستند میتوانند به اقتصاد ملّی کمک کنند.

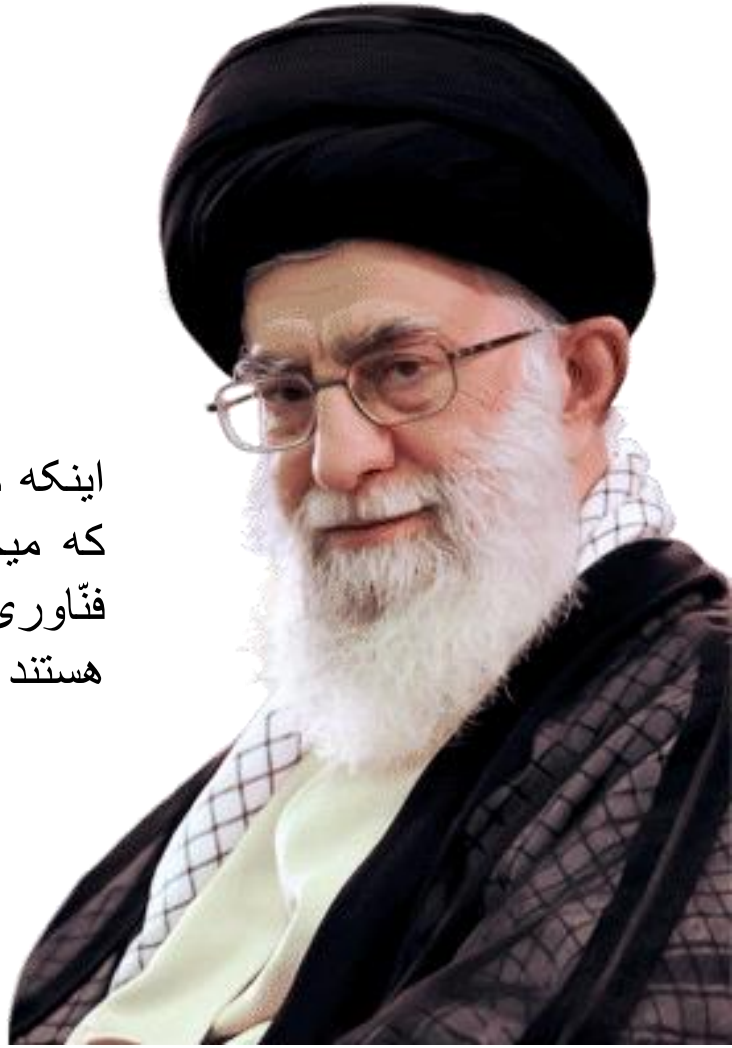

نگاهی بر روش آنالیز FTIR

IR Application Segmentation

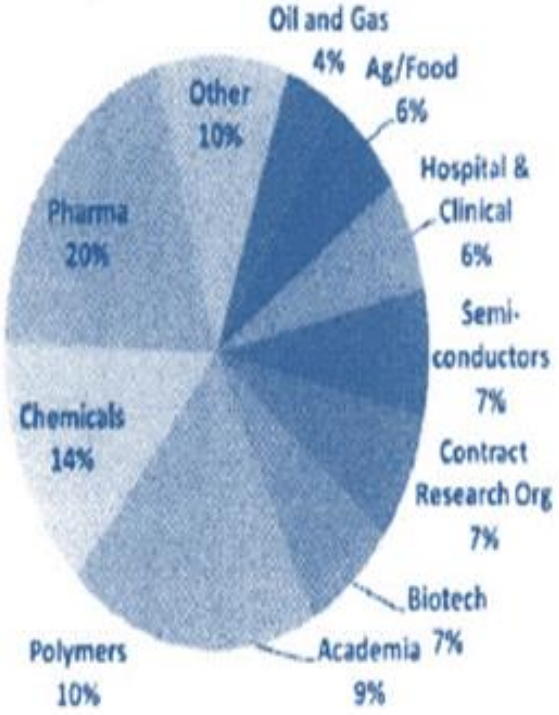

IR Functional Segmentation

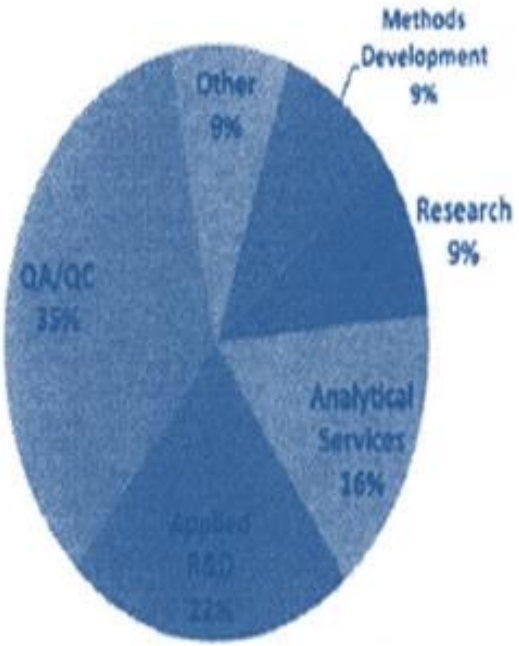

IR Regional Segmentation

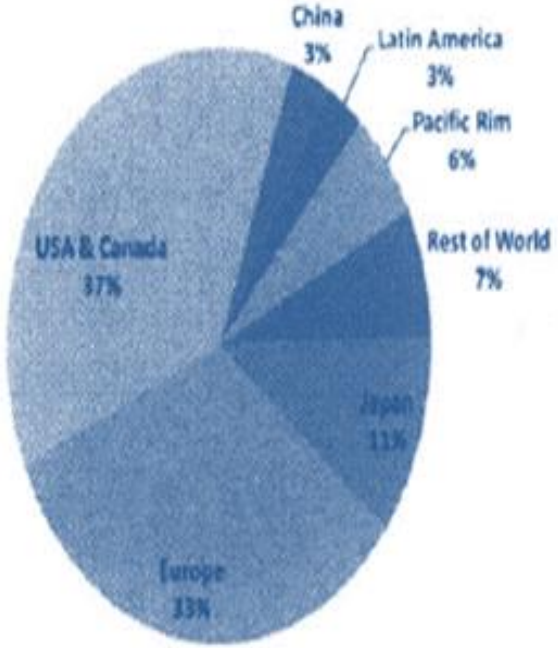

NIR Market Share

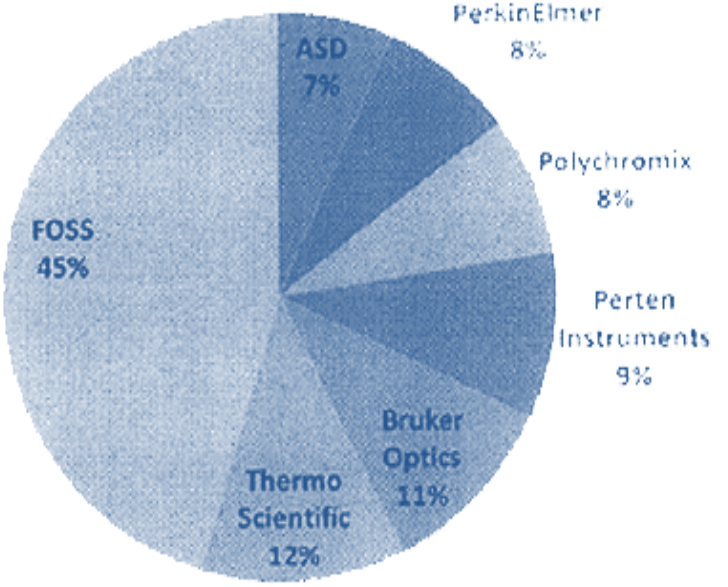

NIR Market Share Value ($M)

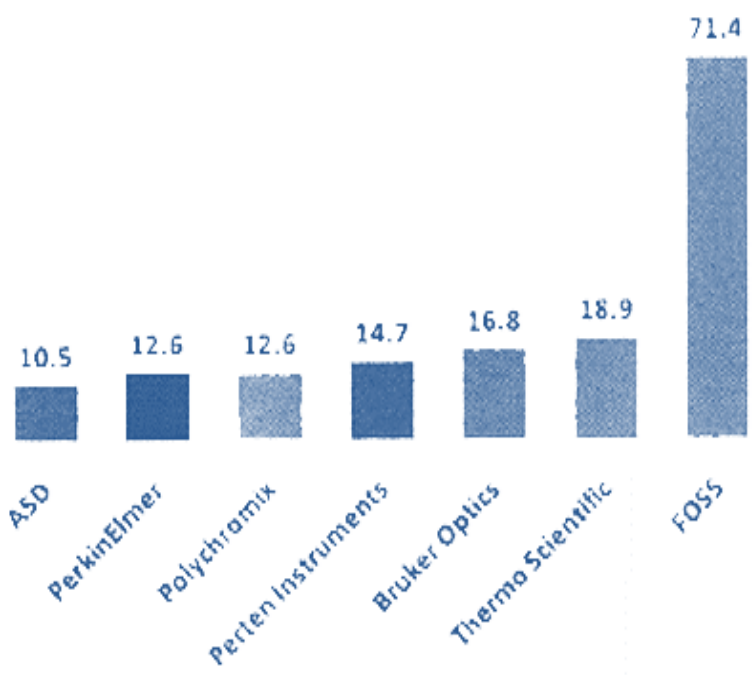

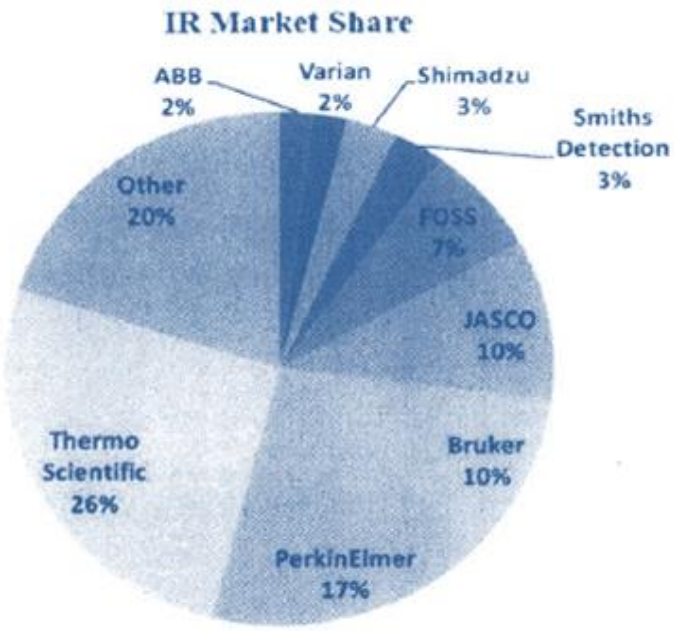
IR Market Share
ABB 2%
Varian 2%
Shimadzu 3%
Smiths Detection 3%
FOSS 7%
JASCO 10%
Bruker 10%
PerkinElmer 17%
Thermo Scientific 26%
Other 20%


IR Market Share Value (SM)
120
100
80
60
40
20
0
8.3
8.3
12.45
12.45
29.05
41.5
41.5
70.55
107.9
83
ABB
Varian
Shimadzu
Smiths Detection
FOSS
JASCO
Bruker
PerkinElmer
Thermo Scientific
Other

Infrared radiation

- Wave Number

$$\nu = \frac{1}{\lambda}$$

Region	cm^{-1}	µm	eV
Near	12000 – 4000	0.8 – 2.5	1.55 – 0.5
Mid	**4000 – 400**	**2.5 – 25**	**0.5 – 0.05**
Far	400 – 10	25 – 1000	0.05 – 0.0012

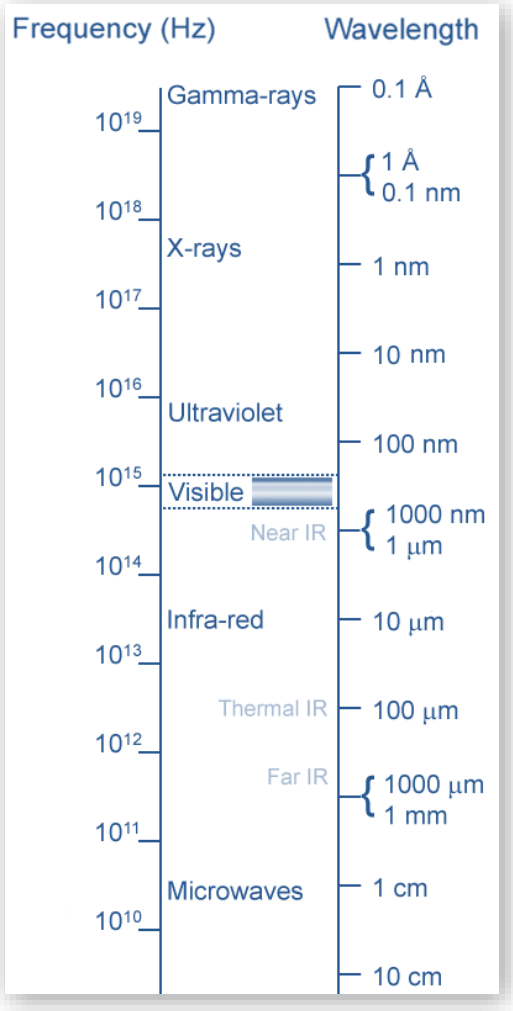

TABLE 1 Examples of Class and Individual Characteristics for Common Evidence

Evidence	Class Characteristics	Individual Characteristics
Fingerprints	General pattern type (arch, loop, whorl)	Relative location of fine detail (bifurcations and ridge endings)
Bullets	Diameter, # of land and groove impressions, mass, and direction of twist	Individual striations (scratches) imparted from the barrel
Hair	Color, length, and diameter	DNA only found in the root or attached skin cells
Glass	Color, thickness, density, refractive index, and curvature	Physical match
Soil	Color, pH, particle size distribution, and density distribution	Uncommon
Fibers	Color, cross section, chemical composition, microscopic features, refractive index, and solubility	Uncommon

Methamphetamine

Courtesy of Texas DPS Crime Laboratory Services

FIGURE 6 The presumptive color test for methamphetamine shows a deep blue-colored product.

Molecular processes

Bond breaking and ionization

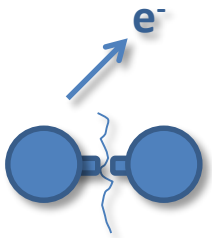

Electronic excitation

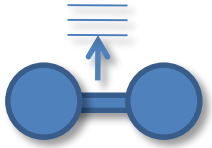

Vibration

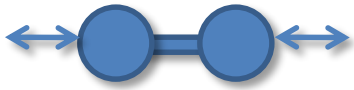

Rotation

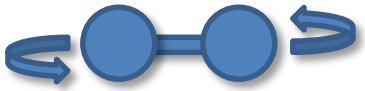

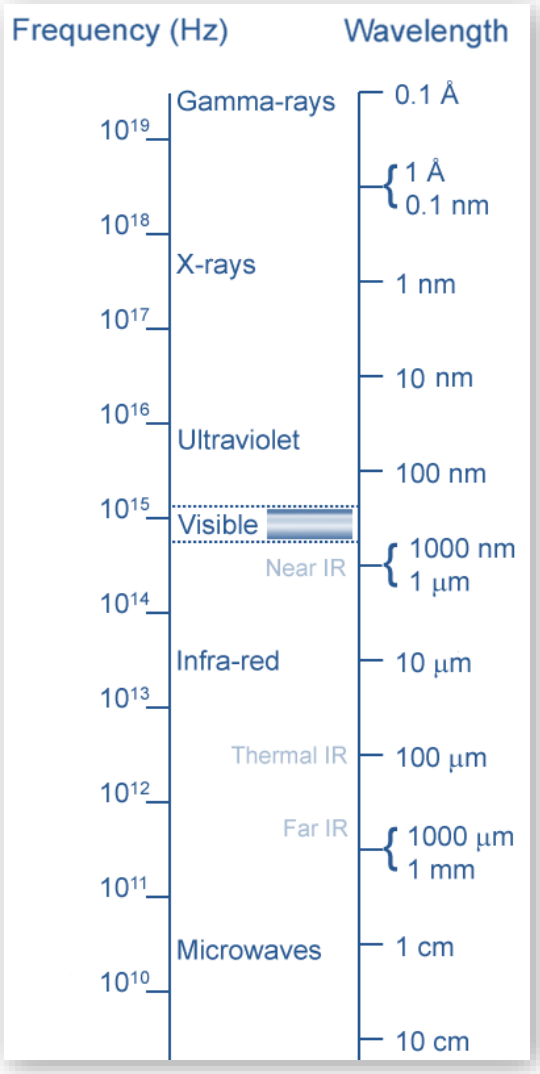

$\Delta E = h\nu$

- There are three types of molecular transitions that occur in IR

a) Rotational transitions

- When an asymmetric molecule rotates about its center of mass, the dipole moment seems to fluctuate.
- ΔE for these transitions correspond to $\bar{\nu} < 100\ cm^{-1}$
- Quite low energy, show up as sharp lines that subdivide vibrational peaks in gas phase spectra.

b) Vibrational-rotational transitions

- complex transitions that arise from changes in the molecular dipole moment due to the combination of a bond vibration and molecular rotation.

c) Vibrational transitions

- The most important transitions observed in qualitative mid-IR spectroscopy.
- $\bar{\nu} = 13{,}000 - 675\ cm^{-1}$ (0.78 – 15 μM)

Vibrational Modes

1. Stretching - the rhythmic movement along a bond axis wit a subsequent increase and decrease in bond length.

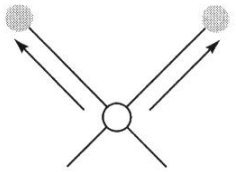

Symmetric

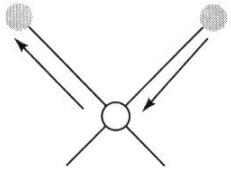

Asymmetric

2. Bending - a change in bond angle or movement of a group of atoms with respect to the rest of the molecule.

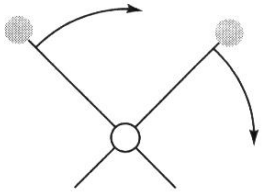

In-plane rocking

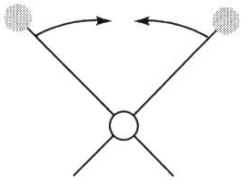

In-plane scissoring

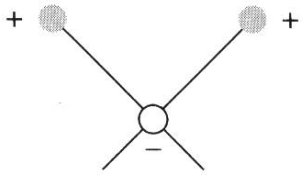

Out-of-plane wagging

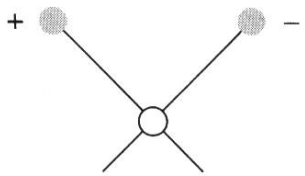

Out-of-plane twisting

…continued…

- **Quantum Treatment of Vibrations**

$$\Delta E = h\nu_m = \frac{h}{2\pi}\sqrt{\frac{k}{\mu}}$$

$$E_{radiation} = h\nu = \Delta E = h\nu_m = \frac{h}{2\pi}\sqrt{\frac{k}{\mu}}$$

The radiation in wavenumbers,

$$\bar{\nu} = \frac{1}{2\pi c}\sqrt{\frac{k}{\mu}} = 5.3 \times 10^{-12}\sqrt{\frac{k}{\mu}}$$

Infrared Spectrum of Hexane

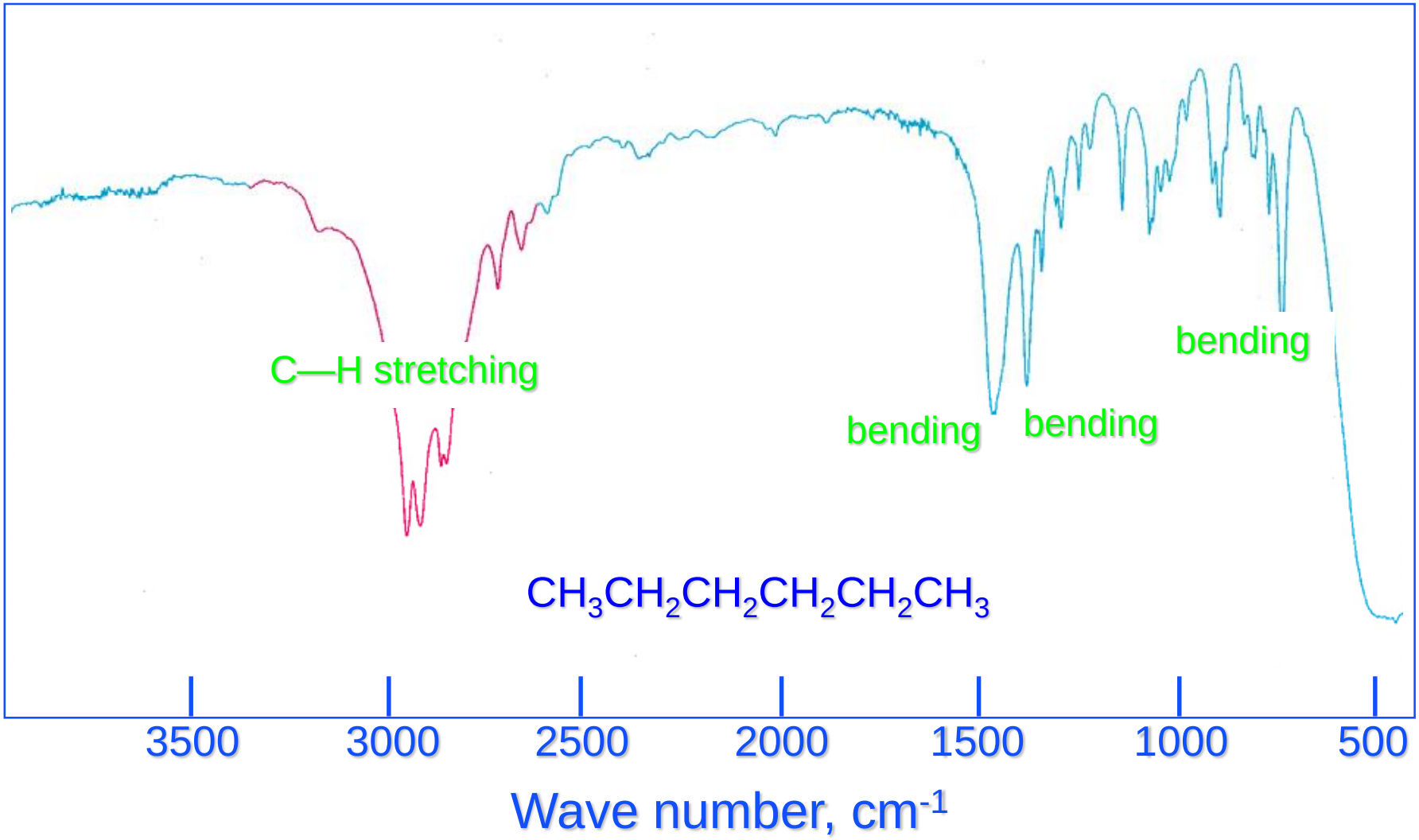

Infrared Spectrum of 2-Hexanol

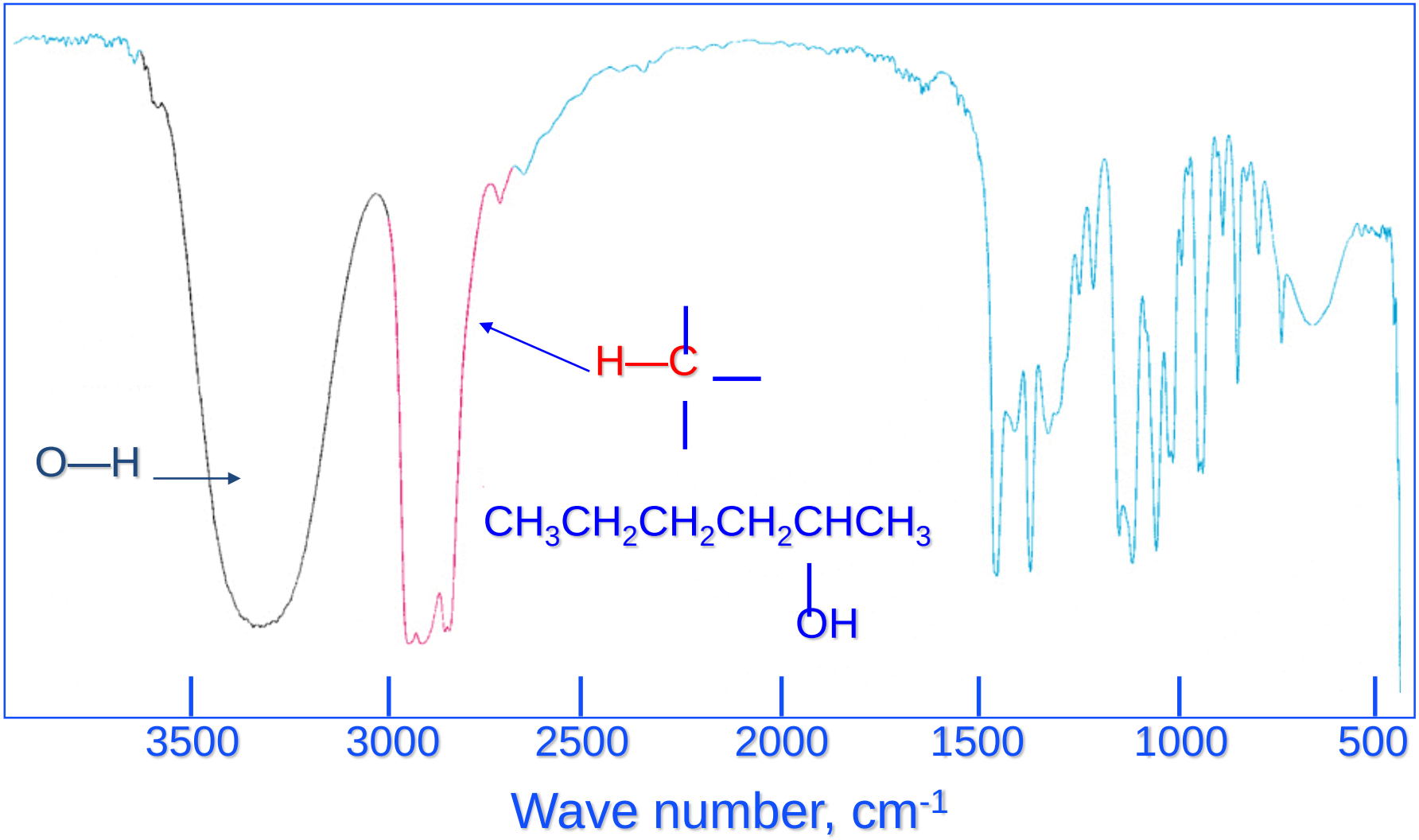

Dispersion spectrometer

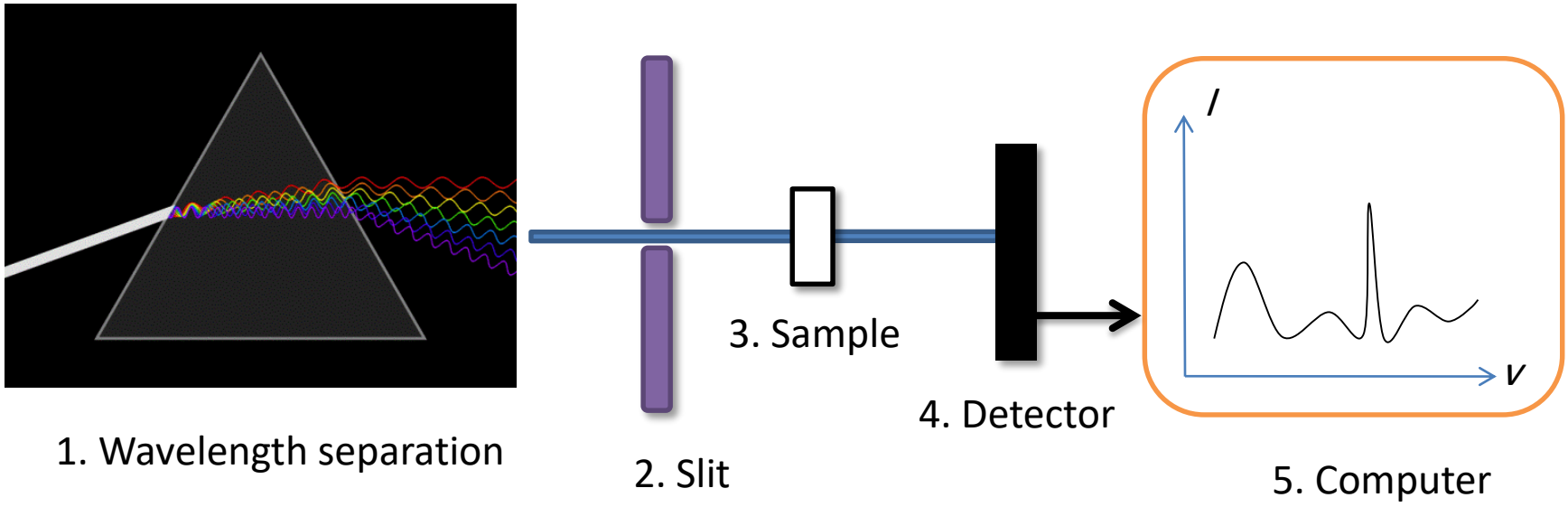

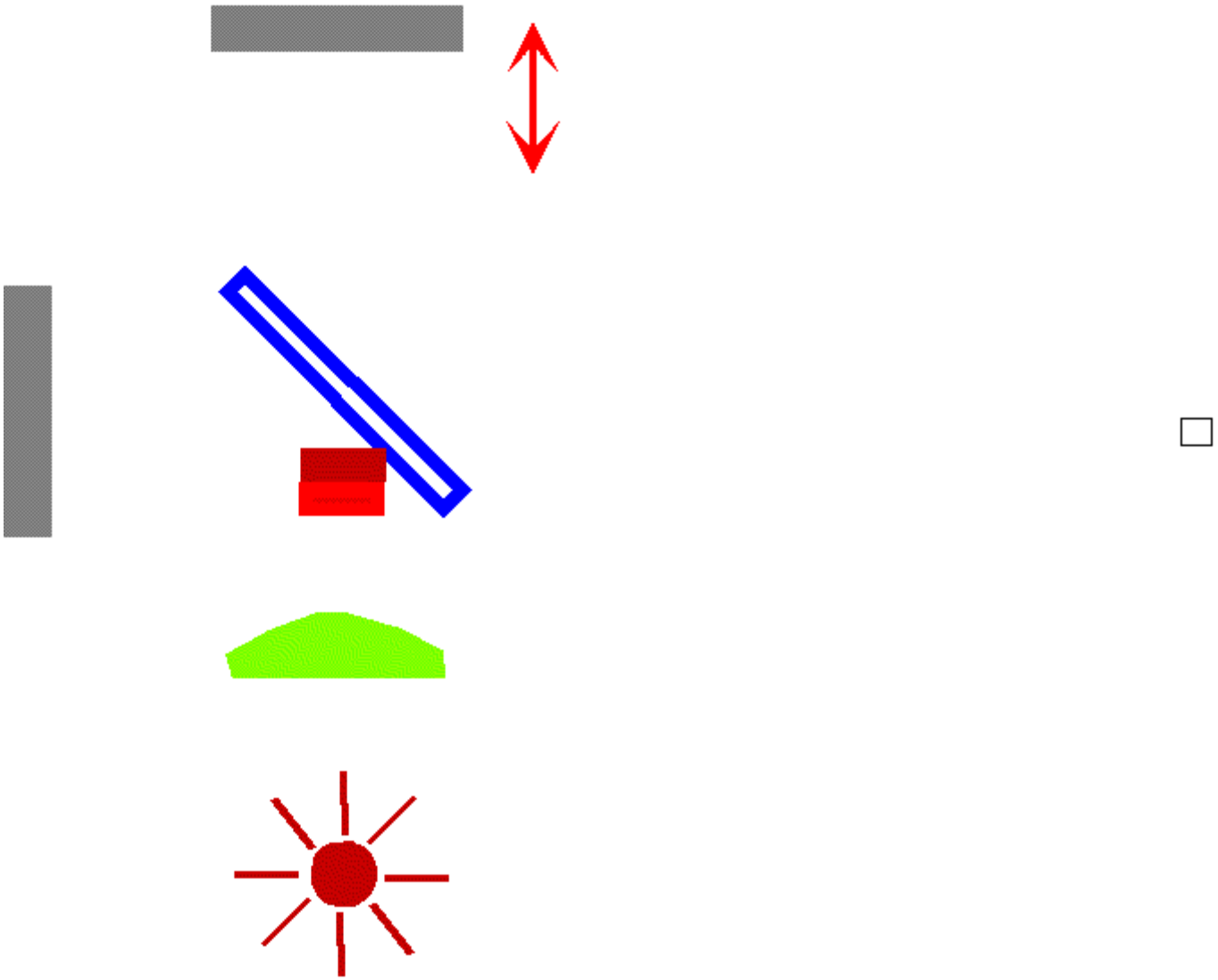

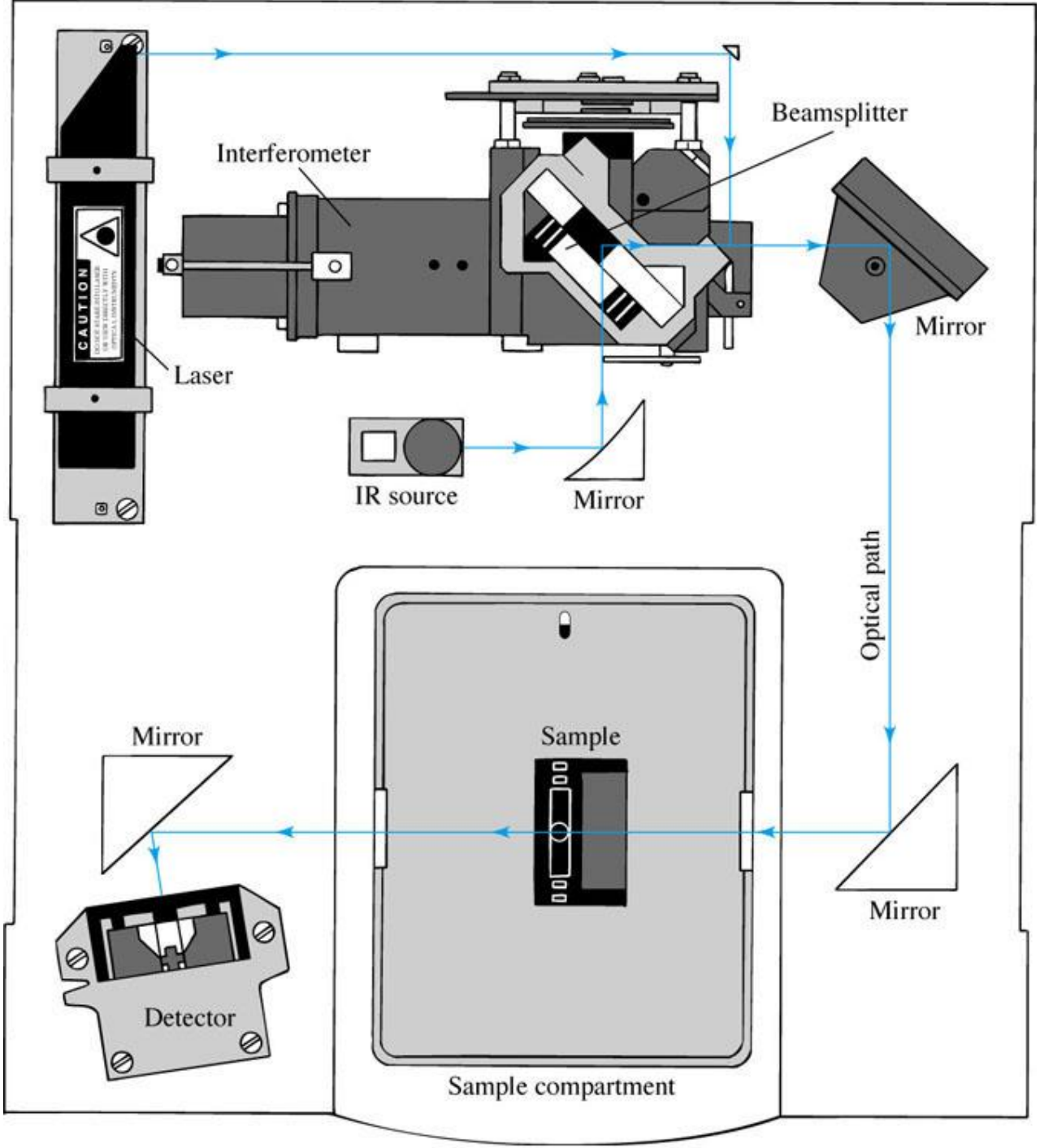

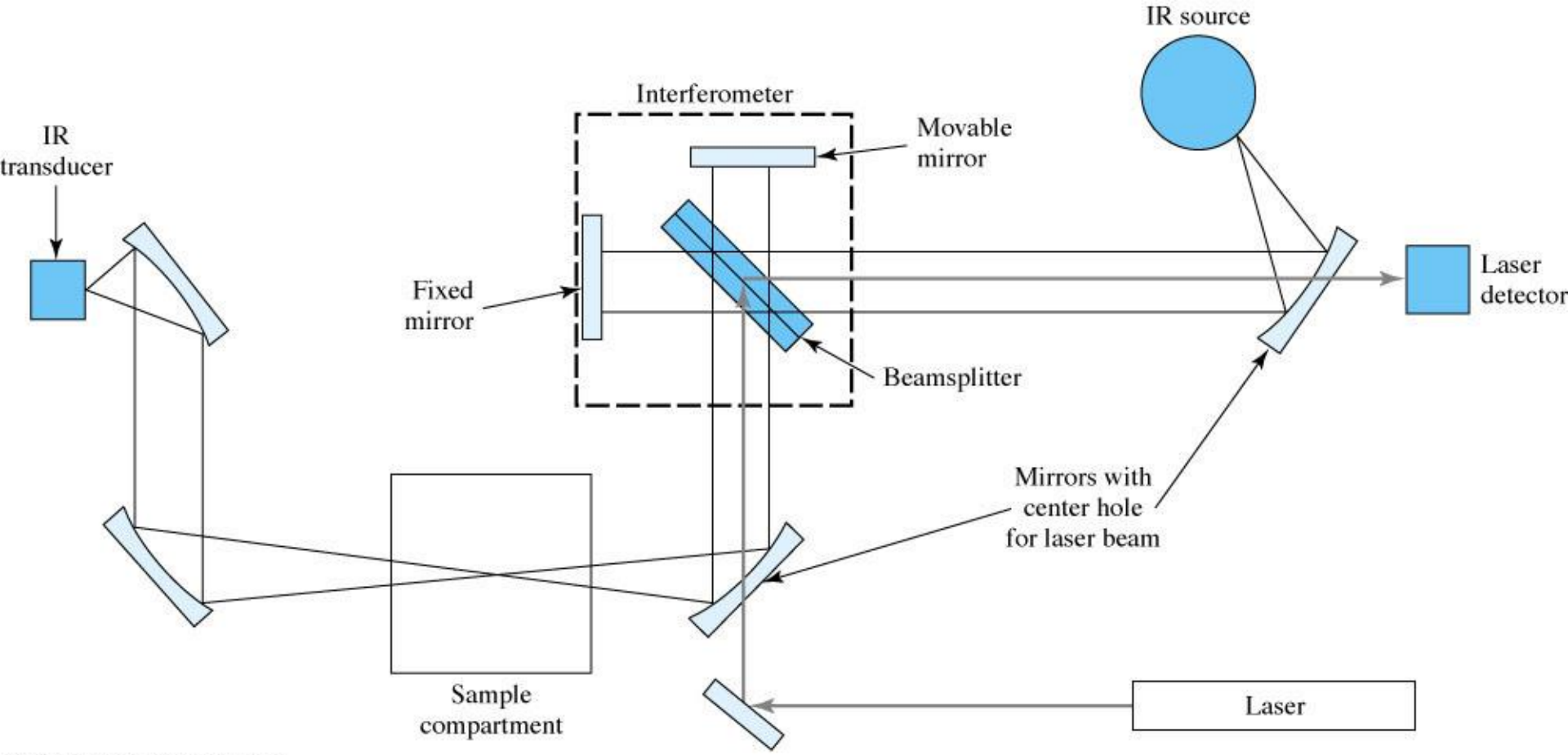

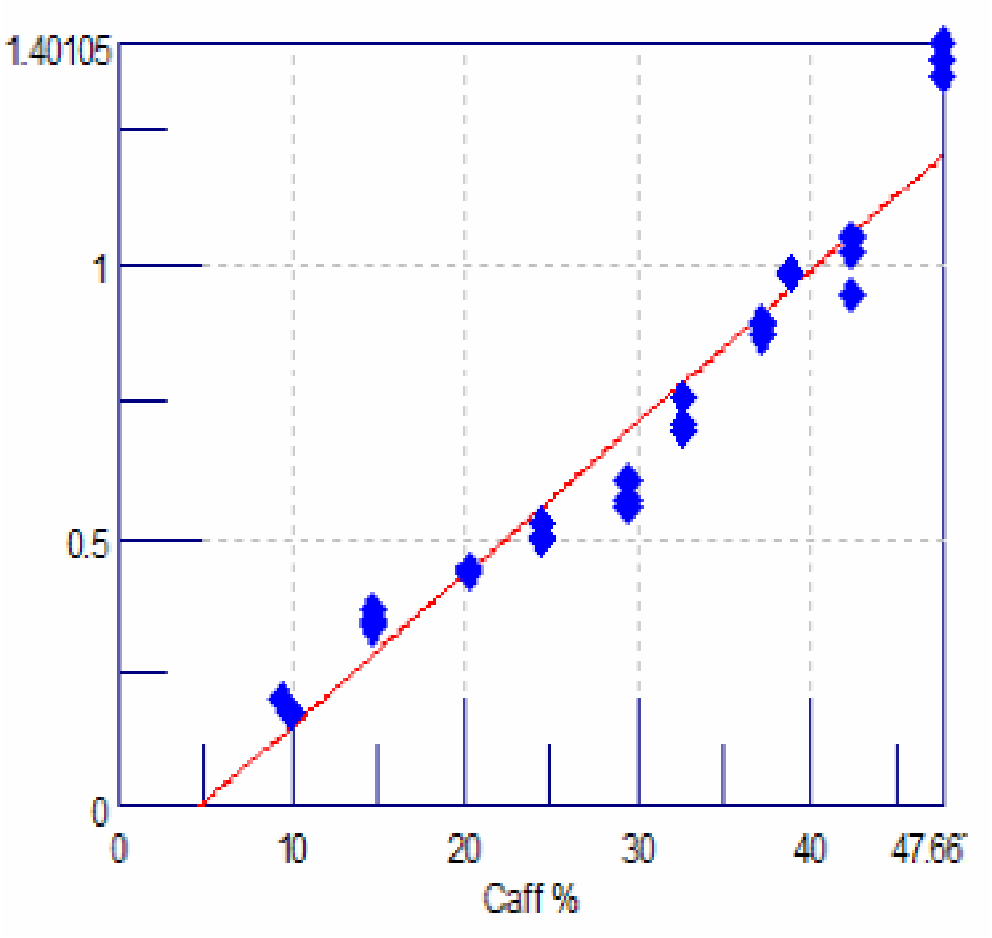
1.40105
1
0.5
0
0
10
20
30
40
47.66
Caff %

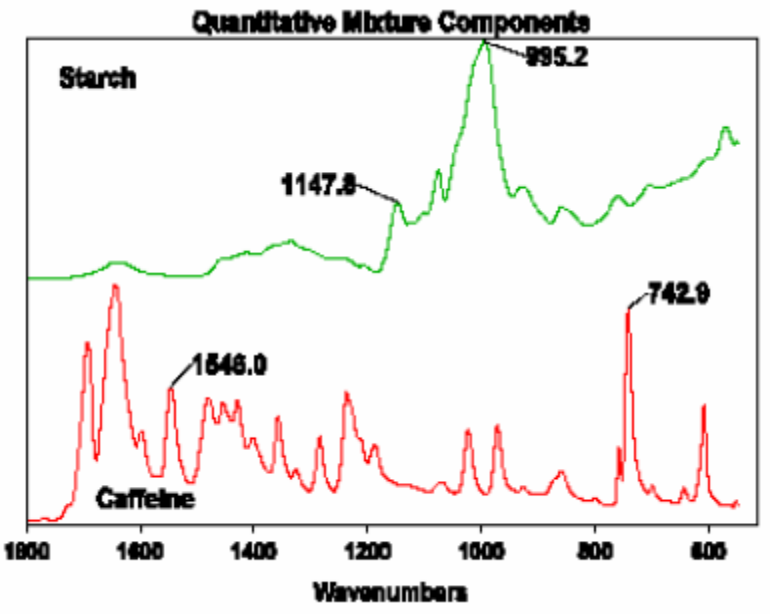
Quantitative Mixture Components
Starch
995.2
1147.8
742.9
1548.0
Caffeine
1800
1600
1400
1200
1000
800
600
Wavenumbers

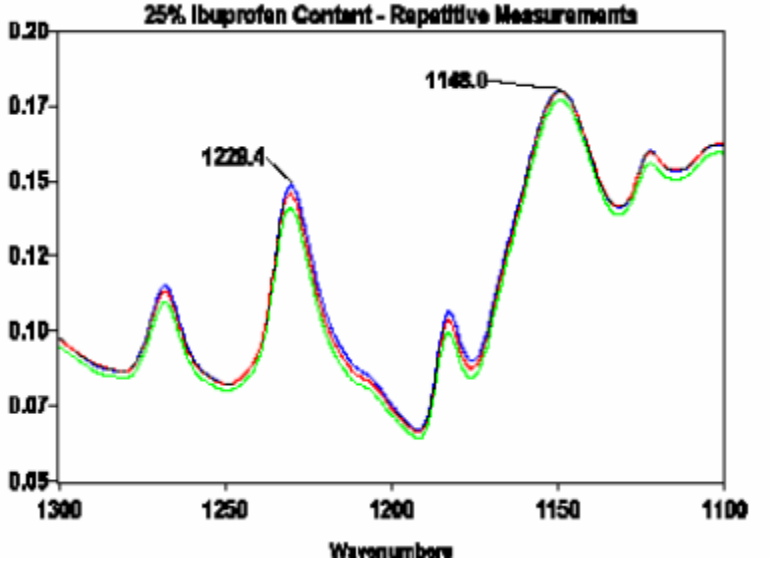
25% Ibuprofen Content - Repetitive Measurements
0.20
0.17
0.15
0.12
0.10
0.07
0.05
1148.0
1229.4
1300
1250
1200
1150
1100
Wavenumbers

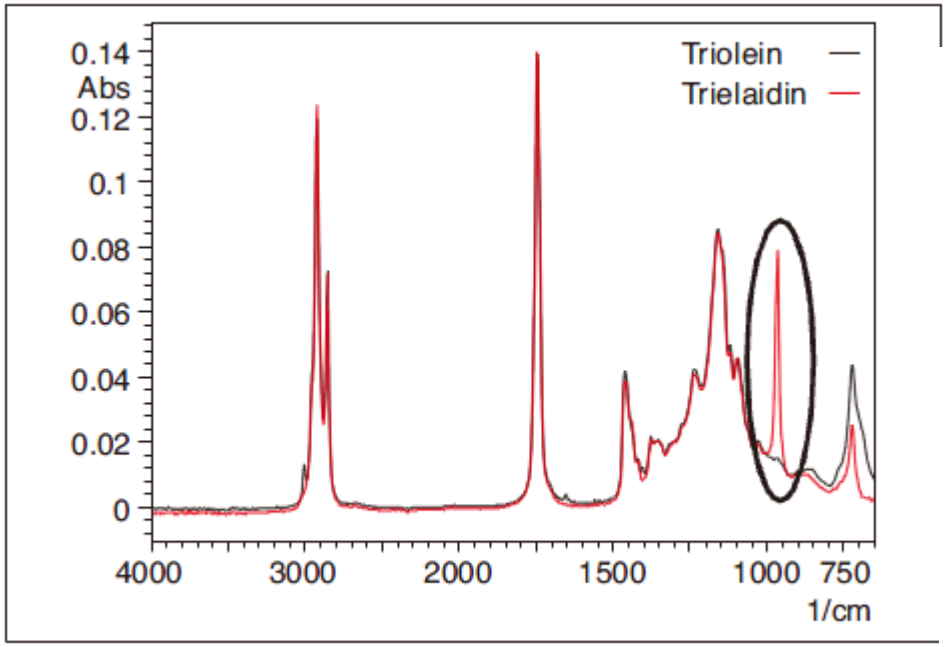

Fig. 3 Infrared Spectra of Triolein and Trielaidin

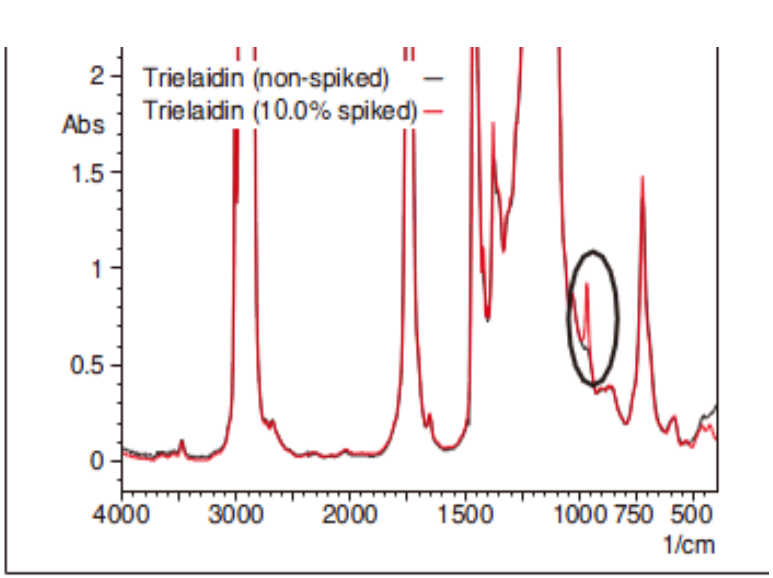

Fig. 6 Infrared Spectra of Unspiked Olive Oil and Olive Oil Spiked with Trielaidin

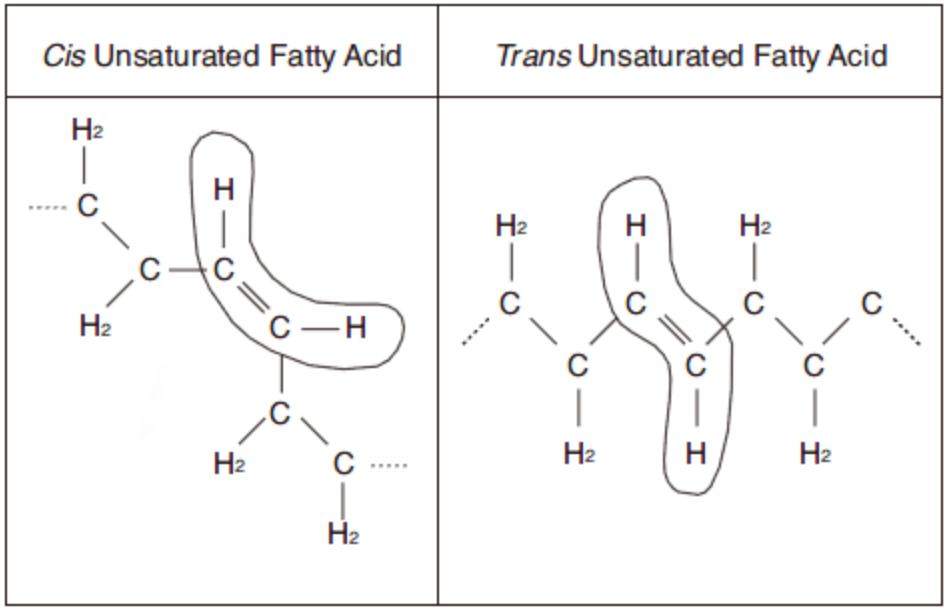

Fig. 2 Structures of *Cis* and *Trans* Fatty Acids

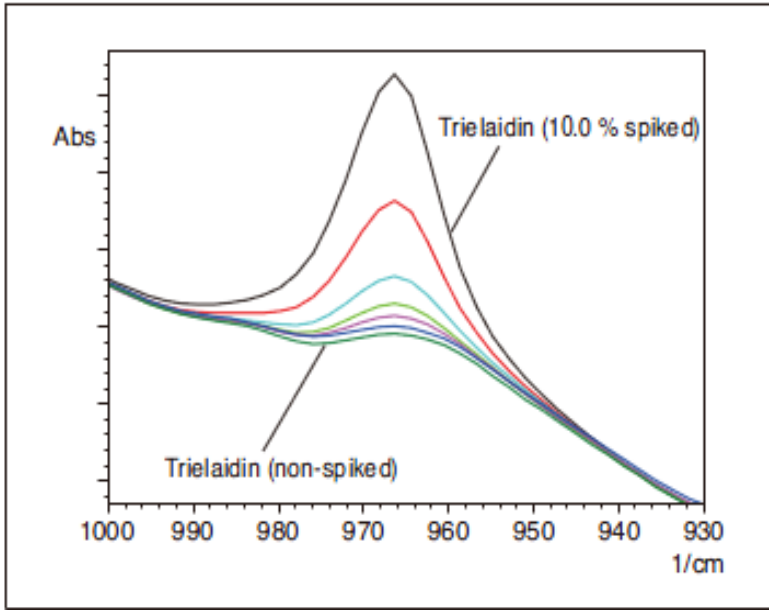

- The Michelson interferometer principle
- 1. example: Monochromatic light

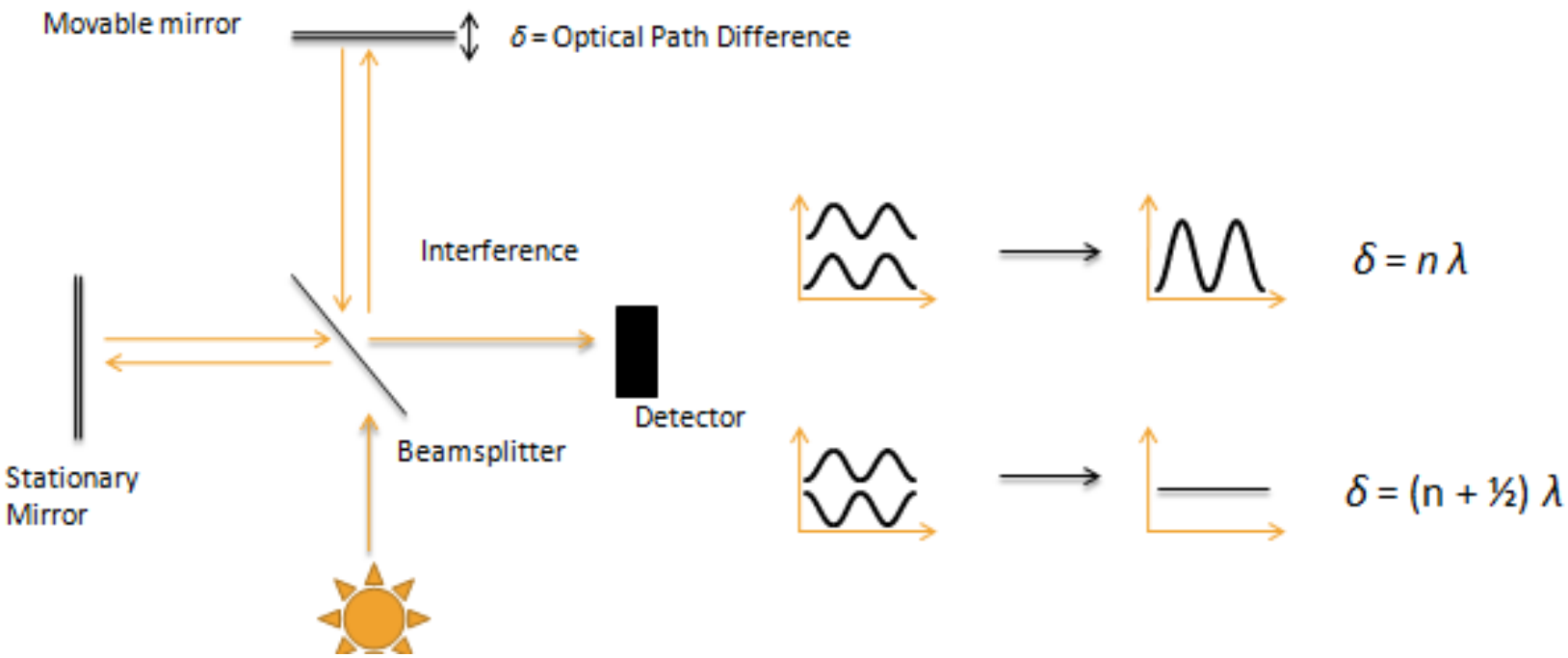

Mathematics (contd.)

- **The resulting interferogram is described as an infinitely long cosine wave**
- $B(\nu)\cos(2\pi\frac{\delta}{\lambda})$ **where** $B(\nu)$ **=intensity as F(v)**
- **For non-monochromatic source treat each frequency as if it resulted in a separate cosine train.**

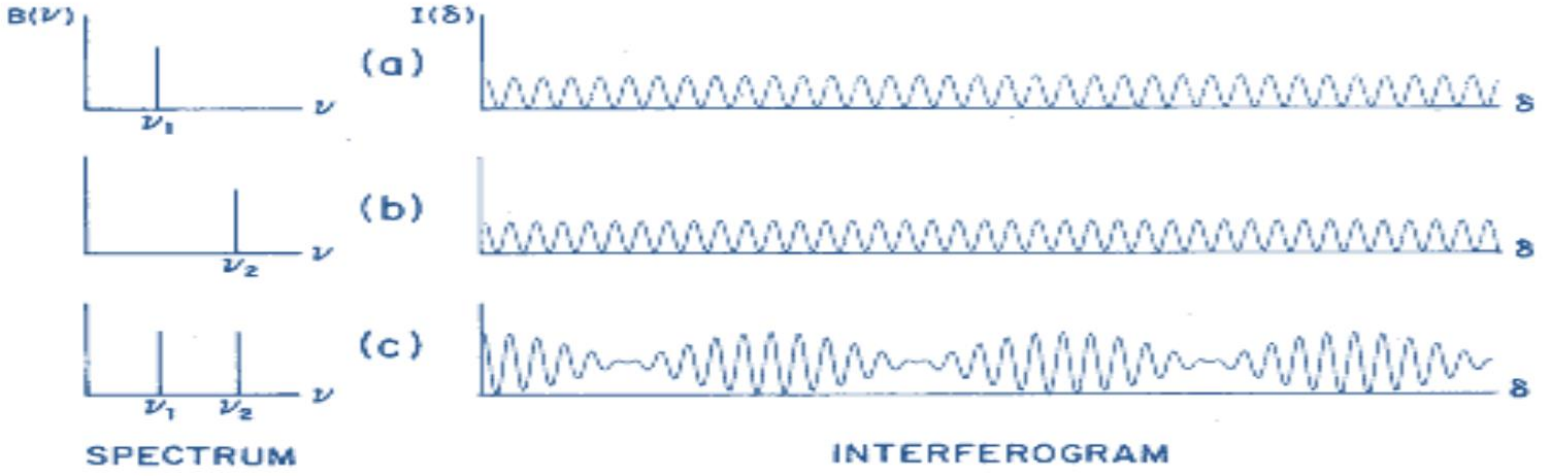

FTIR

- Broadband source

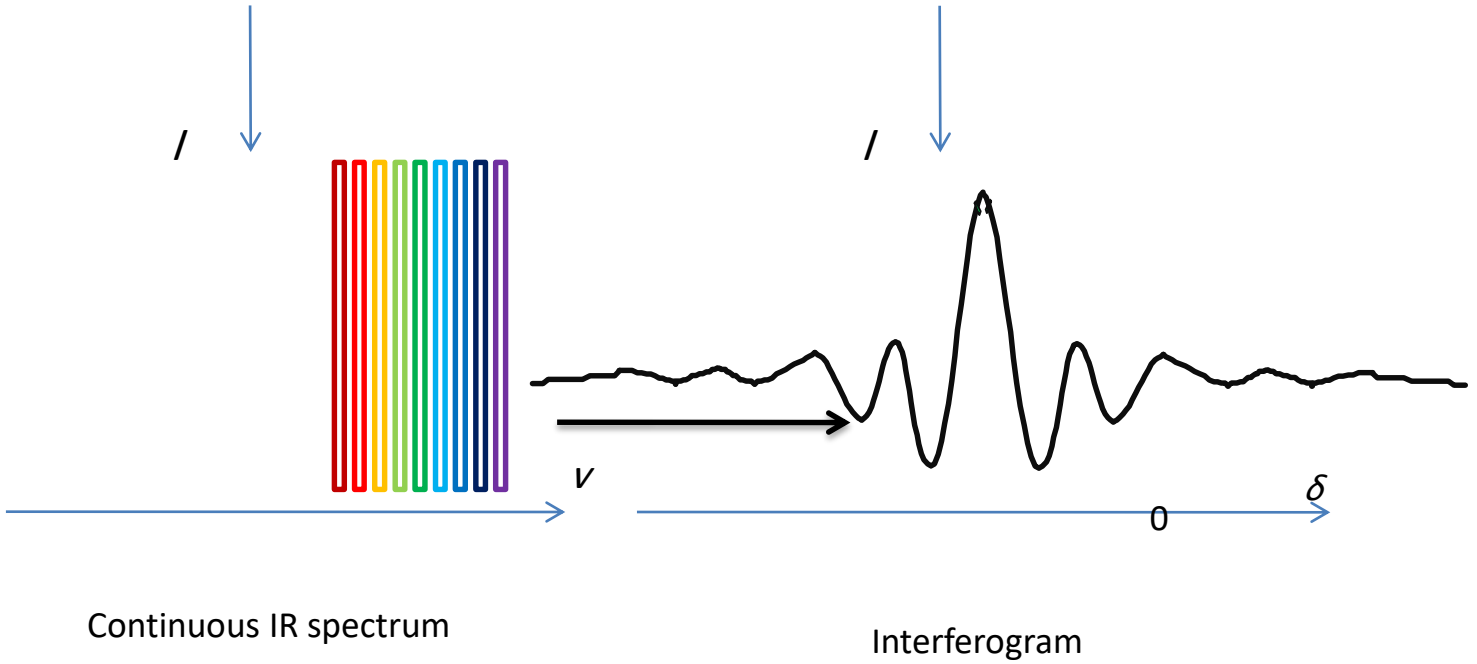

Multiplexing (FT) Spectrometers

- Collect data in the time domain and convert to the frequency domain by Fourier Transform.

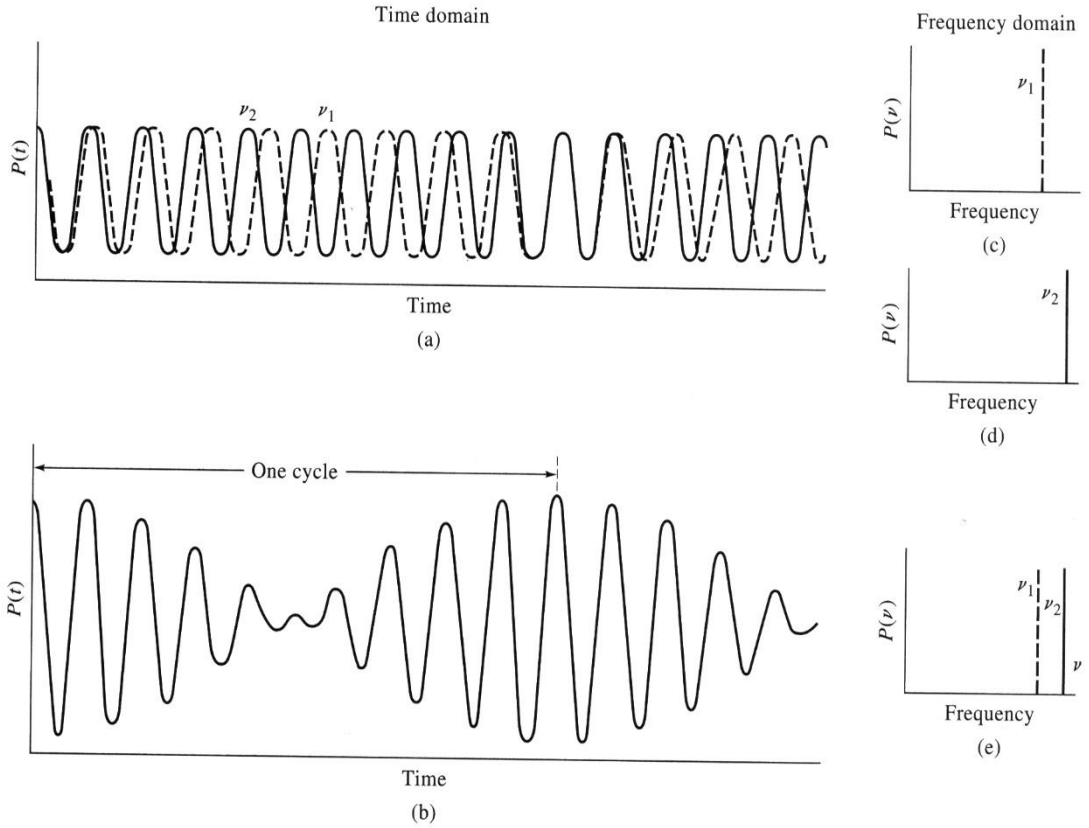

- Detectors are not fast enough to respond to power variations at high frequency (10^{12} to 10^{15} Hz) so the signal is modulated by a *Michelson interferometer* to a lower frequency that is directly proportional to the high frequency.

Fourier Transform

$$I(\delta) = \int_{-\infty}^{\infty} B(\nu)\cos(2\pi\nu\delta)d\nu$$

FT

$$B(\nu) = \int_{-\infty}^{\infty} I(\delta)\cos(2\pi\nu\delta)d\delta$$

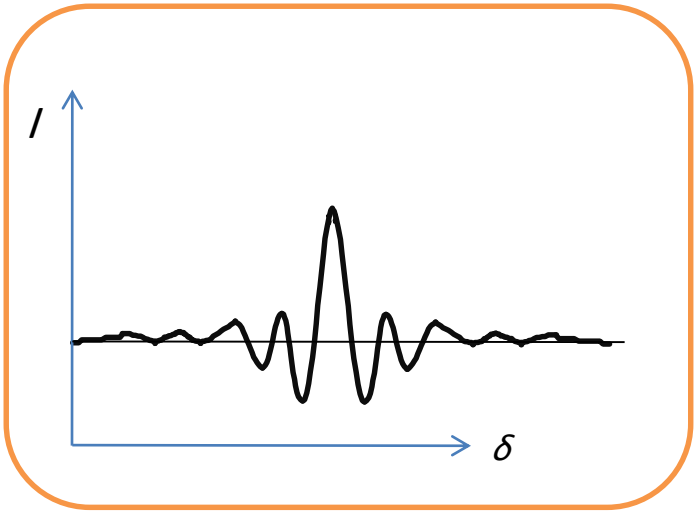

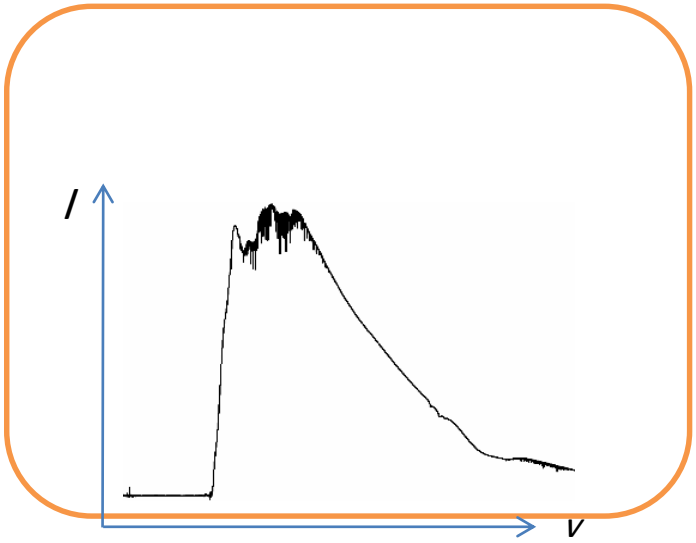

Time domain: *I* vs. δ

Frequency domain: *I* vs. ν

Measurement Techniques(contd.)

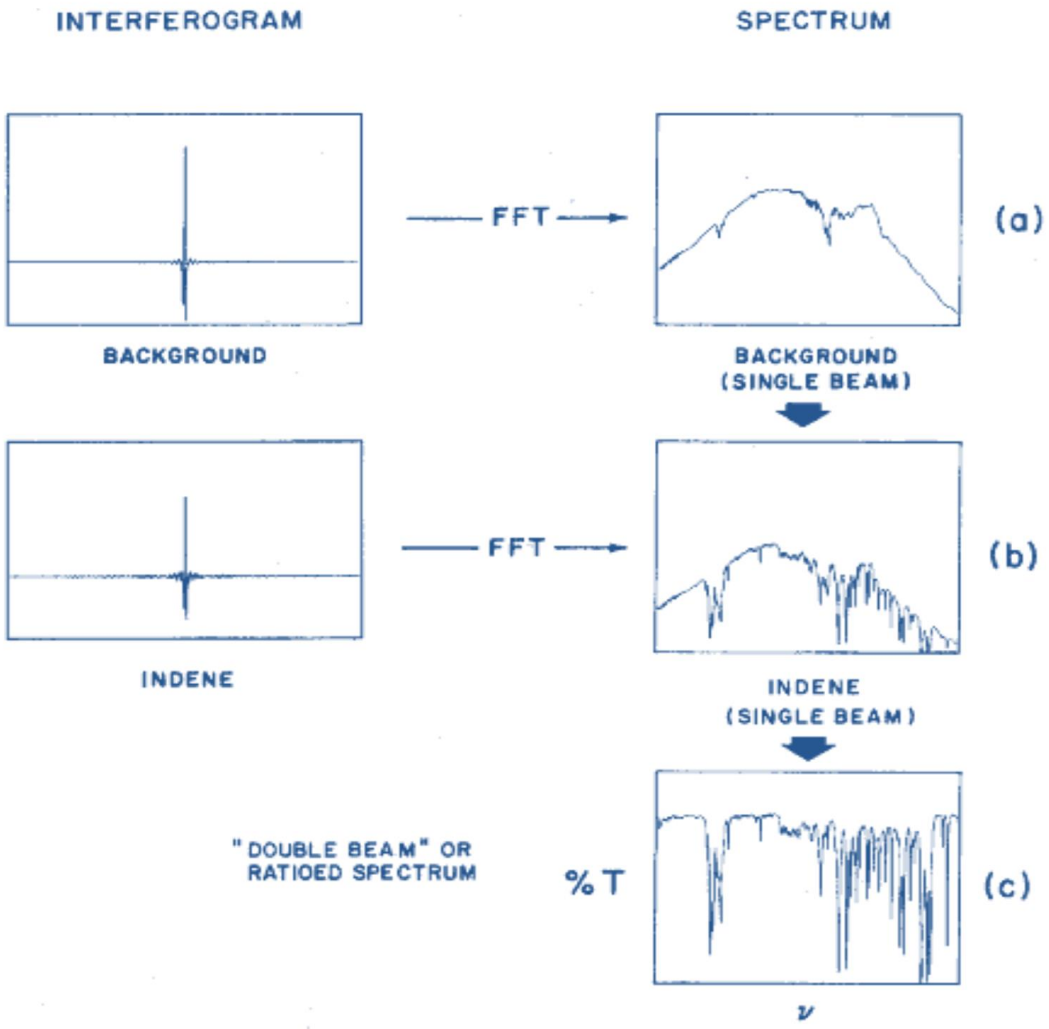

Infrared radiation

- Wavenumber

$$\nu = \frac{1}{\lambda}$$

Region	cm^{-1}	µm	eV
Near	12000 – 4000	0.8 – 2.5	1.55 – 0.5
Mid	**4000 – 400**	**2.5 – 25**	**0.5 – 0.05**
Far	400 – 10	25 – 1000	0.05 – 0.0012

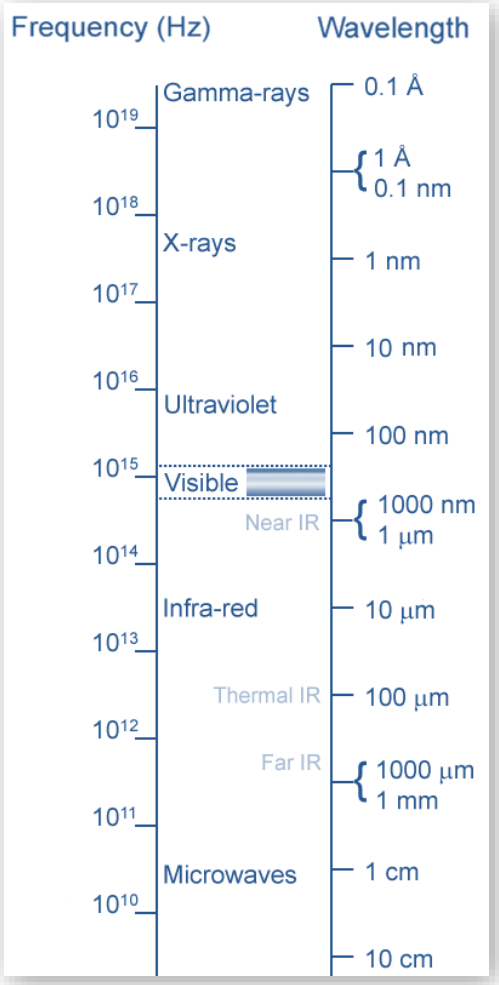

منبع

Component Type	Component Name	Material	Spectral Range
Source	Mercury Arc Lamp	Mercury Gas	FIR
Source	Globar	Silicon Carbide	FIR/MIR
Source	Tungsten Lamp	Tungsten	MIR/NIR
Source	Xenon Arc Lamp	Xenon Gas	VIS/UV
Mirror	Mirror	Gold Coated	FIR/MIR/NIR
Mirror	Mirror	Aluminum Coated	MIR/NIR/VIS/UV
Beam Splitter	Mylar™	Mylar™	FIR
Beam Splitter	KBr	Germanium-Potassium Bromide	MIR
Beam Splitter	CaF_2	Calcium Fluoride	MIR/NIR/VIS
Beam Splitter	Quartz	Quartz	VIS/UV
Detector	Bolometer	Silicon Photodiode	FIR/MIR
Detector	DTGS	Deuterated Triglycine Sulfate	FIR/MIR
Detector	MCT	Mercury Cadmium Telluride	MIR
Detector	InSb	Indium Antimonide	MIR/NIR
Detector	InGaAs	Indium Gallium Arsenide	NIR
Detector	Si-Diode	Silicon Diode	VIS/UV
Detector	GaP-Diode	Gallium Phosphide	VIS/UV

منبع


Parts of the Nernst Lamp

The elements of the Nernst Lamp are the glower, heater (made up of two or four *heater tubes*), ballast and cut-out. These are assembled in the lamp body and the holder.

FIG. 3. NAMES OF PARTS OF THE NERNST LAMP HOLDER

- composition
  - Zirconium oxide ZrO_2 90% wt/wt
  - Yttrium oxide Y_2O_3 7% wt/wt
  - Erbium oxide Er_2O_3 3% wt/wt
- operating temperature: 2300 K
- preheating necessary
- applications
  - general lighting purposes
  - first functional long distance fax
  - ophthalmology
  - projection

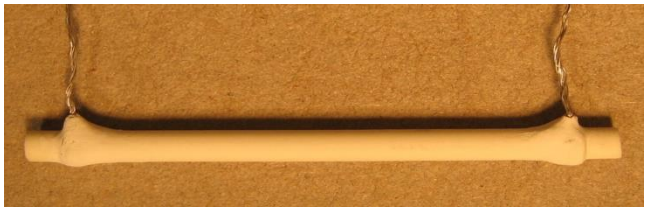

Beamsplitters

Beamsplitter	Range [cm⁻¹]	TENSOR 27*	TENSOR 37	VERTEX 70/70v	VERTEX 80/80v
Mid-Infrared					
Ge on KBr Substrate	7,800 - 370	T 303/7	T 303/3	T 303/3	T 303/8
Ge on KBr (Wide Range)	10,000 - 400	T 304/7	T 304/3	T 304/3	T 304/8
Ge on CsI	5,000 - 200	T 302/7		on request	
ZnSe	5,000 - 500	T 310/7			
Near-Infrared					
Si on CaF_2	15,000 - 1,200		T 401/3	T 401/3	T 401/8
Visible & UV					
VIS Quartz	28,000 - 4,000			T 502/3	
UV/VIS-NIR-CaF_2	50,000 - 4,000				T 602/8
Far Infrared					
Multilayer	680 - 30			T 222/3	T 222/8
Silicon solid state	600 - 10		T 230/3	T 230/3	
Mylar 25 Micron	120 - 20			T 204/3	T 204/8
Mylar 50 Micron	60 - 10			T 205/3	T 205/8
Mylar 125 Micron**	22 - 5				T 206/8
Alignment			T 410/3	T 410/3	T 410/8

Available spectral range: TENSOR 27: 10,000 - 200cm⁻¹, TENSOR 37: 15,000 - 50cm⁻¹, VERTEX 70: 28,000 - 15cm⁻¹, VERTEX 70v: 28,000 - 10cm⁻¹, VERTEX 80: 50,000 - 15cm⁻¹, VERTEX 80v: 50,000 - 5cm⁻¹.

* On the TENSOR 27 the beamsplitter is permanently installed and available as part of the spectral range extension.

** Available for VERTEX 80v vacuum optics only. Liquid He cooled bolometer detector recommended.

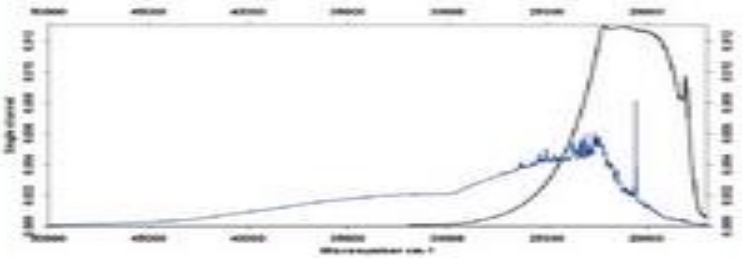

Fig. 3 shows the single beam characteristics of the UV/VIS/NIR beamsplitter T602/8 measured on the VERTEX 80 the using the GaP diode. For the black spectrum the internal Tungsten lamp and for the blue one the Deuterium source was used. The sharp lines in the blue spectrum are due to Deuterium vapour emission.

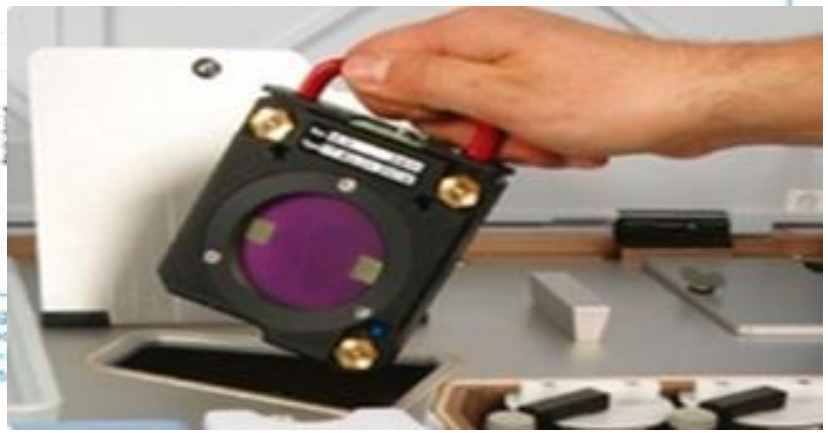

Bruker Optics offers a broad variety of different types of detectors which provide optimum results and maximum experimental flexibility. The full spectral range from the very far IR (or THz) through the mid and near IR up to the visible and UV spectral ranges are covered. The advanced DigiTect detector technology prevents external signal disturbances and guarantees the highest signal-to-noise ratios.
The data acquisition of the VERTEX and TENSOR series FT-IR spectrometers are based on 2-channel delta-sigma ADC's with true 24-bit dynamic range which are integrated into the detector preamplifier electronics.

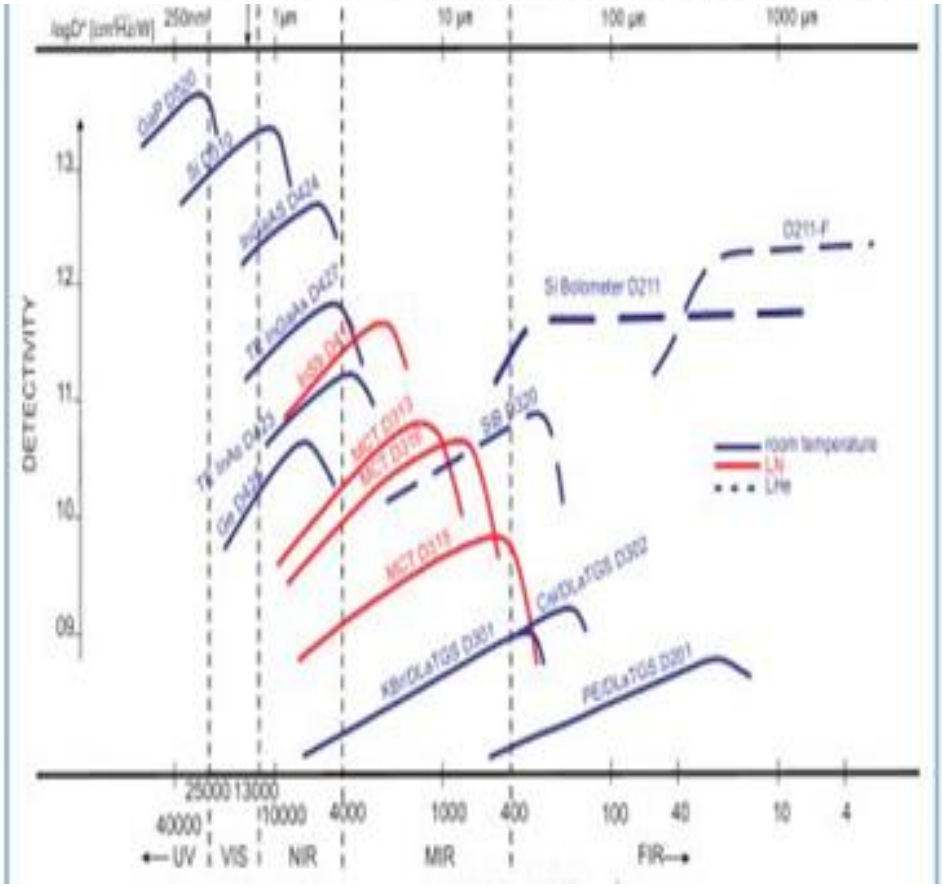

Bruker Optics DigiTect detector technology (US Patent 5,963,322) together with the applied data acquisition electronics of the TENSOR and VERTEX series spectrometer provide as a final result oustanding signal-to-noise-ratio. In the following table the major DigiTect advantages are listed.

DigiTect advantages

- True 24 bit dynamic range
- No gain-switching artefacts
- Parallel dual channel technology
- Integrated detector electronics
- Short analog signal lines
- No disturbing "spikes" in the IR spectrum
- Compact electronics design
- Well suited to harsh environments.

Detector Element/Window	Element Size	Spectral Range	Typical D* cm $Hz^{1/2}$ W^{-1}	Minimum Responsivity	Operating Temperature	Typical Preamplifier Bandwidth
Mid-infrared						
DLaTGS/KBr	1.3 mm	12500-350 cm^{-1}	2.7 E8	50 V/W	Room temp.	170 kHz
DLaTGS/KBr	1.3 mm	12500-350 cm^{-1}	2.7 E8	50 V/W	TE cooled	170 kHz
DLaTGS/CsI	1.3 mm	6400-200 cm^{-1}	2.4 E8	50 V/W	Room temp.	170 kHz
$LiTaO_3$/KBr	1.5 mm	10000-400 cm^{-1}	1.0 E8	20 V/W	Room temp.	170 kHz
MCT-A*/CdTe	1.0 x 1.0 mm^2	11700-800 cm^{-1}	6.4 E10	1,200 V/W	Liquid N_2	175 kHz
MCT-A/CdTe	1.0 x 1.0 mm^2	11700-600 cm^{-1}	4.7 E10	750 V/W	Liquid N_2	175 kHz
MCT-B/KRS-5	1.0 x 1.0 mm^2	11700-400 cm^{-1}	8.0 E9	50 V/W	Liquid N_2	175 kHz
Near-infrared						
InGaAs/glass	1.0 mm	12000-3800 cm^{-1}	4.4 E10	1.3 A/W	Room temp.	170 kHz
InGaAs/glass	1.0 mm	12000-3800 cm^{-1}	3.0 E11	1.4 A/W	TE cooled	50 kHz
PbSe/sapphire	1.0 x 1.0 mm^2	11000-2000 cm^{-1}	2.5 E9	6,000 V/W	Room temp.	100 kHz
InSb/CdTe	2.0 x 2.0 mm^2	10000-1850 cm^{-1}	2.2 E11	2.2 A/W	Liquid N_2	250 kHz
Visible						
Si/Quartz	2.5 mm	27000-8600 cm^{-1}	2.8 E12	0.4 A/W	Room temp.	170 kHz
DLaTGS/Quartz	1.3 mm	25000-2000 cm^{-1}	2.7 E8	50 V/W	Room temp.	170 kHz
Far-infrared						
DLaTGS/Poly	1.5 x 1.5 mm^2	700-50 cm^{-1}	4.8 E8	300 V/W	Room temp.	1.5 kHz
Si/Teflon®	2.5 x 2.5 mm^2	600-20 cm^{-1}	1.6 E12	170,000 V/W	Liquid He	250 Hz
IR Microscope						
MCT-A*/CdTe	0.05 x 0.05 mm^2	11700-700 cm^{-1}	6.4 E10	60,000 V/W	Liquid N_2	175 kHz
MCT-A*/CdTe	0.25 x 0.25 mm^2	11700-750 cm^{-1}	6.4 E10	7,000V/W	Liquid N_2	175 kHz
MCT-A/CdTe	0.25 x 0.25 mm^2	11700-600 cm^{-1}	4.7 E10	6,500 V/W	Liquid N_2	175 kHz

FTIRs Often Use MCT Detectors: Mercury Cadmium Telluride

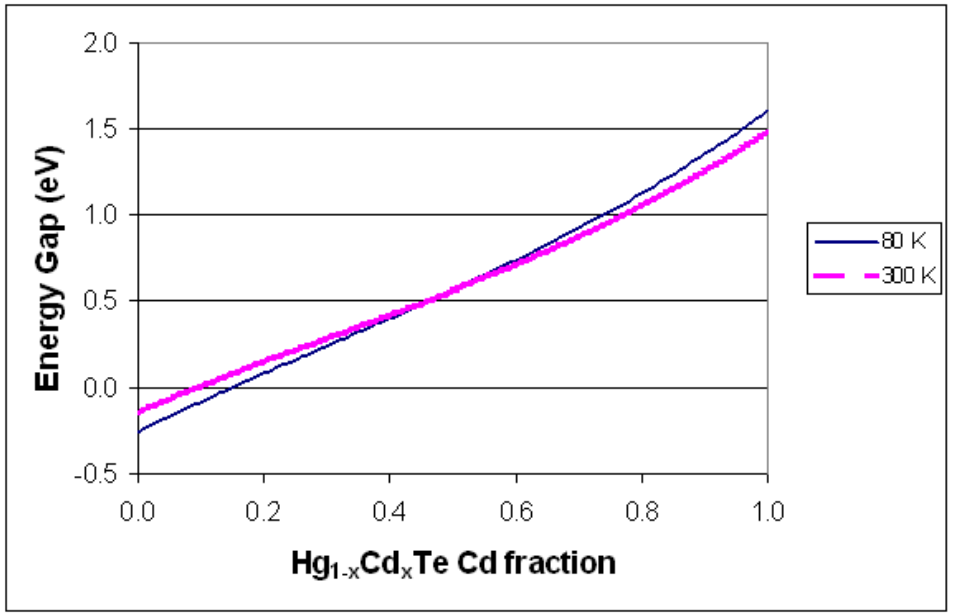

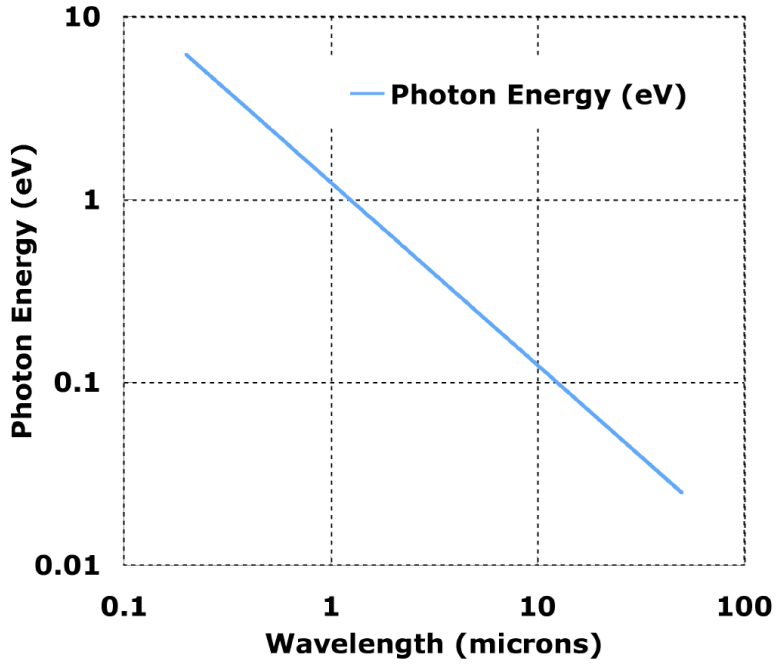

HgCdTe or Mercury cadmium telluride (also Cadmium Mercury Telluride, MCT or CMT) is an alloy of CdTe and HgTe and is sometimes claimed to be the third semiconductor of technological importance after Silicon and Gallium(III) arsenide. The amount of cadmium (Cd) in the alloy (the alloy composition) can be chosen so as to tune the optical absorption of the material to the desired infrared wavelength.
(from http://en.wikipedia.org/wiki/Mercury_cadmium_telluride)

IR ABSORPTION RANGE

The typical IR absorption range for covalent bonds is **600 - 4000 cm^{-1}**. The graph shows the regions of the spectrum where the following types of bonds normally absorb. For example a sharp band around 2200-2400 cm^{-1} would indicate the possible presence of a C-N or a C-C triple bond.

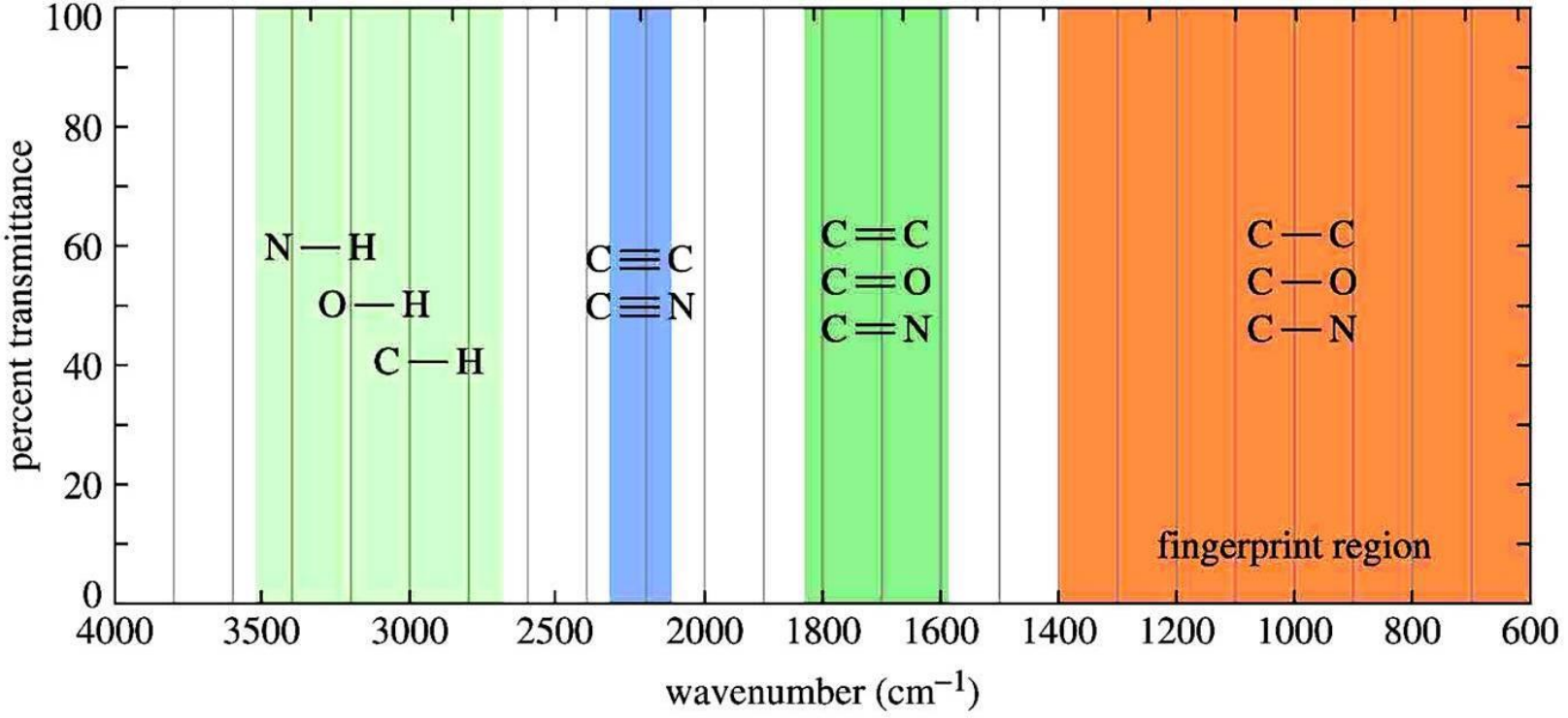

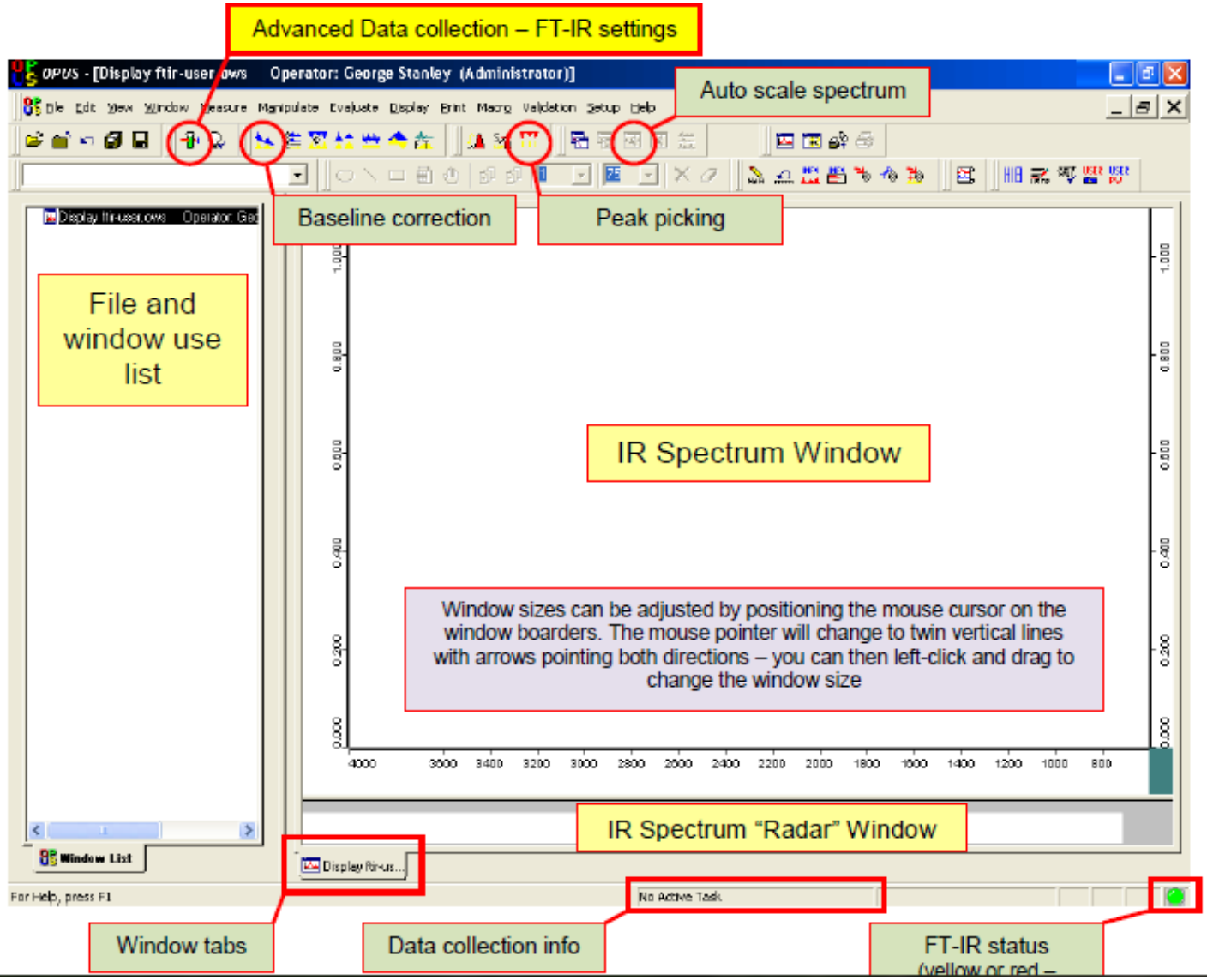
Advanced Data collection – FT-IR settings
Auto scale spectrum
Baseline correction
Peak picking
File and window use list
IR Spectrum Window
Window sizes can be adjusted by positioning the mouse cursor on the window boarders. The mouse pointer will change to twin vertical lines with arrows pointing both directions – you can then left-click and drag to change the window size
IR Spectrum "Radar" Window
Window tabs
Data collection info
FT-IR status

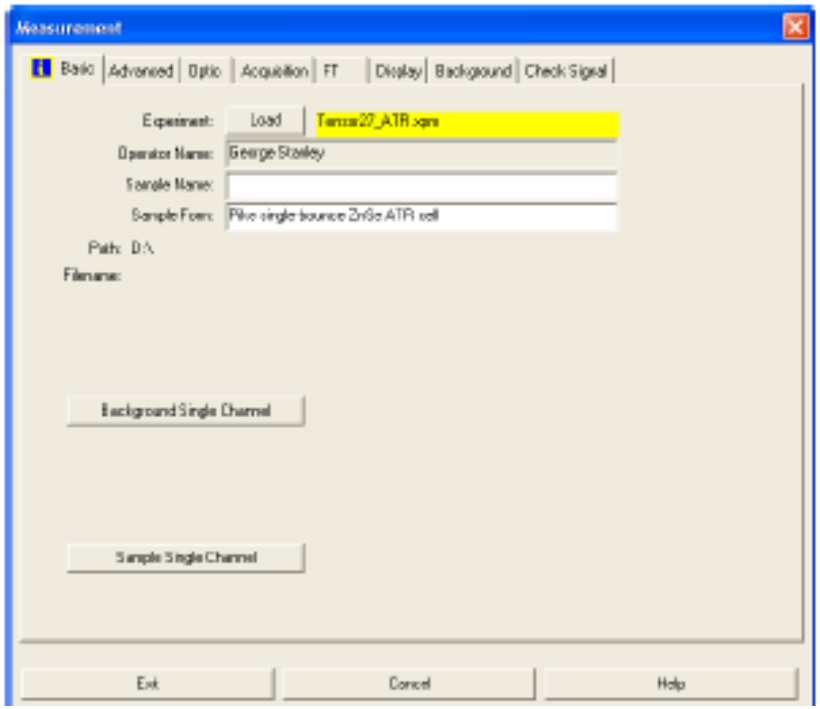
Measurement
Basic
Advanced
Optic
Acquisition
FT
Display
Background
Check Signal
Experiment:
Load
Tensor27_ATR.xpm
Operator Name:
George Stanley
Sample Name:
Sample Form:
Pike single bounce ZnSe ATR cell
Path: D:\
Filename:
Background Single Channel
Sample Single Channel
Exit
Cancel
Help

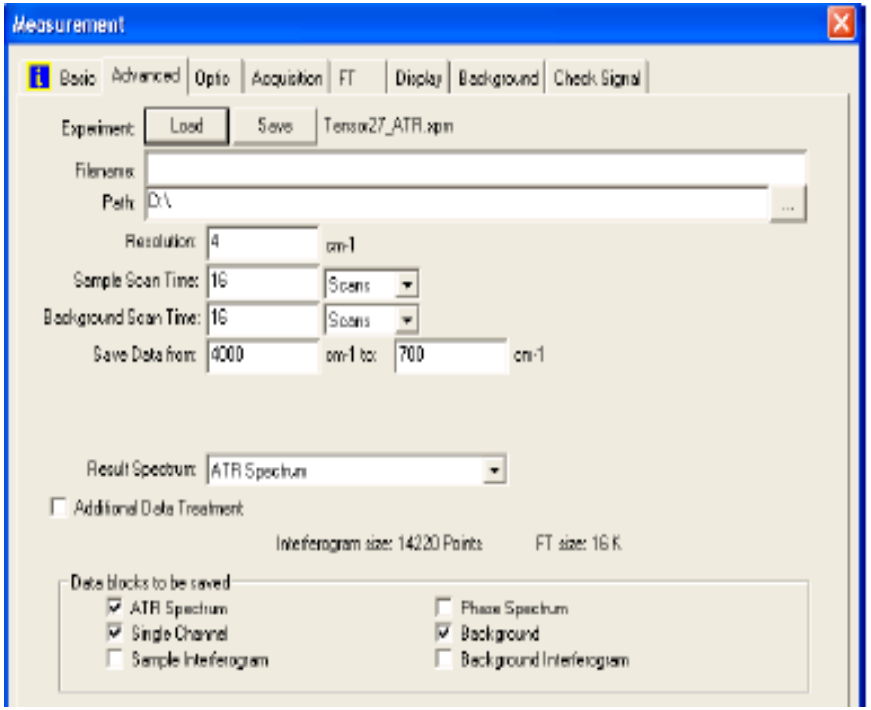
Measurement
Basic
Advanced
Optic
Acquisition
FT
Display
Background
Check Signal
Experiment:
Load
Save
Tensor27_ATR.xpm
Filename:
Path: D:\
Resolution: 4 cm-1
Sample Scan Time: 16 Scans
Background Scan Time: 16 Scans
Save Data from: 4000 cm-1 to: 700 cm-1
Result Spectrum: ATR Spectrum
Additional Data Treatment
Interferogram size: 14220 Points
FT size: 16 K
Data blocks to be saved
ATR Spectrum
Single Channel
Sample Interferogram
Phase Spectrum
Background
Background Interferogram

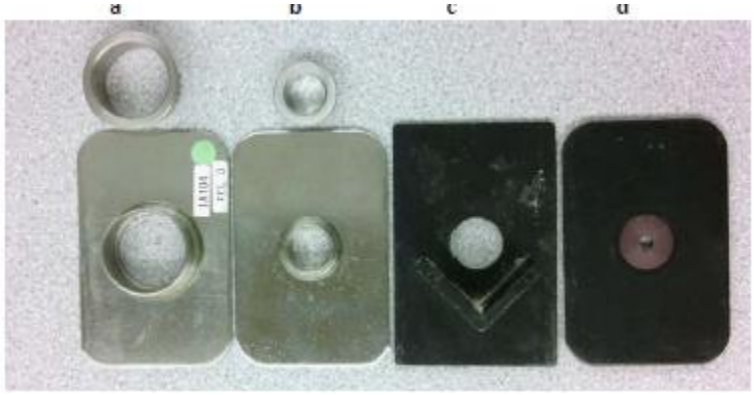
a
b
c
d

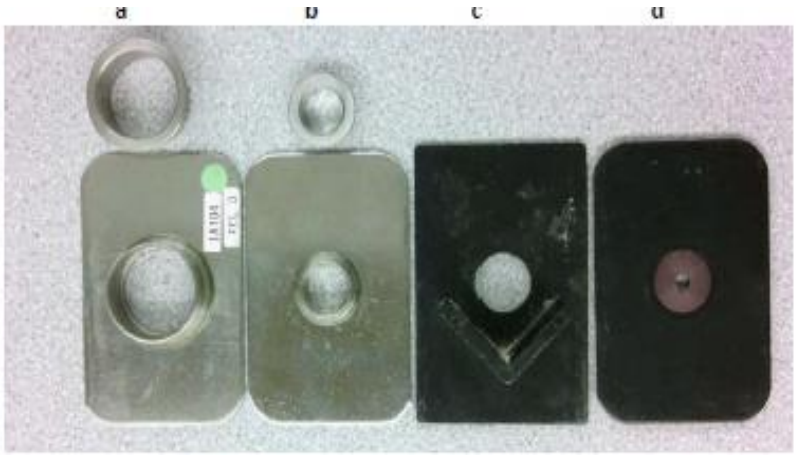
a
b
c
d

گاز و مایع

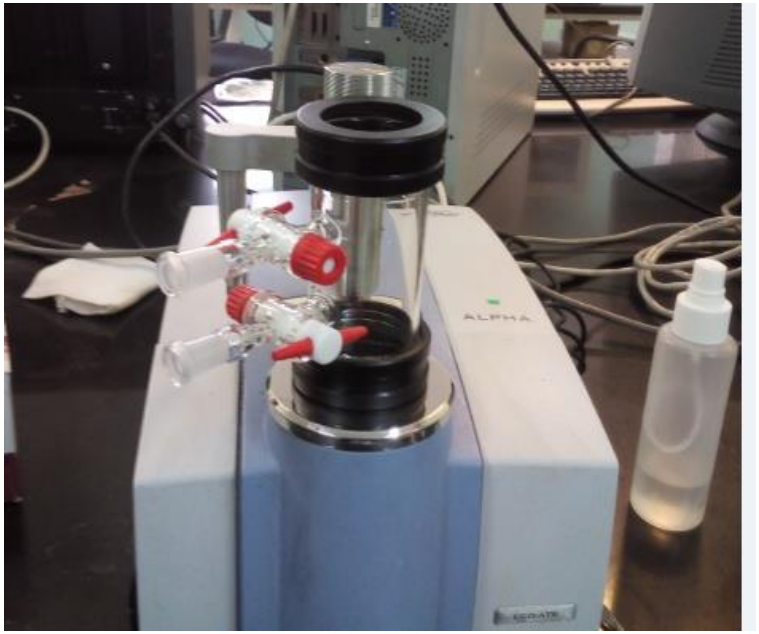

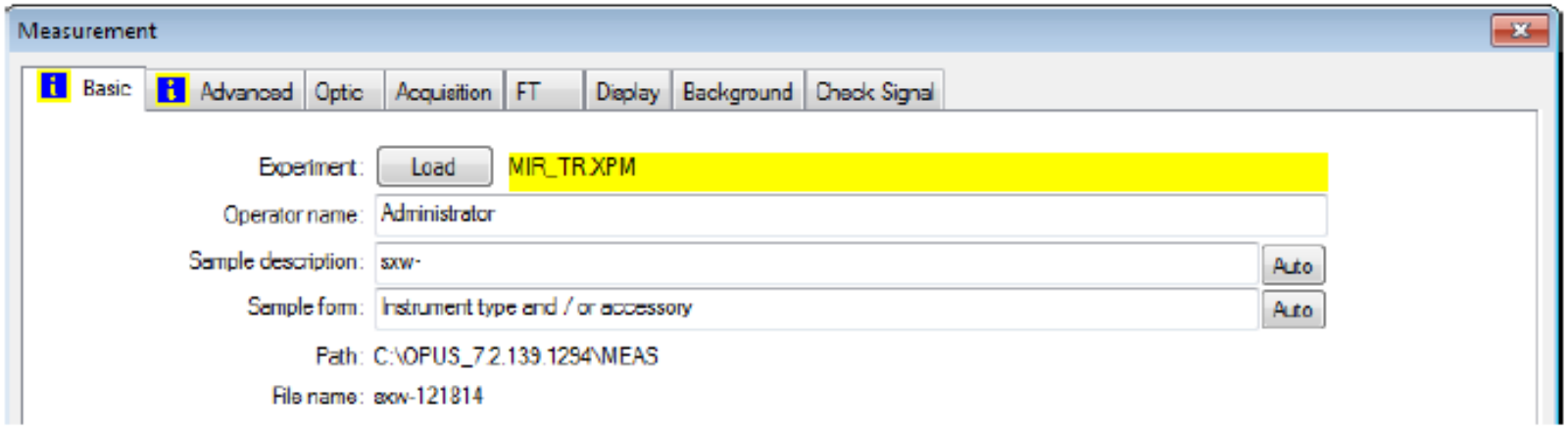

Measurement - Basic Tab

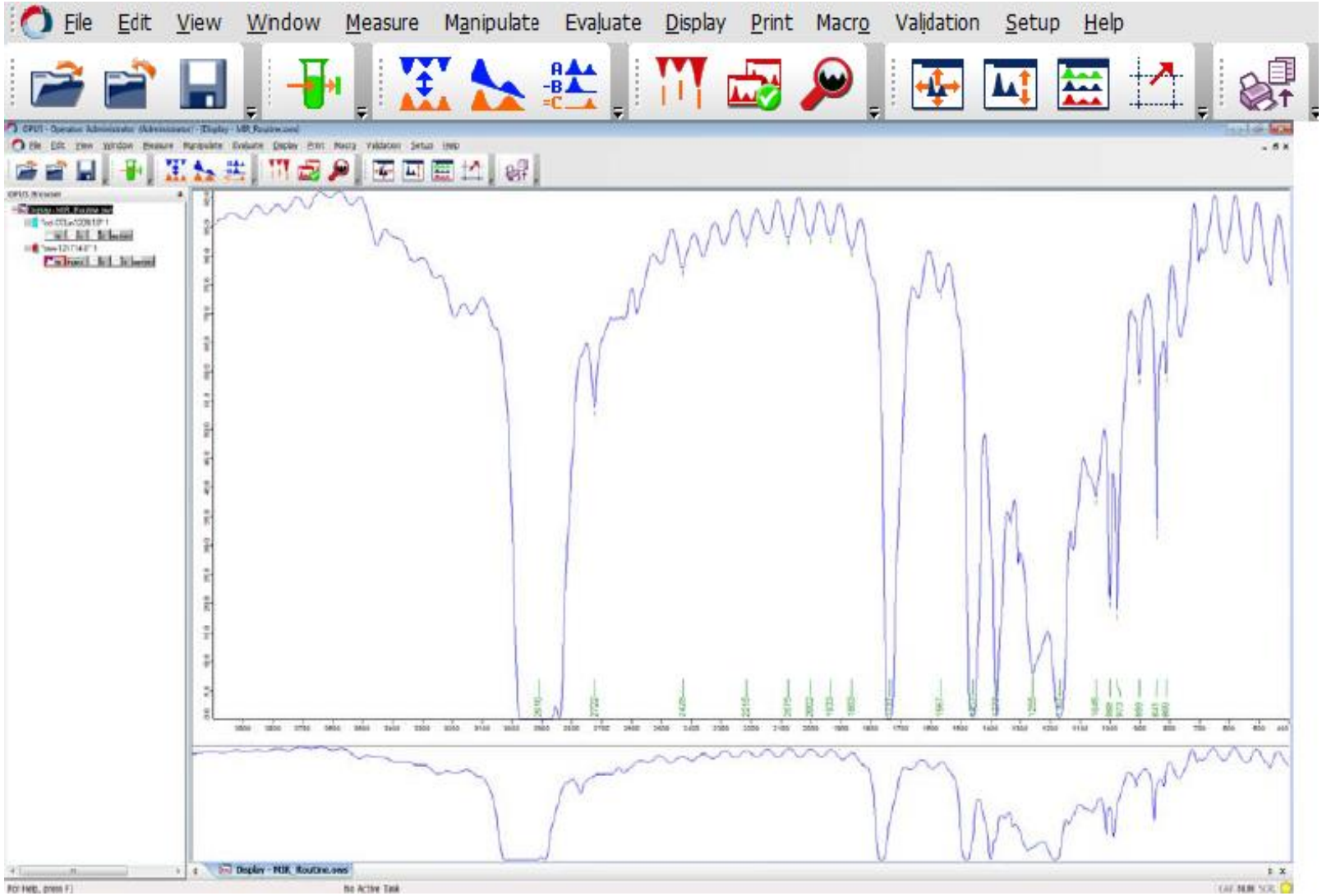
File
Edit
View
Window
Measure
Manipulate
Evaluate
Display
Print
Macro
Validation
Setup
Help

Courtesy of Texas DPS Crime Laboratory Services

FIGURE 9 Natural variation seen in hairs under a microscope.

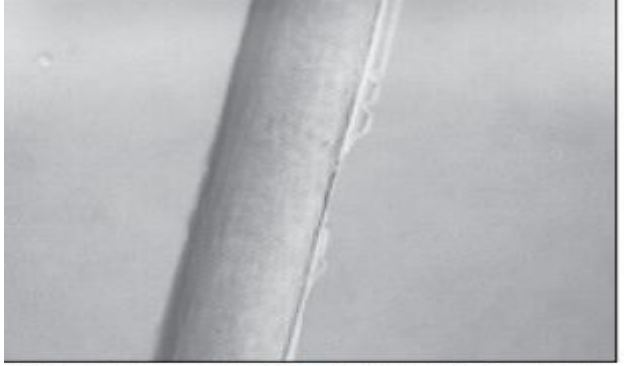

e 2: Video image capture of a hair fiber with hair spray visible on the surface

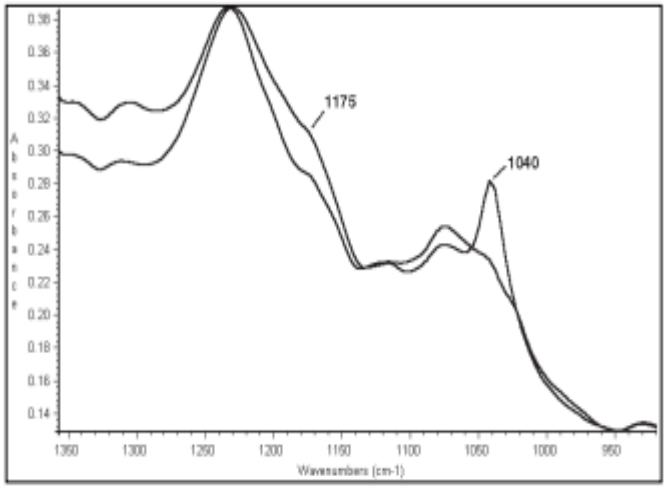

Figure 1: Infrared spectra of a normal, untreated hair fiber and a chemically damaged hair fiber

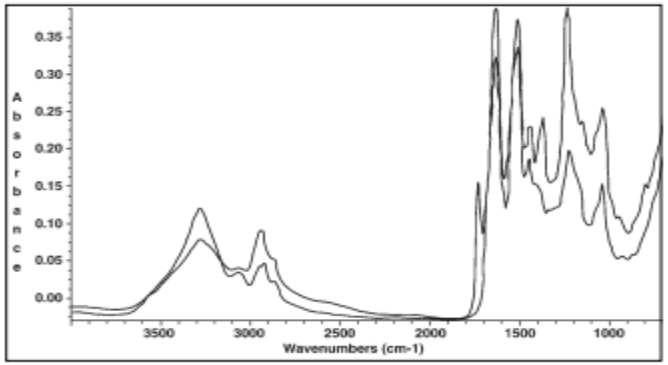

Figure 3: Infrared spectra of a clean hair fiber and a hair spray coated hair fiber

Hair Treatment	Oxidation Products
Alkaline Hydrogen Peroxide	Cysteic acid (1040 cm^{-1} and 1175 cm^{-1})
Metabisulfite Treatment	S-sulfonate (Bunte-salt) (1022 cm^{-1})
Natural Weathering	Cystine monoxide (1071 cm^{-1}), cysteic acid (1040 cm^{-1} and 1175 cm^{-1}), Bunte-salt (1022 cm^{-1})

Table 1: Oxidation products resulting from different hair treatments[1]

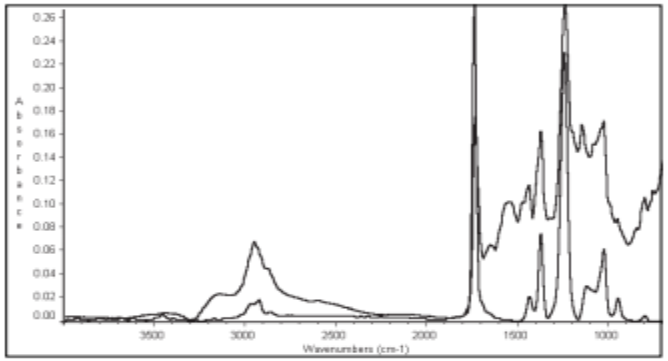

Figure 4: Infrared difference spectrum of the clean hair from the hair sprayed hair, and a reference spectrum of poly(vinylacetate)

Cryogenic measurements

- Sample compartment configurable for third party cryostats
- Far-IR operation for advanced materials and semiconductor research

Far-IR ATR

- All diamond ATR systems for convenient far-IR sampling
- Rapid IR-FIR switchover
- Rapid, efficient purge operation for faster measurement
- Ideal for measurement of inorganic material

TL8000 TG-IR Interface

- Designed for high performance and reliability
- Wide temperature range
- Robust transfer line
- Balanced gas flow design for improved flow regulation gas component resolution
- Ideal for characterization of bioenergy materials, polymer performance measurements and residual solvent analysis

Integrating sphere measurements

- Mid-IR integrating sphere
- Reflection and transmission sampling
- Dedicated detector for high performance sampling

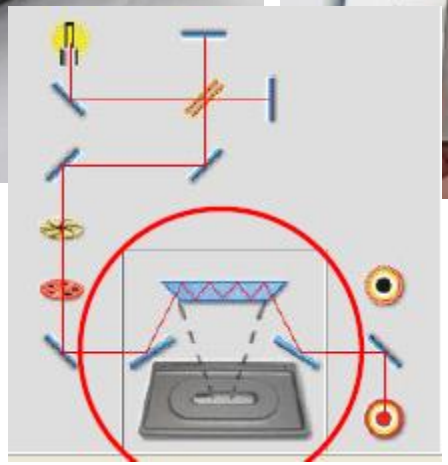

FT-IR Reflection Techniques

Internal Reflection Spectroscopy:

Attenuated Total Reflection (ATR)

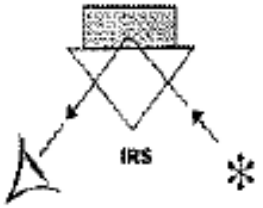

External Reflection Spectroscopy:

Specular Reflection (smooth surfaces)

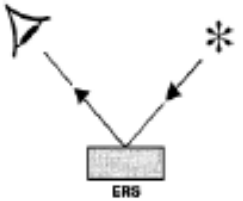

Combination of Internal and External Reflection:

Diffuse Reflection (DRIFTs) (rough surfaces)

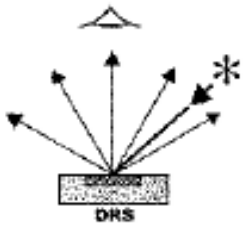

Attenuated Total Reflection (ATR)

Total internal reflection

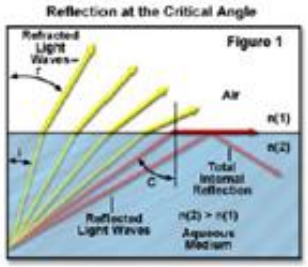

- **critical angle** - when the angle of refraction (**r**) becomes equal to 90 degrees and Snell's law reduces to:

$\sin(\theta) = n(1)/n(2)$ $\quad n(1) \neq n(2)$

where (θ) is termed the **critical angle c**

When the critical angle is exceeded for a particular light wave, it exhibits **total internal reflection** back into the medium.

The larger the angle to the normal, the smaller is the fraction of light transmitted, until the angle when **total internal reflection** occurs.

FT-IR Reflection Techniques

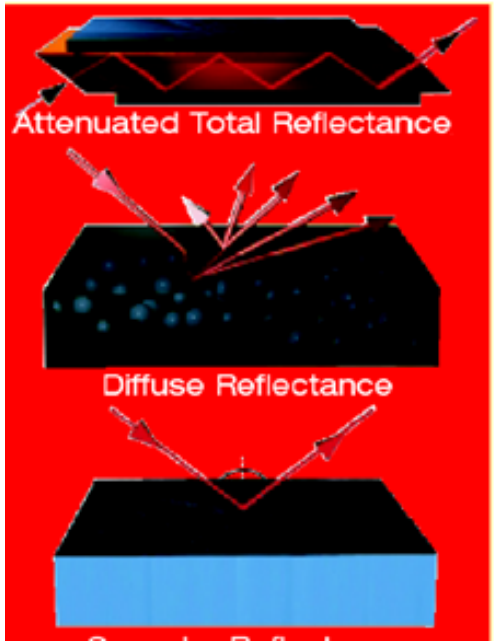

- Infrared beam reflects from a interface via total internal reflectance
- Sample must be in optical contact with the crystal
- Collected information is from the surface

- Solids and powders, diluted in a IR transparent matrix if needed
- Information provided is from the bulk matrix

- Sample must be reflective or on a reflective surface
- Information provided is from the thin layers

Attenuated Total Reflection (ATR)

Critical Angle depends on n_{IRE} and n_{smp}

- increasing $n_{IRE} \Rightarrow$ decreasing θ and d_P

$$\theta_c = \sin^{-1}\left(\frac{n_{smp}}{n_{IRE}}\right)$$

$\Rightarrow$ high values of n_{IRE} needed

Materials of ATR crystals (IRE elements)

Table 1: MIRacle Crystal Plate Specifications

MIRacle Crystal Plate	Application	Hardness kg/mm²	Cutoff cm⁻¹, Spectral Range	Refractive Index @ 1000 cm⁻¹	Depth of Penetration @ 45°,μ	pH Range of Sample
AMTIR	Harder than ZnSe, ok with acid samples	170	630	2.5	1.70	1 – 9
Diamond/KRS-5	When you need full mid-IR spectral range	5700	250	2.4	2.00	1 – 14
Diamond/ZnSe	Ideal for hard samples, acids or alkaline	5700	525	2.4	2.00	1 – 14
Ge	General purpose and carbon filled or rubber	550	575	4.0	0.66	1 – 14
Si/ZnSe	General purpose – only below diamond for hardness	1150	550	3.4	0.85	1 – 12
Si	Excellent for far-IR spectral measurement	1150	8900-1500, 475-40	3.4	0.85	1 – 12
ZnSe	General purpose ATR crystal	120	520	2.4	2.00	5 – 9

Attenuated Total Reflection (ATR)

Experimental Setup - horizontal arrangement (HATR)

Single Bounce ATR

Small sampling area
- use for strong absorbers
- solid samples, liquids

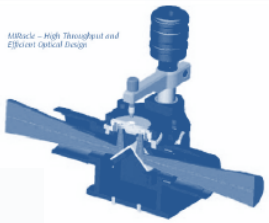

Multi-Bounce ATR

Broad sampling area provides
- greater contact with the sample
- use for weak absorbers or dilute solutions

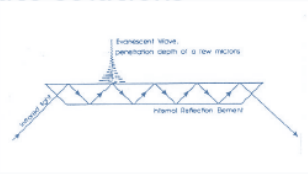

Attenuated Total Reflection (ATR)

Experimental Setup

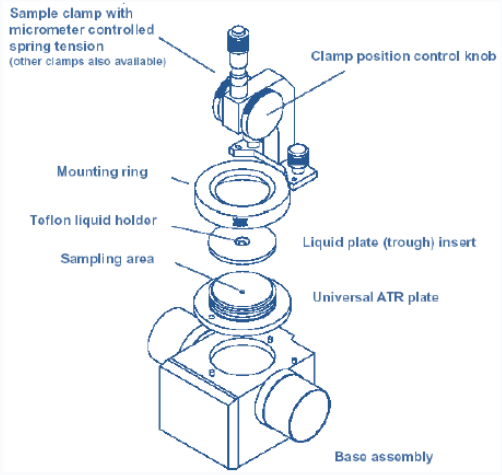

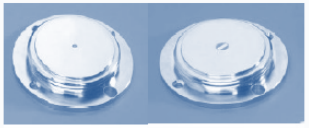

Single Reflection ATR Plate

3 Reflection ATR Plate (includes 5mm swivel tip)

Detection of illicit drugs on Fingerprint

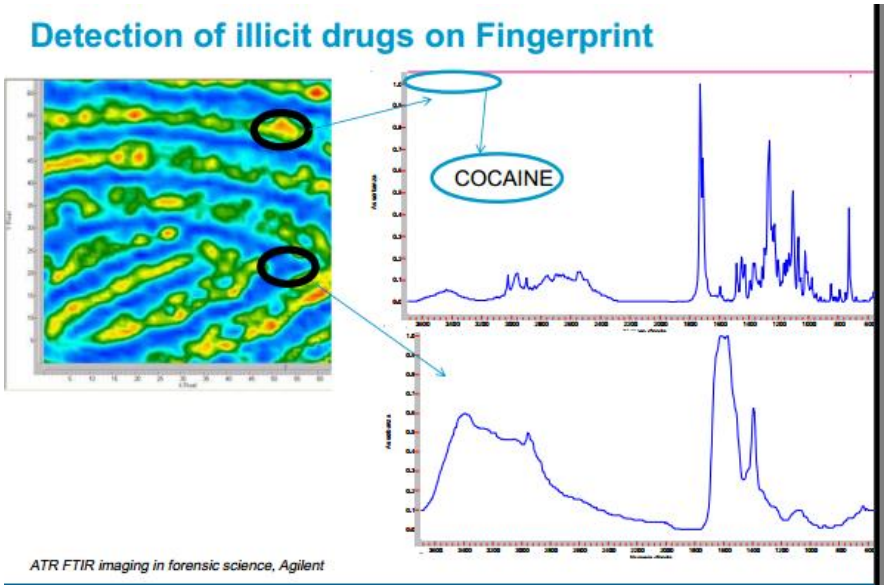

ATR FTIR imaging in forensic science, Agilent

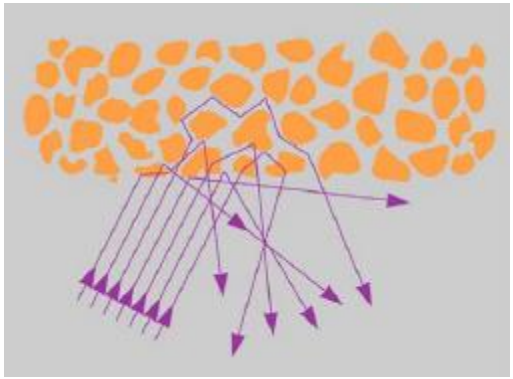

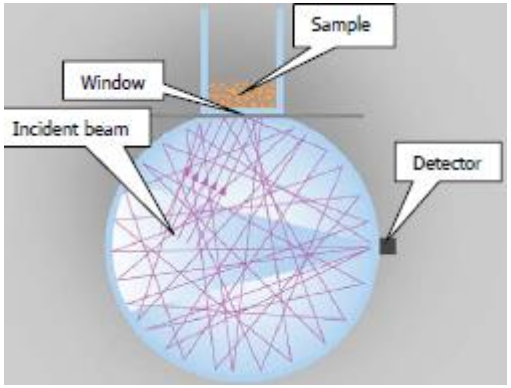
Sample
Window
Incident beam
Detector

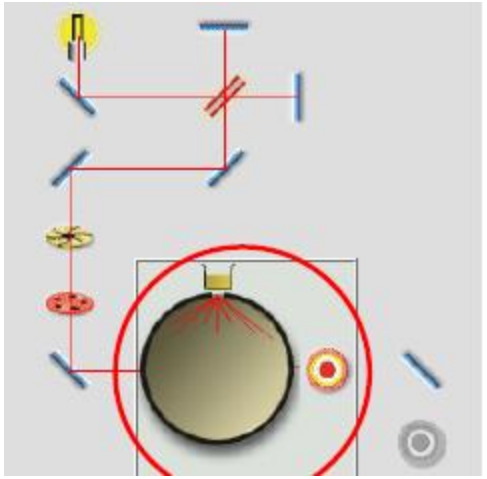

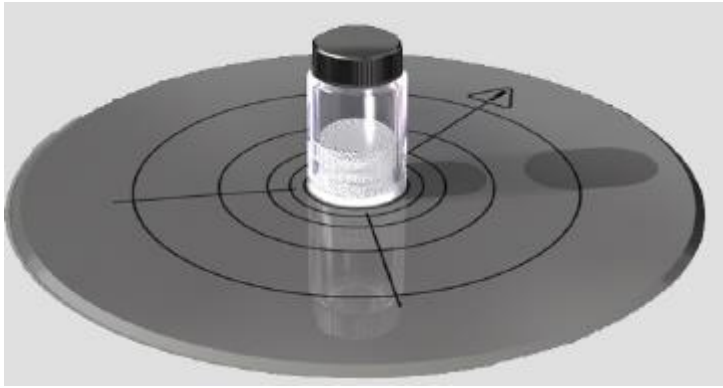

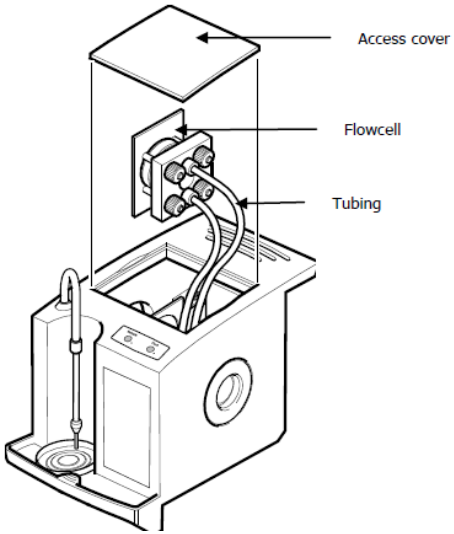
Access cover
Flowcell
Tubing

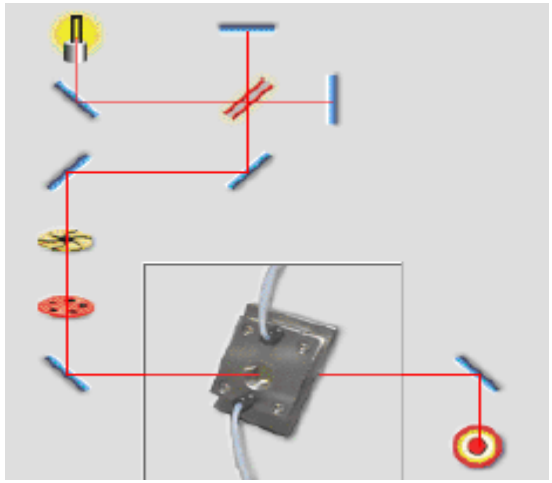

Diffuse Reflection

Experimental Setup

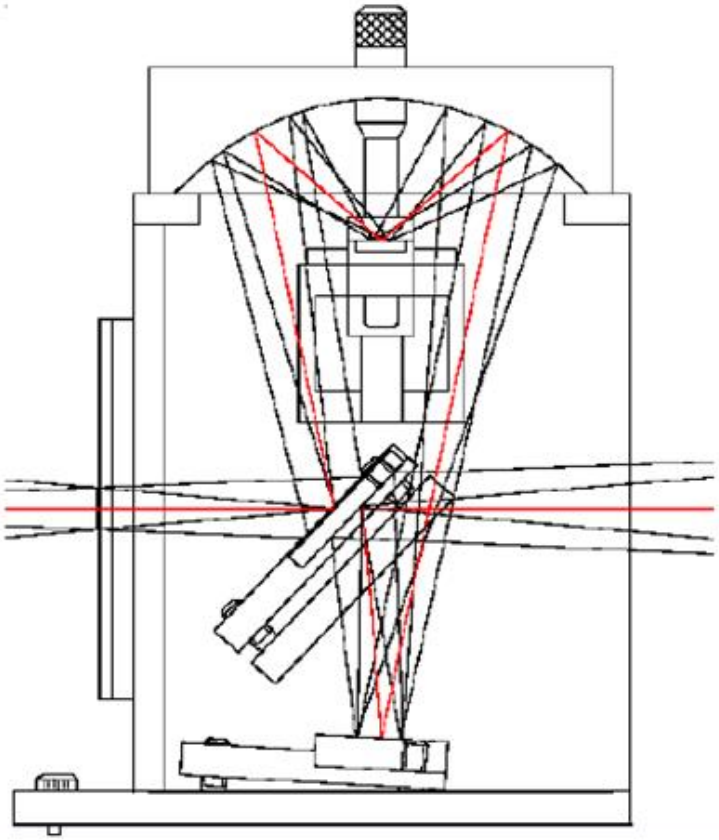

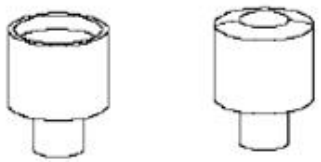

Large and Small Sample Cups

TYPICAL ROCK SPECTRA

- Rock spectra usually more complex than mineral spectra
- Rock spectra combine features of their main mineralogy
- Acidic rocks show reststrahlenband at lower wavelength than basic rocks
- Change in emissivity minimum can be used for mapping igneous rocks of variable SiO2 content

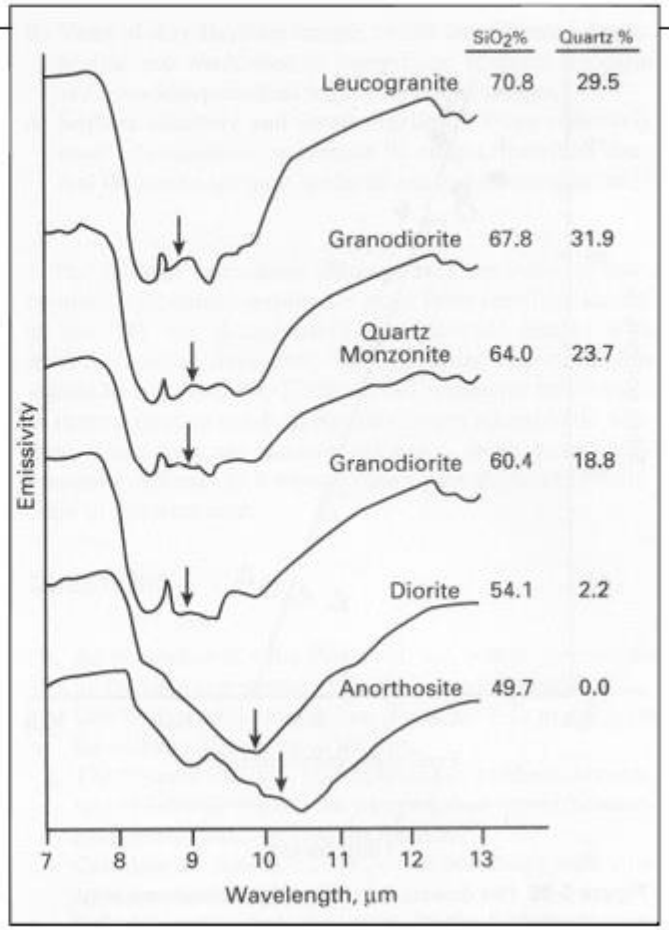

- Source: Sabins (1997)

Sample Shuttle accessory

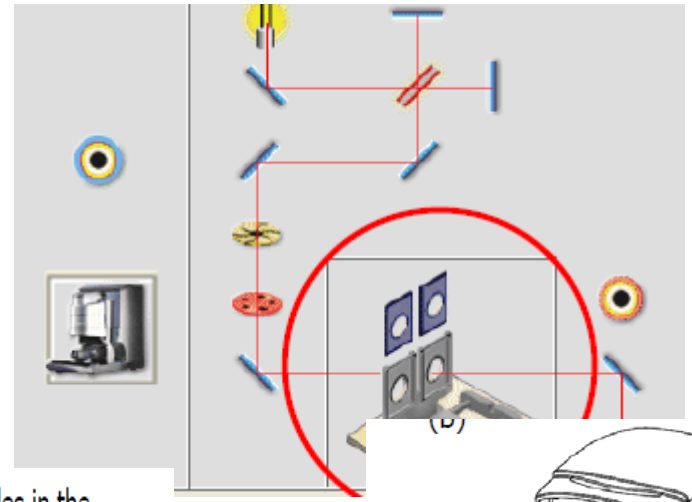

The Sample Shuttle enables you to automatically locate either of two sample slides in the optical beam of the spectrometer without opening the sample compartment. This prevents carbon dioxide and water vapor from entering the sample compartment each time you switch from a background scan to a sample scan.

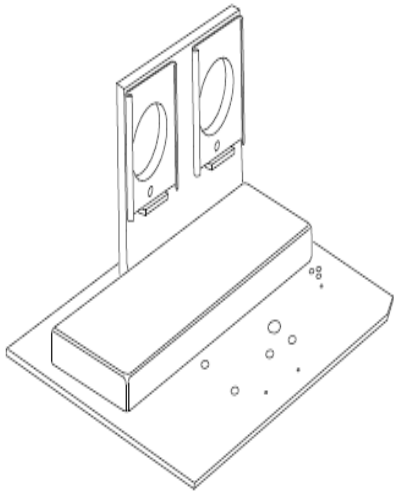

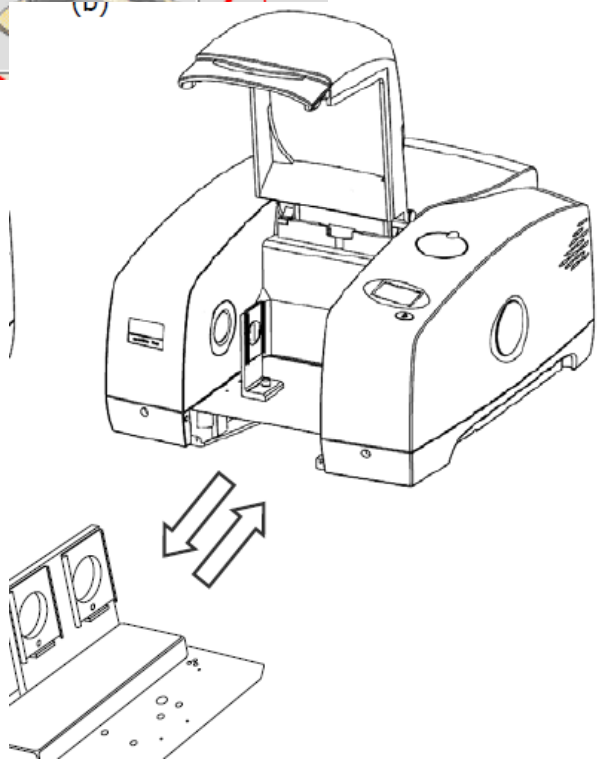

Optical Bench with External $LiTaO_3$ Detector

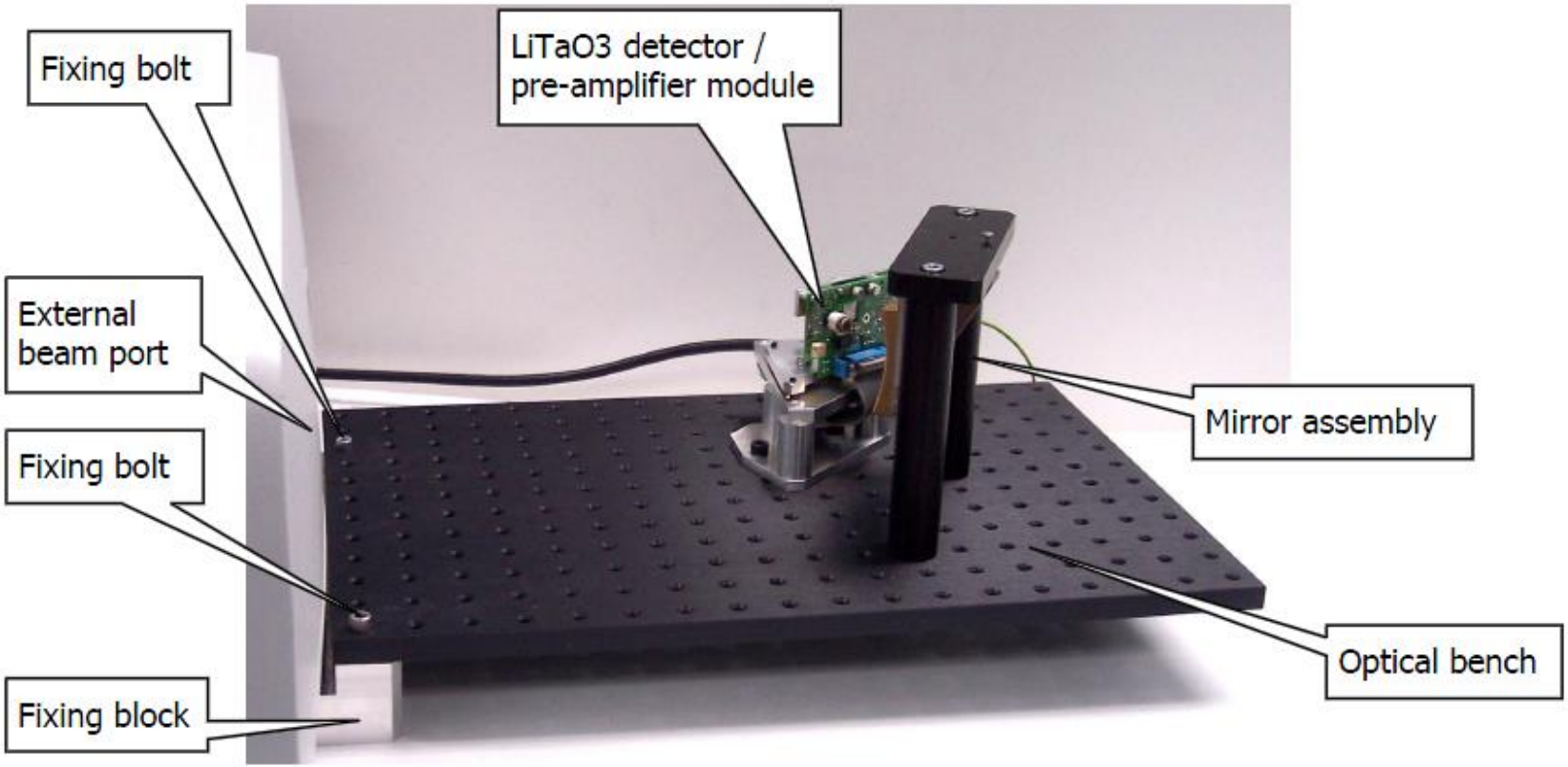

fiber optic interface

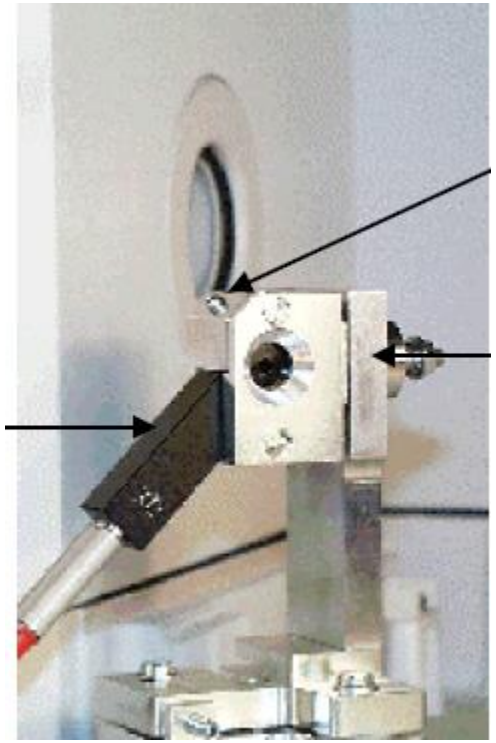

Photoacoustic – Areas of Application

- Carbons
- Coals
- Hydrocarbons
- Hydrocarbon Fuels
- Corrosion
- Clays & Clay Minerals
- Wood & Paper
- Polymers
- Gases
- Food Products
- Biology & Biochemistry
- Medical Applications
- Carbonyl Compounds
- Textiles
- Catalysts

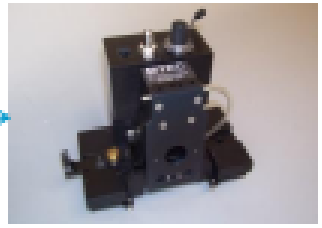

- Raw Materials
- In Process Control
- Final Product QA/QC
- Decomposition
- Pyrolysis
- Distillation Fraction
- Forensics

- UV-Visible
- Near-Infrared
- Mid-Infrared
- Far-Infrared

Quantitative Analysis

Calibration curves can be generated using both linear (or classical) least squares or chemometric techniques, such as partial least squares, for quantitating the amount of analyte present.

Quantitative Analysis

Resolutions Pro integrated quantitative analysis capability allows for one to generate a calibration curve in minutes. This curve can then be applied using a single icon click to quantitate the amount of analyte present.

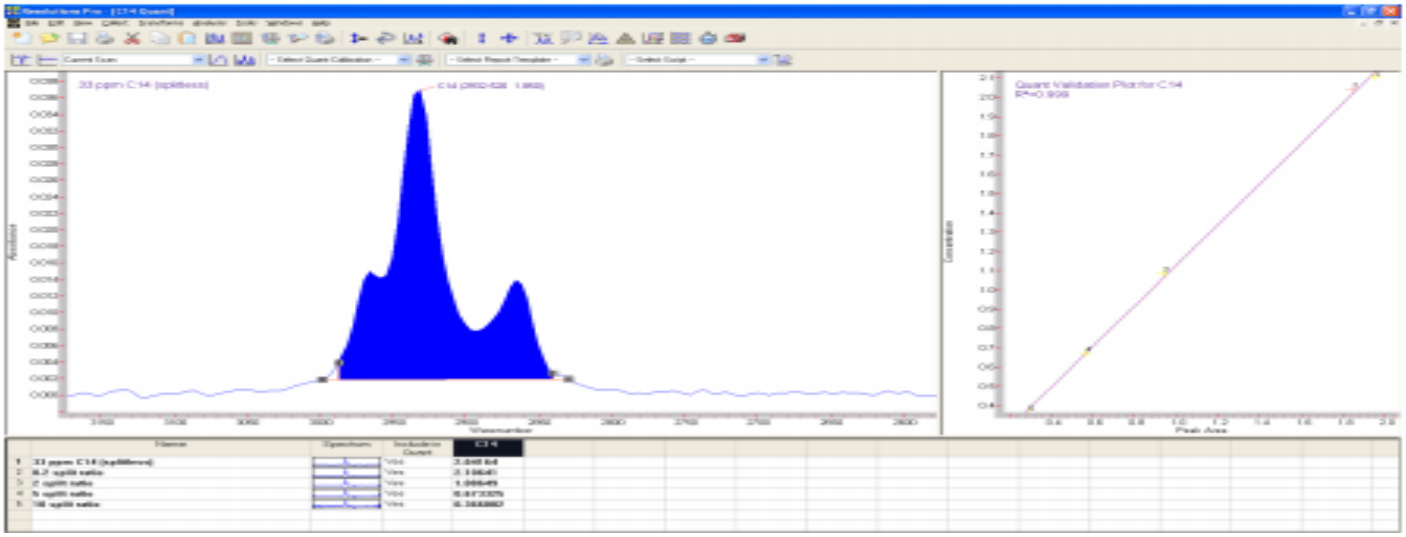

Solid Sample Injection: Pyrolysis GC-IR

CDS Pyroprobe with Agilent GC-IR System making the ultimate solid phase forensic tool.

- Single Step Pyrolyzer
- Needle Connection through Injection Port
- Temperature Programmable to 1400C

Pyrolysis GC-IR Example: Kraton

A Piece of Kraton polymer
njected on Pyrolysis GC-IR

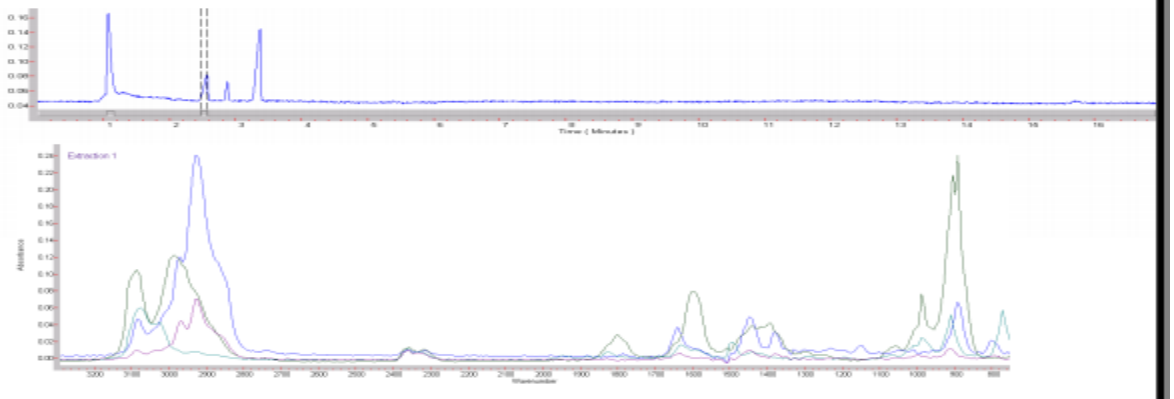

Chart of Common Crystal Materials

Material	ATR Spectral Range (cm^{-1})	Refractive Index	Depth of Penetration (μ) (at 45° & 1000 cm^{-1})	Uses
Germanium	5,500 - 675	4	0.66	Good for most samples. Strong absorbing samples, such as dark polymers.
Silicon	8,900 - 1,500 & 360-120	3.4	0.85	Resistant to basic solutions.
AMTIR	11,000 - 725	2.5	1.77	Very resistant to acidic solutions.
ZnSe	15,000 - 650	2.4	2.01	General use.
Diamond	25,000 - 100	2.4	2.01	Good for most samples. Extremely caustic or hard samples.

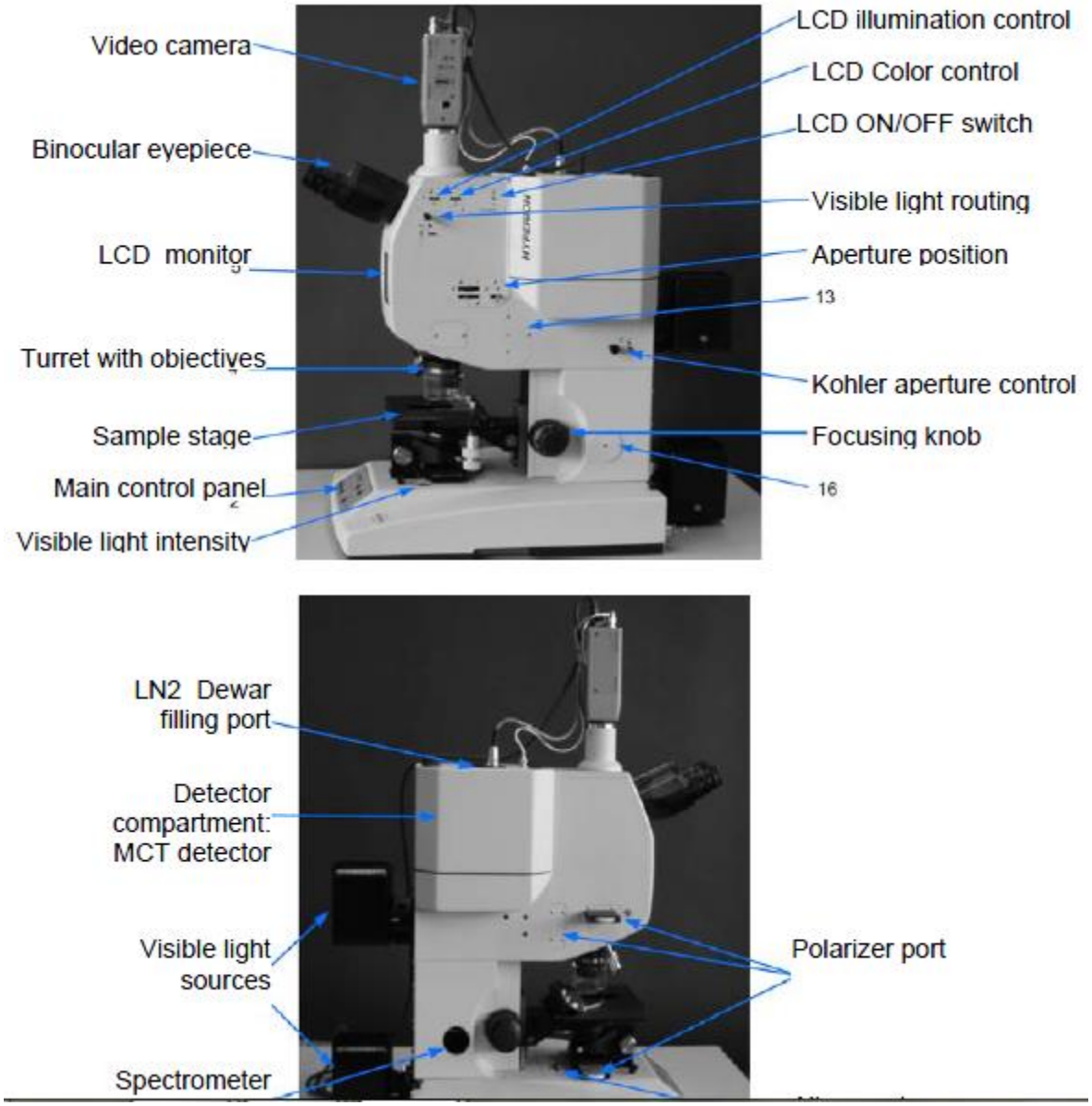
Video camera
Binocular eyepiece
LCD monitor
Turret with objectives
Sample stage
Main control panel
Visible light intensity
LCD illumination control
LCD Color control
LCD ON/OFF switch
Visible light routing
Aperture position
13
Kohler aperture control
Focusing knob
16
LN2 Dewar filling port
Detector compartment: MCT detector
Visible light sources
Spectrometer
Polarizer port

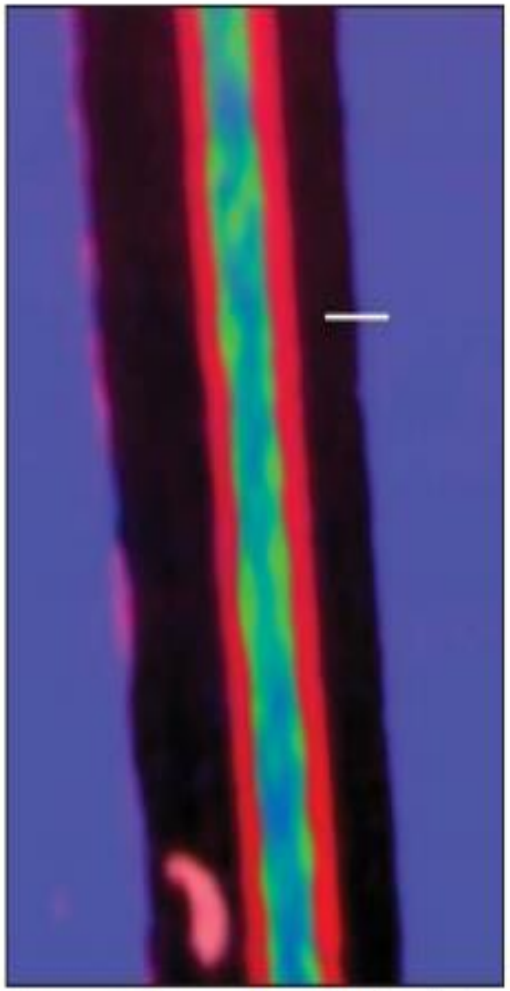

Figure 7. ATR image of a section of a plastic laminate. The image covers 150 microns width by 200 microns height, and has been sampled on a 1.56 micron pitch. The white bar indicates the position where spectra have been extracted. This image is a composite of three principal component images to show

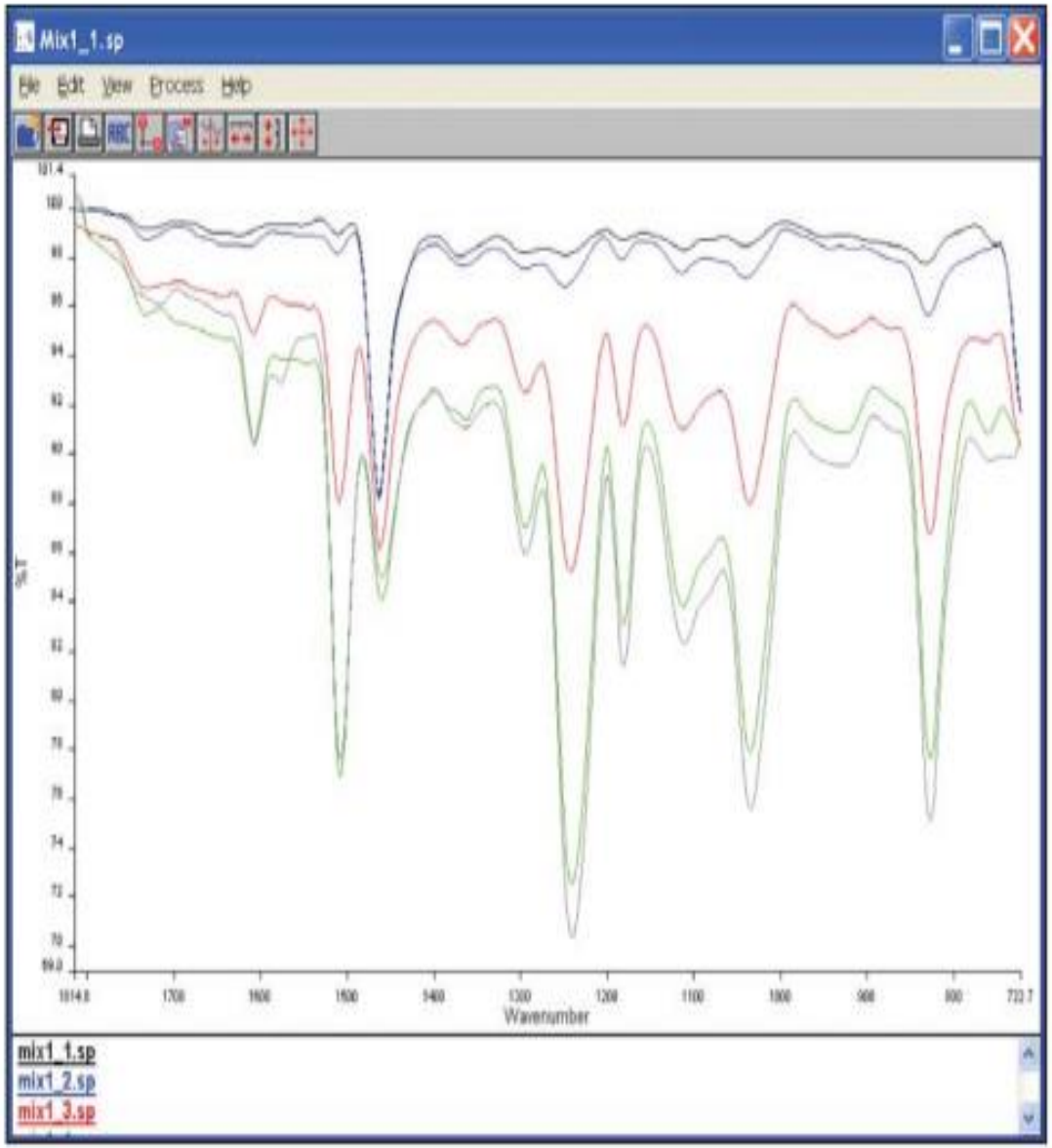

Figure 8. Five spectra obtained from every other pixel along the sampling line in Figure 7. The spatial interval is 3.12 microns.

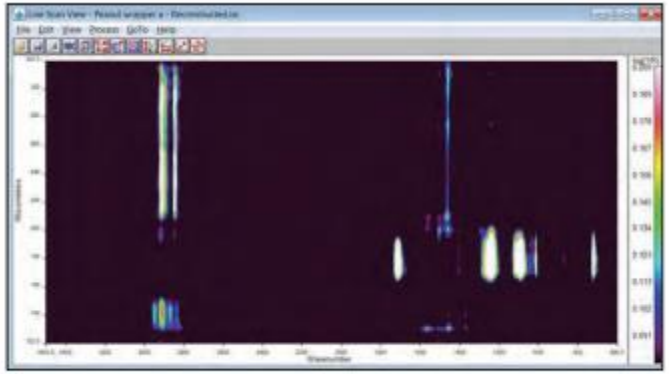

Figure 8: Linescan data for food packaging material.

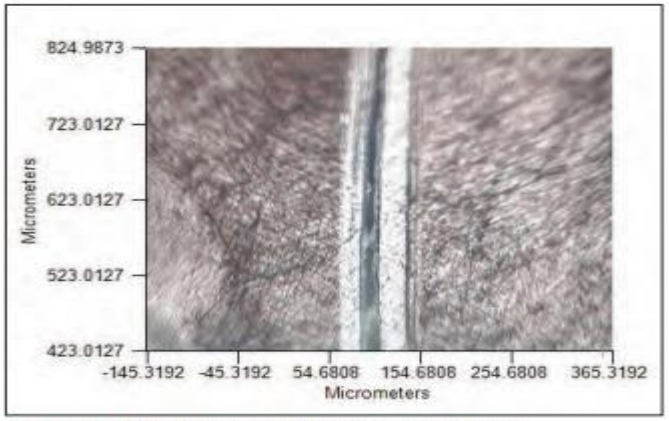

Figure 11: Visible image of a compostable food packaging laminate.

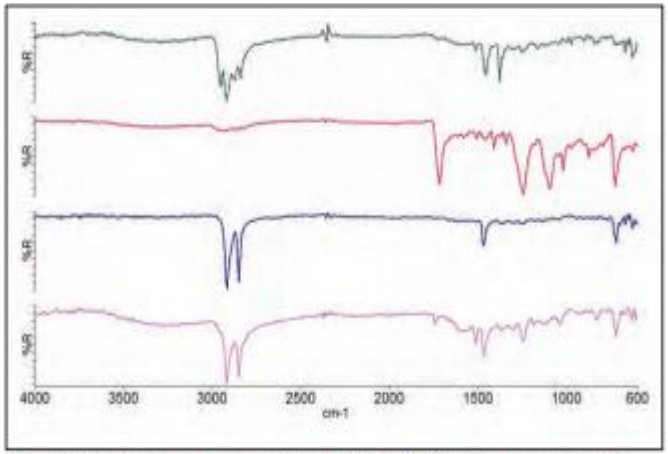

Figure 9: Spectra of major layers are identified as PP, PET, PE and modified PE.

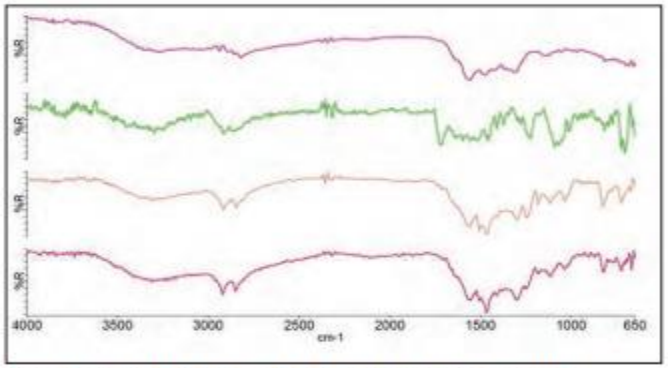

Figure 10: Spectra of minor layers in multilayer food packaging material.

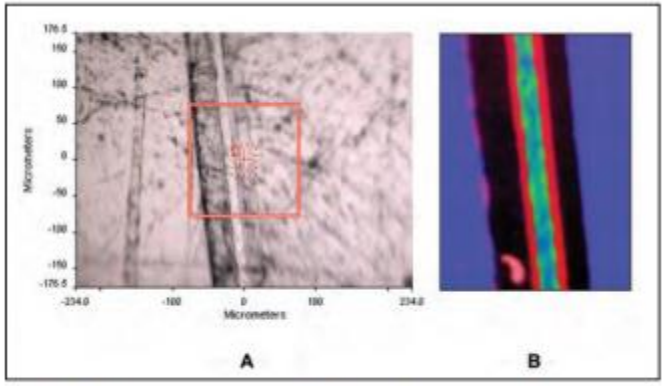

Figure 3. Visible and IR-reconstructed images from embedded laminate.

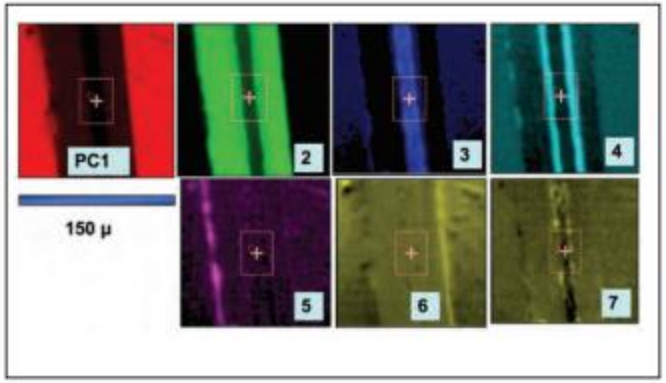

Figure 4. Principal component score images.

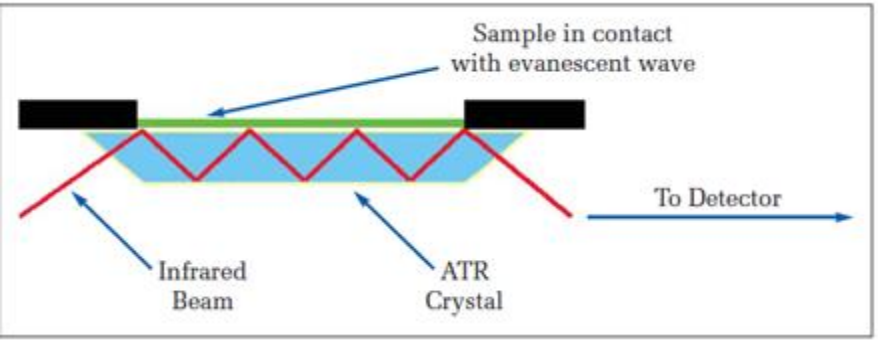

- Test for the presence of blood under certain conditions
  - Burning blood
  - Serial dilution of blood
  - Denaturing by using bleach
  - Aging over a period of time

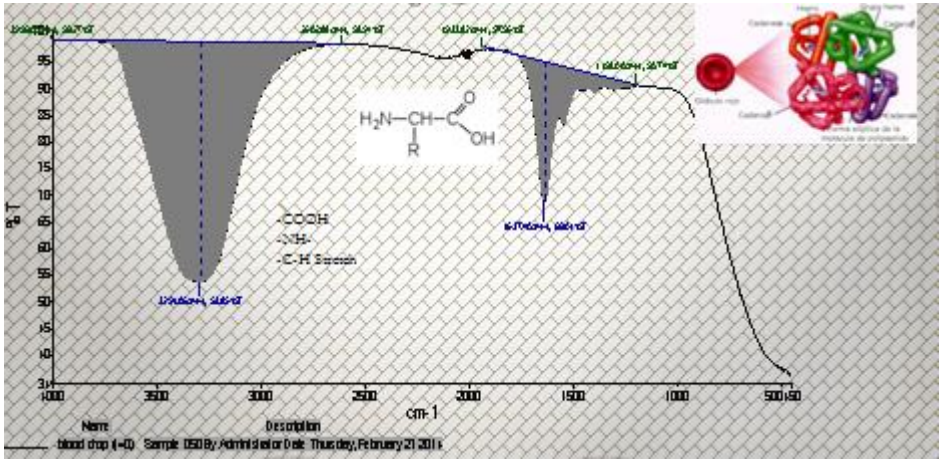

Figure 1. Linkam variable temperature sample cell.

Figure 2. Hot Stage accessory with heating block.

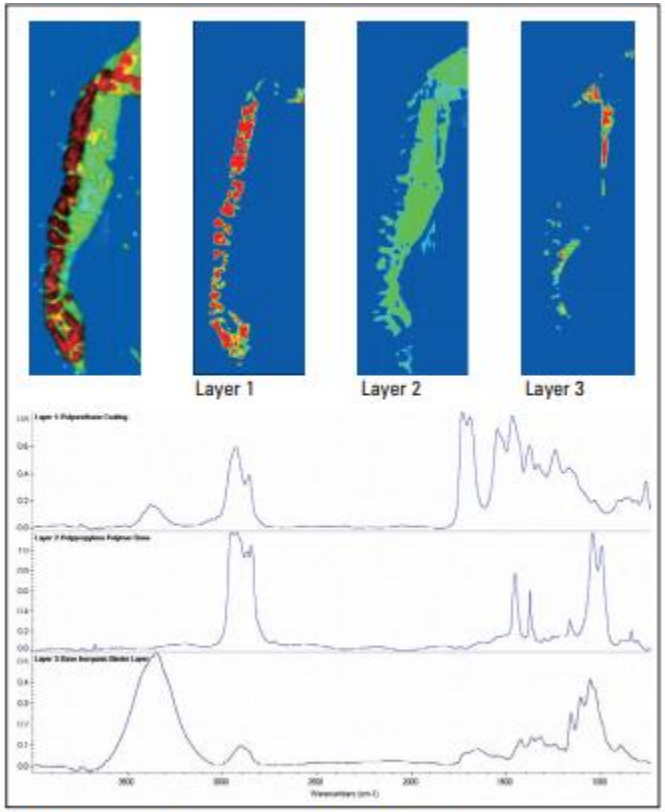

Figure 7: (Upper) Chemical image of a car bumper paint chip layers. (Lower) Spectra of identified layers: Layer 1: protective coating. Layer 2: base coat and polypropylene polymer, Layer 3: binder layer.

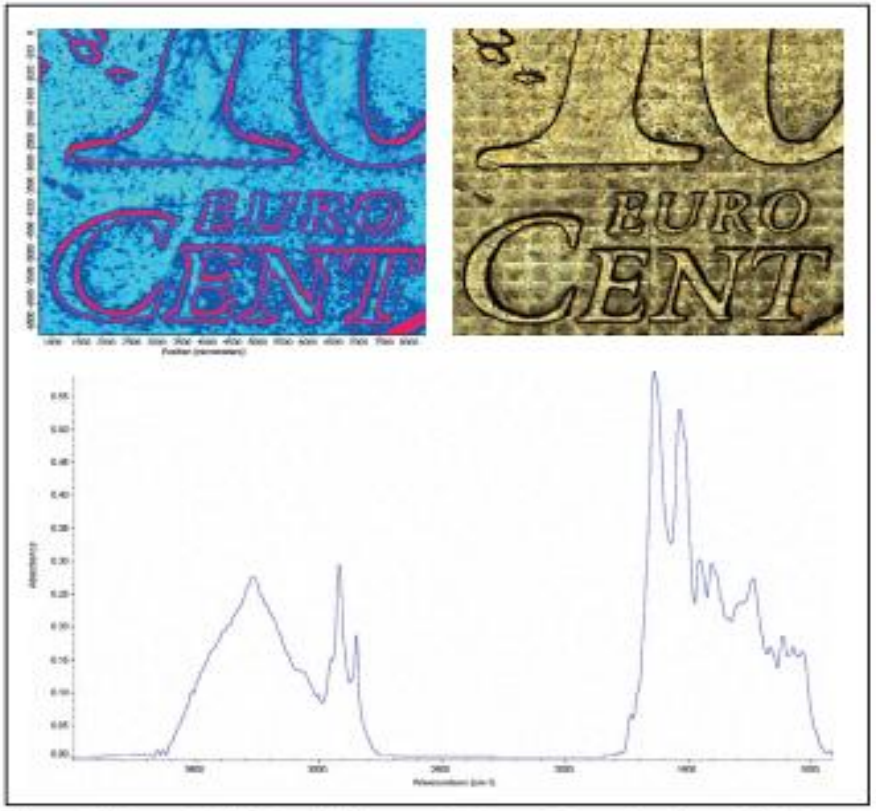

Figure 8: (Upper Left) Chemical image of 10-cent Euro coin (Upper Right) Mosaic video capture of coin sample area (Lower) Spectrum of amide residue.

LABORATORY – SAMPLE CONSIDERATIONS

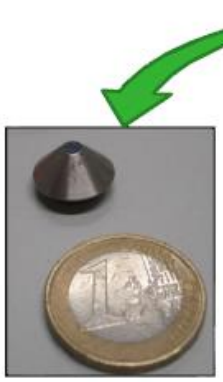

-Designed for small powder samples
-Sampling spot and space too small for most geologic samples

EXTERNAL INTEGRATING SPHERE MEASUREMENT (CONT'D

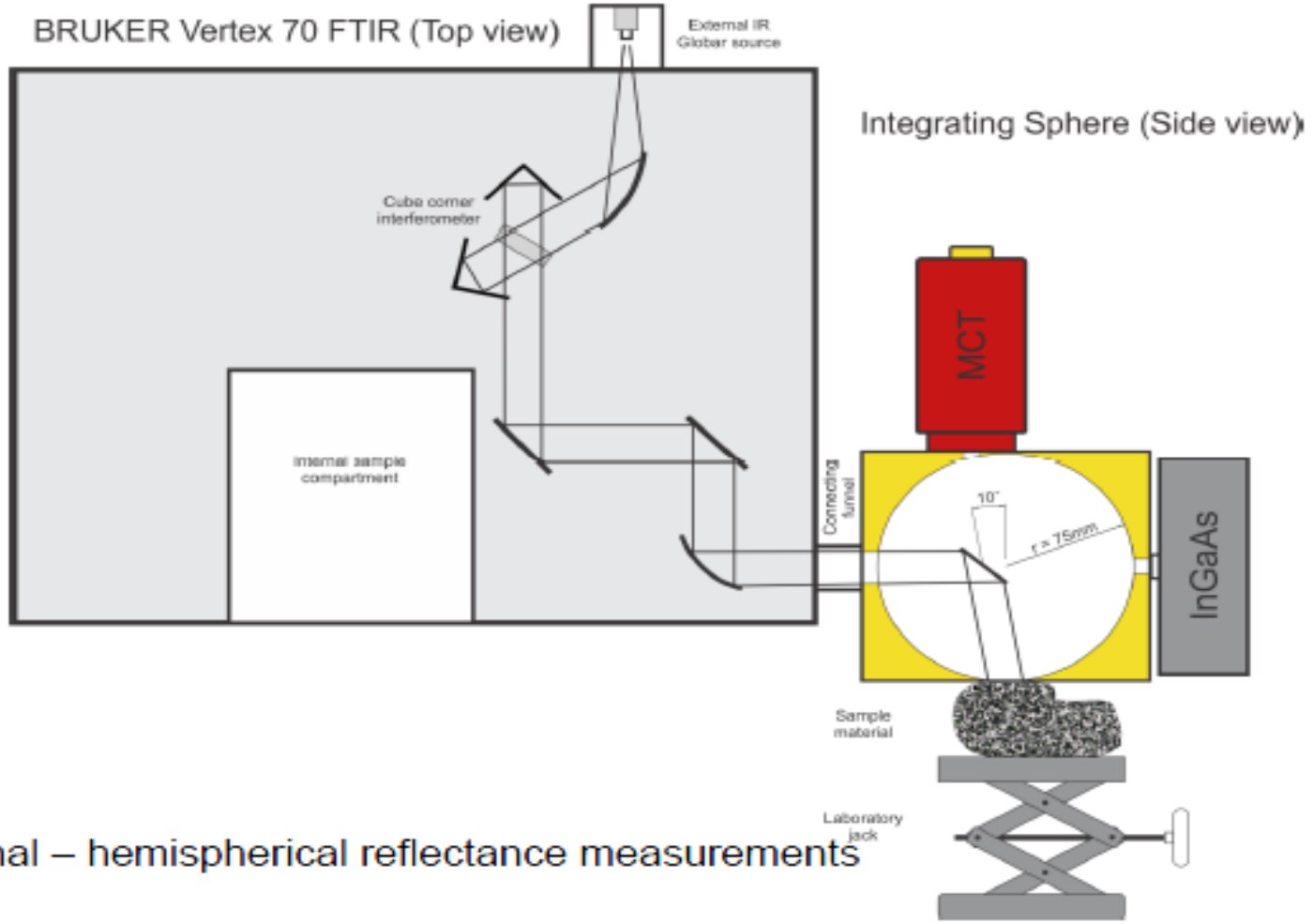

Directional – hemispherical reflectance measurements

Diffuse Reflection

Pt/Al_2O_3 DRIFTs spectra, variation in species at the surface during 1 h of nitration at 423 K (background first spectrum, activated surface).

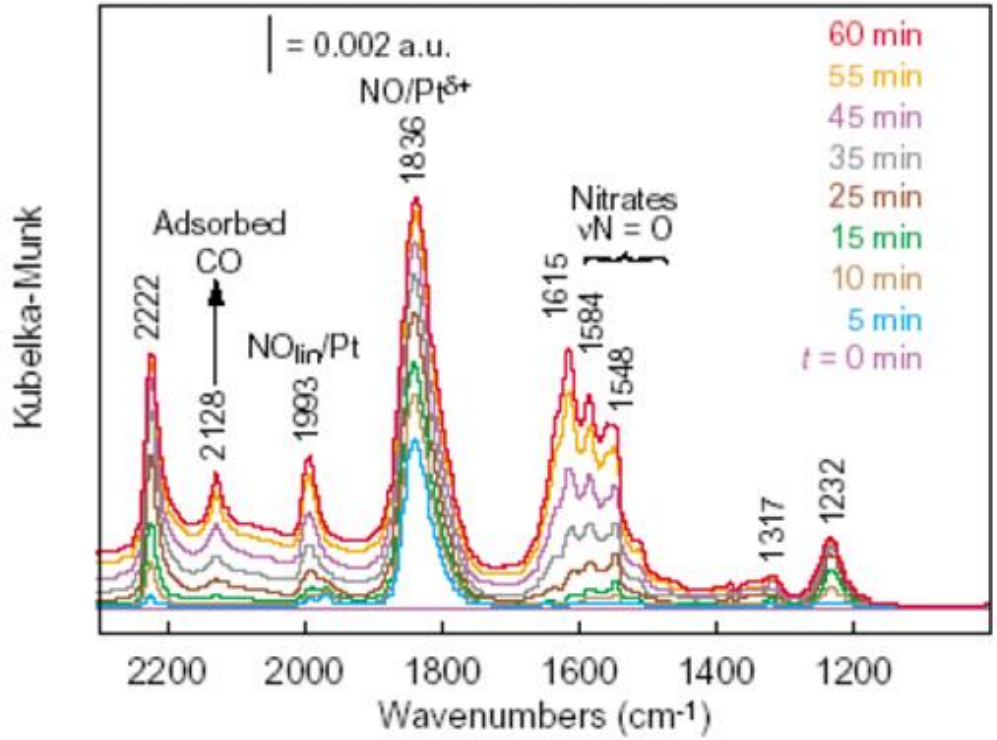

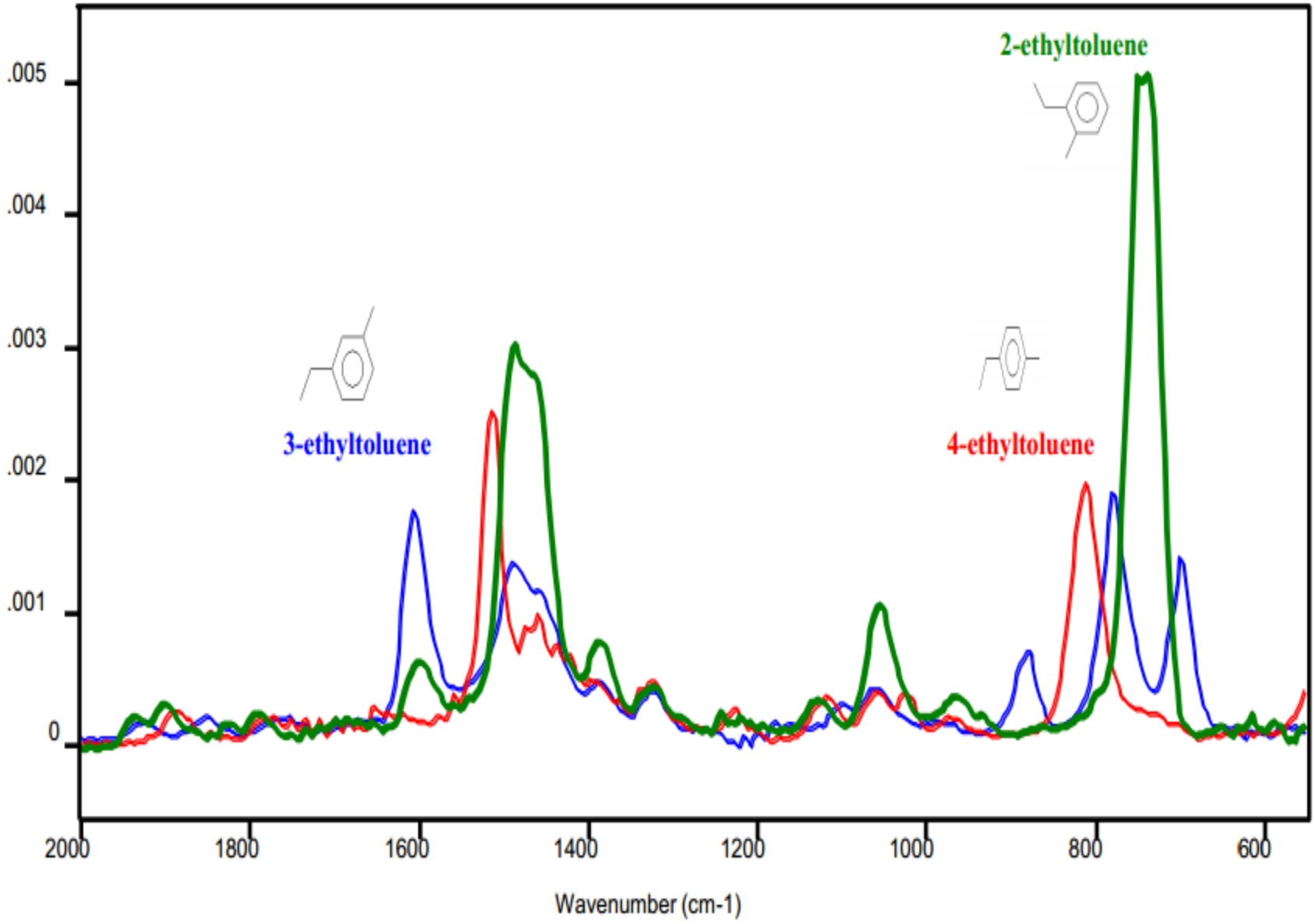
2-ethyltoluene
3-ethyltoluene
4-ethyltoluene
.005
.004
.003
.002
.001
0
2000
1800
1600
1400
1200
1000
800
600
Wavenumber (cm-1)

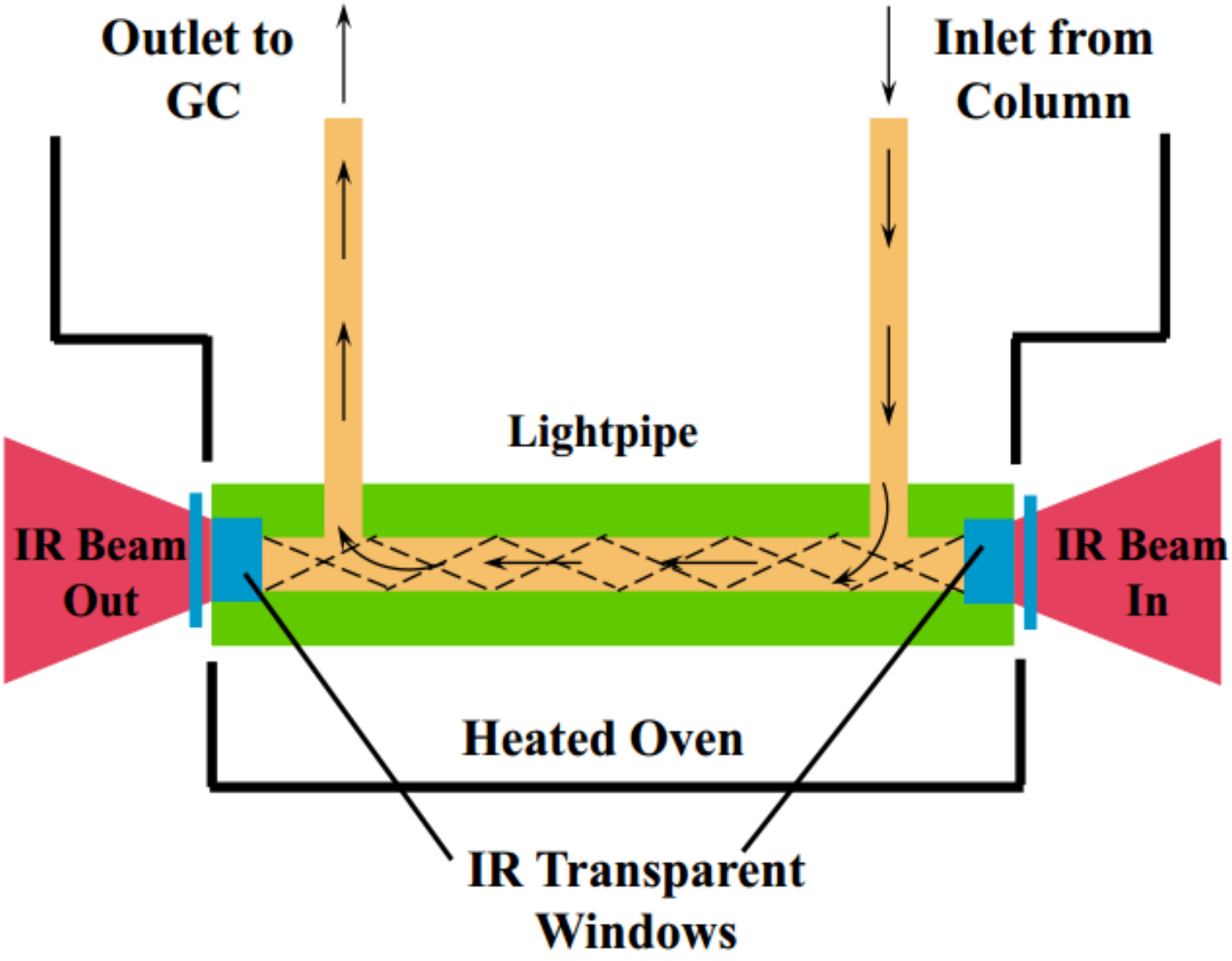
Outlet to GC
Inlet from Column
Lightpipe
IR Beam Out
IR Beam In
Heated Oven
IR Transparent Windows

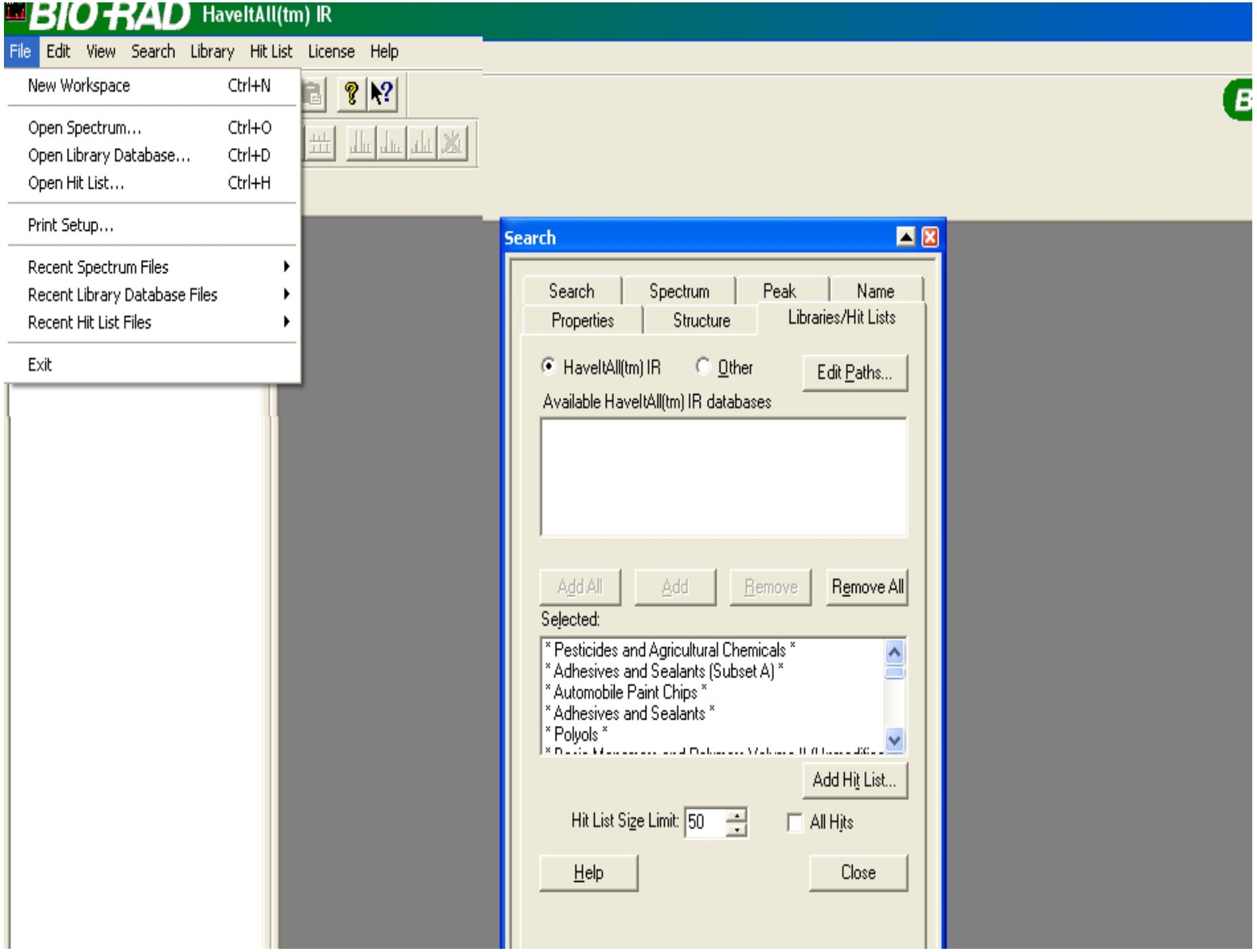
BIO-RAD HaveItAll(tm) IR
File Edit View Search Library Hit List License Help
New Workspace Ctrl+N
Open Spectrum... Ctrl+O
Open Library Database... Ctrl+D
Open Hit List... Ctrl+H
Print Setup...
Recent Spectrum Files
Recent Library Database Files
Recent Hit List Files
Exit
Search
Search Spectrum Peak Name
Properties Structure Libraries/Hit Lists
HaveItAll(tm) IR Other
Edit Paths...
Available HaveItAll(tm) IR databases
Add All Add Remove Remove All
Selected:
* Pesticides and Agricultural Chemicals *
* Adhesives and Sealants (Subset A) *
* Automobile Paint Chips *
* Adhesives and Sealants *
* Polyols *
Add Hit List...
Hit List Size Limit: 50
All Hits
Help
Close

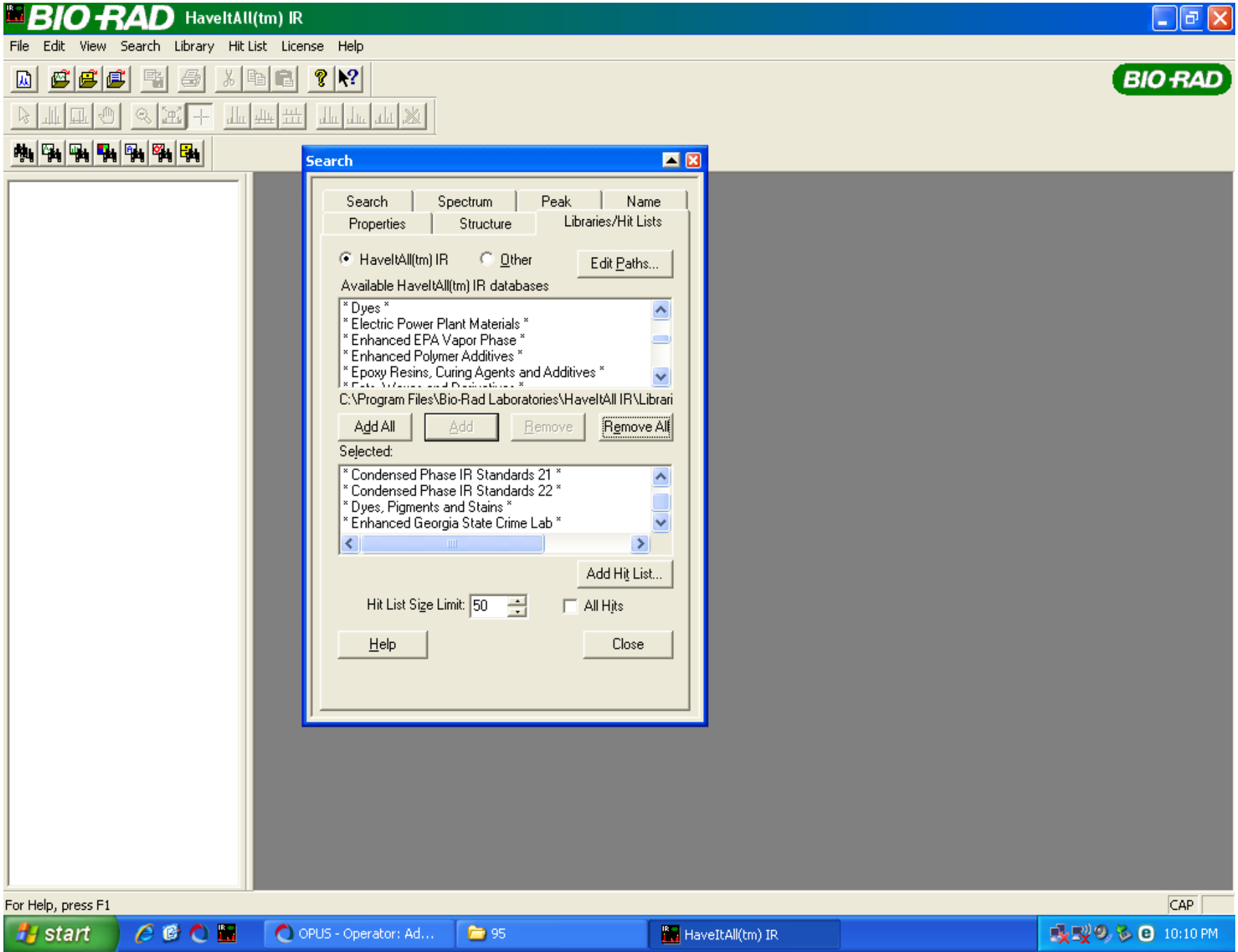
BIO-RAD HaveItAll(tm) IR
File Edit View Search Library Hit List License Help
BIO-RAD
Search
Search Spectrum Peak Name
Properties Structure Libraries/Hit Lists
HaveItAll(tm) IR Other
Edit Paths...
Available HaveItAll(tm) IR databases
* Dyes *
* Electric Power Plant Materials *
* Enhanced EPA Vapor Phase *
* Enhanced Polymer Additives *
* Epoxy Resins, Curing Agents and Additives *
C:\Program Files\Bio-Rad Laboratories\HaveItAll IR\Librari
Add All
Add
Remove
Remove All
Selected:
* Condensed Phase IR Standards 21 *
* Condensed Phase IR Standards 22 *
* Dyes, Pigments and Stains *
* Enhanced Georgia State Crime Lab *
Add Hit List...
Hit List Size Limit: 50
All Hits
Help
Close
For Help, press F1
CAP
start
OPUS - Operator: Ad...
95
HaveItAll(tm) IR
10:10 PM

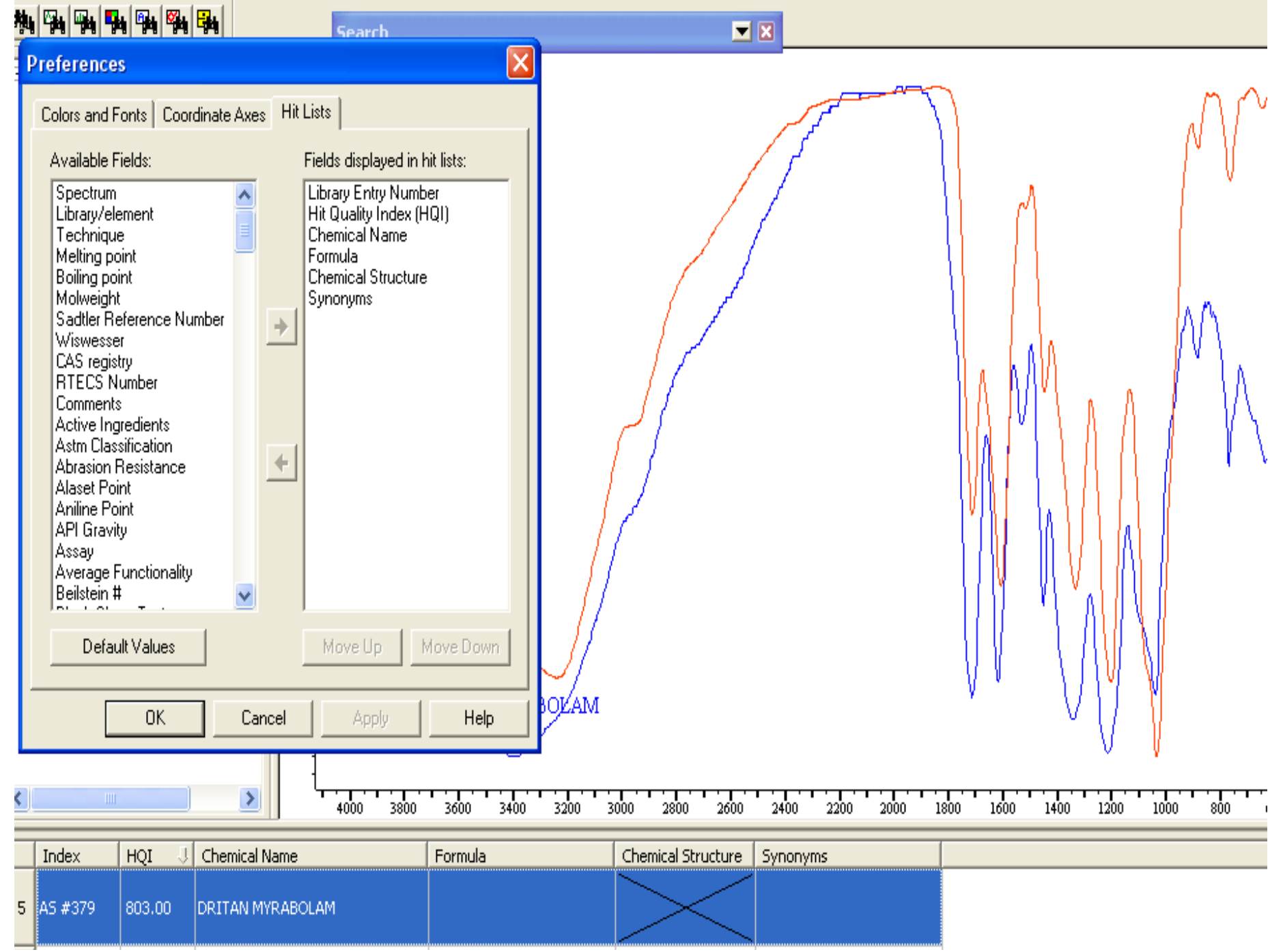
Search
Preferences
Colors and Fonts
Coordinate Axes
Hit Lists
Available Fields:
Spectrum
Library/element
Technique
Melting point
Boiling point
Molweight
Sadtler Reference Number
Wiswesser
CAS registry
RTECS Number
Comments
Active Ingredients
Astm Classification
Abrasion Resistance
Alaset Point
Aniline Point
API Gravity
Assay
Average Functionality
Beilstein #
Fields displayed in hit lists:
Library Entry Number
Hit Quality Index (HQI)
Chemical Name
Formula
Chemical Structure
Synonyms
Default Values
Move Up
Move Down
OK
Cancel
Apply
Help
BOLAM
4000
3800
3600
3400
3200
3000
2800
2600
2400
2200
2000
1800
1600
1400
1200
1000
800
Index
HQI
Chemical Name
Formula
Chemical Structure
Synonyms
5
AS #379
803.00
DRITAN MYRABOLAM

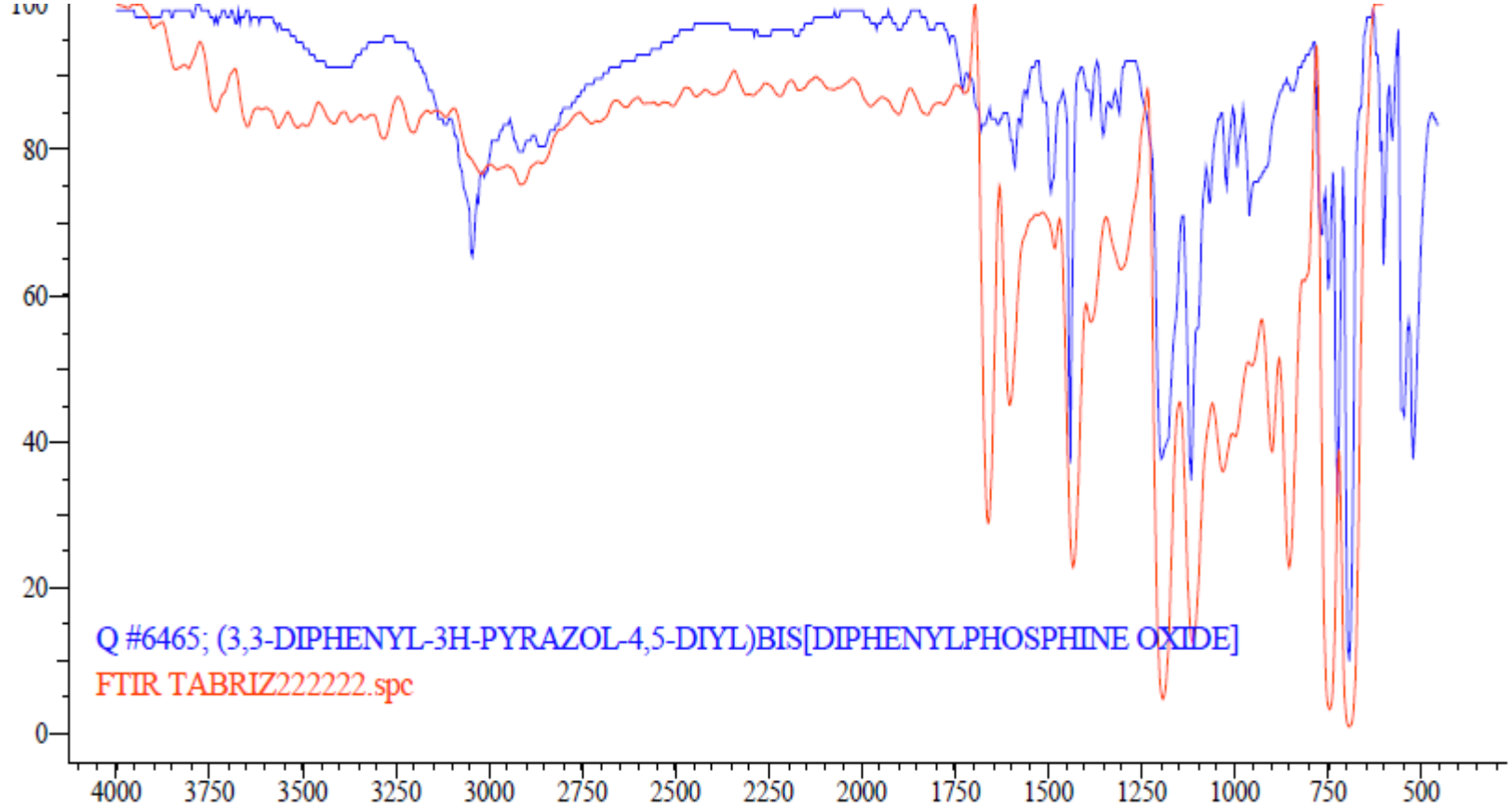

Q #6465	66.95	(3,3-DIPHENYL-3H-PYRAZOL-4,...		
ST #57484	66.95	(3,3-DIPHENYL-3H-PYRAZOL-4,...		
Q #9482	63.95	1-(DIPHENYLPHOSPHINYL)-4-(...		